



ON ISOPARAMETRIC CATMULL–CLARK FINITE ELEMENTS
FOR MEAN CURVATURE FLOW

DISSERTATION

zur Erlangung des Grades
eines Doktors der Naturwissenschaften (Dr. rer. nat.)
am Fachbereich Mathematik und Informatik
der FREIEN UNIVERSITÄT BERLIN

ANNA WAWRZINEK

Berlin 2016

Erstgutachter (Betreuer): Prof. Dr. Konrad POLTHIER

Zweitgutachter: Prof. David LEVIN

Tag der Disputation: 2. November 2016

Diese Dissertation wurde gefördert von der Deutschen Forschungsgemeinschaft e.V. (DFG)
SFB Transregio 109 "Discretization in Geometry and Dynamics".

MEINEN ELTERN

CONTENTS

1	Introduction	1
1.1	Summary of main achievements	3
1.2	Publications	4
2	Classical Theory of Subdivision	5
2.1	Combinatorial structure	5
2.2	Subdivision schemes	11
2.3	Fundamentals of subdivision surfaces	14
3	Generalized B-Splines of Catmull–Clark Type	23
3.1	Introduction to Catmull–Clark subdivision scheme	24
3.2	Natural parametrization of the limit surface	26
3.3	Characteristic surface parameterization	38
4	Isoparametric Catmull–Clark Finite Elements	47
4.1	About the isoparametric concept	48
4.2	Catmull–Clark finite elements	50
4.3	Integrals over subdivision surfaces	58
4.4	Assembly tasks	67
5	Boundary Conditions for PDEs	77
5.1	Subdivision boundary issue	78
5.2	Symmetry constraints	83
5.3	Conditions for PDEs	86
5.4	Constrained optimization	91

6	Catmull–Clark Limit Surfaces of Minimal Area	93
6.1	Perspectives on minimal spline surfaces	94
6.2	Mean curvature flow	97
6.3	Discretization using subdivision finite element	105
6.4	Implementation and experimental results	106
7	Conclusions	121
	Appendix	123
	Bibliography	126

CHAPTER 1

INTRODUCTION

In classical analysis, the behaviour and time evolution of physical phenomena, such as sound, heat, flow, elasticity, etc., are described by partial differential equations (PDEs). These have also found a place in areas such as product design and engineering, scientific computing, and animated film production. In this framework, PDEs are used to model a variety of real world problems. Due to the complexity of the problems described generally on sophisticated domains that represent everyday objects, one has to rely on numerical methods for the computation of the modal parameters. An essential approach to approximate the solution of PDEs on surfaces or volumes are finite elements, thereby, the problem is assembled piece by piece on smaller easier to handle subdomains. On the other hand, the underlying discerning domains require a detailed geometric description. From the beginning, two separate research areas have been managing the geometry representation and the analysis tasks. Over the years, this has led to more barriers for the data exchange, and, consequently, has slowed down the communication between both areas.

In recent years, isogeometric analysis is a rapidly growing research field that unifies the concepts of geometric design and numerical simulation. The focus of interest is an interoperability system based on parametric surface representations for the finite element approximations of analysis problems. One set of basis functions is used for the representation of the geometry and the approximation of the solution space. The expensive data exchange between design and analysis, and the associated data errors can be entirely eliminated. However, the choice of the underlying geometry representation, originally prescribed by non-uniform rational B-splines (NURBS), is the decisive point of the challenging problems to focus on.

Subdivision surfaces are a common geometry representation tool in geometric modelling, especially in computer graphics and computer animation. For a long time, the refinement based construction of smooth surfaces has formed the key focal point of research in this area, i.e. one has been interested in smooth surfaces obtained from repetitive refinement operations on coarse control grids. Due to the simplicity, flexibility and efficiency, a range of different schemes has

been developed. For some of the schemes, the subdivision or, equivalently, limit surfaces, defined by the surfaces in the limit of the corresponding subdivision operations, exhibit a closed parametric representation in addition to its high smoothness. In this regard, subdivision surfaces can serve as a base framework for the construction of finite element methods. The multiple capabilities for applications, such as parameterization, modelling, simulation and manufacturing, make subdivision surfaces to a universally usable processing tool.

This work focuses on quadrilateral control grids and the generalized bicubic B-spline surfaces of Catmull–Clark subdivision type. The basic subdivision algorithm is simple, however, the properties of the limit surface may be quite complicated and difficult to analyze. One may have in mind the existence of extraordinary vertices that influences the smoothness of the surfaces. In [Stam, 1998], the first explicit parameterization of the limit surface has been introduced. Owing to the so-called natural parameterization, the labour-intensive subdivision process can be avoided and the limit surface can be generated without any explicit subdivision operation. Nevertheless, the simplification is not free of defects. At extraordinary vertices, the smoothness of the limit surface defined in the classical manner has been lost. This work describes how to rescue the parameterization by using the classical concept of the characteristic mapping. The associated reparameterization is consistent with the classical definition of subdivision surfaces, i.e. the smoothness of the limit surface at the singularities is retained. However, it is expensive to compute, and therefore not applicable for CAD-systems.

Linking to isogeometric analysis, subdivision finite elements become a fast-growing field of research. Based on the subdivision basis functions, we describe a solid theoretical and algorithmic definition of subdivision finite elements. We introduce the characteristic subdivision finite element for the discretization and study of PDEs on Catmull–Clark surfaces. The conversion of the characteristic parameterization came up as an effective finite element construction. The reason for this, in the integral representation, the expensive inversion of the characteristic map reduces to a scaling factor that depends on the valence of the extraordinary vertex. Furthermore, we compare the results we achieve using the natural and the characteristic subdivision finite element approach solving the mean curvature flow on curved surfaces. Despite good results, a particular challenge is still an efficient numerical integration of non-polynomial functions.

The classical examples of minimal surfaces include the helicoid, catenoid, Schwarz P surface, Schwarz D surface, etc., where each section of the surface is again a minimal surface. Due to the least area property, surfaces such as these are interesting for many natural sciences, engineering and architectural applications. However, the standard minimal surface formulation cannot be used in a custom implementation or simulation. To expand the applicability, algorithms are needed to represent minimal surfaces accurately as a part of the design process. In order to achieve this, we introduce the subdivision suitable analogon of minimal surfaces, i.e. the aim of this work are minimal Catmull–Clark limit surfaces. Using the mean curvature flow, minimal Catmull–Clark surfaces are those surfaces, which are the critical points of the flow on given Catmull–Clark geometries, allowing for specified boundary conditions. In this thesis, we focus on periodic minimal surfaces that fulfil Schwarz’s reflection principle. Accordingly, we describe a set of symmetry preserving boundary constraints for subdivision surfaces. We establish the relevant algorithm and present some examples of minimal Catmull–Clark surfaces.

1.1 Summary of main achievements

The goal of this thesis is to establish the theoretical foundation of Catmull–Clark subdivision surfaces for finite element applications. To determine the reliability and operability of the framework, we apply the corresponding finite elements to the mean curvature flow on curved subdivision surfaces. The results are obtained over a step-by-step changing initial geometry. Furthermore, a framework for the construction of periodic Catmull–Clark limit surfaces of minimal area is achieved. Broadly speaking, this thesis brings together the knowledge about the subdivision surfaces, finite element and numerical methods. The following summarizes our contributions to the problem we consider:

- Based on Stam’s parameterization scheme, we give a detailed definition of the generating splines of Catmull–Clark type in terms of the natural and the characteristic parameterization over the characteristic domain. On the latter definition, we discuss in detail the formalism of the characteristic mapping in the context of Catmull–Clark subdivision surfaces. Properties of the characteristic parameterization are presented relevant to the application for constructing finite element approaches.
- Based on the characteristic parameterization, we introduce a new subdivision finite element. Although the expensive characteristic parameterization is utilized, the computational complexity of the obtained finite element approach is comparable to the previously used natural approach. Owing to the pullback to the domain of the B-spline basis, we show that the usage of the characteristic parameterization reduces to a scaling factor. This is given by the subdominant eigenvalue of the subdivision matrix that corresponds to the valence of the affecting extraordinary vertex. The advantage in comparison with the natural approach is that the characteristic finite elements maintain the compatibility with the classical definition of subdivision surfaces. The described H^2 -regularity of the basis functions is preserved.
- Using the so far best integration method, i.e. applying Gauss quadrature to the regular patches, and to the regular subpatches up to a prescribed number of subdivision levels on the irregular element, we present a valence dependent option for the choice of the number of levels for integration.
- Based on Schwarz’s reflection principle, we construct symmetry conditions that get along with subdivision surfaces. The conditions are applied to the control grid vertices and can be used for the construction of symmetric limit surfaces. In that regard, we present a framework to solve PDEs with symmetric boundary conditions on Catmull–Clark limit surfaces using constrained optimization.
- We present the discretization of the mean curvature flow on Catmull–Clark limit surfaces. We give a detailed definition of the mass and stiffness matrices using the two previously described finite element approaches. As an application, we calculate the flow on curved subdivision surfaces with and without boundary conditions. Furthermore, the calculation is done on the step-by-step changing geometry. Considering this, we compare the characteristic finite element approach to the natural approach used in the literature.
- Finally, we introduce a framework to construct periodic Catmull–Clark limit surfaces of minimal area. In particular, we study the relevance of limit surfaces corresponding to the critical points of the mean curvature flow for the approximation of minimal surfaces. We consider an interoperability system between Catmull–Clark limit surfaces and Catmull–Clark finite elements.

1.2 Publications

A part of this dissertation results in a scientific publication that will be published as a special issue in the Computer-Aided Design Journal (Elsevier). In [Wawrzinek and Polthier, 2016], we deal with the theoretical backgrounds for the integration of generalized B-spline functions on Catmull–Clark limit surfaces close to singularities. Additionally, we will present this research work on the "Symposium on Solid & Physical Modeling 2016" in June 2016.

CHAPTER 2

CLASSICAL THEORY OF SUBDIVISION

Subdivision surfaces are certain types of geometries, firstly introduced in computer graphics, for the representation of smooth surfaces starting from coarse piecewise linear polyhedral meshes, called control grids. They allow a designer to specify and easily modify the desired shape of an object. Subdivision surfaces can be described from two different approaches at once, i.e. as the limit of repetitive operations, and using local spline based parameterization over the control grid as piecewise spline surfaces.

In this chapter, we provide a short introduction to the subdivision surface formalism. We present the basic idea of subdivision, briefly review the history and give a general overview of the underlying structures. These have some crucial properties that we want present to the reader for better understanding of its functional power. The classical, namely, the refinement operation based point of view is to the fore here. Using the subdivision map, we are able to evaluate the subdivision surfaces pointwise, i.e. in the vertices of the control grid. However, a link to the smooth subdivision surface function cannot be avoided. This emphasises the strong connection between the two approaches of subdivision surfaces.

We start with the definition of a polyhedral mesh and consider some fundamental concepts, which we will utilize in the next chapters. A subdivision control grid, described by a polyhedral grid, can be viewed as the elementary combinatorial structure of the subdivision concept. It gives the basic building block for the graph-theoretical patterns on which the evaluation of the geometrical surface is described.

2.1 Combinatorial structure

The basic concept of subdivision surfaces is an algorithm that produces a series of increasingly finer geometries. The geometries are prescribed to be compact sets in the Euclidean space \mathbb{R}^3

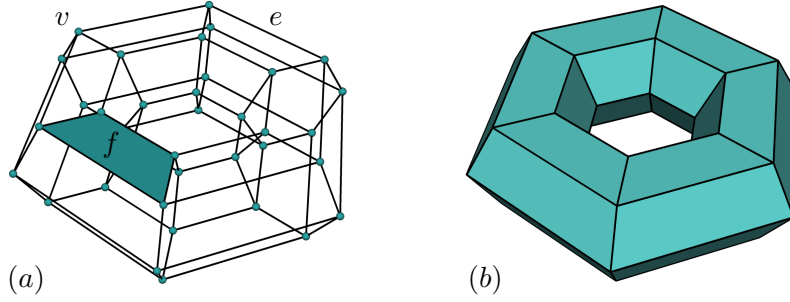


Figure 2.1: *Combinatorial and polyhedral mesh. (a) An example of a combinatorial mesh and its elements: a vertex v (blue points), an edge e (black lines) and a face f (blue quad). (b) A possible geometric realisation the combinatorial mesh.*

that fulfil given properties. In this section, we review the definition of a polyhedral mesh, in the subdivision setting the so-called control grid. A polyhedral mesh is the most basic geometric structure used for the representation of shapes in modelling and engineering systems. The main feature of polyhedral meshes is the finiteness of its dimensionality. Therefore, a smooth surface representation is expressed and visualized by a finite set of vertices with the corresponding connectivity that look as much smooth as desired by the designer. In this thesis, we restrict ourselves to polyhedral meshes that are locally manifolds. Some elementary concepts are presented; the following definitions are based on those described in [Andersson and Stewart, 2010].

2.1.1 Polyhedral meshes

A geometric model embedded in the Euclidean space \mathbb{R}^n base on two preliminary descriptions, the combinatorial and the geometrical description. The combinatorial description is characterizing the entities of the model, i.e. vertices, edges, faces, solids, etc., and the connectivity between them. Each entity is bound by a set of entities of the lower dimension. Solids are bounded by faces, faces are bounded by edges and edges are bounded by vertices. We assume that there are no isolated vertices, i.e. vertices that are not part of an edge. Isolated edges or faces are also not allowed, i.e. edges that are not part of a face and faces that are not part of a solid. The geometrical description defines where the individual entities of the model are situated in the space \mathbb{R}^n . Combining both descriptions by applying geometric information to the underlying combinatorial structure is described as a mesh. Some might ask why separating combinatorics from geometry would make sense? An advantage of doing this is that the entities of the mesh can be immediately identified by their vertices. Especially in the context of subdivision surfaces, the answer is to be found in the fact that subdivision rules are solely described by the combinatorial description of the mesh.

In this work, a geometrical model is described to be a two-dimensional mesh, i.e. we consider the sets of vertices, edges and faces. We use alternating the term grid for the term mesh. Moreover, the Euclidean space is considered here by \mathbb{R}^3 . For the notation, we label the entities of a mesh with small letters. A set of entities is notated with small "typewriter"-font or enclosed within curly brackets " $\{ \}$ ". An ordered set is denoted by round brackets " $()$ ". The adjacency relation is represented by square brackets " $[]$ ".

We begin with the specification of the combinatorial description. From this point of view, all entities are abstract, this means of purely theoretical nature without an underlying space. Let be given the finite sets of vertices

$$\mathbf{v} = \{v_i \mid i \in \mathbb{Z}_V = \{0, 1, \dots, V - 1\}\},$$

unordered edges

$$\mathbf{e} = \{e_{ij} = \{v_i, v_j\} \mid i \neq j, i, j \in \mathbb{Z}_V\}$$

that join two vertices, and faces $\mathbf{f} = \{f\}$, such that a face $f \in \mathbf{f}$ is a finite ordered tuple

$$f = (v_{i_0}, v_{i_1}, \dots, v_{i_{E-1}}), \quad i_k \in \mathbb{Z}_V, \quad k \in \mathbb{Z}_E,$$

of E different vertices, where $\mathbb{Z}_E = \{0, 1, \dots, E-1\}$. All told, sets obtained by cyclic permutation of each element of these are considered. A face f with E vertices is called an E -gon. For each face $f \in \mathbf{f}$, we require $E \geq 3$. We assume that the vertices are arranged in a counter-clockwise sequence; this determines a positive orientation of the face. Furthermore, given a face f , we consider the corresponding set of unordered face edges

$$\mathbf{e}[f] = \{e_{i_0 i_1}, e_{i_1 i_2}, \dots, e_{i_{E-1} i_0}\}.$$

The size of the edge set $\mathbf{e}[f]$ is equal to the number of vertices characterizing the face f , i.e. $|\mathbf{e}[f]| = E$.

Definition 2.1 (Combinatorial mesh). Let $\mathbf{v} = \{v_i\}_{i \in \mathbb{Z}_V}$ be a set of vertices. A *combinatorial mesh* K is defined by a finite set of faces \mathbf{f} obtained from the set of vertices \mathbf{v} and the corresponding set of unordered edges $\mathbf{e}[\mathbf{f}] = \{\mathbf{e}[f] \mid f \in \mathbf{f}\}$. Considering a face $f \in K$, its edges are in K , where for each edge $e \in K$ its vertices are in K . Two faces sharing an edge $e \in K$ are called *neighbours*.

We assume, there are no isolated vertices or edges in K . A combinatorial mesh is called *pure*, if all faces are the same E -gons. For more precise definitions of a mesh and its entities we refer to the books on algebraic topology, for example see [Munkres, 1984; Spanier, 1981]. An example of a combinatorial mesh and its entities is given in Figure 2.1.

In addition, we will distinguish between meshes with or without boundary. We consider therefore the concept of inner and boundary vertices, edges and faces, respectively.

Definition 2.2 (Interior/boundary edge/vertex/face). An edge e is called *interior edge* if it is shared by exactly two faces. If an edge belong to a single face, then it is called a *boundary edge*. An *interior vertex* is a vertex v that is not contained in a boundary edge, otherwise it is a *boundary vertex*. A face f is called *boundary face*, if at least one of the vertices of f is described to be boundary vertex. An *interior face* is characterized by only interior vertices.

Hence, each edge of a mesh belongs to at least one and at most two faces f of the mesh. A boundary is therefore defined as

Definition 2.3 (Boundary and closed mesh). The *boundary* of a combinatorial mesh K , denoted by ∂K , is the set of all boundary edges. We describe a mesh to be *closed* or without boundary, iff the boundary set is empty, otherwise the mesh has a boundary.

Additionally, a combinatorial meshes have to satisfy the following property

Definition 2.4 (Local planarity). We call a combinatorial mesh *locally planar* if each edge is an inner or boundary edge. Additionally, if for all vertices $v \in K$, the $k+1$ faces f_i that coincide at a vertex v can be ordered in such a way that f_i meets f_{i+1} at an edge containing v , for $i = 0, \dots, k-1$. For inner vertices $v \in K$, the face f_k meets f_0 along an edge. Non-consecutive faces do not share a vertex apart from v .

According to this definition, a combinatorial mesh consisting of faces that meet only in a single vertex is not locally planar. In Figure 2.2, allowed and not allowed cases are shown.

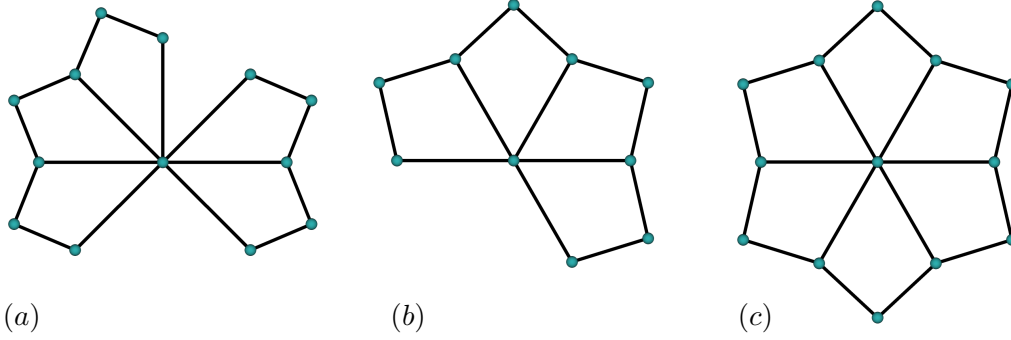


Figure 2.2: *Local planarity. Examples of: (a) a non-local planar mesh, (b) a local planar mesh with solely boundary vertices and (c) a local planar mesh with one inner vertex.*

In the subdivision literature, the concept of meshes with "arbitrary topology" is an often used catchword. The "arbitrary topology" allows for different connectivities of the mesh entities in order to enhance the shape of the mesh. The local planarity of this mesh has to be ensured. Due to this property, the combinatorics are not any more completely arbitrary.

At this point, we consider a mesh enclosed in the Euclidean space \mathbb{R}^3 . We obtain an embedding of the combinatorial mesh into the space \mathbb{R}^3 . The vertices $v \in K$ are therefore attached to geometric positions in \mathbb{R}^3 . We consider for each vertex $v \in \mathbf{v}$ a point $c \in \mathbb{R}^3$ that describes its position. The embedded mesh is defined as follows

Definition 2.5 (Polyhedral mesh). Let $\mathbf{v} = \{v_i\}_{i \in \mathbb{Z}_V}$ be a set of abstract vertices and K be a combinatorial mesh on \mathbf{v} . A *polyhedral mesh* \mathcal{C} of the mesh K is given by the pair $\mathcal{C} = (K, \mathbf{c})$, where $\mathbf{c} = \{c_i\}_{i \in \mathbb{Z}_V}$ is the set of geometric points $c_i \in \mathbb{R}^3$. The points c_i describes the positions of the corresponding abstract vertices $v_i \in \mathbf{v}$ in the Euclidean space \mathbb{R}^3 . A polyhedral mesh is called a mesh without boundary if K is a mesh without boundary. Additionally, \mathcal{C} is called manifold if it describes a subspace of \mathbb{R}^3 and is locally planar.

Remark 2.6. Given an indexing of the vertices v_i in K with $|\mathbf{v}| = V$, V is the number of vertices. There exist a isomorphism $\varphi : K \rightarrow \mathcal{C}$ between the vertices $v_i \in K$ and the geometric positions $c_i \in \mathcal{C}$, such that

$$\varphi(v_i) = c_i$$

is bijective and consequently $|\mathbf{c}| = V$. It is easy to see that, if $\mathcal{C}' = (K, \mathbf{c}')$ is another polyhedral mesh of K with the isomorphism $\varphi' : K \rightarrow \mathcal{C}'$, then $\varphi' \circ \varphi^{-1} : \mathcal{C} \rightarrow \mathcal{C}'$ is also an isomorphism.

Additionally, let $\mathcal{C}' = (K', \mathbf{c}')$ be a polyhedral mesh, such that $\mathcal{C}' \subset \mathcal{C}$. We call \mathcal{C}' a subgrid of \mathcal{C} .

Considering the above, the given isomorphisms maps vertices to vertices, edges to edges, and faces to faces. Through the choice of the combinatorial mesh K and the geometric positions \mathbf{c} , we determine the shape of the polyhedral mesh in \mathbb{R}^3 .

2.1.2 Mesh structures for subdivision

We consider a polyhedral mesh $\mathcal{C} = (K, \mathbf{c})$ over the combinatorial mesh K with the set of geometric positions \mathbf{c} to use it for the construction of a subdivision surface. In this context, the polyhedral mesh \mathcal{C} specify the so called control grid and the geometric positions c_i are called the positions of the control vertex. Additionally, the faces of \mathcal{C} are called elements of the grid. Thus, the shape of the control grid is controlled through the change of positions of the control points.

Definition 2.7 (Valence). The *valence* ν of a vertex $v \in K$ is described by the number of edges e incident in v .

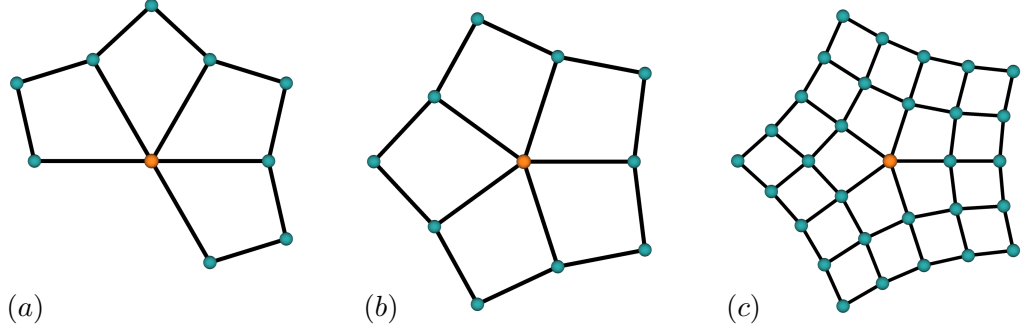


Figure 2.3: The neighbourhood of a vertex (orange vertex). Examples of: (a) an incomplete and (b) a complete one-neighbourhood of a vertex of valence five, and (c) a two-neighbourhood of a vertex of valence five.

We take into account two types of vertices, *ordinary* and *extraordinary* vertices. The type is determined by the valence of the vertices after performing some refinement steps, i.e. it depends on the applied refinement rules. Therefore, an ordinary vertex is prescribed by the most appearing vertex valence. The remaining vertices are called extraordinary. However, a regular tiling of the plain with identical elements is a crucial factor for the refinement rules. In the case of triangular and quadrilateral tilings, it is common to define rules that produce ordinary vertices of valence six and four, respectively.

There are three fundamental types of grids to be distinguished by their combinatorics: the *regular*, ν -*regular* and *irregular* mesh. The first type is characterized through the regular tiling of the plain by identical elements with identical connectivities. The regular mesh is a pure mesh, such that each vertex has the same valence. Purity of a grid concerns only the elements, i.e. the grid is pure, if each element have the same number of edges, otherwise it is called nonpure.

At this point, we add one irregularity to the regular grid. By doing so, we obtain a grid, such that the valence of one of the vertices is different than the other. We consider the so called ν -regular grid

Definition 2.8 (ν -regular grid). A ν -regular grid is a pure grid for that all inner vertices has the same valence except one vertex v_c with the valence ν unequal to the dominant valence. We call the vertex v_c the central vertex of the ν -regular grid.

The ν -regular grid is a grid with a single vertex of extraordinary valence ν . In general, the central vertex will be identified with zero in the plane. For the last type, the valence of the vertices is arbitrary; we distinguish between pure and nonpure irregular grids.

We consider two important submeshes of K that we will use more often in this work. For the following definition, we examine the neighbourhood of a control vertex.

Definition 2.9 (One-/n-neighbourhood). An *one-neighbourhood* of a vertex $v \in K$ is the sub-mesh of K consisting of all faces of the grid that have v as a vertex. A *n-neighbourhood* of v is defined recursively as the union of all one-neighbourhoods of all vertices in the $(n - 1)$ -neighbourhood of the vertex v . A one-neighbourhood is called *complete*, if v is an interior vertex, and *incomplete*, if v is a boundary vertex.

Examples of a complete and an incomplete one-neighbourhoods and a two-neighbourhood of a vertex are shown in Figure 2.3.

Additionally, we examine the neighbourhood of a single element in the grid K and consider the following definition:

Definition 2.10 (One-/n-ring). An *one-ring* of a face f is the union of f and all faces sharing at least one vertex with f . A *n-ring* of f is the union of the one-rings of all faces in the $(n - 1)$ -ring

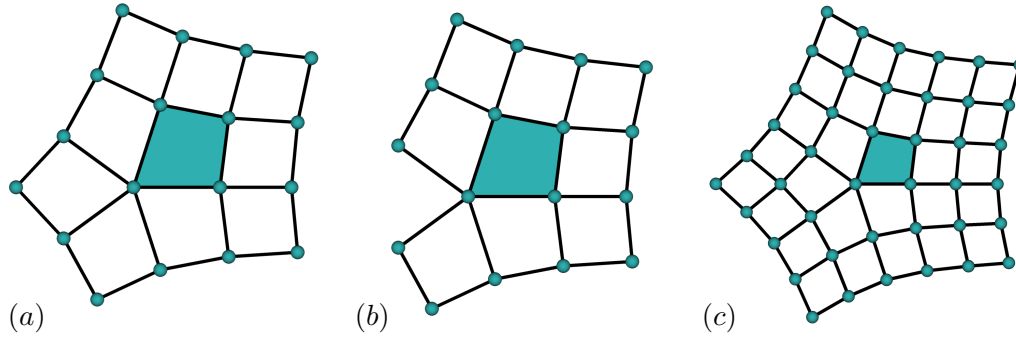


Figure 2.4: The ring of an element (blue quad). Examples of: (a) an incomplete one-ring, (b) a complete one-ring and (c) a two-ring of an irregular element with one extraordinary vertex of valence five.

around f . The one-ring of a face f is *complete* if all vertices of f are interior in the one-ring. Otherwise, the one-ring is called *incomplete*.

In Figure 2.4, different n -rings of a quadrangular element are shown. Considering complete one-rings, we distinguish between regular and irregular elements. An element f is called *regular* if all of its vertices are ordinary. If at least one of the vertices is extraordinary, then the element is called *irregular*.

2.1.3 Refinement of meshes

Given a control grid $\mathcal{C} = (K, \mathbf{c})$ with the underlying combinatorial grid K and the set of vertex positions \mathbf{c} . A new grid K' based on the grid K is constructed by two steps. In the first step, a new vertex set \mathbf{v}' is established by adding new vertices to the vertex set \mathbf{v} of the mesh K . Connecting appropriate vertices in \mathbf{v}' leads to a new grid K' . This procedure is called a combinatorial refinement of a control grid. It can be adopted directly by the control grid \mathcal{C} leading to a new control grid \mathcal{C}' over K' . However, we ignore here the procedure of finding geometric positions of the new vertices.

Considering the connectivity of K and the resultant K' , we distinguish between primal and dual refinement methods. The primal method produces meshes that can be seen as pure refined versions of the considered mesh. In this context, we describe the splitting operation over K , that is, the edges are split in two edges, and the elements into E elements, where E is the number of edges of an element. Moreover, we add one vertex for each edge and one vertex for each face, if necessary. We distinguish between prior, edge and face vertices in K' , that corresponds to vertices, edges and faces in K , respectively. We connect the vertices in K' according to the following rule: each prior vertex has to be connected to the edge vertices of the edges incident to the vertex in the grid K . If there are face vertices, each edge vertex has to be connected with the face vertices of the faces sharing this edge in the grid K . Otherwise, the edge vertices are connected among each other. An example of a primal refinement is shown in Figure 2.5 (a).

Looking now at the dual method, the idea is to construct the dual mesh K' of the given mesh K . The mesh K' is a mesh that has a similar scaled face for each face of K and has one edge whenever the corresponding endpoints of the parallel edges of two scaled faces are separated from each other by an edge in K . Thus, each vertex has a corresponding dual face, whose edges are the edges of the faces corresponding to the edges incident in the vertex. This operation is known as corner cutting, whereby the illustrative construction is described as follows: we first cut off the vertices and then the edges of the K , such that the resulting edges meet in the new vertices of the vertex cutoffs. This justifies the naming of the corner cutting operation. An example of a dual method is shown in Figure 2.5(b).

2.2 Subdivision schemes

One of the main challenges facing the area of computer graphics and applied mathematics is the representation of smooth complex surfaces in the computer. Over the years, many different approaches to this topic have been constructed. The most common constructions are based on parametric representations, as for example B-spline and NURBS surfaces. Moreover, these approaches are described using a control grid. This is, the corresponding smooth surface is created as a weighted sum of the vertices of the grid, i.e. the surface is characterized to be a blend of the vertices with the corresponding basis functions. The parametric approach offers a number of decisive advantages, but it also has weaknesses. For example, it allows to construct complex, high quality shapes that are directly evaluated over a coarse control grid. Therefore, we can start with a rough idea of a shape, while at the same time operating with a smooth surface. However, the obtained shapes are restricted to a rectangular parameter space. More complex shapes, such as spheres or geometries with handles, cannot be represented by a single surface patch. Although, almost any closed surface has to be composed of more than one surface patch. The smooth transition between the individual patches is very important for the representation, but this can be very difficult to achieve. Cases such as this are the reason why the goal would be to find a surface representation that is compact and simple to manipulate, and allows for any topological structure of the parameter space.

A very promising alternative is a concept called subdivision surfaces. It has been designed in order to repair the major issues of the parametric representations known at that time. Subdivision surfaces are piecewise smooth surfaces having no restrictions to the topology of the geometry. As already mentioned, the classical underlying principle of subdivision surfaces is a scheme using repeated subdivision of coarse control grids that allows for intermediate shape manipulation. The schemes utilize subdivision rules for regular elements and generalize these for elements with irregularities. The iterative process generates step by step a series of increasingly finer geometries. If the mesh series converges, we say that the subdivision scheme is well-defined, and therefore results in a surface called *subdivision* or *limit surface*. The topology of the limit surface is determined by the topology of the initial control grid. The shape and smoothness of such a limit surface depend on the applied subdivision scheme.

In the following, we give a general view to the motivation behind subdivision surfaces. Additionally, the basic principles and an overview of the existing schemes are presented to the reader.

2.2.1 Brief overview of existing subdivision schemes

Subdivision surfaces have been firstly introduced by Catmull and Clark [Catmull and Clark, 1978], and Doo and Sabin [Doo and Sabin, 1978] in 1978. At that time, due to the needs of the industry, the two independent research groups presented their ideas on the subdivision scheme

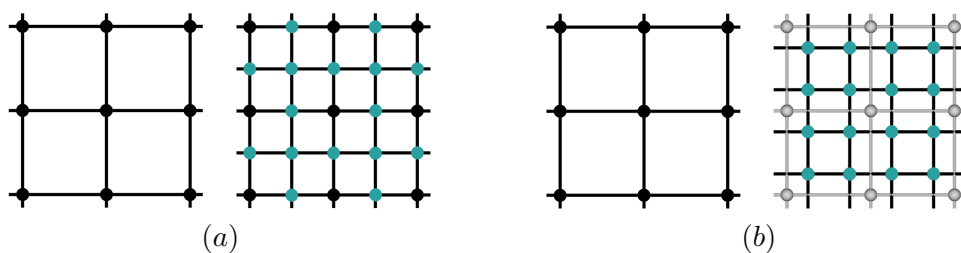


Figure 2.5: Refinement of meshes. Illustrations of (a) the primal and (b) the dual refinement. The initial grid is shown in black. In the primal refinement, the refined grid is given by all points, where the black vertices are the adopted points from the previous mesh and the blue vertices are new. In the dual refinement, the new mesh is given by the blue vertices, the grey mesh represents the rejected old mesh.

Year	Algorithm	Grid	Surface	Degree	Class
1978	Catmull-Clark [Catmull and Clark, 1978]	□	approx	bicubic	C^2
1978	Doo-Sabin [Doo and Sabin, 1978]	□	approx	biquadratic	C^2
1987	Loop [Loop, 1987]	△	approx	quartic	C^2
1990	Butterfly [Dyn et al., 1990]	△	interpol	n/a	C^1
1996	Kobbelt [Kobbelt, 1996]	□	interpol	n/a	C^1
1997	Simplest [Peters and Reif, 1997]	□	approx	quadratic	C^1
1998	TURBS [Reif, 1998]	□	approx	bi-($2k + 2$)	C^k
2000	$\sqrt{3}$ -Subdivision [Kobbelt, 2000]	△	approx	n/a	C^2
2001	4-8 - Subdivision [Velho and Zorin, 2001]	△	approx	sixtic	C^4
2001	Circle preserving [Morin et al., 2001]	□	approx	cubic, trigonom.	C^2
2002	Ternary triangle [Loop, 2002]	△	approx	quartic	C^4
2003	Quad/triangle [Stam and Loop, 2003]	△, □	approx	bicubic, quartic	C^2
2004	4-3 [Peters and Shiue, 2004]	△, □	approx	quartic	C^2
2004	$\sqrt{2}$ -Subdivision [Li et al., 2004]	□	interpol	sixtic	C^4

Table 2.1: *Subdivision zoo. An overview of some of the existing subdivision algorithms, in a chronological order. Additionally, some of their properties are given.*

that has been used for the design of smooth looking object in the computer. The construction of the so-called free-form surfaces has been invented. The underlying principle is the following: the elements of an initially designed coarse control grid are divided into smaller elements that better approximate the piecewise smooth limit surface [Schröder and Zorin, 1998]. Consequently, smooth free-form surfaces are defined algorithmically as the limit of the recursive process of subdivision. The two algorithms of the subdivision pioneers are generalizing bicubic and biquadratic B-spline refinement, respectively, producing quad meshes. The limit surfaces are almost everywhere of the appropriate smoothness. Using this idea, subdivision schemes for triangular meshes immediately followed by Loop’s [Loop, 1987] and the Butterfly subdivision schemes [Dyn et al., 1990].

Over the years, various subdivision algorithms have been invented or adapted to meet specified quality requirements for applications. An example is the quad/triangle subdivision [Stam and Loop, 2003]. The scheme combines Catmull–Clark’s with Loop’s subdivision. These are applied separately to the quad and triangular part of an arbitrary mesh, whereby for the connecting elements new rules have been developed. Thus, along the connecting elements the limit surface loses on quality and it is only C^1 -continuous. Since the Catmull–Clark subdivision by itself has been designed for quad meshes and has an undesirable shape on triangular elements, its combination with Loops algorithm improves the overall surface quality and became more applicable. Also the circle preserving algorithm of Morin et al. [Morin et al., 2001] has been designed to construct an individual type of surfaces, i.e. surfaces of revolution are in the focus of this subdivision. Therefore, using cubic polynomials, the subdivision is capable to reproduce circles and hyperbolic functions. A tension parameter is introduced that allows to obtain C^2 -continuous surfaces everywhere except at extraordinary vertices, where it is C^1 -continuous. Further on, the simplest subdivision [Peters and Reif, 1997], 4-8-subdivision [Velho and Zorin, 2001] and $\sqrt{3}$ -subdivision [Kobbelt, 2000] have been invented to lower the number of newly added vertices. Additionally, a greater control over the size of the refined mesh is one of the most important aims. Notable constructions are free-form splines [Prautzsch, 1997] and TURBS [Reif, 1998]. They support an arbitrary degree of surface smoothness, even at the extraordinary vertices. Both subdivision techniques are based on functions of bi-degree ($2k + 2$) and describe a total C^k -continuous surface. For a deeper survey of subdivision schemes we refer to [Zorin and Schröder, 2000; Peters and Reif, 2008; Cashman, 2012; Ma, 2005].

In summary, considering the existing subdivision zoo, all of the subdivision algorithms has been constructed to produce almost everywhere quad or triangular meshes. Some of the schemes follow the idea to interpolate the vertices of the initially used control grid, whereas others have an interest in certain smoothness requirements producing approximate surfaces. Although subdivision surfaces are defined by its algorithmic idea, for some of the algorithms an analytical representation is known. Furthermore, there are many known subdivision surfaces with tangent (C^1 -), curvature (C^2 -) and also higher continuity. All of the subdivision surfaces contain some isolated points, called singularities. We describe with the term singularity individual points where the general well-behaving differentiability fails. For example, the subdivision surface of the Catmull–Clark scheme is C^2 -continuous everywhere except the limit positions of the extraordinary vertices where the surface is only C^1 -continuous. A list of several well-known refinement algorithms and their properties is given in Table 2.1.

2.2.2 Subdivision basics

The basic idea of subdivision has been summarized in [Zorin and Schröder, 2000] as follows: "Subdivision defines a smooth curve or surface as the limit of a sequence of successive refinements". Building on this, subdivision is an iterative process to generate increasingly finer and smoother looking control grids from an arbitrary control grid by applying a set of operations. This is, each newly generated mesh has a larger number of vertices, edges and elements. We understand the corresponding subdivision scheme as the underlying tool kit with the rules governing the operations. To find these rules, we start with the refinement of regular grids and study how the subdivision effects and what properties characterize the limit surface. The generalization of these rules to an arbitrary grid determines the final subdivision scheme.

A subdivision scheme describes how to proceed in each level of the process. In general, each level is obtained applying a similar set of operations, but it is not a necessity. Two operations per level are specified, the refinement and the smoothing operation. In the refinement operation, we add new vertices to the control grid as has been described in Section 2.1.3. Applying the smoothing operation, we assign the geometric positions to the new set of vertices. These are derived from the vertex positions in the previous grid.

The repositioning rules of a newly added vertex are defined from vertex positions in a fairly small neighbourhood of this vertex in the previous grid. The rules can be visualized using the so-called subdivision masks.

Definition 2.11 (Subdivision masks). A *subdivision mask* illustrates graphically the weightings of the vertices in the old grid that are considered for the computation of the positions of a particular vertex in the new control grid obtained after one level of subdivision.

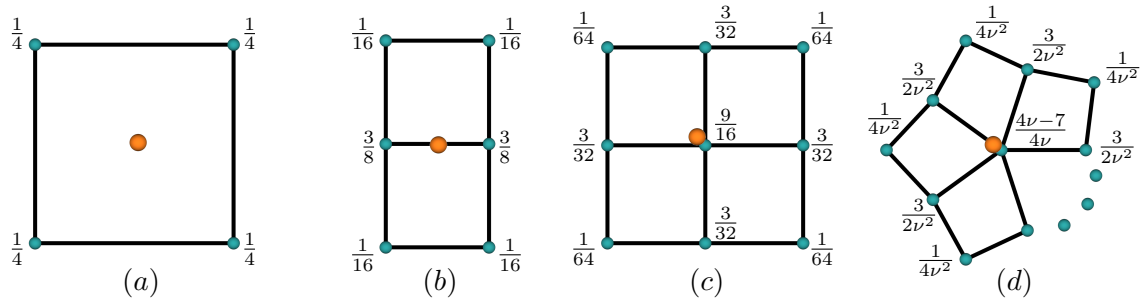


Figure 2.6: Subdivision masks of the Catmull–Clark subdivision scheme. The current grid is used to compute the position of the newly added (a) face points, (b) edge points, and (c) regular and (d) irregular vertex points (orange vertices), where ν is the valence of the central vertex. The weights are assigned to the corresponding vertices (blue) of the current mesh.

The subdivision masks provide an intuitive, index free representation of subdivision rules. If the sum of the weights in the mask is one, the scheme is affine invariant. In Figure 2.6, subdivision masks of the Catmull–Clark scheme are shown.

The scheme is called stationary if in each step the applied operations are identical. Otherwise, the scheme is a dynamical scheme. Note that during the subdivision process the number of extraordinary vertices is constant. It can increase insignificantly in the first level, if the mesh is nonpure, but in the subsequent levels only ordinary vertices will be generated. This leads to the isolation of the existing extraordinary vertices.

2.3 Fundamentals of subdivision surfaces

As already mentioned, the subdivision process is an iterative process generating a series of control grids. The progressively finer grids have an exponentially growing number of entities. In that sense, data storing is one of the accompanying challenges of using this concept. Additionally, the computation of the following series member is described by a global change, i.e. it influences the total control grid. Due to the locality of the subdivision rules, the global issue can be split into a sequence of local refinements that exhibits some important qualities. However, a particular challenge is to determine the limit surface and its properties. The properties of the arising subdivision surface can be obtained by studying the local subdivision.

In the following, we review some strong conceptual and technical backgrounds to calculate the limit surface. Additionally, we discuss elementary concepts that allow us to understand subdivision surfaces as limits of iterative operations on control grids.

2.3.1 Subdivision process

Starting from scratch, let

$$\mathcal{C}_0 = \left(K_0, \mathbf{c}_0 = \{c_i^0\}_{i \in I_0} \right)$$

be an arbitrary control grid described by the combinatorial mesh K_0 together with the set \mathbf{c}_0 of vertex positions c_i^0 in \mathbb{R}^3 , where $i \in I_0$ is the index of a vertex and $I_0 \subset \mathbb{N}$ is the ordered vertex index set of K_0 . We call \mathcal{C}_0 the initial control grid.

The subdivision is described by the repeated application of prescribed subdivision rules to the control grid. The iterative process can be graphically represented as the chain

$$\mathcal{C}_0 \rightarrow \mathcal{C}_1 \rightarrow \mathcal{C}_2 \rightarrow \dots,$$

of successive control grids \mathcal{C}_k , $k \geq 0$, where " \rightarrow " symbolizes one level of the process. Here, the mesh \mathcal{C}_{k+1} is described over the mesh \mathcal{C}_k and by an ongoing repetition of the procedure, we can find its roots in \mathcal{C}_0 . According to that, we consider the set

$$\mathcal{C}[K_0] := \left\{ \mathcal{C}_k \left| \mathcal{C}_k \left(K_k, \mathbf{c}_k = \{c_i^k\}_{i \in I_k} \right) \right. \right\}_{k \in \mathbb{N}} \quad (2.1)$$

of all increasingly finer meshes over K_0 , i.e. the number of vertices is increasing and $I_k \subset I_{k+1}$. Furthermore, for each control grid $\mathcal{C}_k \in \mathcal{C}[K_0]$, we assign a control vertex matrix $\mathbf{C}_k^{*T} = (c_0^k, c_1^k, c_2^k, \dots)^T$. The entries c_i^k , $i \in I_k$, are the position vectors of the control vertices in \mathcal{C}_k . Corresponding to the averaging operation, the positions of the vertices in the refined mesh are obtained from the vertex positions in the previous mesh. Moreover, the relation is linear. A

subdivision scheme describes the following mapping

$$\begin{aligned} \mathcal{S}_* : \mathcal{C}_k &\rightarrow \mathcal{C}_{k+1} \\ \mathcal{C}_{k+1}^* &= \mathcal{S}_* \mathcal{C}_k^*, \end{aligned}$$

with the adaptive matrix \mathcal{S}_* , called the global subdivision matrix. The mapping \mathcal{S}^* corresponds to the refinement rules used to construct the combinatorial mesh K_{k+1} from K_k . It assigns spatial positions \mathcal{C}_{k+1} to the vertices in \mathcal{C}_{k+1} . It should be noted that \mathcal{S}_* is growing with each following level according to the increased number of control grid vertices. As mentioned before, we are able to rewrite \mathcal{C}_k^* back to the initial grid \mathcal{C}_0 . This is given as follows:

$$\mathcal{C}_k^* = \mathcal{S}_* \mathcal{C}_{k-1}^* = \mathcal{S}_*^2 \mathcal{C}_{k-2}^* = \dots = \mathcal{S}_*^k \mathcal{C}_0^*,$$

where $\mathcal{S}_*^k = \mathcal{S}_* \mathcal{S}_*^{k-1} = \mathcal{S}_* \mathcal{S}_* \dots \mathcal{S}_*$ is a product of matrices of increasing sizes. The matrices are prescribed by the connectivity of the vertices and the subdivision masks. That is, the matrix entries are prescribed by the weights used to obtain the newly added vertices distributed in such a way that relation between the new and old vertices is fulfilled.

If a subdivision scheme is convergent, then the series

$$\mathcal{C}_0 \rightarrow \mathcal{C}_1 \rightarrow \mathcal{C}_2 \rightarrow \dots \rightarrow \mathcal{S}^\infty \mathcal{C}_0,$$

converges to a smooth limit surface $\mathcal{S}^\infty \mathcal{C}_0$. After all, applying \mathcal{S}_* infinitely many times should lead to the same limit surface, i.e.

$$\mathcal{S}^\infty \mathcal{C}_0 = \lim_{k \rightarrow \infty} \mathcal{S}_*^k \mathcal{C}_0^*.$$

The question that is addressed in the upcoming section is: what does it mean to the scheme that it is convergent?

2.3.2 Subdivision surface function

Considering an arbitrary initial control grid \mathcal{C}_0 and a given subdivision scheme \mathcal{S}_* , let $\mathcal{C}[K_0]$ be the set of control grids over K_0 generated by means of the subdivision process. Let the vertices of two successive control grids be labelled in such a way that the old vertices keep their indices and the new vertices get new indices. When applying subdivision, for a control point $c_j^k \in \mathcal{C}_k$ in $\mathcal{C}_k \in \mathcal{C}[K_0]$, where $j \in I_k$. The set $I_k \subset \mathbb{N}$ is the ordered set of vertex indices of K_k in \mathcal{C}_k . Let c_j^{k+i} be the position of c_j^k after i levels of subdivision, $i \in \mathbb{N}$, i.e.

$$c_j^{k+i} = [C_{k+i}^*]_j^T = [S_*^i C_k^*]_j^T \in \mathcal{C}_{k+i},$$

where $c_j^k = [C_k^*]_j$. The term $[\cdot]_j$ denotes the restriction of the control vertex matrix to the position of the vertex c_j^k .

A subdivision scheme is called convergent if, for each vertex $c_j^k \in \mathcal{C}_k$, and each $k \in \mathbb{N}$, there exists a continuous function $\mathcal{S}^\infty \mathcal{C}_k \in C(K_k)$, such that

$$\lim_{i \rightarrow \infty} \sup_{i \in I_k} \left\| c_j^{k+i} - \mathcal{S}^\infty \mathcal{C}_k \left(c_j^k \right) \right\| = 0. \quad (2.2)$$

The function $\mathcal{S}^\infty \mathcal{C}_k$ is called the subdivision or limit surface function.

For a given combinatorial mesh K , let $C(K) = \mathcal{S}^\infty \mathcal{C}[K]$ be the space of all continuous functions over K called the *shape space* over K . In the following, we denote by $\mathcal{C}[K]$ the set of

all control grids over K . Furthermore, since the map \mathcal{S}_* is linear, the operator

$$\mathcal{S}^\infty : \mathcal{C}[K] \rightarrow C(K).$$

is linear. The subdivision surface function $\mathcal{S}^\infty \mathcal{C}$ describes the limit surface of a given control grid $\mathcal{C} = (K, \mathbf{c})$ over the mesh K and a prescribed set of geometric positions \mathbf{c} .

Suppose K_k with the set $\mathbf{v}_k = \{v_i^k\}_{i \in I_k}$ of abstract vertices is a k times refined combinatorial mesh generated from an initial grid K_0 by means of the subdivision process. Let $\mathcal{S}^\infty \mathcal{C}[K_k]$ be the space of subdivision surface functions over K_k . Considering the structure of $\mathcal{S}^\infty \mathcal{C}[K_k]$ underlying the fixed combinatorial mesh K_k , we may ask for a basis of the shape space $\mathcal{S}^\infty \mathcal{C}_k$. An obvious choice of the basis is given by the knot basis

$$\delta_i^k(v_j^k) = \begin{cases} 1 & \text{if } i = j \\ 0 & \text{if } i \neq j \end{cases}$$

for all $i \in I_k$. The union of all knot functions corresponding to K_k describes the set $\{\delta_i^k\}_{i \in I_k}$ of linear functions. Now, for each $i \in I_k$, we consider $\delta_i^k K_k$ to be an almost flat control grid in $\mathcal{C}[K_k]$, where only the i th vertex is one higher than the others. The i th subdivision surface basis functions B_i^k is therefore obtained by applying the subdivision surface function to the control grid $\delta_i^k K_k$, i.e. $B_i^k = \mathcal{S}^\infty \delta_i^k K_k$. Based on the locality of the subdivision scheme, the basis function B_i^k is non-zero only in a closed neighbourhood corresponding to the vertex v_i^k in $\delta_i^k K_k$. Consequently, for an arbitrary control grid \mathcal{C}_k in $\mathcal{C}[K_k]$, the control points c_i^k can be written using the knot basis as $c_i^k = c_i^k \delta_i^k K_k$. The subdivision surface corresponding to \mathcal{C}_k can be obtained from the linear combination

$$\mathcal{S}^\infty \mathcal{C}_k = \sum_{i \in I_k} c_i^k B_i^k.$$

Additionally, let \mathcal{C}_k be obtained from an initial control grid \mathcal{C}_0 by applying k levels of a converging stationary subdivision scheme, such that $\mathcal{C}_k \in \mathcal{C}[K_0]$. For the subdivision surface $\mathcal{S}^\infty \mathcal{C}_k$, we have

$$\mathcal{S}^\infty \mathcal{C}_k = \sum_{i \in I_k} c_i^k B_i^k = \sum_{i \in I_k} \left[S_*^k C_0^* \right]_i^T B_i^k = \sum_{i \in I_k} c_i^0 \left(S_*^k \right)^T B_i^k.$$

Considering the initial control grid \mathcal{C}_0 and the associated subdivision surface basis $\{B_i^0\}_{i \in I_0}$, the limit surface $\mathcal{S}^\infty \mathcal{C}_0 \in C(K_0)$ is given by

$$\mathcal{S}^\infty \mathcal{C}_0 = \sum_{i \in I_0} c_i^0 B_i^0.$$

If $B_i^0 = (S_*^k)^T B_i^k$, then $\mathcal{S}^\infty \mathcal{C}_0^* = \mathcal{S}^\infty \mathcal{C}_k^*$ is satisfied. Consequently, this means, the limit surface do not change during the subdivision. Hence, we observe the relation $\mathcal{S}^\infty \mathcal{C}_0^* \subset \mathcal{S}^\infty \mathcal{C}_k^*$. For more information on the stationary subdivision and the representation of subdivision surfaces, please refer to [Cavaretta et al., 1991].

Finally, we establish an elementwise description of the subdivision surface. We consider an element f in the control grid \mathcal{C}_k ; this is described by its vertices. Let $\{b_i^f\}_{i \in I_k}$ be the set of pieces of the subdivision basis functions $\{B_i^k\}_{i \in I_k}$ corresponding to the element f . Assume, for all b_i^f a parameterization over a common domain $\Omega \subset \mathbb{R}^2$ is given, such that $b_i^f : \Omega \rightarrow \mathbb{R}$. Due to the subdivision basis functions, only a finite number of local basis functions b_i^f is unequal to zero in f . Let I_f be the set of indices of the basis functions with a non-zero support in f . The set

$\{b_i^f\}_{i \in I_k^f \subset I_k}$ is called the *generating spline* of f . Moreover, it is the maximal set of basis functions to parameterize the element f . The generating spline is consequently the set of all basis functions needed to parameterize the limit surface over the appropriate control grid element f .

Definition 2.12 (Maximal basis subgrid). Let f be an element of \mathcal{C}_k and $\{b_i^f\}_{i \in I_k^f}$ its generating spline. The set of corresponding control vertices describes a local subgrid \mathcal{C}_f of \mathcal{C}_k . We call the subgrid \mathcal{C}_f the *maximal basis subgrid* of f .

As a result, the surface $\mathcal{S}^\infty \mathcal{C}_k$ can be parameterized elementwise. The limit surface patch over each element f of the control grid can be described by

$$\mathcal{S}^\infty \mathcal{C}_k|_f = \sum_{i \in I_f} c_i^k b_i^f(u, v), \quad (u, v) \in \Omega,$$

where $\mathcal{S}^\infty \mathcal{C}_k|_f$ is the restriction of the limit surface $\mathcal{S}^\infty \mathcal{C}_k$ to the element f . Nevertheless, an explicit parametric representation of the subdivision basis and the generating spline are not known. An inverse construction is described in Section 3.2.5 for the Catmull–Clark subdivision surface. Therefore, a parameterization of the subdivision surface basis functions is determined from a certain parameterization of the generating spline.

2.3.3 Subdivision map and its eigenstructure

In practice, we do not need to handle the global subdivision and the corresponding matrix S_* that grows with each subdivision step. Because of the locality of the subdivision scheme that, the subsequent control grid \mathcal{C}_{k+1} can be generated by applying the subdivision rules piece by piece to a portion of the control grid \mathcal{C}_k . Let

$$\mathcal{C}_0^K = \left(K, \{c_i^0\}_{i \in I} \right)$$

be a subgrid of the initial control grid \mathcal{C}_0 , such that $K \subset K_0$ is a combinatorial subgrid of K_0 with a specified ordering of vertices $v_i^K \in K$, for $i \in I$, where I is the local index set of K . The ordering is given as follows: we select a central vertex $v_c = v_0^K \in K$. The vertex v_c remains fixed to the global index during the subdivision, whereby all the other local vertices will change its global indices according to the refinement of K .

Definition 2.13 (Subdivision map). Given an initial subgrid $\mathcal{C}_0^K \subset \mathcal{C}_l$ over a specified combinatorial grid K . A control vertex matrix C_0 is assembled based on the vertex positions $\{c_i^0\}_{i \in I}$. We select an internal vertex $v_c \in K$ to be the central vertex. Let S be the local subdivision matrix that determines the subdivision near the vertex v_c , such that v_c remains fixed. Additionally, the matrix S is preserving the prescribed grid K . The mapping

$$\begin{aligned} S : \mathcal{C}_k^K &\rightarrow \mathcal{C}_{k+1}^K \\ \mathcal{C}_{k+1} &= S \mathcal{C}_k \end{aligned}$$

is called the *subdivision map*.

For all $k \in \mathbb{N}$, the control grid $\mathcal{C}_k^K \subset \mathcal{C}_{l+k}$ is a subgrid of \mathcal{C}_{l+k} restricted to K . In the process, a reordering of the vertices is obtained. This means, the local indices except the central vertex will be assigned to the appropriate vertex indices in the global ordering.

The subdivision map is defined as a linear transformation of the neighbourhood \mathcal{C}_k^K fixed by K close to the central vertex v_c . Due to the fact that the combinatorial structure before and

after the local subdivision does not change, the matrix S remains unchanged for each subdivision level. This means, the size of S depends on the subgrid K and will not change during the process. Moreover, the local matrix S is given by an appropriate clipping of the global matrix S_* to the subgrid K . In Figure 2.7, an example of a subdivision map of a given subgrid $\mathcal{C}_0^K \subset \mathcal{C}_k$ is shown.

The subdivision map plays an important role to prove the convergence and smoothness of the subdivision process. For analysis purposes, such as convergence analysis of subdivision schemes in irregular vertices, the choice of K is predetermined by the influence of the subdivision rules and the in-depth investigation purpose, see [Andersson and Stewart, 2010] Chapter 5.5. Thus, the converse problem has to be obtained: Consider a set of local subdivision masks, and the associated subdivision matrix for a given combinatorial mesh K . When applying the associated subdivision, does this scheme define a good-behaving surface? Note, the separation of the combinatorial mesh from its geometric positions is a significant issue of the subdivision process that we will make use of in this section.

In the following, we review some concepts from linear algebra that we will use for the study of the local subdivision matrix, for more details see for example [Fischer, 2009]. Let B be an arbitrary square $m \times m$ -matrix. The matrix B is called non-defective, if it is nonsingular and has a complete basis of eigenvectors. If this is the case, then the matrix is diagonalizable and a complete eigenstructure of the matrix is given by the set of its eigenvectors and the corresponding eigenvalues. On the other hand, to each eigenvalue λ_i are associated exactly two eigenvectors v_i^r and v_i^l , $i = 0, \dots, m - 1$. These are called the right and the left eigenvector, respectively. We define the pair (Λ, V) , where Λ is a diagonal matrix defined by the ordered set of eigenvalues $\{\lambda_i\}$, and V is an invertible matrix. We call the pair of matrices the eigenstructure of matrix B . However, to determine the eigenstructure of the matrix B we have to solve one of the following eigenproblems

$$BV_R = V_R\Lambda \quad \text{or} \quad V_L B = \Lambda V_L$$

where the i th eigenvalue corresponds to the right eigenvector in the i th column of the matrix V_R and the left eigenvector in the i th row of the matrix V_L , respectively. Hence, the eigenstructure is determined by the considered eigenvalue problem, i.e. V is described by the right or left eigenvectors, respectively. Now let v^r be a right eigenvector to the eigenvalue λ . Because $(v^r)^T B = (B^T v^r)^T = \lambda (v^r)^T$, the left eigenvectors of B are just the right eigenvectors of the transposed matrix B^T . Consequently, the following relation holds $V_R = V_L^{-1} = V$.

For the given submesh \mathcal{C}_0^K over K , we assemble the control vertex matrix $C_0^T = (c_0^0, c_1^0, \dots)$, where the entries $c_i^0 \in \mathbb{R}^n$, $i \in I$, are position vectors of the vertices in \mathcal{C}_0^K . Let S be the local

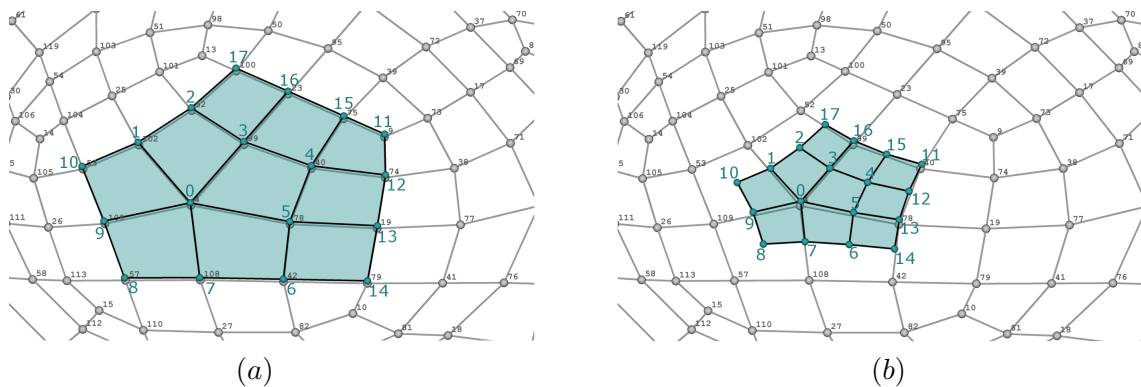


Figure 2.7: Local subdivision. The relation between the local and global indices and the reordering by means of the local subdivision. We consider the subgrid $\mathcal{C}_0^K \subset \mathcal{C}_k$. In Figure (a), the grid \mathcal{C}_0^K is shown with elements and labels coloured in blue. The global labels are grey. Figure (b) shows the grid \mathcal{C}_1^K , the first subdivision of the grid \mathcal{C}_0^K . The vertex $v_c = v_0^K$ is the central vertex of the local grid, the vertex remains associated to the same global vertex.

subdivision matrix given as in Definition 2.13. In the following, we examine the eigenstructure of S . Due to the desired properties, all known subdivision schemes have a non-defective subdivision matrix S . For schemes with defective matrix S , a similar analysis can be performed using Jordan decomposition of S . Therefore, suppose S is a non-defective subdivision matrix. Let V a the matrix, such that the columns of the matrix are described by the right eigenvectors v_i^r , $i = 0, 1, \dots, m - 1$, of S . Hence, the following equation holds

$$SV = V\Lambda, \quad (2.3)$$

with the eigenvalue matrix Λ , where the eigenvalues λ_i , $i \in I$, describes the diagonal entries of Λ . Let the eigenvalues λ_i be sorted in a non-increasing order, i.e. $\lambda_0 \geq \lambda_1 \geq \dots \geq \lambda_{m-1}$. Thus, the i th right eigenvector v_i^r corresponds to the eigenvalue λ_i and $Sv_i^r = \lambda_i v_i^r$, due to Equation 2.3. Once we calculated the right eigenvectors, we can determine the left eigenvectors by the orthogonality condition

$$\left(v_j^l\right)^T v_i^r = \delta_{ij}, \quad (2.4)$$

where δ_{ij} is the Kronecker delta.

As a consequence, the matrix C_0 can be expressed uniquely in terms of the basis of eigenvectors. This is described by

$$C_0 = \sum_{i \in I} v_i^r a_i^T, \quad (2.5)$$

where a_i , $i \in I$, are the corresponding n -dimensional coefficient vectors. Applying an arbitrary left eigenvector v_j^l to control vertex matrix C_0 will result in

$$\left(v_j^l\right)^T C_0 = \left(v_j^l\right)^T \sum_{i \in I} v_i^r a_i^T = \sum_{i \in I} \left(v_j^l\right)^T v_i^r a_i^T = a_j^T,$$

due to Relation 2.4. Further, applying the subdivision matrix S to C_0 will lead to the sum

$$S^k C_0 = \sum_{i \in I} \lambda_i^k v_i^r a_i^T.$$

Considering the limit configuration for $k \rightarrow \infty$, we have

$$S^\infty C_0^K = \lim_{k \rightarrow \infty} S^k C_0.$$

A subdivision algorithm converges, if $\lambda_0 = 1 > \lambda_1$, i.e. λ_0 is a strictly dominant eigenvalue, in the sense that all other eigenvalues are smaller than 1. For the proof, we refer to [Reif, 1995]. Additionally, we assume that a scheme is affine invariant. Therefore, the subdivision matrix S is stochastic, i.e. the rows of the subdivision matrix S sum to one. Thus, the eigenvector v_0^r associated with the eigenvalue $\lambda_0 = 1$ is the m -dimensional vector $v_0^r = (1, 1, \dots, 1)^T$.

Theorem 2.14. *Given a control subgrid C_0^K with a prescribed central vertex v_c , where C_0 is the corresponding control vertex matrix. Let S be the associated non-defective subdivision matrix, such that the eigenvalues λ_i , $i = 0, \dots, m - 1$, fulfil $\lambda_0 = 1 > \lambda_1 \geq \dots$. That is, λ_0 is the dominant eigenvalue. Additionally, we assume that the subdivision scheme defined through S converges. The limit position of the vertex v_c is given by*

$$c_\infty = C_0^T v_0^l = a_0. \quad (2.6)$$

This follows from the fact that all other eigenvalues raised to a higher order become negligible. Considering the above mentioned approaches, the proof is straightforward.

Proof. Let $\{v_i^r\}$ be an orthogonal basis given by the right eigenvectors of the subdivision matrix S . The vertex position matrix C_0 can be expressed as a combination of these eigenvectors v_i^r of the form $C_0 = \sum_{i=0}^{m-1} v_i^r a_i^T$. Thus,

$$C_k = S^k C_0 = \sum_i \lambda_i^k v_i^r a_i^T.$$

If $\lambda_0 = 1$ is the strictly dominant eigenvalue of S , then the transition $k \rightarrow \infty$ is of the form

$$C_\infty = \lim_{k \rightarrow \infty} S^k C_0 = \lim_{k \rightarrow \infty} \sum_i \lambda_i^k v_i^r a_i^T = v_0^r a_0^T$$

Assume S is a stochastic matrix with $v_0^r = (1, 1, \dots, 1)^T$, where the left eigenvectors v_i^l are given as in Equation 2.4. On the other hand, from applying v_0^l to the transition $k \rightarrow \infty$ follows

$$(v_0^l)^T C_0 = (v_0^l)^T v_0^r a_0^T = a_0^T,$$

see Equation 2.5. Transposing the last result provides the assumption. \square

We assume the scheme is a standard subdivision scheme.

Definition 2.15 (Standard subdivision scheme). A *standard subdivision scheme* is defined by a convergent and stationary subdivision. For every valence ν , the distinct and ordered by non-increasing magnitude eigenvalues λ_i of the subdivision matrix S are given according to the following:

- the dominant eigenvalue $\lambda_0 = 1$,
- there are two equal second largest eigenvalues λ_1 and λ_2 , i.e. $\lambda = \lambda_1 = \lambda_2$
- the other eigenvalues, λ_i for $i > 2$, are of magnitude strictly less than λ .

The double eigenvalue λ is called the subdominant eigenvalue of S .

The definition is taken from Peters and Reif [2008]. Assume, λ is real and positive, and the geometric and algebraic multiplicity of λ is equal 2. Consequently, the two eigenvectors v_1^l and v_2^l associated with λ are linearly independent eigenvectors of S . Moreover, the vectors

$$t_1 = v_1^l C_0 \quad \text{and} \quad t_2 = v_2^l C_0 \tag{2.7}$$

describes the tangent plane of the limit surface at the point c_∞ . The unit normal vector of c_∞ can be defined by

$$n_\infty = \frac{t_1 \times t_2}{|t_1 \times t_2|}. \tag{2.8}$$

The properties of the subdominant eigenvalue λ of S are shown in the work of Reif [Reif, 1995]. For example, the structure of S encodes the C^1 -smoothness of the subdivision surface in the neighbourhood of the vertex c_∞ .

Summarizing the above, we consider the following aspect: the position and the normal of the limit surface can be expressed explicitly in terms of the vertices of the control mesh. On the other hand, even if the limit position and the tangent plane in each control point is given, the surface might still not be unique in the singularities. The limit surface is therefore not single-sheeted if the subdivision matrix does not fulfils the prescribed conditions. Hence, a thorough analysis of the convergence and smoothness in the neighbourhood of the irregular vertex have to be executed. We do not want to delve into detail, important references on this topic are [Zorin,

1998; Peters and Reif, 2008]. In the next section, we address the problem of single-sheetedness to the exact choice of the parametric domain.

2.3.4 Characteristic map

Given a standard stationary subdivision scheme, we consider the following definition:

Definition 2.16 (Characteristic map). Considering an element f in the control grid \mathcal{C}_k , let \mathcal{C}_f be the maximal basis subgrid of f and $\{b_i^f\}_{i \in I_k^f}$ be the corresponding generating spline. Let v_c be the central vertex of \mathcal{C}_f and c_∞ its limit position. Given the corresponding subdivision matrix S , let $\{\lambda_i\}_{i \in I_k^f}$ be the ordered set of nonincreasing eigenvalues λ_i of S with the corresponding set of eigenvectors $\{v_i\}_{i \in I_k^f}$. The continuous map

$$\begin{aligned} \chi : \Omega &\rightarrow \mathbb{R}^2 \\ \chi(u, v) &:= V_\lambda^T b^f, \end{aligned}$$

is called the *characteristic map*. Thereby, b^f is a vector with the basis functions b_i^f as entries. The matrix $V_\lambda = (v_1, v_2)$ is called the subdominant matrix. The columns v_i , $i = 1, 2$, of V_λ are given by the two eigenvectors of S corresponding to the subdominant eigenvalue λ . The map χ is regular, if the Jacobian determinant of χ is unequal zero for all $(u, v) \in \Omega$.

The characteristic map is a smooth mapping from the compact domain Ω to \mathbb{R}^2 , that depends only on the structure of the algorithm and not on the control grid data. It can be seen as the limit surface of a control grid in \mathbb{R}^2 , where its vertices are described by the rows of the matrix V_λ . The important components of the characteristic map are the two eigenvectors v_i , $i = 1, 2$. These determine the local structure of the limit surface in the neighbourhood of the limit surface in the neighbourhood of the vertex c_∞ , see Equation 2.7. In [Reif, 1995], the characteristic map has been introduced for the analysis of the smoothness of subdivision schemes at extraordinary vertices. The existence of the characteristic map is proven using its injectivity, see [Peters and Reif, 1997].

A subdivision scheme generates surfaces that are locally manifolds close to the extraordinary vertices, if its characteristic map χ is regular, to be more precise χ is bijective everywhere. If this is the case, then the inverse map χ^{-1} exists everywhere. Moreover, the reversibility of the characteristic map guarantees single sheetedness and C^1 -continuity of the surface, see [Andersson and Stewart, 2010]. The reparametrization of the subdivision surface by means of the characteristic map provide a functional form for the parametric description of the surface. For a more precise analysis of the characteristic map, we refer to [Schweitzer, 1996; Zorin, 1998].

The following corollary shows that the eigenvectors of the subdivision matrix S can be extended to a larger portion of the mesh surrounding the extraordinary vertex. Let \bar{S} be the enlarged subdivision matrix corresponding to an extension of the maximal submesh \mathcal{C}_f . The following relation between the non-zero eigenvalues of S and \bar{S} can be established

Corollary 2.17. *Let λ be the eigenvalue associated with the subdominant matrix V_λ . Applying the enlarged subdivision matrix \bar{S} to V_λ is equal to*

$$\bar{S}V_\lambda = \lambda\bar{V}_\lambda,$$

where \bar{V}_λ is an extension of the eigenvectors of V_λ to the larger portion of the grid.

Proof. For any enlarged grid K' of the grid K surrounding the extraordinary vertex, we can decompose the control grid $\mathcal{C}^{K'}$ into \mathcal{C}^K and $\mathcal{C}^{K'} \setminus \mathcal{C}^K$. The matrix \bar{S} is an extension of the subdi-

vision matrix S to the larger portion of the grid \mathcal{C}^K given by $\mathcal{C}^{\bar{K}} \setminus \mathcal{C}^K$. Due to the decomposition of the control grid, the matrix \bar{S} has the following block structure:

$$\bar{S} = \begin{pmatrix} S & 0 \\ * & * \end{pmatrix},$$

where $*$ corresponds to the $\mathcal{C}^{\bar{K}} \setminus \mathcal{C}^K$ portion of the grid. Note, an eigenvector of S can be given by restricting eigenvalues of matrix \bar{S} to the smaller grid. Is λ the subdominant eigenvalue related to matrix V_λ of S , then the columns of V_λ are part of the appropriate column of the matrix \bar{V}_λ . Therefore, multiplying by the factor $1/\lambda$ will lead to the matrix \bar{V}_λ . \square

In short, the eigenvectors can be enlarged to a larger portion of the grid and have an self-similar structure with respect to the associated subdivision matrix. The matrix S described in Definition 2.16 is the smallest subdivision matrix that allows to determine the characteristic map. Thus, there exists a smallest subdivision matrix to determine the eigenstructure of all larger subdivision matrices \bar{S} . For more details, see [Arden, 2001].

CHAPTER 3

GENERALIZED B-SPLINES OF CATMULL-CLARK TYPE

As described in the previous chapter, there are many different subdivision schemes, each with its own valuable advantages. A homogeneous mesh construction or reasonable limit surface properties describe only some possible examples. In this work, we focus on the Catmull-Clark subdivision surfaces. As provided by subdivision, it is used to produce smooth surfaces from coarse control grids enabling an arbitrary topology. Additional to the inherited subdivision properties, the Catmull-Clark scheme indicates some scheme specific characteristics. For example, they allow for a compact geometry encoding, have a quad structure good for texturing, and specific surface qualities. Moreover, they are widely utilized in areas such as geometry processing, computer graphics, animation and nowadays also in engineering. At each stage of the process, a finer quadrangular mesh is generated from the previous one. Using the classical refinement idea, the limit surface of a given control grid is C^2 -continuous everywhere except at the singularities [Reif, 1995]. It is proven in [Reif and Schröder, 2001] that the limit surface is $C^1 \cup H^2$ -continuous at singularities.

Using Stam's parameterization method [Stam, 1998], we can directly parameterize the limit surface without explicitly applying the time consuming refinement process to the control grid. At the limit of the extraordinary vertices, this so-called natural parameterization shows a behaviour that is undesirable for the prescribed high quality surface. This means, the surface quality is not any more consistent with the quality given by the classical approach, i.e. the C^1 -continuity of the surface at singularities related to the extraordinary vertices has got lost. In order to remedy this, we consider a parameterization that preserves the continuity. It is based on the characteristic map. Using this map, the characteristic parameterization is defined by a reparameterization of the natural representation onto the characteristic domain, the image of the characteristic map. Due

to the complexity of this framework, the computational effort to evaluate the surface becomes very high.

This chapter serves as an introduction into the concept of Catmull–Clark subdivision surfaces. We consider both approaches, the repetitive operations on control grids and the limit surface parameterization with piecewise B-spline functions. We start with the Catmull–Clark subdivision concept concerning the rules to generate finer quadrangular control grids. Based on [Stam, 1998], the natural parameterization of Catmull–Clark subdivision surfaces is discussed. We review the evaluation procedure and describe the so-called natural generating spline that allow for an elementwise evaluation of the limit surface. Because of the lack of smoothness, the closely linked characteristic parameterization is presented. We discuss the characteristic map in the context of Catmull–Clark surfaces. At this point, we introduce the corresponding elementwise parameterization called the characteristic generating splines, and discuss its properties.

3.1 Introduction to Catmull–Clark subdivision scheme

The Catmull–Clark subdivision scheme has been introduced in 1978 by Edwin Catmull and James H. Clark [Catmull and Clark, 1978]. The scheme describes a generalization of the refinement of uniform bicubic B-spline surfaces to meshes of arbitrary topology. Given an initial control grid, after one level of subdivision we obtain a fully quadrangular grid. Performing the corresponding operations iteratively, a set of increasingly finer quadrangular meshes is produced that converges to the smooth Catmull–Clark limit surface. In the following, we review the rules of the scheme describing one level of subdivision and, consequently, the whole process. In Figure 3.1, a schematic illustration of some stages of the subdivision process are shown.

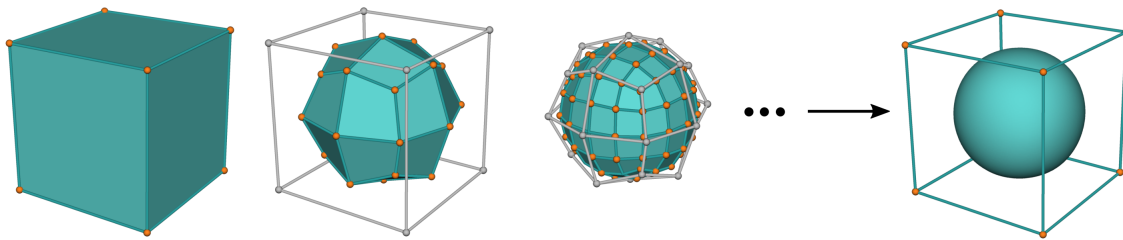


Figure 3.1: *Subdivision process. A schematic illustration of the process is shown by some of the intermediate stages: the initial control grid, the grid in the first and the second subdivision stage enclosed by the grid of the previous stage (grey scaffold), and the corresponding limit surface enclosed by the initial grid are illustrated. The limit surface is equal to the image of the subdivision surface function related to the initial control grid.*

3.1.1 Subdivision rules

As known from the previous chapter, the subdivision process is an iterative process such that at each level some specified operations are applied to the control grid. Starting with the initial control grid $\mathcal{C}_0 = \{K_0, \mathbf{c}^0\}$, at each stage of the subdivision process we obtain a refined quad grid $\mathcal{C}_k = \{K_k, \mathbf{c}^k\}$, $k \in \mathbb{N}$, by introducing new vertices and connecting them appropriately. Considering the Catmull–Clark scheme, three types of new vertices are generated:

- *face points*: newly added vertices to the mesh \mathcal{C}_k that corresponds to the faces of the mesh \mathcal{C}_{k-1} . The position of these vertices is given as the average of the vertices of the according face.
- *edge points*: newly added vertices to the mesh \mathcal{C}_k that corresponds to the midpoints of the edges in \mathcal{C}_{k-1} . The position of an edge point can be calculated as the average of the center point of the considered edge and the new face points of the faces containing this edge.

- *vertex points*: newly added points to the mesh \mathcal{C}_k that can be seen as the repositioned versions of the vertices in \mathcal{C}_{k-1} . The new position of a vertex point is equal to a linear combination of the positions of the adjacent faces, the midpoints of the adjacent edges, and the position of the particular vertex in the mesh \mathcal{C}_{k-1} . This is described by the formula:

$$c_{\bar{v}} = \frac{c_f}{n} + \frac{2c_e}{n} + \frac{(n-3)c_v}{n}$$

where $c_{\bar{v}}$ and c_v are the new and old vertex position, respectively, of the vertex point. Let ν describes the valence of the vertex c_v . The average of the ν new faces is denoted by c_f , c_e is the average of the midpoints of the adjacent edges to vertex c_v .

Now, the new control grid is generated by connecting the vertices in the following manner: each face point and all adjacent edge points, as well as each vertex point and all adjacent edge points are connected by an edge. The new elements are defined by surfaces within the connected edges. The subdivision rules can be illustrated using subdivision masks. The masks related to the element, edge and vertex points of a regular quad grid are the same as for bicubic B-splines. Additionally, there are masks for extraordinary vertices, nonquadrilateral elements and edges between nonquadrilateral elements. The standard masks are shown in Figure 2.6.

The Catmull–Clark scheme describes a primal subdivision. According to this, the refinement can be seen as a splitting of the elements of the grid \mathcal{C}_{k-1} . The splitting of the element is given by a " $1 \rightarrow |e[f]|$ " rule. That means, the element f is divided into $|e[f]|$ new elements, where $|e[f]|$ is the number of edges of f .

After the first subdivision step, an arbitrary control grid is subdivided into a fully quadrilateral grid. Two steps are all that are needed in order to isolate the extraordinary vertices of a grid. This means, each irregular element will contain exactly one extraordinary vertex. With each following step, no new extraordinary vertices will be added into the control grid, only ordinary vertices and regular elements will newly appear. The total amount of the irregular elements is constant after the first step, but the ratio of the total number of irregular to the total number of regular elements decreases. Four stages of the subdivision process of an arbitrary control grid are shown in Figure 3.2.

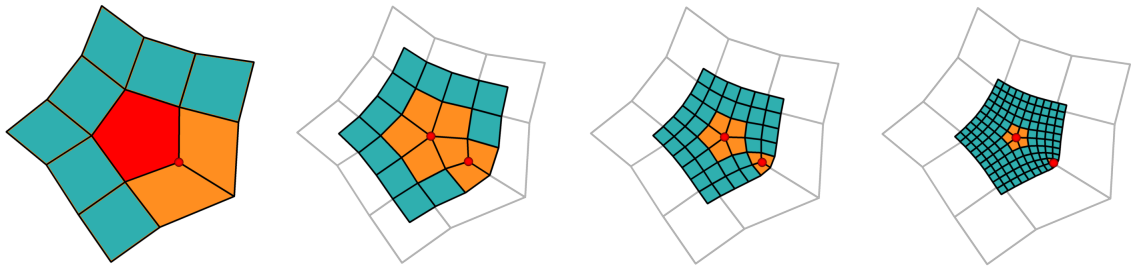


Figure 3.2: *Isolation of extraordinary vertices. The initial control grid and its first three subdivision stages. The initial control grid with boundary is containing a nonquadrilateral element (red element) and an extraordinary vertex (red vertex). The irregular quadrilateral elements are coloured orange, the regular elements are coloured blue. The grey grid is illustrating the initial grid. A reduction of the boundary elements is obtained.*

Within the classical subdivision theory, the generation of edge and vertex points on the boundary has not been defined. Considering a control grid with boundary, we calculate all possible to determine vertices. Consequently, the boundary elements shrinks with each following step in the subdivision process. Moreover, in the limit, the subdivision surface does not exist on boundary elements. An example of a shrinking control grid with boundary is shown in Figure 3.2.

For a given control grid, using the Catmull–Clark subdivision process the series of subsequent grids converges to a smooth limit surface. Thus, the resulting surface approximates the emerging

control grids. Nevertheless, the concept permits to adapt the control grid during the subdivision process to the individual requirements of the designer. This means, the limit surface will be also adjusted to the shape of the new control grid. The altered control grid is therefore seen as a new initial grid. However, the modified and unmodified control grids are based on the same initial configuration where the modification is described by a linear operation on the control grid. It may be that the limit surfaces of both grids are different, but the shape space of both is consequently the same. This flexibility makes subdivision surfaces particularly interesting for applications where operations in the shape space are regarded.

In Section 2.3.3, a method to calculate the limit surface according the control grid vertices have been reviewed. Therefore, to determine the limit position of a control grid vertex, an appropriate subgrid \mathcal{C}_k^K of the control grid \mathcal{C}_k is taken into account. For the Catmull–Clark scheme, the valuable subgrid \mathcal{C}_k^K for this operation is described by the one-neighbourhood of the vertex of which we want to calculate the limit position. The eigenstructure of the corresponding local subdivision matrix S has to be calculated. The limit position of the vertex is defined by the dominant eigenvalue and the corresponding eigenvector of S applied to the associated control vertex matrix C_k . The same holds for the tangent vectors of the control vertex.

At this point, we are interested in the subdivision surface of the Catmull–Clark scheme. For each vertex of the control grid \mathcal{C}_k , we obtain a subdivision basis function. The non-zero support of one function corresponds to the two-neighbourhood of the associated control vertex. The generating spline is described by the non-zero parts of the subdivision basis functions corresponding to an element of \mathcal{C}_k . This allows to parameterize the limit surface piece by piece over each element in the control grid, see Section 2.3.2. As aforementioned, the Catmull–Clark subdivision describes the generalization of the refinement of uniform bicubic B-splines. Due to the subdivision rules, the maximal subgrid of an element is given by its one-ring, see Definition 2.12. Using the one-ring, we distinguish between regular and irregular elements, see Figure 3.3. Therefore, for a regular element, i.e. all vertices of the element have valence 4, the one-ring is given by a 3×3 quad grid described by 16 vertices. The generating spline is defined by the 16 appropriate bicubic B-spline basis function patches. If the element is irregular, i.e. at least one of the vertices is an extraordinary vertex, the number of entities describing the one-ring depends on the irregularity. Consequently, the generating spline is not that simple any more. A closer look at the subdivision process shows that in each subdivision stage the irregular element is being replaced by one irregular element and three regular elements. This results in the partition of the irregular element in series of regular elements that can be represented piece by piece by bicubic B-spline patches except the extraordinary vertex. Thus, the generating spline is formed by an infinite decomposition into regular elements and the limit of the extraordinary vertex. The resulting functions are prescribed to be a piecewise bicubic B-spline. The limit surface can be obtained by a brute force repeated subdivision of the element. The given procedure has been proven to be valuable and sufficient in the area of computer graphics. Therefore, the Catmull–Clark limit surface is a C^2 -continuous surface except at finitely many extraordinary vertices, where it is at least C^1 -continuous. The smoothness of the Catmull–Clark limit surface has been proven in [Peters and Reif, 1998].

3.2 Natural parametrization of the limit surface

So far, we have an idea of how we can calculate the limit surface element by element using the generating spline. We distinguish between the regular and the irregular element of the control grid. Consequently, the limit surface is established by bicubic and piecewise bicubic B-spline surface patches, respectively. To avoid the time consuming subdivision process, a parameterization of the surface patches can be determined, because of the properties of the underlying surface. A

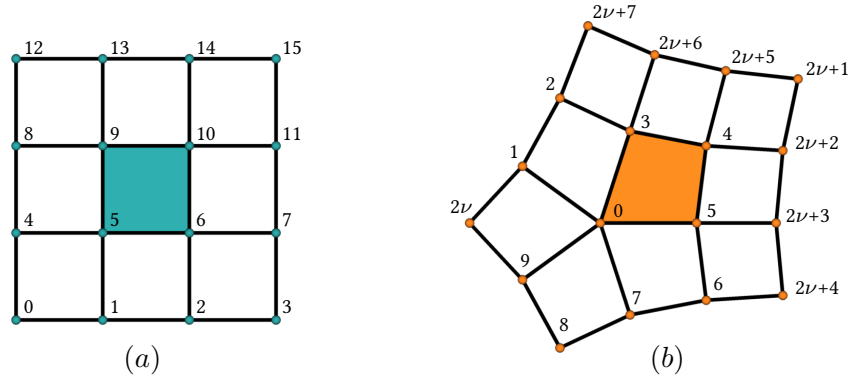


Figure 3.3: *Elements one-rings. The one-rings of (a) a regular element and (b) an irregular element with an extraordinary vertex of valence five are shown. Additionally, the orders of the vertices in the one-rings are shown.*

stable and efficient scheme for the evaluation of the Catmull–Clark limit surface has been presented in Stam [1998]. Therefore, the limit surface can be exactly determined at any point on the surface without explicitly subdividing the considered control grid.

In this section we review Stam’s algorithm that will be used for the elementwise representation of the Catmull–Clark limit surface. To use Stam’s algorithm, one essential requirement has to be fulfilled: the control grid has to be a fully quadrilateral grid with isolated extraordinary vertices. This means, each irregular element has to contain at most one extraordinary vertex. For any arbitrary grid, this is easily satisfied by subdividing the grid at most twice. However, the theory can be easily extended to any desired control element avoiding the refinement. From the parametric description of the generating spline, we determine a suitable parameterization of the subdivision surface functions called here the generalized B-spline basis functions of Catmull–Clark type. The following notation has been inherited from [Stam, 1998] and adjusted to our requirements.

3.2.1 Regular surface patch

Given an arbitrary control grid \mathcal{C} , consider a regular element with its one-ring, see Figure 3.3 (a). The limit surface of a regular element is parametrized by uniform bi-cubic B-spline functions. We assemble the control vertex matrix

$$C^T = (c_0, \dots, c_{15})$$

where the columns c_i , $i = 0, \dots, 15$, are given by the position vectors of the sixteen vertices in the one-ring. The order of the vertices is equivalent to the order shown in Figure 3.3 (a). The generating spline of a regular element is defined by

Definition 3.1 (Regular generating spline). Let $b(u, v)$ be the vector where the entries are given by the 16 bi-cubic B-spline basis functions b_i . The basis functions $b_i : [0, 1]^2 \rightarrow \mathbb{R}$ are defined by the formula

$$b_i(u, v) := n_{i \% 4}(u) n_{i/4}(v), \quad i = 0, \dots, 15, \quad (3.1)$$

where “%” and “/” represents the remainder and the division operation, respectively. The func-

tions $n_j(t)$, with $t \in [0, 1]$, denote the four cubic basis polynomials:

$$\begin{aligned} n_0(t) &:= \frac{1}{6} (1-t)^3 \\ n_1(t) &:= \frac{1}{6} (4-6t^2+3t^3) \\ n_2(t) &:= \frac{1}{6} (1+3t+3t^2-3t^3) \\ n_3(t) &:= \frac{1}{6} t^3. \end{aligned} \tag{3.2}$$

We call b the *generating B-spline* or the *regular generating spline* of the element.

The cubic B-spline functions n_i , $i = 0, \dots, 3$, have the following properties:

- pointwise nonnegativity over the entire domain: $n_i(t) \geq 0$ for all $t \in [0, 1]$,
- strong convex hull property,
- compact local support: $n_i(t) = 0$ falls $t \notin (0, 1)$,
- partition of unity: $\sum_{j=0}^3 n_j(t) = 1$ for all $t \in [0, 1]$,
- C^2 -continuity.

The properties are inherited directly by the tensor product functions b_i . The functions n_i can be written as a linear combination of dilated and translated copies of itself. This principle has been used for the definition of the subdivision rules. Additionally, considering a control grid with only regular elements, the generating splines of the control grid elements are dilated and shifted copies of itself.

The parametrization of the limit surface patch is defined by the linear combination of the basis functions $b_i(u, v)$ weighted by the control vertices c_i . This is given by the sum:

$$s(u, v) = \sum_{i=0}^{15} c_i b_i(u, v).$$

The equation can be rewritten into the product of the control vertex matrix C and the generating spline b , i.e.

$$s(u, v) = C^T b(u, v), \quad (u, v) \in [0, 1]^2.$$

The partial derivatives of the surface parameterization are obtained by the partial derivatives of the bicubic B-splines. For example, we consider the partial derivative with respect to the first variable u . The partial derivative of the surface is given by

$$\frac{\partial}{\partial u} s(u, v) = C^T \frac{\partial}{\partial u} b(u, v)$$

where the derivative of the vector $b(u, v)$ has to be derived componentwise, i.e. for each entry we have

$$\frac{\partial}{\partial u} (b_i(u, v)) = n'_{i\%4}(u) n_{i/4}(v), \quad i = 0, \dots, 15.$$

This means, the derivatives of the bicubic functions are described by the derivatives of the relevant cubic basis functions $n'_j(\cdot)$, $j = 0, \dots, 3$. The same applies to the second variable, respectively.

3.2.2 Irregular surface patch

Given an arbitrary control grid \mathcal{C}_0 , consider an irregular element and its one-ring, see Figure 3.3 (b). Let ν be the valence of the extraordinary vertex characterizing this element. The one-ring is given by the subgrid \mathcal{C}_0^K , where K is the corresponding combinatorial grid. There are $2\nu + 8$ vertices in K . We assemble the control vertex matrix

$$C_0^T = (c_0^0, \dots, c_{2\nu+7}^0),$$

with the entries $c_i^0, i = 0, \dots, 2\nu + 7$ given by the positions of the vertices in the prescribed order shown in Figure 3.3 (b). Actually, the order does not matter, but the given order simplifies the handling of the neighbourhood of the extraordinary vertex with different valences. The index n of the matrix C_n is used as the indicator for the level of subdivision.

Considering the subdivision process, with each step of subdivision the irregular element is replaced by an increasing number of regular elements. Therefore, it can be described by a piecewise bicubic B-spline everywhere except at the extraordinary vertex. To determine the parameterization, we first take a look at the first stage of subdivision of the one-ring. Here, the one-ring is needed to determine the subdivision of the entire irregular element, see Figure 3.5 (c). On the other hand, the one-ring is the maximal basis subgrid of the element. Furthermore, the subdivision is performed in two manners. One manner is to obtain a local subdivision with the extraordinary vertex being the central vertex, see Section 2.3.3. This provides a control grid \mathcal{C}_1^K that is a scaled copy of the initial grid \mathcal{C}_0^K , i.e. the grid \mathcal{C}_1^K is given by the irregular element and its one-ring. A second manner is to subdivide the grid \mathcal{C}_0^K globally to obtain the larger grid \mathcal{C}_1^{K*} . The grid \mathcal{C}_1^{K*} is an enlarged version of the grid \mathcal{C}_1^K , i.e. the combinatorial mesh K_* is given by the mesh K and an additional array of elements, see Figure 3.5. The grid \mathcal{C}_1^{K*} consists of $m = 2\nu + 17$ vertices. Moreover, from the mesh K_* we recognise that the irregular element has been subdivided in one irregular and three regular elements. Additionally, we can determine the one-rings of all four subelements. The two subdivision manners are shown in Figure 3.5. The order of the vertices in the enlarged grid K_* is shown in Figure 3.4.

The limit surface of the three regular subelements can be parametrized via the regular generating spline as described in Section 3.2.1. For this purpose, we assemble the control vertex

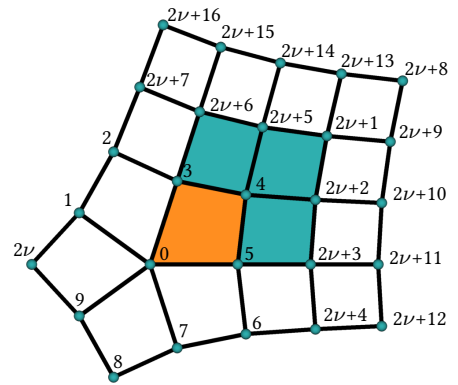


Figure 3.4: *Global one-ring subdivision. The order of vertices after one global subdivision of an irregular element. The resulting irregular and regular subelements are coloured orange and blue, respectively.*

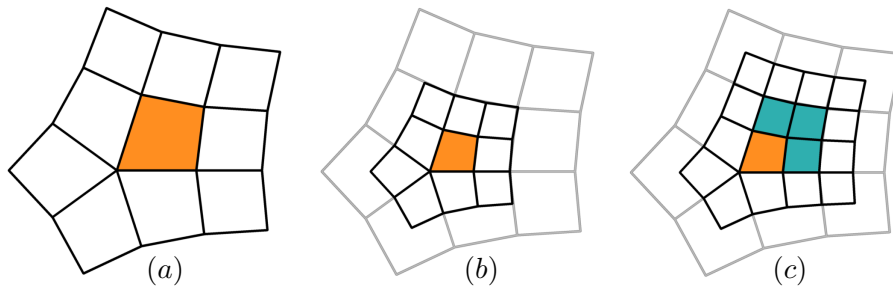


Figure 3.5: *Subdivision manners. We illustrate (a) the one-ring of an irregular element (orange), (b) the local subdivision and (c) the global subdivision of the one-ring of an irregular element. The regular subelements are coloured blue.*

matrices of the two subgrids related to the corresponding subdivision manner

$$C_1^T = (c_0^1, \dots, c_{2\nu+7}^1) \quad \text{and} \quad \bar{C}_1^T = (C_1^T, c_{2\nu+8}^1, \dots, c_{m-1}^1),$$

where C_1 corresponds to the grid \mathcal{C}_1^K and \bar{C}_1 to the enlarged grid \mathcal{C}_1^{K*} . The entries c_i^1 , $i = 0, \dots, m-1$, are the position vectors of the corresponding vertices in the subgrids. Based on the subdivision concept, the positions of the vertices in the subgrids \mathcal{C}_1^K and \mathcal{C}_1^{K*} are given by the linear combination of the vertex positions of the grid \mathcal{C}_0^K . We consider the two subdivision equations: For the local subdivision we write

$$C_1 = AC_0,$$

with the quadratic subdivision matrix A , whereas the larger control grid is given by

$$\bar{C}_1 = \bar{A}C_0,$$

where \bar{A} denotes the enlarged subdivision matrix. Both matrices are determined by the relevant subdivision weights characterized by the subdivision masks. Due to the order of the vertices, A has the following block structure:

$$A = \begin{pmatrix} S & 0 \\ S_{00} & S_{01} \end{pmatrix}, \quad (3.3)$$

where S is an $(2\nu+1) \times (2\nu+1)$ -matrix determined by the one-neighbourhood of the irregular vertex. The matrix S is nondefective for all valences ν , i.e. S has $2\nu+1$ linear independent eigenvectors. Additionally, S has a single dominant eigenvalue equal one, and consequently fulfils the necessary and sufficient convergence condition. This is, at the extraordinary vertex, the set of step-by-step subdivided control grids converges to a single point. We assume that the corresponding eigenvector is a vector of ones, i.e. with a one in every entry. Thus, the entries of every row of S sum up to one. The matrices S_{00} and S_{01} are defined by the subdivision weights for the remaining vertices. A schematic definition of matrices S , S_{00} and S_{01} is given in Appendix 7.

For the enlarged matrix \bar{A} the following block structure is obtained:

$$\bar{A} = \begin{pmatrix} & A & \\ S_{10} & S_{11} & \end{pmatrix} = \begin{pmatrix} S & 0 \\ S_{00} & S_{01} \\ S_{10} & S_{11} \end{pmatrix}.$$

The blocks S_{10} and S_{11} correspond to the array of additional vertices in \mathcal{C}_1^{K*} . For the assembling of the matrices, see Appendix 7. Furthermore, the Catmull–Clark subdivision is stationary. We can easily determine the positions of the vertices in any level of subdivision. In accordance with the two resulting subgrids, the n th subdivision stage can be obtained by the following two formulas:

$$C_n = AC_{n-1} = A^n C_0 \quad \text{and} \quad \bar{C}_n = \bar{A}C_{n-1} = \bar{A}A^{n-1}C_0, \quad n \geq 1.$$

Consequently, with each step of subdivision the irregular element shrinks more and more.

To parameterize the three regular elements in the following subgrids, we have to select the relevant one-rings, see Figure 3.6. The order of the vertices has to be adjusted in accordance with the order of the vertices in the one-ring of a regular element. For this purpose, we define three picking matrices P_k , $k = 1, 2, 3$. These are given as follows: in each row of matrix P_k every

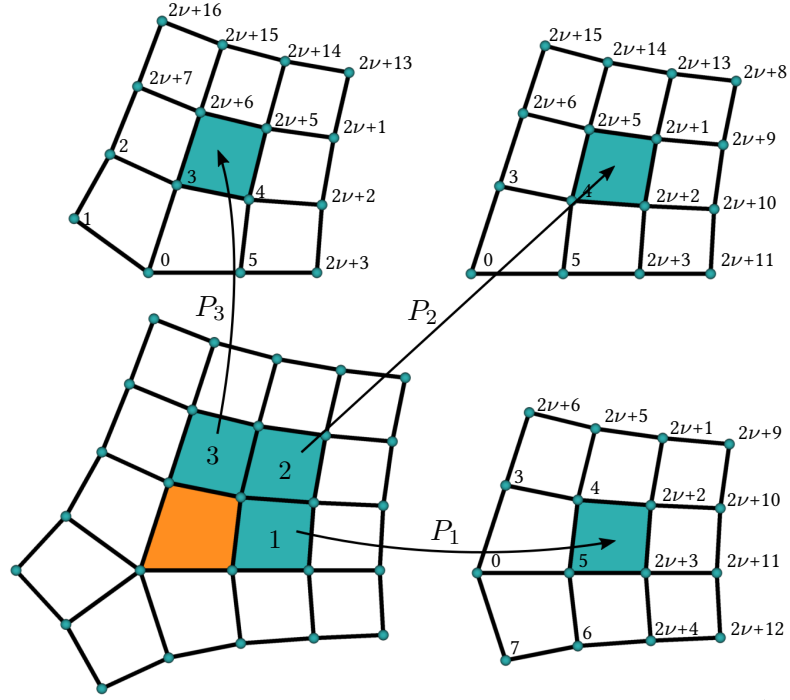


Figure 3.6: Picking of regular subelements. The order of the vertices in the one-ring of a regular subelement before renumbering these for the calculation of the three bicubic B-spline patches in the submesh C_n^{K*} .

entry is zero except for the ones in the rows corresponding to the indices in the k th one-ring of subelement shown in Figure 3.6. If m is an index of the k th subelement, for $m = 0, \dots, 2\nu + 16$, then in the m th row a one is located in the column corresponding to the index of the vertex in accordance with the order shown in Figure 3.3 (a). In Figure 3.6, the indices of the one-ring vertices of the three sub-elements are shown. Finally, the vertices of the k th subelement in the n th subdivision level are obtained by

$$P_k \bar{C}_n = S_{k,n} C_0,$$

where $S_{k,n} = P_k \bar{A} A^{n-1}$ describes the subdivision matrix providing the positions of the appropriate vertices from the initial grid C_0 .

The parameterization of the limit surface patch of the k th subelement in the n th subdivision level is defined by the product of the positions of the control vertices selected by $P_k \bar{C}_n$, and the regular generating spline, i.e.

$$s_{k,n}(u, v) = C_0^T S_{k,n}^T b(u, v), \quad (u, v) \in [0, 1]^2$$

where $n \geq 1$ denote the index of the refinement level and $k = 0, 1, 2$ is the index of the subelement in this level. Note, $s_{k,n}$ is a regular B-spline patch.

Due to the continuity of B-splines and the subdivision properties, the subdivision does not change the limit. Consequently, the parameterization of the limit surface over the irregular element is given by collecting the individual surface patches. This is given by postponing the domain of the subpatches to the relevant subdomain of the domain of the irregular element. Let $\Omega = [0, 1]^2$ be the domain of the irregular element. The given subdivision is defining a partition of the domain by means of a topological refinement, see Figure 3.7. Thus, we consider

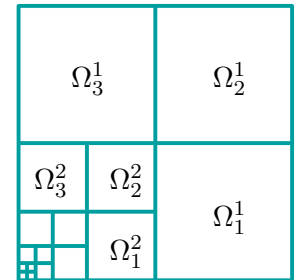


Figure 3.7: Partition of Ω into subdomains Ω_k^n .

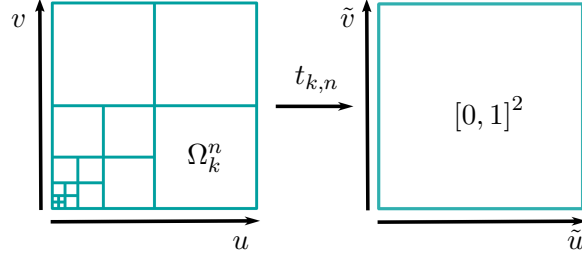


Figure 3.8: Transformation of the regular subdomains. Mapping $t_{k,n}$ represents the transformation of the subdomain $\Omega_k^n \subset \Omega$ into the B-spline domain $[0, 1]^2$.

the partition of the domain Ω into the subdomains Ω_k^n and the point $(0, 0)$ corresponding to the extraordinary vertex. In the n th subdivision level the three subdomains Ω_k^n are characterized by

$$\begin{aligned}\Omega_0^n &= \left[\frac{1}{2^n}, \frac{1}{2^{n-1}} \right] \times \left[0, \frac{1}{2^n} \right], \\ \Omega_1^n &= \left[\frac{1}{2^n}, \frac{1}{2^{n-1}} \right] \times \left[\frac{1}{2^n}, \frac{1}{2^{n-1}} \right], \\ \Omega_2^n &= \left[0, \frac{1}{2^n} \right] \times \left[\frac{1}{2^n}, \frac{1}{2^{n-1}} \right].\end{aligned}$$

The parameterization of the limit surface over the entire irregular element is given by a set of B-spline subpatches and the limit position of the extraordinary vertex, i.e.

$$s(u, v) = \begin{cases} s_{k,n} \circ t_{k,n}(u, v) & \text{for } (u, v) \in \Omega_k^n \\ s_\infty & \text{for } (u, v) = (0, 0) \end{cases},$$

where the mapping $t_{k,n}$ corresponds to the transformation of the subdomain Ω_k^n onto the unit square $[0, 1]^2$. For the n th subdivision level, the transformations are given as follows

$$\begin{aligned}t_{0,n}(u, v) &:= (2^n u - 1, 2^n v), \\ t_{1,n}(u, v) &:= (2^n u - 1, 2^n v - 1), \\ t_{2,n}(u, v) &:= (2^n u, 2^n v - 1),\end{aligned}\tag{3.4}$$

where we assume that the point $(0, 0)$ corresponds to the extraordinary vertex of the element. The limit surface of the extraordinary vertex can be calculated using the classical evaluation scheme, see Section 2.3.3. For the computation, we consider the one-neighbourhood of the extraordinary vertex and the corresponding subdivision matrix S , see Theorem 2.14.

At this point, the evaluation of the limit surface is still very expensive. For each of the subelements in the n th level $n - 1$ matrix multiplication of matrix A have to be performed. To simplify the evaluation of the matrix powers, Stam introduced a decomposition of the subdivision matrix A into its eigencomponents. We review this in the next section and give some details on it that facilitate the calculation.

3.2.3 Eigenstruktüre of the subdivision matrices

To investigate the eigenstructure of matrices, it is often inevitable to use numerical methods. Unfortunately, the decomposition is numerically unstable. To avoid this, we will firstly apply spectral techniques to find an algebraic form for the eigenstructure of the subdivision matrix A , i.e. the diagonal matrix Λ and the eigenvector matrix V are to be determined.

The subdivision matrix A is defined to be a square and nondefective matrix. The eigenstructure of A is given by the pair (Λ, V) . Therefore, the following eigenvalue problem has to be solved

$$AV = V\Lambda.$$

Due to the given order of the vertices, the matrix A is undistributed for an arbitrary valence ν of the extraordinary control vertex. Considering the block structure of A , the explicit representation of the eigenstructure can be derived piece by piece. Therefore, we obtain the diagonal matrix Λ to be of the following form:

$$\Lambda = \begin{pmatrix} \Sigma & 0 \\ 0 & \Delta \end{pmatrix},$$

where the diagonals of Σ and Δ are given by the eigenvalues of the matrices S and S_{01} , respectively. Moreover, it can be shown that the eigenvector matrix V has the form

$$V = \begin{pmatrix} U_0 & 0 \\ U_1 & W_1 \end{pmatrix}.$$

Consequently, the eigenstructures of S and S_{01} are described by the pairs (Σ, U_0) and (Δ, W_1) , respectively. The analytical calculation of these two structures is given in detail [Stam, 1998]. To calculate the block U_1 of the eigenvector matrix V that is determined by the equality $AV = V\Lambda$, i.e.

$$\begin{pmatrix} SU_0 & 0 \\ S_{00}U_0 + S_{01}U_1 & S_{01}W_1 \end{pmatrix} = \begin{pmatrix} U_0\Sigma & 0 \\ U_1\Sigma & W_1\Delta \end{pmatrix}$$

we consider the following equality to be solved

$$S_{00}U_0 + S_{01}U_1 = U_1\Sigma$$

with the unknown matrix U_1 . Using the eigenstructure of S_{01} , to find U_1 means to solve $2\nu + 1$ linear systems

$$\begin{pmatrix} \sigma_i - \delta_0 & & 0 \\ & \ddots & \\ 0 & & \sigma_i - \delta_6 \end{pmatrix} [U_1^*]_{.,i} = [W_1^{-1}S_{00}U_0]_{.,i},$$

where $U_1^* = W_1^{-1}U_1$. The entries σ_i and δ_j are the entries of the diagonal matrices Σ and Δ , respectively, for $i = 0, \dots, 2\nu$ and $j = 0, \dots, 6$. The term $[\cdot]_{.,l}$ denote the restriction to the l th column of the considered matrix.

The matrix V is invertible. Based on the block structure, the inverse of V has the following representation

$$V^{-1} = \begin{pmatrix} U_0^{-1} & 0 \\ -W_1^{-1}U_1U_0^{-1} & W_1^{-1} \end{pmatrix},$$

where the inverse matrices of U_0 and W_1 can be explicitly specified, see Appendix.

3.2.4 Natural parametrization

We consider the diagonalized representation of the subdivision matrix A . This is given by the formula

$$A = V\Lambda V^{-1}$$

with the individual components Λ and V as stated above. The control points in the n th refinement level can be calculated as follows

$$\bar{C}_n = \bar{A}A^{n-1}C_0 = \bar{A}V\Lambda^{n-1}V^{-1}C_0$$

with the important simplification of the computation of the control vertices in the n th subdivision level. This is, we just need to exponentiate separately the entries of the diagonal matrix Λ . Consequently, the given representation will speed up the calculation.

The parameterization of the limit surface of a regular subpatch is described by

$$s_{k,n}(u, v) = C_0^T S_{k,n}^T b(u, v), \quad (u, v) \in [0, 1]^2$$

where the matrix

$$S_{k,n} = P_k S_n \tag{3.5}$$

is the subdivision matrix that localizes the k th subpatch in the n th subdivision level. The matrix $S_n = \bar{A}V\Lambda^{n-1}V^{-1}$ is the product of the two subdivision matrices A and \bar{A} . Using the transformation from the individual patches to the domain of the irregular element, we obtain the following definition

Definition 3.2 (Natural parameterization). The *natural parameterization* $s : \Omega \rightarrow \mathbb{R}^3$ of the limit surface patch of an irregular element is given by

$$s(u, v) = \begin{cases} s_{k,n} \circ t_{k,n}(u, v) & (u, v) \in \Omega_k^n \\ s_\infty & (u, v) = 0 \end{cases} \tag{3.6}$$

where Ω_k^n is the k th subdomain, $k = 0, 1, 2$, in the n th subdivision level, $n \geq 1$, corresponding to the partition of the domain Ω shown in Figure 3.7. The point s_∞ denotes the limit position of the extraordinary vertex.

Using Stam's simplification, the evaluation cost of the limit surface of the irregular element is comparable to the evaluation cost using bicubic B-splines.

Over the domain $\Omega \setminus (0, 0)$, the partial derivatives of the limit surface are obtained by differentiating the basis functions over the subdomain Ω_k^n . For example, the first partial derivative with respect to u is described by

$$\begin{aligned} \frac{\partial}{\partial u} s(u, v) |_{\Omega_k^n} &= C_0^T S_{k,n}^T \frac{\partial}{\partial u} b(t_{k,n}(u, v)) \\ &= 2^n C_0^T S_{k,n}^T \left(\frac{\partial}{\partial \tilde{u}} b(\tilde{u}, \tilde{v}) \right) \Big|_{(\tilde{u}, \tilde{v})=t_{k,n}(u, v)} \end{aligned}$$

where $(u, v) \in \Omega_k^n$. The partial derivatives of the corresponding B-spline basis functions are described in Section 3.2.1. Due to the derivative of the transformation map $t_{k,n}(u, v)$, the factor 2^n appears in the formula. Note that for the p th partial derivative of the surface, this results in the factor 2^{pn} . Considering a regular element, we are also able to evaluate the limit surface using Stam's method. Therefore, we have to treat one of the element vertices as an extraordinary vertex. However, the representation converges to a bicubic B-spline surface patch as described in Section 3.2.1. For reasons of simplicity, we will use the B-spline representation for the limit surface evaluation on regular elements.

The parameterization is easy to use, but not fully compatible with the classical subdivision surfaces. The natural representation is still C^2 -continuous everywhere except at the singularities corresponding to the extraordinary vertices in the mesh. However, the defect is noticeable

in the surface continuity at the singularity, i.e. the parameterization provides there only a C^0 -continuity. In order to obtain a C^1 -continuity, as in the classical concept, a suitable differentiable structure has to be put on the domain, or, equivalently, a suitable reparameterization of the surface patch has to be obtained.

3.2.5 Natural generating spline

Based on the natural parameterization of the subdivision surface, we are able to derive the set of corresponding element-based basis functions called here the generating spline. Please note that the basis functions are sensitive to the valence of the extraordinary vertex, i.e. its representation have to be adapted to the valence. We consider the following definition:

Definition 3.3 (Natural generating spline). Given an element Q_c of the Catmull–Clark grid \mathcal{C}_Q , we consider the set of basis functions $\{b_j^*\}$, $j = 0, \dots, K - 1$. The factor $K = 2\nu + 8$, describes the size of the set of vertices in the one-ring of Q_c , where ν denotes the valence of the extraordinary vertex. Let $b(u, v)$ be a vector, where the entries b_i , $i = 0, \dots, 15$ are the 16 uniform bi-cubic B-spline basis functions defined over the unit square $[0, 1]^2$. The *natural generating spline* is given by the vector

$$b^* = (b_0^*, b_1^*, \dots, b_{K-1}^*)^T,$$

where the entry b_j^* is the j th basis function corresponding to the j th vertex in the one-ring of the element that are defined by

$$b_j^* : \Omega \rightarrow \mathbb{R}$$

$$b_j^*(u, v) = \begin{cases} [S_{k,n}^T]_{j,\cdot} \cdot b \circ t_{k,n}(u, v) & \text{for } (u, v) \in \Omega_k^n \\ b_j^\infty & \text{for } (u, v) = (0, 0), \end{cases} \quad (3.7)$$

for $n \geq 1$ and $k = 1, 2, 3$. The matrix $S_{k,n} = P_k S_n$ is given by the product of the subdivision matrix $S_n = \bar{A} A^{n-1}$, $n \geq 1$, and the picking matrix P_k , $k = 1, 2, 3$. For the parameter domain $\Omega = [0, 1]^2$, we consider the infinite partition of Ω into subdomains Ω_k^n , as shown in Figure 3.7. The function $t_{k,n}$ describes the transformation from Ω_k^n to $[0, 1]^2$, the parameter domain of the B-spline functions. At the extraordinary vertex, the generalized basis function is described by the value b_j^∞ .

The term $[\cdot]_{j,\cdot}$ denotes the j th row of the matrix. In the regular case, one of the regular vertices is treated as extraordinary. For the valence $\nu = 4$, the $2\nu + 8 = 16$ basis functions of b^* are equivalent to the bi-cubic B-spline basis functions b_j . For simplicity's sake, if we consider a regular element, then we use the B-spline representation for the evaluation, see Formula 3.1. In Figure 3.9, the generating spline of an irregular element with an extraordinary vertex of valence 5 is shown.

To calculate b_j^∞ , we consider the classical limit surface evaluation scheme. Therefore, we examine the one-neighbourhood of the extraordinary vertex and assemble the corresponding subdivision matrix S . The one-neighbourhood is given by $2\nu + 1$ vertices. Note, the matrix S is stochastic and nondefective, i.e. it has a complete basis of eigenvectors. For each vertex v_j , $j = 0, \dots, 2\nu$, in the one-neighbourhood we set up a $(2\nu + 1) \times 1$ control vertex matrix C_j , such that each entry is zero except for a one in the j th entry. Consider the eigendecomposition of the subdivision matrix: The set $\Lambda = \{\lambda_k\}$ of ordered eigenvalues is given such that $\lambda_0 = 1 > \lambda_1 \geq \dots \geq \lambda_{2\nu}$. Let $\{v_k^r\}$ and $\{v_k^l\}$ be the sets of right and left eigenvectors. The limit position of the basis function is given by

$$b_j^\infty = \lim_{n \rightarrow \infty} (S^n C_j)^T v_0^l = C_j^T v_0^l, \quad (3.8)$$

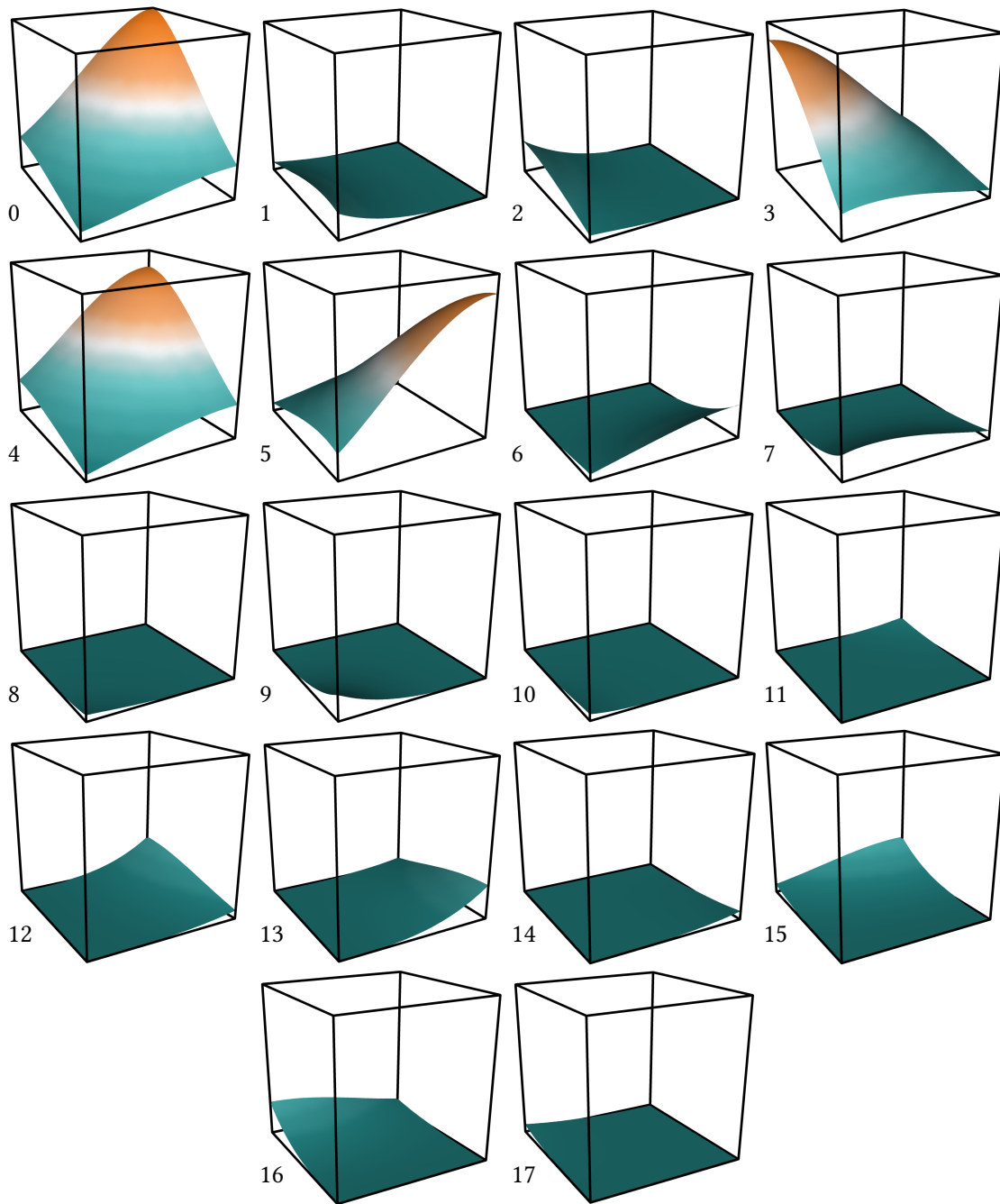


Figure 3.9: *Generating spline. The images of basis functions of an irregular element with an extraordinary vertex of valence 5. The order of the functions is similar to the order of vertices shown in Figure 3.3 (b). The images are oriented, such that the extraordinary vertex is in the lower corner. For visual reasons, in the image 0 the extraordinary vertex is positioned in the opposite corner. Note, the basis function related to the extraordinary vertex, i.e. image 0, is higher than the three functions related to the regular vertices of the element shown in images 3, 4 and 5.*

where v_0^l is the left eigenvector of S corresponding to the largest eigenvalue that by definition is equal 1. For details see Section 2.3.3.

A closer look at the entries of the natural generating spline show that some of the basis functions coincide with some of the bicubic B-spline basis functions. This is true in particular for the basis functions corresponding to vertices in the one-ring of the element that are lying in the outer layer of the two-neighbourhood of the extraordinary vertex of valence ν . Hence, the seven basis functions

$$b_{2\nu+1}^*, \dots, b_{2\nu+7}^*,$$

coincide with the uniform B-spline basis functions in the following order

$$b_{15}, b_{11}, b_7, b_3, b_{14}, b_{13}, b_{12}. \quad (3.9)$$

The remaining functions are compositions of bicubic B-splines as described above.

As mentioned before, considering the generating spline over a control grid element, every basis function of the spline is describing a part of a subdivision basis function associated to one of the vertices in the one-ring of this element. On the other hand, the global functions can be parameterized piece by piece by the relevant element based basis functions. Due to the Catmull–Clark subdivision rules, the non-zero support of the global basis function B_a corresponding to the a th control vertex is given by the two-neighbourhood of this vertex in the control grid \mathcal{C}_Q . Thus, for an element $Q_c \in \mathcal{C}_Q$ in the two-neighbourhood of a vertex, let this vertex corresponds to the j th vertex in the one-ring of Q_c . The generating spline function b_j^* of Q_c describes then the parameterization of the global basis function B_a associated with this vertex on the element Q_c . How to determine the relation between the local and the global indices is described in Section 4.4.2. The subdivision basis functions B_a are called the generalized B-spline basis functions of Catmull–Clark type. These are known to be bicubic polynomials on each regular patch or regular subpatch of the irregular element apart from the extraordinary vertex. Using the global basis, the total representation of the limit surface is given by the linear combination

$$s = \sum_a c_a B_a,$$

where c_a is the vertex position of the a th vertex in the control grid \mathcal{C}_Q . Note, the global representation looks similar to the subdivision function defined in Section 2.3.2. However, keep in mind that the natural parameterization of the generalized B-spline basis is not consistent with the smoothness of the classical subdivision basis functions.

Depending on the two-neighbourhood of a control vertex, we distinguish three possibly emerging basis types. The basis types emerge from the following neighbourhood compositions:

- an extraordinary vertex, i.e. all vertices in the one-neighbourhood are regular, see Figure 3.10 (a). The element-based pieces of the subdivision basis function correspond to piecewise B-splines in the one-neighbourhood of the extraordinary vertex, and appropri-

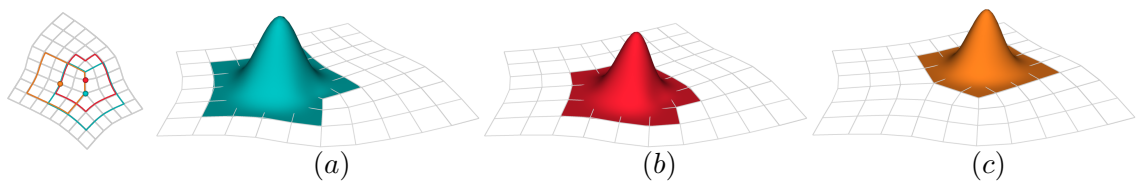


Figure 3.10: *Generalized B-spline basis functions of Catmull–Clark type. The images of the functions corresponding to (a) an irregular vertex, (b) a regular vertex with at least one extraordinary vertex in its one-neighbourhood, and (c) a regular vertex without extraordinary vertices in its one-neighbourhood. The last one is equivalent to a uniform bicubic B-spline basis function.*

ate bicubic B-spline functions listed in Equation 3.9 on the remaining part of the two-neighbourhood,

- a regular vertex with at least one extraordinary vertex in its one-neighbourhood, see Figure 3.10 (b). The element-based pieces of the subdivision basis functions are described by piecewise B-splines in the one-neighbourhood of each extraordinary vertex, and an appropriate bicubic B-spline basis function on the remaining part of the 2-neighbourhood,
- and, a regular vertex without extraordinary vertices in its one-neighbourhood, see Figure 3.10 (c). The element-based pieces of the subdivision basis function corresponds to the appropriate bicubic B-spline basis functions $b_i, i = 0, \dots, 15$.

Using the natural parameterization of the generalized B-splines, we illustrate examples of the emerging function types in Figure 3.10. Just as a reminder, we restrict ourselves to control grids with isolated extraordinary vertices, i.e. each element of the control grid has at most one extraordinary vertex. Considering the global subdivision basis functions, it should be observed that the limit position of a control grid vertex is influenced by $2\nu + 1$ global basis functions. In particular, these are given by the basis functions that corresponds to the vertices lying in the one-neighbourhood of this vertex. Note, the basis functions lying in the second neighbourhood are equal zero for this vertex.

3.3 Characteristic surface parameterization

In the previous section, the natural parameterization of the limit surface has been explained in more detail. It allows for a direct calculation of the limit surface. As mentioned before, it is incompatible with the classical characterization of subdivision surfaces, i.e. the natural parameterization produces a lack of smoothness at the limit of the extraordinary vertices. To repair this defect, a reparameterization has to be established that ensures the provided C^1 -continuity at the limit of these vertices.

The characteristic map is an important concept of subdivision surfaces. The map is associated with the subdivision matrix close to extraordinary vertices and therefore depends on the valence of these vertices. The characteristic map has been introduced in [Reif, 1995] for the investigation of subdivision surfaces at singularities. It is very much linked to the regularity properties of subdivision surfaces, see Section 2.3.4. In [Peters and Reif, 1998], it is shown that a subdivision scheme generates C^1 -continuous surfaces that are locally manifold, if χ is regular and injective (i.e. it has no vanishing Jacobian). Consequently, the concept can be used for the parameterization of the limit surface. In this section, the so-called characteristic parameterization is considered. This idea proves to be promising concerning the preservation of smoothness of limit surfaces, see [Prautzsch, 1998]. In [Boier-Martin and Zorin, 2004], an algorithmic method for the evaluation of the characteristic parameterization has been presented. Due to the complexity of the method, the evaluation cost is enormous. Therefore, the applicability of this method is limited.

In this section, we give a detailed construction of the characteristic parameterization and its element based generating splines for Catmull–Clark subdivision surfaces. Using the natural parameterization, a reparameterization of the corresponding generating spline is described via the transformation of the domain Ω into the characteristic domain Ω_ν . The domain Ω_ν is defined as the image of the characteristic map. One goal of this section is to understand the impact of the characteristic map on the representation of the limit surface close to singularities or, equivalently, extraordinary vertices. We deduce a new concept of characteristic patches and describe its properties. These turn out to be important to understand the differentiability properties of this

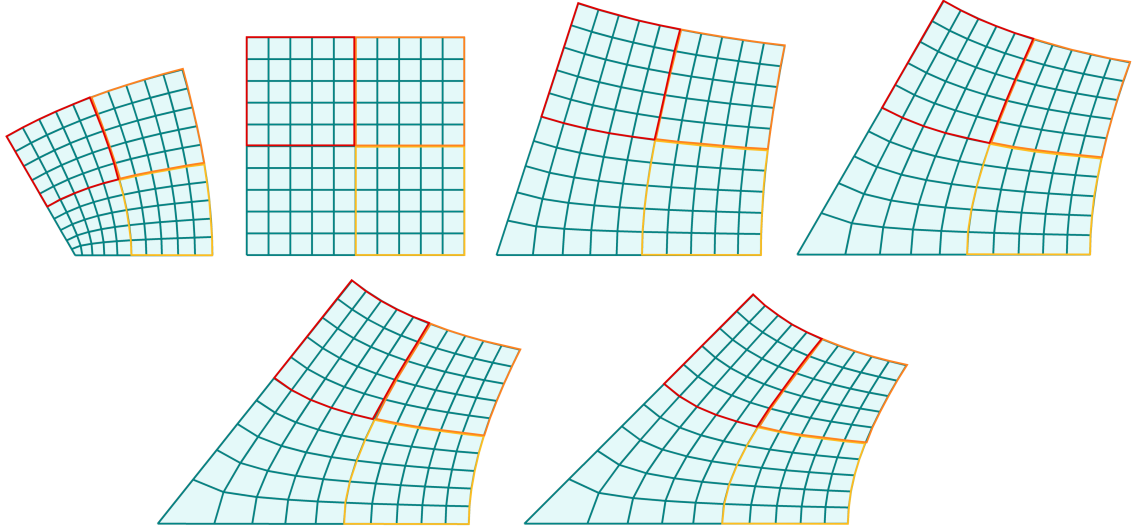


Figure 3.11: Characteristic domains Ω_ν for different vertex valences ν . From left to right, the domains Ω_ν (blue domains) for the valence $\nu = 3, 4, 5, 6, 7, 8$ are shown. The blue grid illustrate the characteristic map of a ten by ten grid on the unit square with uniform spacing. The parts separated by the yellow, orange and red boundaries are illustrating the characteristic domains $\Omega_\nu^{0,1}$, $\Omega_\chi^{1,1}$ and $\Omega_\chi^{2,1}$, respectively.

reparameterization. Our approach is based on Reif's idea of characteristic mappings introduced in [Reif, 1995] and continued in [Peters and Reif, 2008].

3.3.1 Characteristic mapping

Considering a convergent subdivision scheme, the ordered eigenvalues λ_i of the corresponding subdivision matrix fulfil $\lambda_0 = 1 > |\lambda_1| = |\lambda_2| > \dots$. If the subdominant eigenvalue λ satisfies $\lambda = \lambda_1 = \lambda_2$, then the limit position and the tangents of the given control vertex are related to the eigenvectors corresponding to the first three eigenvalues λ_i , $i = 0, 1, 2$. Thus, the characteristic map χ is defined by the two eigenvectors v_1 and v_2 associated with the subdominant eigenvalue λ , see Section 2.3.4.

The Catmull–Clark scheme is convergent for each valence of the extraordinary vertex. Given a control grid element $Q_c \in \mathcal{C}_Q$ and its one-ring, we consider the associated quadratic subdivision matrix A , see Section 3.2.2. Due to the properties of A , we consider the following definition of the characteristic map of the Catmull–Clark scheme.

Definition 3.4 (Characteristic map). Given an element Q_c of the control grid \mathcal{C}_Q . For the associated subdivision matrix A , let (Λ, V) be the corresponding eigenstructure of A , where the ordered set of eigenvalues $\{\lambda_i\}$ fulfils $1 = \lambda_0 > \lambda_1 = \lambda_2 \geq \lambda_3 \geq \dots$. The characteristic map χ of the Catmull–Clark subdivision scheme is therefore defined by

$$\begin{aligned} \chi : \Omega &\rightarrow \mathbb{R}^2 \\ \chi(u, v) &= V_\lambda^T b^*(u, v), \end{aligned}$$

where $b^*(u, v)$ denote the natural generating spline of Q_c at the point $(u, v) \in \Omega$. The subdominant matrix $V_\lambda = (v_1, v_2)$ is given by the two eigenvectors v_i , $i = 1, 2$, associated with the subdominant eigenvalue λ of A .

The characteristic map influences the behaviour of the limit surface close to the extraordinary vertex over an element of the control grid. The image of the characteristic map defines a two-dimensional spline domain in the plane. The domain changes according to the valence ν of the

extraordinary vertex characterizing the irregular element. We denote the domain with Ω_ν and call it the characteristic domain. In Figure 3.11, the characteristic domains for different vertex valences are shown.

Given the definition of b^* , a piecewise representation of the characteristic map can be obtained. That is,

$$\chi(u, v) = \begin{cases} \chi_{k,n} \circ t_{k,n}(u, v) & \text{for } (u, v) \in \Omega_k^n \\ (0, 0)^T & \text{for } (u, v) = (0, 0), \end{cases} \quad (3.10)$$

for

$$\begin{aligned} \chi_{k,n} &: [0, 1]^2 \rightarrow \Omega_\nu \\ \chi_{k,n}(u, v) &= \lambda^{n-1} (P_k \bar{A} V_\lambda)^T b(u, v), \end{aligned}$$

where the mapping $t_{k,n}$ is the transformation from Ω_k^n into the B-spline domain $[0, 1]^2$, see Equation 3.4. The piecewise representation using the mappings $\chi_{k,n}$ describes a division of the characteristic domain Ω_ν into subdomains $\Omega_\nu^{k,n}$, where $\Omega_\nu^{k,n}$ is the k th subpatch in the n th subdivision level of Ω_ν . Thus, a correlation with the partition of the parameter domain Ω arises, compare Figure 3.12 and Figure 3.7. Note, the characteristic domain Ω_ν is equal Ω if the extraordinary vertex has valence $\nu = 4$, i.e. the corresponding element is regular.

Moreover, for a fixed k and for $n \rightarrow \infty$ the subdomains $\Omega_\nu^{k,n}$ can be seen as scaled copies of each other in conformity with the origin $(0, 0) \in \Omega_\nu^{k,n}$. Three independent mappings can be specified.

Remark 3.5. Let $\chi_{k,n}$ be the mapping characterizing the subdomain $\Omega_\nu^{k,n}$. Three mappings χ_k , $k = 1, 2, 3$, can be gained from the following relation:

$$\begin{aligned} \chi_k &: [0, 1]^2 \rightarrow \mathbb{R}^2 \\ \chi_k(u, v) &= \lambda^{-n} \chi_{k,n}(u, v), \end{aligned} \quad (3.11)$$

where χ_k characterizes one of the three neighbouring domains of the characteristic domain. The factor λ is given by the subdominant eigenvalue and depends on the valence ν of the extraordinary vertex.

Thus, the partition of the characteristic domain corresponds to the scaling of the domain described by χ_k . Furthermore, the mapping χ_k forms an elemental foundation for the partition of Ω_ν :

Definition 3.6 (Characteristic patches). Using the natural parameterization, the *characteristic patches* χ_k , $k = 1, 2, 3$, are defined by

$$\chi_k(u, v) = \bar{V}_\lambda^T P_k^T b(u, v) \quad (u, v) \in [0, 1]^2$$

where $\bar{V}_\lambda = \frac{1}{\lambda} \bar{A} V_\lambda$ describes an extension of the eigenvectors to the neighbouring elements of the irregular element. The matrix $V_\lambda = (v_1, v_2)$ is the subdominant matrix and \bar{A} is the extended subdivision matrix, see Section 3.2.2.

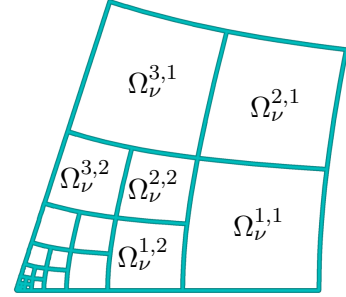


Figure 3.12: Partition of Ω_ν into sub-domains $\Omega_\nu^{k,n}$.

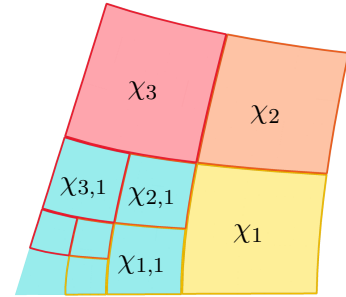


Figure 3.13: Characteristic mappings. The blue quad illustrates the characteristic domain Ω_ν . The characteristic patches χ_0 , χ_1 and χ_2 are shown by the yellow, orange and red quads, respectively. The associated subdomains of Ω_ν , described by the scaling $\chi_{k,n}$ of mapping χ_k is characterized by a frame of the corresponding colour.

The image of the characteristic patches has no overlap with the characteristic domain except for the common boundary, see Figure 3.13. Note, χ_k and χ are defined over the same domain, i.e. $\Omega = [0, 1]^2$. The extension \bar{V}_λ of the eigenvectors relates to the extension of the characteristic domain using the characteristic patches χ_k . Moreover, the images of the characteristic patches χ_k can be seen as the parameter domain of the three neighbouring elements in the control grid in the characteristic domain. The following relations between the characteristic mappings are valid:

Remark 3.7. The characteristic map χ fulfils the scaling relation

$$\chi(u/2, v/2) = \lambda \chi(u, v).$$

The characteristic patches χ_k , $k = 1, 2, 3$, fulfil the scaling relation

$$\lambda^n \chi_k(u, v) = \chi_{k,n}(u, v) = \chi|_{\Omega_{k,n}^{k,n}}, \quad (3.12)$$

where the restriction of the characteristic map χ to $\Omega_\nu^{k,n}$ is similar to the restriction of the domain Ω to Ω_k^n . Additionally, the neighbouring subpatches satisfy the relation

$$\chi_{k,n}(u, v) = \lambda \chi_{k,n-1}(u, v). \quad (3.13)$$

We write here $(\tilde{\xi}, \tilde{\eta}) = \chi(\tilde{u}, \tilde{v})$ for the coordinates of a point in the domain Ω_ν and $(\xi, \eta) = \chi_k(u, v)$ for the coordinates in the image of the characteristic patch χ_k . A schematic illustration is shown in Figure 3.14. Furthermore, we choose a point $(\tilde{\xi}, \tilde{\eta})$ in Ω_ν , such that $(\tilde{\xi}, \tilde{\eta}) = \lambda^n(\xi, \eta)$. Due to the scaling relation described in Remark 3.7, we know that such a point exists for each $n \geq 1$. Considering the transformation from Ω_ν into the subdomains $\Omega_\nu^{k,n}$, we obtain some important properties. For the change of coordinates from Ω_ν to $\Omega_\nu^{k,n}$, we have:

$$\chi^{-1}(\tilde{\xi}, \tilde{\eta}) = \chi^{-1}(\lambda^n \xi, \lambda^n \eta) = \frac{1}{2^n} \chi_k^{-1}(\xi, \eta),$$

where the scaling is proportional to the level of subdivision of the corresponding characteristic patch χ_k . Using the mapping $\chi_{k,n}^{-1}$ instead of χ^{-1} for the reparameterization means to substitute $(\lambda^n \xi, \lambda^n \eta)$ where $(\xi, \eta) \in \chi_{k,n}(\Omega)$.

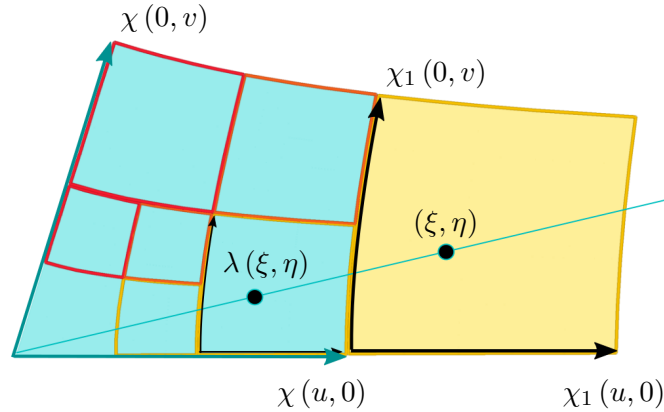


Figure 3.14: Scaling relation. Schematic illustration of the relation between the characteristic patch χ_k and the scaling $\chi_{k,n}$. The blue and the yellow quad illustrates the characteristic domain Ω_ν and the characteristic patch χ_1 , respectively, for $\nu = 5$.

The Jacobian of the transformation is determined by

$$J_\chi = \frac{\partial \left(\tilde{\xi}, \tilde{\eta} \right)}{\partial (\xi, \eta)} = \lambda^n I, \quad (3.14)$$

where I denote the identity matrix. Note, the Jacobian is constant. In particular, the underlying transformation is invertible. We consider the representation of the gradient ∇_χ over the domain $\Omega_\nu = \chi(\Omega)$ restricted to the subdomain $\Omega_\nu^{k,n} = \chi_{k,n}(\Omega)$.

Remark 3.8. The gradient ∇_χ restricted to $\Omega_\nu^{k,n}$ can be represented in the local coordinates by

$$\nabla_\chi|_{\Omega_\nu^{k,n}} = \lambda^{-n} \nabla_{\chi_{k,n}},$$

where $\nabla_{\chi_{k,n}}$ is the surface gradient in the coordinates of $\Omega_\nu^{k,n}$.

The representation of the restriction is given by the change of coordinates, where scaling by λ^{-n} corresponds to the scaling of the characteristic patch $\chi_k(\Omega)$ into the domain $\Omega_\nu^{k,n}$. Moreover, the scaling relation of the characteristic patches provides the same result, see Formula 3.12. For more detailed information about characteristic mappings we refer to Reif [1995]; Reif and Schröder [2001]; Zorin [1998].

3.3.2 Characteristic generating spline

The characteristic map χ determines the behaviour of the limit surface close to the singularity related to an extraordinary vertex in the corresponding control grid. As indicated in [Reif, 1995], the map can be used to parameterize the limit surface, such that the smoothness of the surface remains consistent to the classically defined subdivision surface. Due to the injectivity of the characteristic map χ , we can think of the mapping $\chi^{-1} : \Omega_\nu \rightarrow \Omega$ as a parameterization of the domain Ω . Based on this, we define a reparameterization of the natural representation of the limit surface. More precisely, we apply the transformation of the element-based basis given by the natural generating spline, see Definition 3.3, onto the characteristic domain.

Remark 3.9. For an element Q_c of the control grid \mathcal{C}_Q , we consider the associated generating spline b^* . Let χ be the corresponding characteristic map and

$$\Omega_\nu = \{(\xi, \eta) \in \mathbb{R}^2 \mid (\xi, \eta) = \chi(u, v), (u, v) \in \Omega\}$$

be the associated characteristic domain. The basis functions b_j^* defining the natural generating spline can be reparametrized as follows

$$\begin{aligned} b_j^x &: \Omega_\nu \rightarrow \mathbb{R} \\ b_j^x(\xi, \eta) &= b_j^* \circ \chi^{-1}(\xi, \eta) \quad (\xi, \eta) \in \Omega_\nu \end{aligned} \quad (3.15)$$

where $j = 0, \dots, K - 1$ corresponds to the index of a vertex in the one-ring of Q_c . The basis function b_j^x is at least C^1 -continuous for any $(\xi, \eta) \in \chi(\Omega)$ [Reif, 1995].

The parameterization over the characteristic domain provides the desired compatibility with the classical definition of the Catmull–Clark subdivision surfaces. In Zorin [1998], the characteristic representation has been considered for the continuity investigation of stationary subdivision surfaces. The author shows that χ puts a differentiable structure on the domain Ω . The injectivity of this parameterization is proven in [Boier-Martin and Zorin, 2004].

Based on the piecewise representation of the characteristic map χ , we define the characteristic generating spline.

Definition 3.10 (Characteristic generating spline). For an element Q_c of the control grid \mathcal{C}_Q , let b^* be the associated generating spline. Let χ be the characteristic map described by the piecewise representation as given in Equation 3.10. Using the corresponding partition of Ω_ν into $\Omega_\nu^{k,n}$, the basis functions b_j^χ can be parameterized by

$$b_j^\chi : \Omega_\nu \rightarrow \mathbb{R}$$

$$b_j^\chi(\xi, \eta) = \begin{cases} \left[S_{k,n}^T \right]_{j,\cdot} b \circ \chi_{k,n}^{-1}(\xi, \eta) & \text{for } (\xi, \eta) \in \Omega_\nu^{k,n} \\ b_j^\infty & \text{for } (\xi, \eta) = (0, 0) \end{cases} \quad (3.16)$$

where the mappings b_j^χ are the components of the *characteristic generating spline*

$$b^\chi = (b_0^\chi, b_1^\chi, \dots, b_{K-1}^\chi)^T.$$

The term $[\cdot]_{j,\cdot}$ denotes the restriction to the j th row of the matrix.

A closer look at the definition reveals that the transformation to the reference domain Ω can be neglected. The piecewise basis function b_j^χ is directly parameterized over the partitioned characteristic domain Ω_ν .

At this point, we establish the characteristic parameterization of the limit surface. Using the characteristic generating spline, the limit surface can be described over Ω_ν by

$$s_\chi(\xi, \eta) = \begin{cases} s_{k,n} \circ \chi_{k,n}^{-1}(\xi, \eta) & \text{for } (\xi, \eta) \in \Omega_\nu^{k,n}, \\ s_\infty & \text{for } (\xi, \eta) = (0, 0) \end{cases} \quad (3.17)$$

where $\Omega_\nu^{k,n}$ is the k th subdomain in the n th subdivision level of the partitioned domain Ω_ν .

Due to the fact that the evaluation of the inverse of the characteristic map χ^{-1} is nontrivial, the evaluation of the surface using the characteristic parameterization is much more expensive than the natural parameterization. In [Boier-Martin and Zorin, 2004], an algorithm for the evaluation has been introduced. As the authors report, the efficiency of the assembly is low. Consequently, using this parameterization in systems designed for parametric patches has limitations in the application. For this reason, we use the natural parameterization for the evaluation of the limit surface. Nevertheless, we will use the characteristic parameterization for the definition of subdivision finite elements.

3.3.3 Eigensplines

Considering the definition of the characteristic parameterization, a functional form for the limit surface representation can be derived. This means, a set of functions can be derived that fully depends on the subdivision process. In particular, considering the characteristic parameterization of the limit surface, we can separate the components depending on the subdivision process from the components prescribed by the mesh construction. These functions are called eigensplines. Eigensplines play a fundamental role in the analysis of smoothness of subdivision surfaces. The functions can also be alternatively used for the parameterization of the surface. In the following, we derive an explicit representation of the Catmull–Clark eigensplines.

As described in Section 2.3.3, given a nondefective subdivision matrix, there exists a set of appropriate right and left eigenvectors. For the Catmull–Clark scheme, the quadratic subdivision matrix A that corresponds to the subdivision of the one-ring of an element $Q_c \in \mathcal{C}_Q$ is nondefective. The control vertex matrix C_0 , formed by the position vectors of the vertices in the one-ring of Q_c , can be uniquely expressed in terms of the right eigenvectors v_j^r of A . In particular, C_0 is

given by the sum

$$C_0 = \sum_{j=0}^{K-1} v_j^r a_j^T,$$

where K is the number of vertices in the one-ring. The vectors a_j are the appropriate coefficient vectors that gives the subdivision independent part of the vertices. These can be seen as the projections of the vertex positions into the eigenspace of the subdivision matrix. The basis of the eigenspace is given by the mentioned set of eigensplines. Using the characteristic parameterization $s_\chi = s \circ \chi^{-1}$ of a limit surface patch, we consider a separation of the pure subdivision related part of the parameterization from the part related to the control grid. Using the eigen-decomposition of the matrix C_0 , the surface patches can be represented by an expansion of the form

$$s_\chi(\xi, \eta) = \sum_{j=0}^{K-1} a_j \varphi[v_j^r](\xi, \eta), \quad (3.18)$$

for $(\xi, \eta) \in \Omega_\nu$. The functions $\varphi[v_j^r]$ are the eigenspline functions. These are defined as follows:

Definition 3.11 (Eigensplines). For the subdivision matrix A , let $\{v_i^r\}_{i=0, \dots, K-1}$ be the set of right eigenvectors corresponding to the ordered set of eigenvalues $1 = \lambda_0 > \lambda \geq \lambda_3 \geq \dots$, where $\lambda = \lambda_1 = \lambda_2$ denote the double subdominant eigenvalue of A . The *eigensplines* $\varphi[v_j^r]$, $j = 0, \dots, K-1$, are described by the formula

$$\begin{aligned} \varphi[v_j^r] : \Omega_\nu &\rightarrow \mathbb{R} \\ \varphi[v_j^r](\xi, \eta) &= \begin{cases} \lambda_j^n (\bar{v}_j^r)^T P_k^T b \circ \chi_{k,n}^{-1}(\xi, \eta) & \text{for } (\xi, \eta) \in \Omega_\nu^{k,n}, \\ \delta_{0j} & \text{for } (\xi, \eta) = (0, 0) \end{cases} \end{aligned}$$

where $\bar{v}_j^r = \frac{1}{\lambda_j} \bar{A} v_j^r$ is the extension of the j th eigenvector v_j^r .

Note, the functions are only defined for the eigenvectors v_i^r of the subdivision matrix. A linear functional form is considered. Further, the functions satisfy the following scaling relation:

Theorem 3.12. *Is λ_j an eigenvalue of the subdivision matrix A , then the corresponding eigenvector v_j^r determines the eigenfunction φ_j . The function φ_j satisfies the relation*

$$\varphi[v_j^r](\xi, \eta) = \lambda_j \varphi[v_j^r]\left(\frac{\xi}{\lambda}, \frac{\eta}{\lambda}\right)$$

where λ is the double subdominant eigenvalue of A .

This means, applying one subdivision to the eigenspline, or equivalently, multiplying with the subdivision matrix A^T corresponds to the scaling of the domain Ω_ν with the subdominant eigenvalue λ . The scaling is also equivalent to the subdivision of the parameter domain Ω_ν . Hence, the behaviour of stationary schemes at extraordinary vertices can be reduced to a scaling relation.

Proof. Due to the definition of the characteristic map χ and the corresponding partition of the characteristic domain Ω_ν , for $(\xi, \eta) \in \Omega_\nu$ there is a subdomain $\Omega_\nu^{k,n}$ such that $(\xi, \eta) \in \Omega_\nu^{k,n}$. Considering the mapping $\chi_{k,n}$ that describes the domain $\Omega_\nu^{k,n}$, there exist a point $(u, v) \in [0, 1]^2$, such that $\chi_{k,n}(u, v) = (\xi, \eta)$. Based on the scaling relation 3.13, multiplying the point (ξ, η) with $\frac{1}{\lambda}$ results in the point $\chi_{k,n-1}(u, v) = \left(\frac{\xi}{\lambda}, \frac{\eta}{\lambda}\right) \in \Omega_\nu^{k,n-1}$. Applying the subdivision matrix A to

the eigenspline results in

$$\varphi [v_j^r] (\xi, \eta) = \lambda_j^n (\bar{v}_j^r)^T P_k^T b \circ \chi_{k,n}^{-1} (\xi, \eta) \Big|_{\Omega_\nu^{k,n}}$$

The multiplication with λ_j is similar to applying the subdivision matrix A^T , i.e. $A^T \bar{v}_j^r = \lambda_j \bar{v}_j^r$.

$$= \lambda_j \cdot \lambda_j^{n-1} (\bar{v}_j^r)^T P_k^T b \circ \chi_{k,n-1}^{-1} (\xi, \eta) \Big|_{\Omega_\nu^{k,n}}$$

The coordinates (ξ, η) correlate with the domain $\Omega_\nu^{k,n}$, the dilation to $\Omega_\nu^{k,n-1}$ comply with the scaled coordinates $\left(\frac{\xi}{\lambda}, \frac{\eta}{\lambda}\right)$.

$$\begin{aligned} &= \lambda_j \cdot \lambda_j^{n-1} (\bar{v}_j^r)^T P_k^T b \circ \chi_{k,n-1}^{-1} \left(\frac{\xi}{\lambda}, \frac{\eta}{\lambda}\right) \Big|_{\Omega_\nu^{k,n-1}} \\ &= \lambda_j \cdot \varphi [v_j^r] \left(\frac{\xi}{\lambda}, \frac{\eta}{\lambda}\right) \end{aligned}$$

where $(\xi, \eta) \in \Omega_\nu$. □

The concept of eigenbasis functions has been introduced in [Warren, 1995] for the analysis of the behaviour of subdivision curves. In [Warren and Weimer, 2001], a similar theorem to ours is stated. However, we introduce the parametric formulation of the functions for the Catmull–Clark scheme.

CHAPTER 4

ISOPARAMETRIC CATMULL–CLARK FINITE ELEMENTS

We consider a control grid together with the associated limit surface. Using the previously defined parameterizations, the surface can be described by a patchwork of glued together surface patches corresponding to the elements of the control grid. Given an arbitrary PDE over a prescribed domain. The elementwise representation is similar to the idea of finite elements, where a partition of the problem domain into a collection of smaller easier to handle subdomains is being used. The global problem can be therefore rewritten into a set of local problems over the subdomains. Assume that the problem domain is given by a subdivision surface. Using the subdivision basis functions, a finite element approach can be derived, where the same set of functions is used for the representation of the unknown displacements and the construction of the geometry. Based on this construction, we obtain an isoparametric finite element approach.

In the case of the Catmull–Clark subdivision scheme, the basis functions are at least $C^1 \cap H^2$ -regular [Reif and Schröder, 2001]. In the following, we want to make use of the high regularity for the construction of finite element methods, called subdivision finite elements. Furthermore, a conforming finite element can be obtained for the approximation of partial differential equations up to order four. Based on the two presented limit surface parameterizations, the natural and characteristic finite element approaches can be deduced by means of the isoparametric concept. The underlying generating splines are taken as a basis framework for the construction of the subdivision finite elements. Consequently, a set of element-based shape functions is established in relation to the generating splines associated with the elements of the control grid. Keep in mind, the representation of the generating splines depends on the element type and, if appropriate, on the valence of the extraordinary vertex. Again, we distinguish between regular and irregular surface patches. If the element is regular, the parameter domain is given by the unit

square. Consequently, both finite element representations are identical. The difference between the two approaches lies in the treatment of the irregular element, that is, in the parameter domain of the corresponding parameterization. Compared to the natural parameterization defined over the partitioned unit square, the domain of the characteristic parameterization is given by the characteristic domain, where the latter one is established from the spectral properties of the subdivision matrix and depends on the valence of the extraordinary vertex.

In this chapter, we specify the necessary requirements for the discretization and approximation of geometric partial differential equations on subdivision surfaces. Using the given parameterizations, the subdivision finite elements will be here explored in more detail. Concerning this, we introduce the characteristic finite element that is compatible with the classical subdivision surfaces. Additionally, we derive the PDE specific integrals over subdivision surfaces. Here, we focus on the Catmull–Clark scheme [Catmull and Clark, 1978] on quadrangular meshes, but the presented ideas can be adopted to other subdivision schemes. These requires an identical construction, i.e. a reparameterization onto the characteristic domain.

4.1 About the isoparametric concept

Since the beginning of using computer-aided computation, analysis and simulations for manufacturing, one is interested on more accurate and efficient methods to solve real world problems using the computer. For example, a variety of problems from rather diverse application areas can be modelled by PDEs. The focus of solving PDEs is the investigation of specific material or structural properties that have a compact geometric description and underlie certain loading conditions. This can be very challenging, due to the corresponding equation, the associated initial and boundary conditions, or the problem domain. To find an analytical solution of such problems has turned out to be difficult or even impossible. Current research has proven that simplification of the associated difficulties is much more useful and can be put on a level with the continuous solutions. There are different methods to deal with the PDE simplification, for example, finite elements, finite differences, methods of lines, etc. By now, the finite element method became more and more accurate and reliable compared to other methods.

4.1.1 Finite element method

The finite element method has been developed in the 60's in the field of structural engineering and structural mechanics [Clough, 1960]. It has been adopted to analyse the behaviour of PDEs on heterogeneous domains, for example, on different shaped surfaces, for which the smooth solutions cannot be found. Thus, an approximation of the continuum is obtained using Galerkin's method. Substituting the PDE by a weak formulation, a discretization of the global problem can be obtained. As next, we provide an as good as possible partition of the domain into so-called elements. Consequently, a finite number of smaller, easier to handle problems have to be solved on the individual elements. The elements are connected only at node points located at the corners or at the element boundaries. The solution is represented as a patchwork of such elements, unnecessary details are neglected. The smooth solution space is replaced by a finite dimensional subspace that is defined by a set of basis functions. It is crucial to restrict the support of the basis functions to the disjoint elements that cover the domain. In general, polynomial functions on polyhedral domains are used for the assembly. Thus, the converted problem can then be solved using numerical methods. The approximated solution hopefully converge to the smooth solution, if the discretization becomes increasingly finer. For details on the finite element method, please refer to the book of [Ciarlet, 1978], [Hughes, 2000] and [Braess, 2007].

4.1.2 Isoparametric elements

Choosing an appropriate finite element method, there is one important choice to make: how to represent the solution space? A significant contribution to the field of finite elements is given by the isoparametric approach [Irons and Zienkiewicz, 1968]. The fundamental principle of this approach is to prescribe a set of shape functions defined over the problem domain, such that the same functions can be used to model the global solution space. Consequently, one set of shape functions is required to represent the components of the solution space and the shape of the underlying geometry.

Before the isoparametric element can be defined, we consider the so-called natural coordinates appropriate for quadrilateral elements. In the finite element theory, the natural coordinates are given by Cartesian coordinates (u, v) in the plane, called the reference domain. For $(u, v) \in \Omega$, where Ω is given by the unit square, Ω is describing a quadrilateral element in the plane, called the reference domain. A mapping over the total domain Ω describes another quadrilateral element. Considering higher order quadrilateral elements, the calculation is obtained within each element. The results have to be linked to the nodal degrees of freedom of the problem. We consider the transformation between different elements, this defines the so called isoparametric mapping.

Definition 4.1 (Isoparametric element). Let $x : \Omega \rightarrow \mathbb{R}^n$ of the form

$$x(u, v) = \sum_{a=0}^n N_a(u, v) x_a$$

be a quadrilateral representation of a finite element

$$Q = (\Omega, \mathcal{N}, \mathcal{X}),$$

where $\mathcal{N} = \{N_a\}_{a=0, \dots, n}$ is the set of functions defined over Ω , and \mathcal{X} is the set of linear independent forms x over \mathcal{N} . If the mapping X over Q can be written as

$$X(p) = \sum_{a=0}^n N_a \circ x^{-1}(p) X_a$$

for $p \in Q$, and $X(Q)$ is a closed subset of \mathbb{R}^n with a non-empty interior, the element parameterization X is said to be an *isoparametric finite element*.

A finite element constructed on an other finite element is called isoparametric. Respectively, both elements are isoparametrically equivalent. For a schematic illustration, see Figure 4.1. Considering the definition, note that the shape functions N_a , $a = 0, \dots, n$, describing the mapping $x(u, v)$ also serves as the basis of the mapping $X(p)$. Consequently, the element $Q = x(\Omega)$ and the mapping $X(Q)$ are contained in the same space.

Remark 4.2. The mapping x has to fulfil the following conditions:

- x is one-to-one
- x is onto

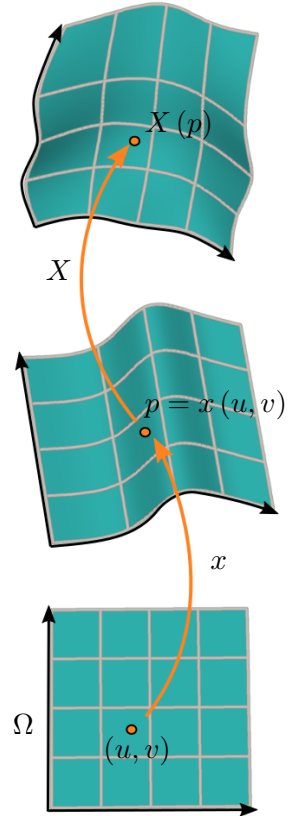


Figure 4.1: Schematic illustration of the isoparametric finite element in \mathbb{R}^3 .

- Let $x : \Omega \rightarrow Q$ be a differentiable mapping, i.e. the determinant of the derivative $|J| = \det \left(\frac{\partial x}{\partial u} \right)$ called the *Jacobian determinant* fulfils $|J| > 0$ for all $u \in \Omega$.

The quality of the approximation depends on the properties of chosen finite element approach. At least one, accuracy or efficiency, can be easily achieved. For the efficiency, the most preferable shape functions are simple polynomials. Accuracy is obtained from the convergence behaviour of the solution. This can be described by the following idea: as we increase the resolution of the mesh specifying the domain, the sequence of the approximated solutions should converge to the exact solution. For more detailed information on isoparametric finite elements see [Ciarlet, 1978].

4.1.3 Link to isogeometric analysis

Back to the beginning of computer-aided manufacturing, another powerful scientific sector has been established, this is, Computer-Aided Design (CAD). The task of CAD is to develop a concept for the design of sufficiently accurate models for production purposes. The exact geometry description is of primary importance. Despite the frequent cooperation of the finite element and CAD sectors, throughout the years, each sector moves independently towards its own aims. Consequently, gaps are emerging in the interworking of both sectors. One of the greatest concerns is the exchange of data. Different models for the representation of the geometry are used for the finite element analysis and CAD modelling technologies. Moreover, complex and time consuming transformation processes become indispensable.

Recently, a new scientific area called Isogeometric Analysis (IgA) has been introduced in [Cottrell et al., 2005, 2009]. The aim of IgA is an integrated system that combines the advantages of finite element analysis and CAD technologies. Hence, CAD tools for representing exact geometrical shapes are used for the investigation of real world problems. One type of shape functions is used for the representation of the geometry and the unknown solution space. However, the idea of an unified approach for the representation of form and function is not new. From the finite element side, the isogeometric approach builds on the isoparametric approach that is founded on this idea. Considering the isoparametric and the isogeometric approach, the difference is in the origin of the shape functions. In the isoparametric concept, the basis functions result from the construction of the solution space. Thus, the choice of shape functions to obtain a sufficient approximation quality of the unknown solution is prescribing the basis for the geometry representation. In the isogeometric concept, the shape functions arise from the exact representation of the geometry in the CAD system.

In the original concept, NURBS has been used for the construction. Nowadays, a variety of geometry representation tools are circulating in the literature, for example, T-splines (an enhancement of NURBS) [Sederberg et al., 2003], subdivision surfaces (mainly used in the animation industry), etc. All of these tools have the capability to describe smooth geometries and avoid the effort of geometry conversion from CAD into a suitable finite element mesh. Consequently, the IgA concept looks very promising for the future of manufacturing.

4.2 Catmull–Clark finite elements

Catmull–Clark subdivision surfaces describe a common tool used for the representation and design of geometric models. Using the locality of the subdivision, the global parameterization is avoidable and we can think of generalized B-spline patches that piecewise describe the surface. Considering the properties of the underlying basis functions, it is a natural consequence to introduce the concept of Catmull–Clark subdivision surfaces into the area of finite element analysis. Combining the geometrical and analytical potential of this concept, a finite element approach

can be obtained that provide consistency for problems which require up to H^2 -regularity. Moreover, we are interested in solving PDE's on arbitrary two-dimensional surfaces based on the subdivision concept. Consequently, the concept exhibits a great robustness and flexibility of the resulting models.

In this section, we introduce the concept of Catmull–Clark subdivision surfaces in the field of finite element analysis. Using the isoparametric approach, we define subdivision finite elements of Catmull–Clark type. Two approaches will be established, the natural and the characteristic finite elements, that base on the natural and the characteristic parameterization, respectively. The representation of the shape functions is described by the corresponding generating spline that is used to calculate the limit geometry, element by element. Here, we present an alternative concept to traditional finite element techniques that allows for an interoperability concept. It builds on subdivision basis functions for the approximation of the solution space.

4.2.1 Subdivision finite element framework

Given an arbitrary control grid $\mathcal{C}_Q = \{K, \mathbf{c}\}$, we obtain a unique Catmull–Clark limit surface \mathcal{Q} . Let the surface \mathcal{Q} be immersed in \mathbb{R}^3 together with the control grid \mathcal{C}_Q . Moreover, \mathcal{Q} is described to be a generalized B-spline surface, i.e. a set of global basis functions is given that corresponds to the set of control grid vertices. The underlying global basis is the set of generalized B-spline basis functions B_a , described in Section 3.2.5. The limit surface can be therefore represented by

$$\mathcal{Q} = \sum_a c_a B_a,$$

where $c_a \in \mathbf{c}$ are the vertex positions of the vertices in the control grid \mathcal{C}_Q , $a \in I_Q$ is the index of a vertex in \mathcal{C}_Q . In the following, we will restrict ourselves to closed limit surfaces, such that for each control grid element the limit surface exists. Note, subdividing a control grid with boundary leads to missing limit surface for the boundary elements, see Section 3.1.1).

Based on the fundamental ideas behind the limit surface \mathcal{Q} , two parameterizations have been described in the previous chapter. Using the natural and the characteristic parameterization, the surface can be seen as a patchwork of glued together subdomains $Q \subset \mathcal{Q}$, called surface patches, corresponding to the elements Q_c of the control grid \mathcal{C}_Q . Therefore, each element $Q_c \in \mathcal{C}_Q$ is associated with a surface patch $Q \subset \mathcal{Q}$. The patches $Q \subset \mathcal{Q}$ characterize a decomposition of the surface \mathcal{Q} , i.e. we obtain the so called physical grid on \mathcal{Q} . An interplay between two meshes is described, the control grid and the physical mesh. The control grid is specified by the control vertices and can be seen as a scaffold of the physical mesh. Moreover, it has the look of a typical finite element mesh. The degrees of freedom are distributed on the vertices of the control grid that stand for the field variables, as for example displacement, temperature, etc.

For each patch Q or, equivalently, each element Q_c , a set of basis functions is described by the associated generating spline. These element-based functions correspond to the vertices in the one-ring of Q_c . Let $I_Q \subset \mathbb{Z}$ be the index set of the one-ring vertices. For simplicity's sake, we distinguish between regular and irregular elements. If the element Q_c is regular, the B-spline representation also called regular representation can be applied. Therefore, the corresponding surface patch Q is described by the mapping $s_Q : [0, 1]^2 \rightarrow \mathbb{R}^3$, i.e.

$$s_Q(u, v) = \sum_{j \in I_Q} c_j b_j(u, v), \quad (u, v) \in [0, 1]^2,$$

where c_j is the position of the j th control vertex in the one-ring of the appropriate element $Q_c \in \mathcal{C}_Q$. The surface s_Q is therefore a uniform bicubic B-spline patch.

If Q_c is an irregular element, the limit surface is a piecewise B-spline patch. Depending on

the parameterization, the natural and the characteristic representations of the surface patch can be used for the parameterization. By means of the natural parameterization, the surface patch Q is defined by the mapping $s_Q : \Omega \rightarrow \mathbb{R}^3$ on the reference domain Ω . The mapping s_Q is defined by the weighted sum

$$s_Q(u, v) = \sum_{j \in I_Q} c_j b_j^*(u, v), \quad (u, v) \in \Omega,$$

where $\{b_j^*\}_{j \in I_Q}$ is the natural generating spline basis, with the patchwise representation

$$s_Q(u, v)|_{\Omega_k^n} = s_{k,n} \circ t_{k,n}(u, v) \quad (u, v) \in \Omega_k^n, \quad (4.1)$$

where $s_{k,n}$ is a regular B-spline parameterization, see Formula 3.2.2. Using the characteristic parameterization, the surface patch Q is given by a reparameterization of s_Q over the associated characteristic domain Ω_ν of Q_c . Thus, the mapping $s_Q \circ \chi^{-1} : \Omega_\nu \rightarrow \mathbb{R}^3$ is described by the weighted sum

$$s_Q \circ \chi^{-1}(\xi, \eta) = \sum_{j \in I_Q} c_j b_j^X(\xi, \eta), \quad (\xi, \eta) \in \Omega_\nu,$$

with the characteristic generating spline basis $\{b_j^X\}_{j \in I_Q}$. The patchwise representation is given by

$$s_Q \circ \chi^{-1}(\xi, \eta)|_{\Omega_\nu^{k,n}} = s_{k,n} \circ \chi_{k,n}^{-1}(\xi, \eta) \quad (\xi, \eta) \in \Omega_\nu^{k,n}, \quad (4.2)$$

where the mapping $\chi_{k,n}$ describes the subdomain $\Omega_\nu^{k,n}$ of the partitioned characteristic domain.

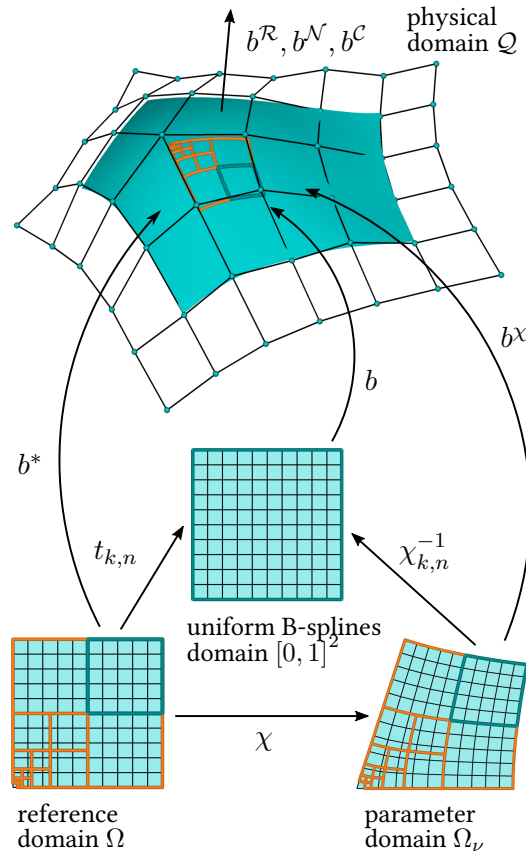


Figure 4.2: Element based basis functions. Schematic illustration of the domains and the appropriate generating splines together with the shape functions.

Using a parameterization, the limit surface \mathcal{Q} is therefore given by the union

$$\mathcal{Q} := \bigcup_{Q \subset \mathcal{Q}} Q$$

of all surface patches Q . Accordingly, if the control grid element Q_c is regular, then all three parameterizations can be used for representation of the related limit surface patch. However, the natural and the characteristic parameterizations are equivalent to the B-spline representation, see Section 3.3.2. In the irregular case, the choice of parameterization has an essential influence on the quality of the surface.

In the following, we consider different notions of element based basis functions. Depending on the representation and the domain, we distinguish between:

- the uniform B-spline basis b on $[0, 1]^2$, see Definition 4.3,
- the regular shape function $b^{\mathcal{R}}$ on the surface patch $Q \subset \mathcal{Q}$ in the physical space \mathbb{R}^3 with the reference domain $[0, 1]^2$,
- the natural generating spline basis b^* on the reference domain $\Omega = \bigcup_{k,n} \Omega_k^n = [0, 1]^2$, see Definition 4.4,
- the natural shape function $b^{\mathcal{N}}$ on the surface patch $Q \subset \mathcal{Q}$ in \mathbb{R}^3 with the reference domain Ω ,
- the characteristic generating spline basis b^{χ} on the characteristic domain $\Omega_{\nu} = \bigcup_{k,n} \Omega_{\nu}^{k,n} \subset \mathbb{R}^2$, see Definition 4.5,
- and, the characteristic shape functions $b^{\mathcal{C}}$ on the surface patch $Q \subset \mathcal{Q}$ in \mathbb{R}^3 with the reference domain Ω_{ν} .

The particular basis functions are illustrated in Figure 4.2. As imposed by the isoparametric approach, the same basis functions are used for the definition of the solution space as for the representation of the surface. The shape functions are characterized on the surface \mathcal{Q} and can be therefore defined by the pullback of the generating spline by the inverse of the associated surface parameterization. In this context, it is important to remember that for a given surface representation the generating splines represent the basis for the parameterization of the surface \mathcal{Q} , whereas the shape functions are defined on the surface \mathcal{Q} and specify the basis of the function space over \mathcal{Q} .

Accordingly, we distinguish between the regular and irregular element. If the corresponding control grid element Q_c of $Q \subset \mathcal{Q}$ is regular, the reference domain Ω of the natural representation coincide with the characteristic domain Ω_{ν} and the B-spline domain $[0, 1]^2$. The generating spline $b^{\chi} = b^* = b$ is given by the 16 bicubic B-spline basis functions b_j , $j = 0, \dots, 15$. Therefore, the shape functions can be summarized by a single definition, that is, the shape functions for a regular element are defined by

Definition 4.3 (Regular finite element). Given the regular representation s_Q of a surface patch $Q \subset \mathcal{Q}$ that is related to a regular element $Q_c \in \mathcal{C}_Q$. The *regular shape functions* $b_i^{\mathcal{R}} : Q \rightarrow \mathbb{R}$ on Q , $i \in I_Q$, are defined as the push-forwards of the uniform bicubic B-spline functions b_i , to be precise

$$b_i^{\mathcal{R}}(q) = b_i \circ s_Q^{-1}(q) \quad (4.3)$$

for $q \in Q$, where i is the index of the i th vertex in the one-ring of the element Q_c . The function space over the patch Q is given by

$$V_Q^{\mathcal{R}} = \{x_Q^{\mathcal{R}} \in \text{span} \{b_i^{\mathcal{R}}\} \mid i \in I_Q\}, \quad (4.4)$$

where $x_Q^{\mathcal{R}}$ is the *regular finite element* on Q . The set $I_Q \subset \mathbb{Z}$ is the one-ring index set of the regular element.

If the given control grid element Q_c of $Q \subset \mathcal{Q}$ is irregular, we consider the following definitions:

Definition 4.4 (Natural finite element). Considering the natural parameterization s_Q of the patch $Q \subset \mathcal{Q}$. The *natural shape functions* $b_i^{\mathcal{N}} : Q \rightarrow \mathbb{R}$, $i \in I_Q$, on Q are defined as the push-forwards of the natural generating spline functions b_i^* (see Definition 3.3), i.e.

$$b_i^{\mathcal{N}}(q) = b_i^* \circ s_Q^{-1}(q) \quad (4.5)$$

for $q \in Q$, where $i \in I_Q$ is the index of the i th vertex in the one-ring of the according control grid element Q_c . The function space over Q is given by

$$V_Q^{\mathcal{N}} = \{x_Q^{\mathcal{N}} \in \text{span} \{b_i^{\mathcal{N}}\} \mid i \in I_Q\}, \quad (4.6)$$

where $x_Q^{\mathcal{N}} : Q \rightarrow \mathbb{R}^n$ is the *natural finite element* mapping over the surface patch Q . The set $I_Q \subset \mathbb{Z}$ is the one-ring index set of element Q_c .

Due to the continuity of the basis functions, the function space over the whole surface \mathcal{Q} is given by the union of all element function spaces. Considering the natural parameterization of \mathcal{Q} , the function space V_h is given by the set

$$V_h = \bigcup_Q V_Q^{\mathcal{N}} = \left\{ x^{\mathcal{N}} = \bigcup_Q x_Q^{\mathcal{N}} \mid x_Q^{\mathcal{N}} \in V_Q^{\mathcal{N}} \right\}.$$

However, if an element is regular, we will use the regular finite element. Equivalently, the natural shape space V_h can be described by

$$V_h = \bigcup_{Q \text{ reg}} V_Q^{\mathcal{R}} \cup \bigcup_{Q \text{ irreg}} V_Q^{\mathcal{N}} = \left\{ x^{\mathcal{N}} = \bigcup_{Q \text{ reg}} x_Q^{\mathcal{R}} \cup \bigcup_{Q \text{ irreg}} x_Q^{\mathcal{N}} \mid x_Q^{\mathcal{R}} \in V_Q^{\mathcal{R}} \text{ and } x_Q^{\mathcal{N}} \in V_Q^{\mathcal{N}} \right\}.$$

The natural finite element is a common approach appearing in the subdivision finite element literature. Nevertheless, a precise definition hasn't been introduced to the community.

Finally, based on the characteristic representation, we introduce a new subdivision finite element approach.

Definition 4.5 (Characteristic finite element). We consider the reparameterization of s_Q over the characteristic domain given by $s_Q \circ \chi^{-1}$. The *characteristic shape functions* $b^{\mathcal{C}} : Q \rightarrow \mathbb{R}$ over surface patch $Q \subset \mathcal{Q}$ are defined as the push-forwards of the characteristic generating spline functions $b_i^{\mathcal{X}}$ (see Definition 3.10), i.e.

$$b_i^{\mathcal{C}}(q) = b_i^{\mathcal{X}} \circ \chi \circ s_Q^{-1}(q) \quad (4.7)$$

for $q \in Q$, where $i \in I_Q$ is the index of the i th vertex in the one-ring of the related control grid

element Q_c . The function space over the surface patch Q is given by

$$V_Q^C = \{x_Q^C \in \text{span} \{b_i^C\} \mid i \in I_Q\}, \quad (4.8)$$

where $x_Q^C : Q \rightarrow \mathbb{R}^n$ is the *characteristic finite element* over the surface patch Q .

The definition of the element is based on the characteristic parameterization and therefore consistent with the classical subdivision surfaces. The reference domain of an element is given by the characteristic domain Ω_ν that changes depending on the valence of the extraordinary vertex. The function space over the surface Q is described equivalently to the natural function space by

$$V_h = \bigcup_{Q \text{ reg}} V_Q^R \cup \bigcup_{Q \text{ irreg}} V_Q^C = \left\{ x^C = \bigcup_{Q \text{ reg}} x_Q^R \cup \bigcup_{Q \text{ irreg}} x_Q^C \mid x_Q^R \in V_Q^R \text{ and } x_Q^C \in V_Q^C \right\},$$

with respect to the regular representation x_Q^R on regular grid elements.

4.2.2 Subdivision finite elements at a glance

The Catmull–Clark limit surface is a C^2 -continuous surface except at finitely many extraordinary vertices, where it is only $C^1 \cap H^2$ -continuous. It guarantees a high continuity of the approximation that is highly promising for the construction of finite elements assuring an appropriate regularity. Consequently, the Catmull–Clark subdivision provides a conforming finite element approach for PDEs up to fourth order.

The degrees of freedom, or the so-called nodal variables of the finite element model, are referring to the control vertices and the corresponding global basis functions given by the generalized B-splines. The generalized B-spline basis functions are not interpolating, unlike most shape functions. Consequently, nodal variables can not be interpreted by themselves, but only with reference to the basis functions. That is, the solution of a PDE is construed from a linear combination of the nodal variables weighted with the appropriate basis function. However, the support of each of the generalized B-spline basis function is spanned over the two-neighbourhood of the related control vertex. Considering the physical mesh, the global functions can be handled locally using the element-based shape functions. Here, the set of element-based functions is influenced by the valence of the element vertices. Additionally, the impact of the underlying basis functions goes beyond the vertices of an element, i.e. the vertices in the one-ring of the element are affected.

In contrast to the classical finite theory, the framework of a subdivision finite element does not coincide with the boundary of the reference domain. Due to the fact that the whole one-ring is affected by the set of element based basis functions, the subdivision finite element approach requires new concepts for surfaces with boundary, or, equivalently, for boundary value problems. This is due to the fact that, given a surface with boundary, the boundary elements have an incomplete one-ring. A possible approach could be to establish new basis functions that are compatible with the one-ring construction. However, in doing so, it is a non-trivial problem to determine basis functions fulfilling prescribed boundary conditions. Another idea would be to extend the control grid to complete the one-ring of the boundary element to satisfy the requirements for the element based generating spline. The treatment of boundary constraints compatible with the construction of subdivision surfaces is discussed in Chapter 5.

4.2.3 Derivatives on surfaces

Here, we briefly summarize some concepts relevant for the application of finite elements for the computation of integrals over curved surfaces. For the general definition, let Ω be an open set in \mathbb{R}^2 . We consider a mapping $s : \Omega \rightarrow \mathbb{R}^3$ from the reference domain Ω to the physical space \mathbb{R}^3 , such that

$$(u, v) \mapsto s(u, v).$$

The mapping s describes a regular surface \mathcal{Q} in \mathbb{R}^3 , i.e. s is a diffeomorphism. The Jacobian matrix of s is a 3×2 matrix defined by

$$J_s = (s_{,1} \ s_{,2}),$$

where the entries $s_{,i}$, $i \in \{1, 2\}$, are column vectors given by the partial derivatives of the surface mapping, i.e.

$$s_{,1} = \frac{\partial s(u, v)}{\partial u} \quad \text{and} \quad s_{,2} = \frac{\partial s(u, v)}{\partial v}$$

describing the independent tangent vectors of the surface. By $G_s = J_s^T J_s$ we denote the first fundamental form of s . Equivalently, we can write G_s as follows

$$G_s = \begin{pmatrix} g_{11} & g_{12} \\ g_{21} & g_{22} \end{pmatrix},$$

where $g_{ij} = s_{,i}^T s_{,j}$. The first fundamental form describes intrinsic measurements of the surface, as length and area, that do not depend on the position of the surface in the ambient space. The Jacobian determinant $|J_s|$ is defined by

$$|J_s| = \sqrt{\det(G_s)}.$$

It describes the change of the area in the surface element. Under the change of coordinates, the area element of s is defined by $ds = |J_s| \, dudv$, where the change is given by the absolute value of the Jacobian determinant J_s . If J_s is the Jacobian of s , such that G_s is invertible, then

$$J_s^\dagger = G_s^{-1} J_s^T, \tag{4.9}$$

where the operator J_s^\dagger is called the Moore–Penrose pseudo-inverse of J_s . The inverse of G_s is given by $G_s^{-1} = (g^{ij})_{ij}$, or, more precisely by

$$G_s^{-1} = \frac{1}{\det(G_s)} \begin{pmatrix} g_{22} & -g_{12} \\ -g_{21} & g_{11} \end{pmatrix}.$$

The pseudo-inverse describes the generalization of an inverse matrix for singular and non-quadratic matrices.

The unit normal vector of s can be determined by

$$n = \frac{s_{,1} \times s_{,2}}{|s_{,1} \times s_{,2}|}.$$

If n is continuous over Ω , then the surface s is orientable. The second fundamental form has the following matrix description

$$H_s = \begin{pmatrix} h_{11} & h_{12} \\ h_{21} & h_{22} \end{pmatrix},$$

where the coefficients can be computed by $h_{ij} = n \cdot s_{,ij}$. Thus, the vectors $s_{,ij}$ are the second partial derivatives of s . The second fundamental form depends on the position of the surface in the ambient space. It is used to describe different curvature types of the surface. One of the important curvatures is the mean curvature H , that measures the mean of the maximal and the minimal curvature at each point on the surface. Using the first and the second fundamental form, the formula describing H is given by

$$H = \frac{h_{11}g_{22} - 2h_{12}g_{12} + h_{22}g_{11}}{2(g_{11}g_{22} - g_{12}^2)}, \quad (4.10)$$

where the symmetry of G_s and H_s have been used. The two extremes are the two principal curvatures κ_1 and κ_2 . The principal curvatures correspond to the two eigenvalues of the shape operator, whereby the associated eigenvectors are the corresponding principal directions. The shape operator is given in terms of the components of the first and second fundamental form, i.e.

$$S = G_s^{-1}H_s.$$

The shape operator defines a type of extrinsic curvature. Thus, the mean curvature is equal to

$$H = \frac{\kappa_1 + \kappa_2}{2}.$$

To deal with PDEs on surfaces, we consider the smooth function $f : \mathbb{R}^3 \rightarrow \mathbb{R}$ defined over the image of the mapping s . In order to handle f , a standard procedure is to transform f onto the reference domain Ω of s . For this purpose, we consider the pullback of f by s through the smooth function composition

$$f(q) = f \circ s(u, v),$$

where $q = s(u, v) \in Q$ for $(u, v) \in \Omega$. The surface gradient ∇_Q is defined as the tangential part of the gradient ∇ of f in the physical space of s . It can be computed by the formula (see do Carmo [1993])

$$\nabla_Q f(q) = \left(J_s^\dagger \right)^T \nabla (f \circ s)(u, v), \quad (4.11)$$

for $q = s(u, v)$ and $(u, v) \in \Omega$ and the gradient $\nabla (f \circ s)(u, v)$ of the function $f \circ s$ in the reference domain. The gradient of $f \circ s$ in the reference domain is directly given by

$$\nabla (f \circ s)(u, v) = \left(\frac{\partial (f \circ s)(u, v)}{\partial u}, \frac{\partial (f \circ s)(u, v)}{\partial v} \right)^T.$$

Note, the surface gradient ∇_Q is similar to the conventional gradient ∇ , i.e. the surface gradient ∇_Q is the projection of the gradient ∇ onto the surface. The generalization of the Laplace operator Δ for operations on surfaces is described by the Laplace–Beltrami operator

$$\Delta_Q f = \text{div}_Q (\nabla_Q f),$$

where div_Q is the divergence operator on surface Q . The representation of the divergence of a vector X is

$$\text{div}_Q X = \frac{1}{\sqrt{\det G_s}} \left(\frac{\partial}{\partial u}, \frac{\partial}{\partial v} \right) \sqrt{\det G_s} J_s^\dagger X.$$

Like the Laplace operator, the Laplace–Beltrami operator is defined as the divergence of the gradient, where the gradient and the divergence operator in the context of surfaces are considered to be the surface gradient ∇_Q and the divergence operator div_Q . Hence, we obtain the following

formula for the Laplace–Beltrami of the mapping f :

$$\Delta_Q f = \frac{1}{\sqrt{\det G_s}} \left(\frac{\partial}{\partial u}, \frac{\partial}{\partial v} \right) \sqrt{\det G_s} G_s^{-1} \nabla (f \circ s) (u, v)$$

It describes the generalization of the Laplace operator Δ to operate on arbitrary surfaces, for instance, curved surfaces.

4.3 Integrals over subdivision surfaces

Let \mathcal{Q} be a smooth subdivision surface immersed in \mathbb{R}^3 . Furthermore, \mathcal{Q} can be represented by a piecewise generalized B-spline surface partitioned into patches $Q \subset \mathcal{Q}$. In this section, we derive some finite element concepts for solving PDEs defined on subdivision surfaces. This includes the projection of a function onto the subdivision finite element space V_h and the weak Laplacian of a pair of functions over the surface \mathcal{Q} . Considering the element based construction of the finite elements, both problems can be piecewise solved piece by piece over the patches Q of surface \mathcal{Q} .

4.3.1 Finite element projection

Let $x : \mathcal{Q} \rightarrow \mathbb{R}$ be a function described on the surface \mathcal{Q} . The projection of x onto a finite element space V_h is given by the integral of the product of x with a test function $v \in V_h$, i.e.

$$\int_{\mathcal{Q}} xv \, d\mathcal{Q}.$$

We refer here to the subdivision finite element space that is given by the union

$$V_h = \bigcup_{Q \subset \mathcal{Q}} V_Q$$

of the element based spaces V_Q . Each of the subspaces V_Q is finite-dimensional and can be determined by a basis $\{\beta_i\}_{i \in I_Q}$, where I_Q is the index set of the vertices in the one-ring of Q . Thus, we consider the restriction $x|_Q = x_Q$ of function x to an element $Q \subset \mathcal{Q}$. Using the basis functions β_i , we may write x_Q as the sum

$$x_Q = \sum_{i \in I_Q} x_i^Q \beta_i, \quad (4.12)$$

where x_i^Q is the coefficient of the expansion x_Q associated with the i th basis function β_i . By setting the test function to be equal to the basis, i.e. $v|_Q = v_Q = \beta_j$ for each $j \in I_Q$, the integral can be rewritten as follows

$$\int_{\mathcal{Q}} x\beta_j \, d\mathcal{Q} = \int_Q x_Q \beta_j \, dQ = \sum_i x_i^Q \int_Q \beta_i \beta_j \, dQ,$$

where

$$M_{ij}^Q = \int_Q \beta_i \beta_j \, dQ$$

is the integral of the product of basis functions β_i and β_j defined over Q . Moreover, M_{ij}^Q describes the ij th entry of the local mass matrix M^Q on element Q . Considering the global problem, i.e.

the integral over all surface patches $Q \subset \mathcal{Q}$ and all $\beta_j, j \in I_Q$, we obtain the formula

$$M = \sum_{Q \subset \mathcal{Q}} M^Q = \sum_{Q \subset \mathcal{Q}} \sum_{i,j \in I_Q} M_{ij}^Q,$$

where M is the global mass matrix. As can be seen, the assembling of the global mass matrix M is done locally, whereby the sums of integrals over each individual patch $Q \subset \mathcal{Q}$ have to be evaluated. Keep in mind, the local indices i and j of the element Q are related to the global indices of the vertices of the entire surface \mathcal{Q} . For each element, the local evaluation have to be postponed to the appropriate entries of the global system.

In the following, let \mathcal{Q} be the limit surface associated with the control grid \mathcal{C}_Q . For simplicity's sake, we distinguish between $Q_c \in \mathcal{C}_Q$ being a regular or an irregular control grid element. If Q_c is regular, then the surface patch $Q \subset \mathcal{Q}$ is specified to be a B-spline surface patch. Without the restriction to one of the two finite element approaches, the reference domain of Q is given by $[0, 1]^2$, and even $\Omega = \Omega_\nu = [0, 1]^2$. The pullback of the shape functions $b_j^{\mathcal{R}} : Q \rightarrow \mathbb{R}$ to the reference domain $[0, 1]^2$ is given by the composition

$$b_j^{\mathcal{R}}(q) = b_j \circ s_Q^{-1}(q) = b_j(u, v), \quad (4.13)$$

where s_Q is the parameterization of the surface patch Q with B-spline basis functions $b_j : \Omega \rightarrow \mathbb{R}$, $j \in I_Q$. Using the change of coordinates, the ij th entry M_{ij}^Q of the local mass matrix M^Q can be calculated from the formula:

$$M_{ij}^Q = \int_Q b_i^{\mathcal{R}}(q) b_j^{\mathcal{R}}(q) dQ = \int_{[0,1]^2} b_i(u, v) b_j(u, v) |J_{s_Q}| d\omega, \quad (4.14)$$

where J_{s_Q} is the Jacobian of the surface mapping s_Q and $|J_{s_Q}|$ is the related Jacobian determinant.

If the element Q_c of the control grid \mathcal{C}_Q is irregular, then the surface patch $Q \subset \mathcal{Q}$ is determined to be a piecewise B-spline patch. We distinguish between the natural and the characteristic finite elements, where $V_Q^{\mathcal{N}}$ and $V_Q^{\mathcal{C}}$ are the corresponding function spaces. For the natural approach, the reference domain Ω remains the same, whereas the characteristic domain Ω_ν depends on the valence ν of the extraordinary vertex.

Considering the natural finite elements, the shape function $b_j^{\mathcal{N}}$ is defined by the pullback of the basis function b_j^* (described in Formula 4.5) by the inverse of the surface parameterization, i.e.

$$b_j^{\mathcal{N}}(q) = b_j^* \circ s_Q^{-1}(q) = b_j^*(\bar{u}, \bar{v}), \quad (4.15)$$

where s_Q is the natural parameterization of the patch Q and $q \in Q$ is given by $q = s(\bar{u}, \bar{v})$. Based on the partition of the domain $\Omega = \bigcup_{k,n} \Omega_k^n$, the basis functions $b_j^* : \Omega \rightarrow \mathbb{R}$ can be described by the composition

$$b_j^*(\bar{u}, \bar{v})|_{\Omega_k^n} = \sum_{k,n} [S_{k,n}^T]_{j,\cdot} \cdot b \circ t_{k,n}(\bar{u}, \bar{v})|_{\Omega_k^n} = \sum_{k,n} [S_{k,n}^T]_{j,\cdot} \cdot b(u, v),$$

where $S_{k,n}$ is the subdivision matrix that maps onto the k th subpatch in the n th subdivision level described as $s_{k,n}$. Note, $s_{k,n}$ is related to the subdomain $\Omega_k^n \in \Omega$. The vector b is the regular generating spline with the 16 B-spline basis functions as entries. We denote by $\sum_{k,n} = \sum_n \sum_k$ the double sum for $k = 1, 2, 3$ and $n \geq 1$. The local mass matrix of the element Q can be calculated as follows:

Theorem 4.6. Let Q be a surface patch corresponding to an irregular control grid element. Using the natural approach, the element mass matrix M^Q is defined by the sum

$$M^Q = \lim_{n \rightarrow \infty} \sum_{k,n} S_{k,n}^T M^{kn} S_{k,n} \quad (4.16)$$

of integrals over the domain $[0, 1]^2$, where $S_{k,n} = P_k S_n$ is the subdivision matrix that localizes the k th subpatch in the n th subdivision level described by the mapping $s_{k,n} \subset Q$. The matrix M^{kn} is the local mass matrix of the domain characterized by $s_{k,n}$. The entries of M^{kn} are given by

$$M_{\sigma\tau}^{kn} = \int_{[0,1]^2} b_\sigma b_\tau |J_{s_{k,n}}| d\omega, \quad (4.17)$$

where b_γ is the γ th uniform B-spline basis function, for $\gamma = 0, \dots, 15$.

The matrix M^{kn} is a 16×16 -matrix that corresponds to the vertices in the one-ring of an element, which results from subdividing the element Q_c with matrix $S_{k,n}$. Applying $S_{k,n}$ to the matrix M^{kn} will distribute the entries to the degrees of freedom of the patch Q corresponding to the appropriate vertices in the one-ring of the element Q_c .

Proof. Let b_i^c and b_j^c be two shape functions described over the surface patch Q . The integral of the product of these functions over Q is defined by

$$M_{ij}^Q = \int_Q b_i^N b_j^N dQ$$

The function b_i^N fulfils the composition $b_i^N(q) = b_i^* \circ s_Q^{-1}(q)$ for $q \in Q$, such that $b_i^N(q) = b_i^*(\bar{u}, \bar{v})$ for $(\bar{u}, \bar{v}) \in \Omega$. Thus, it holds that

$$= \int_\Omega b_i^* b_j^* |J_{s_Q}| d\Omega$$

where $J_{s_Q} = (s_{Q,1} \ s_{Q,2})(\bar{u}, \bar{v})$ is the Jacobian of the mapping s_Q . Consider the infinite partition of Ω into Ω_k^n , see Figure 3.7. Using the restrictions to the subdomains Ω_k^n , we have

$$= \lim_{n \rightarrow \infty} \sum_{k,n} \int_{\Omega_k^n} (b_i^* \circ \iota_{k,n}) (b_j^* \circ \iota_{k,n}) |J_{s_Q}| \circ \iota_{k,n} |J_{\iota_{k,n}}| d\Omega_k^n$$

where $\iota_{k,n}$ is the identity map transforming to the domain Ω_k^n , with $|J_{\iota_{k,n}}| = 1$. Using the patchwise parameterization $s_Q|_{\Omega_k^n} = s_{k,n} \circ \iota_{k,n}$ of the surface s_Q , the restriction of the Jacobian determinant results in $|J_{s_Q}| \circ \iota_{k,n} = |J_{s_{k,n} \circ \iota_{k,n}}|$. For the basis functions, we obtain $b_i^* \circ \iota_{k,n} = [S_{k,n}^T]_{i, \cdot} b \circ \iota_{k,n}$. Hence, we consider the following infinite sum:

$$= \lim_{n \rightarrow \infty} \sum_{k,n} [S_{k,n}^T M_\Omega^{kn} S_{k,n}]_{i,j}$$

with the matrix M_{Ω}^{kn} described over the domain Ω_k^n . The term $[\]_{i,j}$ denotes the ij th entry of the given matrix. The entries $(M_{\Omega}^{kn})_{\sigma\tau}$ are defined by

$$\left(M_{\Omega}^{kn}\right)_{\sigma\tau} = \int_{\Omega_k^n} (b_{\sigma} \circ t_{k,n}) (b_{\tau} \circ t_{k,n}) |J_{s_{k,n} \circ t_{k,n}}| d\Omega_k^n.$$

Now, given $t_{k,n}^{-1}$, we transform Ω_k^n to the B-spline domain $[0, 1]^2$. Using the chain rule, we obtain the formula

$$= \lim_{n \rightarrow \infty} \sum_{k,n} \left[S_{k,n}^T M^{kn} S_{k,n} \right]_{ij}$$

with the matrix M^{kn} , where the entries $M_{\sigma\tau}^{kn}$ are given as in Equation 4.17. \square

As a result, the summands are characterized on the B-spline domain $[0, 1]^2$.

Considering the characteristic finite elements, the shape function b_j^C are defined by the pull-back of the basis function b_j^X (see Formula 4.7) by the inverse of the surface parameterization, this is

$$\bar{b}_j^C(q) = b_j^X \circ \chi \circ s_Q^{-1}(q) = b_j^X(\xi, \eta), \quad (4.18)$$

where $s_Q \circ \chi^{-1}$ is the parameterization of the surface patch Q described over the characteristic domain Ω_{ν} . The characteristic function χ and, equivalently, the characteristic domain Ω_{ν} are given depending on the valence of the extraordinary vertex. Using the partition of the domain $\Omega_{\nu} = \bigcup_{k,n} \Omega_{\nu}^{k,n}$, the basis functions $b_j^X : \Omega_{\nu} \rightarrow \mathbb{R}$ can be described by the composition

$$b_j^X(\xi, \eta) \Big|_{\Omega_{\nu}^{k,n}} = \sum_{k,n} [S_{k,n}^T]_j, b \circ \chi_{k,n}^{-1}(\xi, \eta) \Big|_{\Omega_{\nu}^{k,n}} = \sum_{k,n} [S_{k,n}^T]_j, b(u, v),$$

where $S_{k,n}$ is the subdivision matrix specifying the k th subpatch in the n th subdivision level described by the mapping $s_{k,n}$. Thus, $s_{k,n} \circ \chi_{k,n}^{-1}$ is described over the subdomain $\Omega_{\nu}^{k,n} \subset \Omega_{\nu}$. The vector b is the regular generating spline. The local mass matrix M^Q of element Q can be calculated using the following theorem.

Theorem 4.7. *Let Q be a surface patch corresponding to an irregular control grid element. Using the characteristic approach, the element mass matrix M^Q is given by the infinite sum*

$$M^Q = \lim_{n \rightarrow \infty} \sum_{k,n} S_{k,n}^T M^{kn} S_{k,n} \quad (4.19)$$

where $S_{k,n} = P_k S_n$ is the subdivision matrix that localizes the k th subpatch in the n th subdivision level. The matrix M^{kn} is the mass matrix of the subpatch $s_{k,n} \subset Q$. The entries of M^{kn} are given by

$$M_{\sigma\tau}^{kn} = \int_{[0,1]^2} b_{\sigma} b_{\tau} |J_{s_{k,n}}| d\omega, \quad (4.20)$$

where b_{γ} is the γ th uniform B-spline basis function, for $\gamma = 0, \dots, 15$.

Proof. Let b_i^C and b_j^C be two shape functions described over the surface patch Q . The integral of the product of these functions on Q is defined by

$$M_{ij}^Q = \int_Q b_i^C b_j^C dQ$$

The function b_i^c fulfils the composition $b_i^c(q) = b_i^x \circ \chi \circ s_Q^{-1}(q)$ for $q \in Q$, such that $b_i^c(q) = b_i^x(\xi)$ for $\xi \in \Omega_\nu$. Using the chain rule $(s_Q \circ \chi^{-1})'(\xi) = s_Q'(\chi^{-1}(\xi))(\chi^{-1})'(\xi)$, it holds that

$$= \int_{\Omega_\nu} b_i^x b_j^x \left| J_{s_Q \circ \chi^{-1}} \right| d\Omega_\nu$$

where $J_{s_Q \circ \chi^{-1}} = J_{s_Q} J_{\chi^{-1}}$, with $J_{s_Q} = (s_{Q,1} s_{Q,2})|_{\chi^{-1}(\xi)}$, for $J_{\chi^{-1}}$ (see Eq. 3.14). Consider the infinite partition of Ω_ν into the domains $\Omega_\nu^{k,n}$ (see Figure 3.12). Using piece by piece the restriction to $\Omega_\nu^{k,n}$, we have

$$= \lim_{n \rightarrow \infty} \sum_{k,n} \int_{\Omega_\nu^{k,n}} (b_i^x \circ \iota_{k,n}) (b_j^x \circ \iota_{k,n}) \left| J_{s_Q \circ \chi^{-1}} \right| \circ \iota_{k,n} |J_{\iota_{k,n}}| d\Omega_\nu^{k,n}$$

where $\iota_{k,n}$ is the identity map associated with the domain $\Omega_\nu^{k,n}$, where $|J_{\iota_{k,n}}| = 1$. Using the patchwise parameterization $s_Q|_{\Omega_k^n} \circ \chi^{-1} = s_{k,n} \circ \iota_{k,n} \circ \chi^{-1}$ of the surface s_Q , the restriction to $\Omega_\nu^{k,n}$ is given by $s_Q \circ \chi^{-1} \circ \iota_{k,n} = s_{k,n} \circ \chi_{k,n}^{-1}$. The restriction of the Jacobian determinant results in $\left| J_{s_Q \circ \chi^{-1}} \right| \circ \iota_{k,n} = \left| J_{s_{k,n} \circ \chi_{k,n}^{-1}} \right|$. For the basis functions, we have: $b_i^x \circ \iota_{k,n} = \left[S_{k,n}^T \right]_{i,\cdot} b \circ \chi_{k,n}^{-1}$. Hence, we consider the infinite sum:

$$= \lim_{n \rightarrow \infty} \sum_{k,n} \left[S_{k,n} M_\chi^{kn} S_{k,n} \right]_{i,j}$$

with the local matrices M_χ^{kn} , where the entries $(M_\chi^{kn})_{\alpha\beta}$ are defined by

$$\left(M_\chi^{kn} \right)_{\alpha\beta} = \int_{\Omega_\chi^{k,n}} (b_\alpha \circ \chi_{k,n}^{-1}) (b_\beta \circ \chi_{k,n}^{-1}) |J_{s_{k,n} \circ \chi_{k,n}^{-1}}| d\Omega_\nu^{k,n}.$$

Now, we transform $\Omega_\nu^{k,n}$ to the B-spline domain $[0, 1]^2$ by $\chi_{k,n}$. Using the chain rule, we have

$$= \lim_{n \rightarrow \infty} \sum_{k,n} \left[S_{k,n}^T M^{kn} S_{k,n} \right]_{i,j}$$

with the mass matrix M^{kn} , where the entries $M_{\alpha\beta}^{kn}$ are given as in Equation 4.20. \square

The integrand is therefore transformed onto the B-spline domain $[0, 1]^2$ by the reparameterization onto the parameter domain Ω_ν , where we make use of the partition into the subdomains $\Omega_\nu^{k,n}$. Note, since the extraordinary vertex is just a null set, we do not pay attention to it calculating the integrals.

4.3.2 Weak Laplacian

In the following, we examine the integral corresponding to the weak Laplacian of x and v , a pair of mappings on the surface \mathcal{Q} . This is given by

$$\int_{\mathcal{Q}} \nabla_{\mathcal{Q}} x \cdot \nabla_{\mathcal{Q}} v \, d\mathcal{Q},$$

where $\nabla_{\mathcal{Q}}$ is the surface gradient described in Formula 4.11. As before, we consider the finite element space V_h described by the union of element-based subspaces V_Q , i.e.

$$V_h = \bigcup_{Q \subset \mathcal{Q}} V_Q,$$

where each V_Q is determined by the set of corresponding basis functions $\{\beta_i\}_{i \in I_Q}$. For the mappings x and v , the patchwise representations x_Q and v_Q on element Q are obtained as in Equation 4.12. The global integral can be therefore rewritten into the sum of integrals over the patches $Q \subset \mathcal{Q}$. This is given by

$$\int_{\mathcal{Q}} \nabla_{\mathcal{Q}} x \cdot \nabla_{\mathcal{Q}} v \, d\mathcal{Q} = \sum_{Q \subset \mathcal{Q}} \sum_{i,j} x_i \int_Q \nabla_Q \beta_i \cdot \nabla_Q \beta_j \, dQ \, v_j,$$

where

$$D_{ij}^Q = \int_Q \nabla_Q \beta_i \cdot \nabla_Q \beta_j \, dQ \quad (4.21)$$

is the weak Laplacian of the basis functions β_i and β_j over surface patch $Q \subset \mathcal{Q}$. The change of the Laplace–Beltrami operator $\nabla_{\mathcal{Q}}$ to ∇_Q is here just a renaming. This is due to fact that we consider the restriction of \mathcal{Q} to the patch Q that is done without requiring any further change of coordinates. The term D_{ij}^Q is the ij th entry of the local stiffness matrix D^Q . Moreover, the global problem given by the integral over the whole domain \mathcal{Q} results in the global stiffness matrix described by

$$D = \sum_{Q \subset \mathcal{Q}} D^Q = \sum_{Q \subset \mathcal{Q}} \sum_{ij} D_{ij}^Q. \quad (4.22)$$

We assemble the global matrix D by computing the local integrals over the subpatches $Q \subset \mathcal{Q}$, and postpone the results to the appropriate global matrix entries.

Given the limit surface \mathcal{Q} together with the control grid \mathcal{C}_Q , we consider the element $Q_c \in \mathcal{C}_Q$. Again, we distinguish between Q_c being a regular or an irregular element. If Q_c is regular, the set of basis functions on Q is given by the set of regular shape functions $\{b_i^{\mathcal{R}}\}_{i \in I_Q}$ based on the regular B-spline basis b_i , see Equation 4.13. By means of the change of coordinates, the ij th entry of the local stiffness matrix D^Q is described by the formula

$$D_{ij}^Q = \int_Q \nabla_Q b_i^{\mathcal{R}}(q) \cdot \nabla_Q b_j^{\mathcal{R}}(q) \, dQ = \int_{[0,1]^2} (\nabla b_i(u, v))^T G_{s_Q}^{-T} \nabla b_j(u, v) |J_{s_Q}| \, d\omega, \quad (4.23)$$

where b_i , $i \in I_Q$, is the i th uniform B-spline basis functions. The term ∇b_i is describing the usual gradient of the function b_i . Further, the term $G_{s_Q}^{-T}$ is the transposed inverse of the first fundamental form G_{s_Q} of the surface mapping $s_Q \equiv Q$.

If the element Q_c is irregular, then we distinguish between the natural and the characteristic finite elements given by the set of basis functions $\{b_j^{\mathcal{N}}\}_{j \in I_Q}$ and $\{b_j^{\mathcal{C}}\}_{j \in I_Q}$, respectively. For the natural approach, the pullback of the functions $b_j^{\mathcal{N}}$ is defined as in Equation 4.15. Before specifying the stiffness matrix D^Q , we firstly consider the surface gradient $\nabla_Q b_j^{\mathcal{N}}$ of basis function $b_j^{\mathcal{N}}$.

Theorem 4.8. Let Q be a surface patch corresponding to an irregular element Q_c in the control grid \mathcal{C}_Q . Considering the natural finite element, the surface gradient ∇_Q of the function $b_i^N \in V_Q^N$ can be transformed onto the B-spline domain $[0, 1]^2$ by

$$\nabla_Q b_i^N|_{s_{k,n}} = 2^n \left([S_{k,n}^T]_{i,\cdot} \nabla b(u, v) J_{s_{k,n}}^\dagger \right)^T \quad (u, v) \in [0, 1]^2$$

where $|_{s_{k,n}}$ denotes the restriction to the subpatch $s_{k,n} \subset Q$ defined over $[0, 1]^2$. The term $\nabla b(u, v)$ is given by the 16×2 -matrix and characterize componentwise the gradients of the vector entries $b_j(u, v)$, such that each row is equal to the 1×2 vector $(\nabla b_j)^T$. The term $J_{s_{k,n}}^\dagger$ denotes the Moore–Penrose inverse (see Formula 4.9) of the surface patch $s_{k,n}$.

Thus, the surface gradient $\nabla_Q b_i^C$ is determined piece by piece corresponding to the definition of the natural basis functions b_i^* . That is, the restriction of $\nabla_Q b_i^N$ to $s_{k,n}$ can be rewritten onto the B-spline domain $[0, 1]^2$.

Proof. For the basis function b_i^N , the surface gradient is given by

$$\nabla_Q b_i^N = \nabla_Q \left(b_i^* \circ s_Q^{-1} \right)$$

The function b_i^N fulfils the composition $b_i^N(q) = b_i^* \circ s_Q^{-1}(q)$ for $q \in Q$, such that $b_i^N(q) = b_i^*(\bar{u}, \bar{v})$ for $(\bar{u}, \bar{v}) \in \Omega$. Using the chain rule, we have

$$= \left(J_{s_Q}^\dagger \right)^T \nabla_\Omega b_i^*.$$

This describes the transformation onto the reference domain Ω . The term J_{s_Q} denotes the Moore–Penrose inverse of s_Q . We consider the partitioned domain $\Omega = \bigcup \Omega_k^n$. Using the restrictions to the subdomains Ω_k^n , we have

$$\left(J_{s_Q}^\dagger \right)^T \nabla_\Omega b_i^* \Big|_{\Omega_k^n} = \left(J_{s_Q}^\dagger \right)^T \circ \iota_{k,n} \nabla_\Omega (b_i^* \circ \iota_{k,n})$$

where $\iota_{k,n}$ is the identity mapping, such that $|J_{\iota_{k,n}}^\dagger| = 1$. Using the mapping $t_{k,n}$, we can write

$$= \left(J_{s_{k,n} \circ t_{k,n}}^\dagger \right)^T \lambda^{-n} \nabla_{\Omega_{k,n}} \left([S_{k,n}^T]_{i,\cdot} b \circ t_{k,n} \right)$$

Finally, the transformation onto the B-spline domain $[0, 1]^2$ is described by

$$= \left(\frac{1}{2} \right)^{-n} \left(J_{s_{k,n}}^\dagger \right)^T \left([S_{k,n}^T]_{i,\cdot} \nabla b \right)^T.$$

Due to the patchwise parameterization $s_{k,n}$ of the surface patch s_Q , the restriction of $\nabla_Q b_i^C$ to $\Omega_\chi^{k,n}$ is given by $s_{k,n} \circ \chi_{k,n}^{-1}$. The assumption is derived directly from this equality. \square

At this point, using the above determined surface gradient, the stiffness matrix D^Q is defined as follows:

Theorem 4.9. Let Q be a surface patch corresponding to an irregular control grid element. Using the natural approach, the integral of the product of the gradients of the shape functions b_i^N and b_j^N

defined on Q can be computed over the B-spline domain $[0, 1]^2$ using the equation

$$D^Q = \lim_{n \rightarrow \infty} \sum_{k,n} 4^n S_{k,n}^T D^{kn} S_{k,n}$$

where $S_{k,n} = P_k S_n$ is the subdivision matrix that localize the k th subpatch in the n th subdivision level. The matrix D^{kn} is the stiffness matrix of the subpatch $s_{k,n} \in Q$. The entries are defined by

$$D_{\sigma\tau}^{kn} = \int_{[0,1]^2} (\nabla b_\sigma)^T G_{s_{k,n}}^{-T} \nabla b_\tau |J_{s_{k,n}}| d\omega \quad (4.24)$$

where ∇b_γ is the gradient of the γ th uniform B-spline basis function, for $\gamma = 0, \dots, 15$. The term $G_{s_{k,n}}$ denotes the first fundamental form of the subpatch $s_{k,n}$.

Proof. We consider the ij th entry of the local stiffness matrix D^Q given by the weak Laplacian of the basis functions b_i^C and b_j^C . This is given by

$$D_{ij}^Q = \int_Q (\nabla_Q b_i^N)^T \nabla_Q b_j^N dQ$$

Using Theorem 4.8, we have

$$= \lim_{n \rightarrow \infty} \sum_{k,n} 2^{2n} \int_{[0,1]^2} [S_{k,n}^T]_{i,\cdot} \nabla b G_{s_{k,n}}^{-T} \left([S_{k,n}^T]_{j,\cdot} \nabla b \right)^T |J_{s_{k,n}}| d\omega$$

The rows of ∇b are given by the transposed gradients ∇b_γ , for $\gamma = 0, \dots, 15$. Hence,

$$= \lim_{n \rightarrow \infty} 4^n \sum_{k,n} \left[S_{k,n}^T D^{kn} S_{k,n} \right]_{ij}$$

for the matrix D^{kn} , where the entries $D_{\sigma\tau}^{kn}$ are given as in Equation 4.24. To determine the local matrix D^Q , we have to compute the weak Laplacian for all $i, j \in I_Q$. This coincides with the assumption of Theorem 4.9. \square

Accordingly, we consider a similar procedure for the characteristic finite elements $\{b_j^C\}_{j \in I_Q}$ (see Equation 4.18). The surface gradient ∇_Q can be determined by

Theorem 4.10. *Let Q be a surface patch corresponding to an irregular control grid element. Let λ be the subdominant eigenvalue of the subdivision matrix of the corresponding control element. Considering the characteristic generating spline b_χ , the surface gradient ∇_Q of the function b_i^C can be computed piece by piece over $[0, 1]^2$, this is given by the formula*

$$\nabla_Q b_i^C|_{s_{k,n}} = \lambda^{-n} \left([S_{k,n}^T]_{i,\cdot} \nabla b(u, v) J_{s_{k,n}}^\dagger \right)^T \quad (u, v) \in [0, 1]^2$$

where $|_{s_{k,n}}$ describes the restriction to the subpatch $s_{k,n}$. The term $\nabla b(u, v)$ be given by the 16×2 -matrix, that follows from the componentwise evaluation of the gradient of the vector entries $b_j(u, v)$, such that each row is equal to $\nabla b_j(u, v)$ corresponding to the 1×2 -vector of the partial derivatives of b_j . The term $J_{s_{k,n}}^\dagger$ denote the Moore-Penrose inverse of the surface patch $s_{k,n}$.

Proof. We consider the surface gradient

$$\nabla_Q b_i^C = \nabla_Q \left(b_\chi^i \circ \chi \circ s_Q^{-1} \right)$$

The function b_i^C fulfils the composition $b_i^C(q) = b_i^X \circ \chi \circ s_Q^{-1}(q)$ for $q \in Q$, such that $b_i^C(q) = b_i^X(\xi)$ for $\xi \in \Omega_\nu$. Using the chain rule, we have

$$= \left(J_{s_Q \circ \chi^{-1}}^\dagger \right)^T \nabla_\chi b_\chi^i$$

This is equal to the transformation onto the characteristic domain Ω_ν . The term $J_{s_Q \circ \chi^{-1}}$ is the Moore-Penrose inverse of $s_Q \circ \chi^{-1}$ (see Formula 4.9). We consider the partitioned domain $\Omega_\nu = \bigcup \Omega_\nu^{k,n}$. The restriction to the subdomain $\Omega_\nu^{k,n}$ is given by

$$\left(J_{s_Q \circ \chi^{-1}}^\dagger \right)^T \nabla_\chi b_\chi^i \Big|_{\Omega_\nu^{k,n}} = \left(J_{s_Q \circ \chi^{-1}}^\dagger \right)^T \circ \iota_{k,n} \nabla_\chi b_\chi^i \circ \iota_{k,n}$$

where $\iota_{k,n}$ is the identity mapping, i.e. $\left| J_{\iota_{k,n}}^\dagger \right| = 1$. Using Remark 3.8, we can write

$$= \left(J_{s_{k,n} \circ \chi_{k,n}^{-1}}^\dagger \right)^T \lambda^{-n} \nabla_{\chi_{k,n}} [S_{k,n}^T]_{i,\cdot} \circ b \circ \chi_{k,n}^{-1}$$

At this point, we consider the transformation onto the B-spline domain $[0, 1]^2$, this is equal to

$$= \lambda^{-n} \left(J_{s_{k,n}}^\dagger \right)^T \left([S_{k,n}^T]_{i,\cdot} \nabla b \right)^T.$$

Due to the patchwise parameterization $s_{k,n}$ of the mapping s_Q , the restriction of $\nabla_Q b_i^C$ to $\Omega_\nu^{k,n}$ is given by $s_{k,n} \circ \chi_{k,n}^{-1}$, which by applying to the last equality coincide directly with the assumption. \square

Consequently, the element stiffness matrix D^Q is defined by the following theorem.

Theorem 4.11. *Let Q be a surface patch corresponding to an irregular element in the control grid \mathcal{C}_Q . Using the characteristic finite elements, the integral of the product of the gradients of the shape functions b_i^C and b_j^C over the surface patch Q can be transformed onto the B-spline domain $[0, 1]^2$. By means of the transformation, the element stiffness matrix is defined by*

$$D^Q = \lim_{n \rightarrow \infty} \sum_{k,n} \lambda^{-2n} S_{k,n}^T D^{kn} S_{k,n}$$

where $S_{k,n} = P_k S_n$ is the subdivision matrix that localizes the k th subpatch in the n th subdivision level. The matrix D^{kn} is the stiffness matrix of the subpatch $s_{k,n} \in Q$. The entries $D_{\alpha\beta}^{kn}$ are given by

$$D_{\alpha\beta}^{kn} = \int_{[0,1]^2} (\nabla b_\alpha)^T G_{s_{k,n}}^{-T} \nabla b_\beta |J_{s_{k,n}}| dudv \quad (4.25)$$

where ∇b_γ is the gradient of the γ th uniform B-spline basis function, for $\gamma = 0, \dots, 15$. The term $G_{s_{k,n}}$ denotes the first fundamental form of the subpatch $s_{k,n}$.

Proof. We consider the ij th entry of the local stiffness matrix D^Q given by the weak Laplacian of the basis functions b_i^C and b_j^C , i.e.

$$D_{ij}^Q = \int_Q (\nabla_Q b_i^C)^T \nabla_Q b_j^C dQ$$

Using Theorem 4.10, we have

$$= \lim_{n \rightarrow \infty} \sum_{k,n} \lambda^{-2n} \int_{[0,1]^2} [S_{k,n}^T]_{i,\cdot} \nabla b G_{s_{k,n}}^{-T} \left([S_{k,n}^T]_{j,\cdot} \nabla b \right)^T |J_{s_{k,n}}| d\omega$$

The rows of ∇b are given by the transpose of the gradients ∇b_γ of the B-spline basis function b_γ , for $\gamma = 0, \dots, 15$. Consequently, we obtain

$$= \lim_{n \rightarrow \infty} \lambda^{-2n} \sum_{k,n} \left[S_{k,n}^T D^{kn} S_{k,n} \right]_{ij}$$

where the entries $D_{\alpha\beta}^{kn}$ of the stiffness matrix D^{kn} are given as in Equation 4.25. \square

Considering the representation of the mass and the stiffness matrix assembled by means of the natural or the characteristic finite element approach, we refer to the transformation of the associated integrals onto the B-spline domain $[0, 1]^2$ using the Jacobian and the Moore–Penrose pseudo-inverse (see Formula 4.9). By means of these representations, to compute the mass and the stiffness matrices, we can easily make use of numerical methods.

Even through the complicated definition of the characteristic parameterization and, correspondingly, the characteristic finite elements, the computation of the integral representation is comparable to using the natural approach. To be exact, the definitions of the mass matrices are equal for both approaches.

Additionally, although the formulas of the stiffness matrices look similar, considering the surface gradients, there is a difference given by the emerging scalar factor. In the case of the natural approach with the reference domain Ω , the factor is equal $1/2$ and do not change for the underlying element type. That is, no distinction is made between elements with extraordinary vertices of different valences. On the other hand, for the characteristic shape functions with the reference domain given by the characteristic domain Ω_ν , the factor λ emerge that depends on the valence of the extraordinary vertex of the element, see Theorem 4.10. Keep in mind, λ is the subdominant eigenvalue and therefore coincides with the scaling behaviour of the characteristic mapping, see Section 3.3.1.

4.4 Assembly tasks

In this section, we are interested in the assembling of the matrices presented in the previous section. The given matrices arise when applying subdivision finite elements to the weak form of various PDEs, as for example Poisson’s equation, the eigenvalue problem and the mean curvature flow. On the latter issue, we consider this geometric flow in the following chapter.

We consider the mass and the stiffness matrix described by the appropriate integrals over a given subdivision surface, see Section 4.3.1 and 4.3.2. Because of the complexity of the problems, in particular considering curved limit surfaces, it is inevitable to use numerical methods for the computation of the integrals. Accordingly, the approximation of the integrals can be calculated by applying the numerical quadrature. The following sections present some assembling details that emerge in the context of computing the given PDE problems on Catmull–Clark subdivision surfaces.

4.4.1 Numerical integration

As a general task of the previous section, an integral over the subdivision surface \mathcal{Q} can be first rewritten into a sum of integrals on the surface patches $Q \subset \mathcal{Q}$ describes the physical mesh

on surface \mathcal{Q} . Next, every summand is transformed onto the B-spline domain given by the unit square $[0, 1]^2$. Consequently, this representation can be used to compute the integrals using numerical integration. In the following, we give an overall view on how to apply numerical integration to the presented problems.

For a general function $f : \mathcal{Q} \rightarrow \mathbb{R}$ defined on the surface \mathcal{Q} , we consider the partition of \mathcal{Q} into the set of subpatches Q and rewrite f into the sum

$$\int_{\mathcal{Q}} f \, d\mathcal{Q} = \sum_{Q \subset \mathcal{Q}} \int_Q f_Q \, dq,$$

where f_Q is the projection of f over Q . In doing so, the function f is restricted piece by piece to the surface patches $Q \subset \mathcal{Q}$. Depending on whether type the element Q is, the integral over Q is given by

$$\int_Q f(q) \, dq = \int_{[0,1]^2} (f \circ s_Q |J_{s_Q}|) (u, v) \, dudv,$$

if Q is regular, or

$$\int_Q f(q) \, dq = \lim_{n \rightarrow \infty} \sum_{k,n} \int_{[0,1]^2} (f \circ s_{k,n} |J_{s_{k,n}}|) (u, v) \, dudv$$

if Q is irregular, for $k = 1, 2, 3$ and $n \geq 1$. In particular, s_Q and $s_{k,n}$ are the parameterizations of the surface patches corresponding to a regular element and a regular subelement of an irregular element, respectively.

Using a quadrature scheme, the domain of the integrals has to be adjusted to the quadrature domain ω_q . To be precise, ω_q is here a quadrilateral domain in \mathbb{R}^2 that is prescribed by the scheme. The corresponding transformation is done by using a classical change of variables $g : \omega_q \rightarrow [0, 1]^2$. This is given by

$$\int_{[0,1]^2} (f \circ s |J_s|) (u, v) \, dudv = \int_{\omega_q} (f \circ s \circ g |J_s|_g |J_g|) (\tilde{u}, \tilde{v}) \, d\tilde{u}d\tilde{v},$$

where $s \equiv s_Q$ or $s \equiv s_{k,n}$. We examine the Jacobian determinant $|J_{s \circ g}| = |J_s|_g |J_g|$, where $|J_s|_g$ means that the Jacobian determinant $|J_s|$ have to be calculated at the point $g(\tilde{u}, \tilde{v})$ for $(\tilde{u}, \tilde{v}) \in \omega_q$. The Jacobian determinant $|J_g| = C \in \mathbb{R}$ of g is therefore constant. Furthermore, we consider here quadrature schemes based on interpolating functions. For such a kind of schemes, we can approximate the equation using the following formula:

$$\int_{\omega_q} (f \circ s \circ g |J_s|_g) (\tilde{u}, \tilde{v}) \, d\tilde{u}d\tilde{v} \approx \sum_{q=1}^G w_q (f \circ s \circ g |J_s|_g) (u_q, v_q),$$

where $(u_q, v_q) \in \omega_q \in \mathbb{R}^2$ are the so called quadrature points and w_q are the corresponding weights. This means that we can directly apply this to the mass and stiffness matrices characterized by integrals over the B-spline domain $[0, 1]^2$. As an example, the global mass matrix M of a regular control grid can be computed by the following formula

$$M \approx C \sum_{Q \subset \mathcal{Q}} \sum_{i,j \in I_Q} \sum_{q=1}^G w_q b_i \circ g(u_q, v_q) b_j \circ g(u_q, v_q) |J_{s_Q}|_g(u_q, v_q). \quad (4.26)$$

As a first result, to approximate an integral over a subdivision surface, we need to rewrite the integral into a sum over a possible to handle subdomains. Therefore, a proper quadrature rule

Rule	Index q	Quadrature points u_q	Quadrature weights w_q
$G = 1$	1	0	2
$G = 2$	1	$-\sqrt{\frac{1}{3}}$	1
	2	$\sqrt{\frac{1}{3}}$	1
$G = 3$	1	$-\sqrt{\frac{3}{5}}$	$\frac{5}{9}$
	2	0	$\frac{8}{9}$
	3	$\sqrt{\frac{3}{5}}$	$\frac{5}{9}$
$G = 4$	1	$-\sqrt{\frac{3}{7} + \frac{2}{7}\sqrt{\frac{6}{5}}}$	$\frac{18-\sqrt{30}}{36}$
	2	$-\sqrt{\frac{3}{7} - \frac{2}{7}\sqrt{\frac{6}{5}}}$	$\frac{18+\sqrt{30}}{36}$
	3	$\sqrt{\frac{3}{7} - \frac{2}{7}\sqrt{\frac{6}{5}}}$	$\frac{18+\sqrt{30}}{36}$
	4	$\sqrt{\frac{3}{7} + \frac{2}{7}\sqrt{\frac{6}{5}}}$	$\frac{18-\sqrt{30}}{36}$

Table 4.1: Gaussian quadrature. Quadrature points and weights for $G = 1, 2, 3, 4$ evaluation knots in the one-dimensional case.

have to be found in order to obtain an adequate approximation.

Within the framework of this thesis, the numerical integration is done using the Gaussian quadrature. The Gaussian quadrature is an interpolation function based quadrature method known for the exact integration of univariate polynomial functions up to a prescribed degree. For bivariate functions on square elements that are described by tensor products of appropriate one-dimensional formulas, the same can be applied to the integration rules, i.e. a tensor product quadrature method can be used for the approximation. Here, we use the 2D Gauss quadrature. The notation " G^2 " that means we apply G points in each variable of the to be integrated function. This provides G^2 evaluation points for the total integral over a regular element. For the quadrature in one-dimension, we obtain the Gauss–Legendre-integration with the quadrature domain $[-1, 1]$, where the quadrature points $u_q, q = 1, \dots, G$, and the weights w_q are prescribed by the choice of evaluation points. According to that, we get an exact result for polynomials of degree $2G - 1$ or less by using a suitable choice of points u_q and weights w_q . In Table 4.1, the quadrature points and weights for different number G of evaluation knots are given. For the two-dimensional quadrature, the integration domain is given by $[-1, 1]^2$. The quadrature points (u_{q_1}, u_{q_2}) are given by all possible permutations of two quadrature points in one-dimension. The corresponding weights w_q are therefore given by the products $w_q = w_{q_1} w_{q_2}$.

4.4.2 Index finding routine

Given an arbitrary subdivision surface together with its control grid, we want to calculate integrals over the surface described in the Section 4.3. The size of the global matrices is prescribed by the number of the vertices in the control grid. This is due to the fact that for each control vertex, a global basis function is described by the appropriate generalized B-spline basis function, see Section 3.2.5. The support of a generalized B-spline is equal to the two-neighbourhood of the corresponding vertex. To assemble the problem matrices using the global basis, the loop through all the pairs of basis functions has to be performed. In doing so, we make the effort to integrate functions on the surface, for which we know that their support do not overlap, and, consequently, the integral is equal zero. In Section 4.3.1 and 4.3.2 was shown that using the ele-

ment based finite elements the effort can be reduced, i.e. the global problem is given by a set of local integrals defined over the patches of the surface. Consequently, instead of assembling the global matrix by passing through all pairs generalized B-spline functions, as it is indicated by the global matrix formulation, we run through all elements and all pairs of the generating spline functions, and construct local matrices.

The local matrix is obtained through the restriction of the global integral to a given surface patch. The size of a local matrix depends on the one-ring of the element. Let K describe the number of vertices in the one-ring. Keep in mind, K is changing due to the valence of the extraordinary vertex. Considering the definition of the local mass and stiffness matrices introduced in Section 4.3, the local matrices are $K \times K$ -matrices. For a given pair β_i and β_j of local basis functions, $i, j \in \{0, \dots, K-1\}$, and a given quadrature point $(u_q, v_q) \in \mathbb{R}^2$, the evaluation returns the value of the integrals with respect to the physical coordinates. The local matrix is obtained through the calculation of all the index pairs (i, j) of the basis functions in all quadrature points of the quadrature method, where the assemblies have to be added to the appropriate matrix entry. The advantage of the local evaluation is taken in order to reduce the amount of assembling work. For each element we obtain a dense local matrix, i.e. all element based integrals are non-zero. Given a fully validated local matrix, this have to be transferred into the appropriate entries of the global matrix. This is done by means of the local-global index correspondence is describing the ordering of the indices in the global grid restricted to the local ordering. Considering the local-global index correspondence, we construct a correlation array that links the local numbering described by the order of the vertices in the one-ring, with the global numbering of the vertices in the total control grid. For a surface patch Q , let $Q_c \in \mathcal{C}_Q$ be the associated control grid element together with its one-ring. Let $I_Q = 0, 1, \dots, K-1$ be the index set with the prescribed order of the vertices in the one-ring of element Q_c . The ordering of the vertices in the one-ring of an element is shown in Figure 3.3. The correlation array Π_Q is given by the tuple

$$\Pi_Q = (\pi_0, \dots, \pi_{K-1}),$$

where $\pi_i \in I_Q$, $i \in I_Q$, is the global index corresponding to the i th vertex in the one-ring of Q . K is the number of vertices in the one-ring and the set I_Q is the set of global indices. Next, given a local index i , the corresponding global index a is described by

$$a = [\Pi_Q]_i = \pi_i.$$

On the other hand, let a be a global index. Firstly, we have to find the elements in \mathcal{C}_Q that contains a in the one-ring. Is the element Q_c one of these elements, the local index of a is therefore given by

$$\Pi_Q(a) = i,$$

where i is the position of the a in the local array Π_Q . An example of an correlation array is given

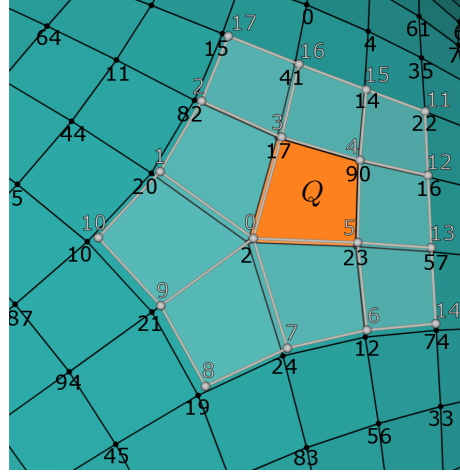


Figure 4.3: Correlation array. An example of the correlation array of element Q : $\Pi_Q = (2, 20, 82, 17, 90, 23, 12, 24, 19, 21, 10, 22, 16, 57, 74, 14, 41, 15)$. The black numbers are the global indices of the control grid, the grey numbers are the vertex indices in the one-ring of element Q_c corresponding to surface patch Q .

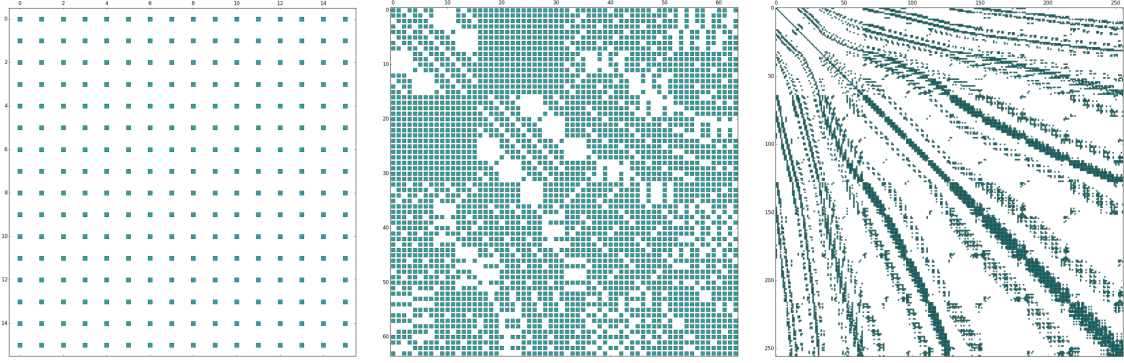


Figure 4.4: *Matrix sparsity plots.* On the example of the closed control grids of increasing resolution shown in Figure 4.5 with 16, 64 and 256 vertices, the plots illustrate the non-zero entries (blue dots) of the corresponding mass matrices. The control grids are regular, this means, for each vertex at most 49 entries are non-zero.

in Figure 4.3. Note, the size of the correlation array is adjusted to the changing element one-ring.

Given a fully calculated local matrix of element Q , each matrix entry can be added to the appropriate entry in the global matrix that is assembled by the means of the correlation array. This is, for the ij th entry there is a global entry ab described by

$$a = [\Pi_Q]_i \text{ and } b = [\Pi_Q]_j,$$

for $i, j \in I_Q$ and $a, b \in I_Q$. The assembling of the global matrix is given by adding up the series of local assemblies. In the end, each entry of the global matrix is given by the sum of the corresponding local entries. In this way, we only take non-zero integrals into the calculation. Note, the global matrix is sparse, due to the size of the two-neighbourhood support of the global basis. Therefore, the patches Q that contribute to the assembling of the global entry lie in the intersection of the two-neighbourhood of the vertices with the indices a and b . For a fixed vertex a , the support of the intersection with a second basis is non-zero, if the corresponding vertex b belongs up to the three-neighbourhood of vertex a .

Compared to classical element-based finite elements, the larger support of the subdivision basis functions result is an increased bandwidth of the global matrix. For example, for a basis function that is related to a regular vertex, such that all vertices in its two-neighbourhood are regular, we obtain overlaps with 49 neighbouring basis functions. This means, the degree of freedom of this vertex is affected by 49 non-zero entries in the corresponding row of the matrix. As a visual reinforcement, sparsity plots of the mass matrices for the geometries shown in Figure 4.5 are shown in Figure 4.4.

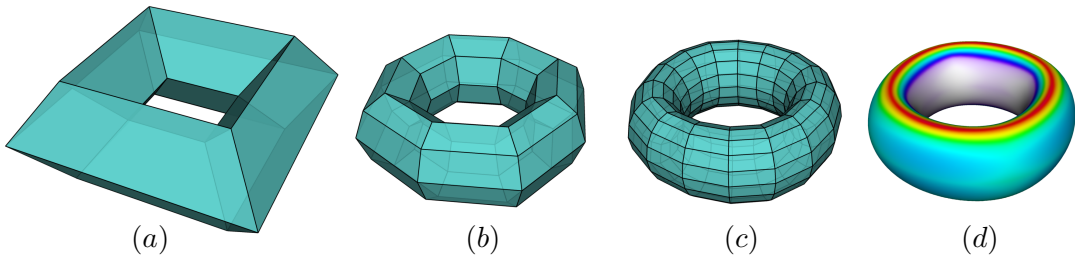


Figure 4.5: *Regular control grids.* Illustration of the control grids used in the experiment: (a) the initial grid: Torus 1, (b) its first subdivision: Torus 2, and (c) its second subdivision: Torus 3. Due to the properties of the subdivision concept, the image of limit surface is identical for all grids. The limit surface is shown in (d). It is coloured by its mean curvature. Note, although the vertices of the initial grid are lying on a torus, the limit surface is not a well-formed torus any more.

4.4.3 Appropriate quadrature rule

In the following, we want to find a sufficiently accurate quadrature method to solve the presented integrals numerically. A closer look at the integrands shows that if the surface is curved the functions are non-polynomial, i.e. the functions to be integrated are products of B-spline functions and/or its derivatives. Although B-splines are simple polynomials, the integrands are rational functions. The reason for this is the non-constant Jacobian determinant $|J|$ or the inverse G^{-1} of the first fundamental form. Both appear because of the transformation of variables from the surface patch onto the parameter domain $[0, 1]^2$. On the other hand, due to Strang's Lemma, an exact integration is not needed to obtain the optimal convergence rate of finite element solutions, see Strang and Fix [1973], Ch. 4. In particular, the quadrature error has to preserve the interpolation error. However, a necessary task for the future is to find a numerical integration scheme for non-polynomial functions.

In the following, although all known quadrature schemes are unsuitable for nonpolynomial functions, we will use the Gaussian quadrature. In [Cottrell et al., 2009], the authors has stated that the choice of evaluation points for the Gaussian quadrature can be made according to the degree of the basis functions. In our case, the basis functions are bicubic polynomials and their derivatives are biquadratic. Thus, a 3^2 - or 2^2 -point quadrature should be sufficient. Because of the fact that the integrands are non-polynomial, this argumentation is inappropriate. Thus, an exact result cannot be achieved using Gaussian quadrature. However, this method seems to be very effective, see [Nguyen et al., 2014; Jüttler et al., 2016]. To determine a sufficient choice of the quadrature, i.e. the number of quadrature points and the subdivision depth in the case of irregular elements, we perform a bunch of research to make a reasonable decision.

Due to the different requirements on the presented integrals, we distinguish between regular and irregular elements. Given a regular element, we can use two different finite element discretizations. That is, a discretization based on the regular approach that can be used only for regular elements, see Formula 4.3, and the piecewise approach. The latter is applicable especially to irregular elements, but can be used also for a regular element. Using the regular approach, the shape functions $b^{\mathcal{R}}$ are given by polynomials of bi-degree three. In this case, the evaluation of the integral is done in one go. For the piecewise approach, one of the vertices of the element has to be treated as extraordinary. Moreover, we consider two piecewise representations, the natural and characteristic representation described in Formula 4.5 and 4.7, respectively. Note, for a regular element, both approaches are equal. This is because of the fact that the subdominant eigenvalue λ of the subdivision matrix of a regular element is equal $1/2$. Furthermore, the corresponding shape functions $b^{\mathcal{N}}$ and $b^{\mathcal{C}}$ are piecewise polynomials of bi-degree three. The integration of piecewise polynomials leads to a set of integrals over the regular pieces of the surface patch. Consequently, we have to apply the Gaussian quadrature to each of the summands, see Section 4.3.1 and 4.3.2. Due to the infinite sums, we have to be satisfied with an another approximation applying Gaussian quadrature up to a chosen subdivision level. We assemble the mass matrix and the stiffness matrix for both types of finite elements using 2^2 -, 3^2 - and 4^2 -point Gaussian quadrature. To verify the results, we calculate the Frobenius norm and the row-sum norm of the matrices.

In the following, we are aiming to find the appropriate number of quadrature knots for the integration on regular elements. In the experiment, we consider control grids with only regular elements, where the initial grid is given by a closed grid its points lie on a torus, see Figure 4.5. Due to the B-spline representation, the limit surfaces is not a torus any more. For comparison, we consider meshes with an increased number of vertices obtained by subdividing the initial grid two times, see Figure 4.5. Moreover, considering the piecewise approach, the quadrature has been done up to different subdivision levels. In table 4.3 and 4.4 the row-sum norms and

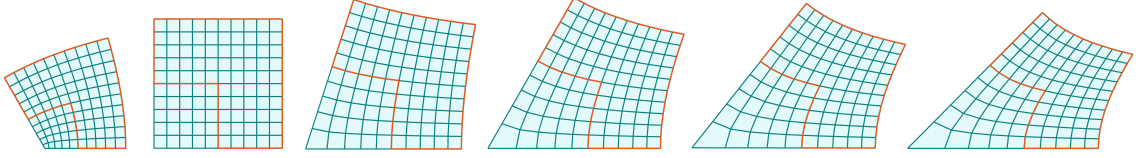


Figure 4.6: *Ratio of regular subpatches. The characteristic domains Ω_ν for different valences $\nu = 3, 4, 5, 6, 7, 8$ of the extraordinary point are illustrated. Note the changing ratio of the three regular subdomains $\Omega_\nu^{k,1}$ all together (orange frame), $k = 1, 2, 3$, to the remaining part of Ω_ν .*

the Frobenius norms of the mass matrices are shown, respectively. Additionally, in Table 4.5 and 4.6 the row-sum norms and the Frobenius norms of the stiffness matrices are shown (see end of this chapter). Comparing the results, the more quadrature knots are used, the better the results seems to be. That is, for the piecewise approach, the norms seems to converge to the norm using the regular approach with 4^2 quadrature points. Consequently, for regular elements, we decide to use the regular approach, including a 4^2 -point Gaussian integration. Considering the piecewise approach, a closer look at the results shows that the 3^2 - and 4^2 -point Gaussian quadrature produces comparably similar results for each of the presented levels of subdivision. In order to minimize the evaluation cost, we relay on a 3^2 -point Gaussian quadrature for the piecewise approach. Additionally, we take the 9th subdivision level as a reference for the integration on regular elements. This provides for the mass and stiffness matrices over an regular element an $O(10^{-6})$ Frobenius norm convergence to the reference value of the regular approach using 4^2 -point Gaussian quadrature.

Considering integrals on irregular elements, thus only the piecewise approaches are relevant for the representation of the surface. Related to this, the natural and the characteristic approach is represented by an infinite sum of integrals. In [Nguyen et al., 2014], the authors are confident with an evaluation up to level seven in terms of the natural approach. Keep in mind that this approach does not pay attention to the valence of the irregularity. That is, the reference domain of each irregular element is given by the partitioned domain Ω , whereby in our approach the reference domain changes accordingly. In the following, we want to find an appropriate number of subdivision levels for a sufficient approximation of the infinite sum of integrals over the corresponding subelements. For the characteristic approach, we additionally take care about the changing reference domain, according to the valence of the extraordinary vertex. According to this, we determine a valence dependent condition for the choice of subdivision levels for the integration on irregular elements with different irregularities.

At this point, let Q_c be an irregular element with an extraordinary vertex of valence ν . For the associated characteristic domain Ω_ν , we obtain the partitioned representation of the domain $\Omega_\nu = \bigcup_{k,n} \Omega_\nu^{k,n}$, see in Section 3.3.1, where $\Omega_\nu^{k,n}$ is the k th subdomain in the n th subdivision level of Ω_ν . For this purpose we assume that the area of Ω_ν is equal

$$\int_{\Omega_\nu} d\xi d\eta = 1.$$

We denote by A_n the area of the three subdomains $\Omega_\nu^{k,n}$, $k = 1, 2, 3$, in the n th subdivision level. In Figure 4.6, we show the domain of the three subdomains $\Omega_\nu^{k,1}$. According to the valence of the extraordinary vertex, note the considerable change of the ratio of the joint domain of the three subdomains to the total characteristic domain Ω_ν . The area of the characteristic domain Ω_ν can be therefore rewritten in

$$1 = (1 - A_1) + A_1 = (1 - A_1 - A_2) + A_1 + A_2 = \dots = (1 - A_1 - \dots - A_n) + A_1 + \dots + A_n = \dots$$

	3	4	5	6	7	8
λ	0.410097	0.5	0.549988	0.579682	0.598510	0.611117
Error (%)						
$1 \cdot 10^{-5}$	7	9	10	11	12	12
$5 \cdot 10^{-6}$	7	9	11	12	12	13
$1 \cdot 10^{-6}$	8	10	12	13	14	15

Table 4.2: Subdivision levels for integration. Number of subdivision levels depending on the valence ν that is sufficient to integrate over the characteristic domain Ω_ν , except for a prescribed area error.

Due to the scaling property, the area after subtracting A_1 is given by

$$1 - A_1 = \int_{\lambda\Omega_\nu} d\xi d\eta = \lambda^2 \int_{\Omega_\nu} d\xi d\eta = \lambda^2,$$

and, consequently, we consider the formula $1 - A_1 - \dots - A_n = \lambda^{2n}$ for the remaining area of the characteristic domain Ω_ν after n subtractions. Now, to integrate at least over a specified portion A_ν of the characteristic domain, we consider the formula:

$$A_\nu < 1 - \lambda^{2n}, \quad (4.27)$$

where $1 - \lambda^{2n} = \sum_{i=1}^n A_i$ is prescribed by the number of subdivision levels. Therefore, we can decide for a precise number of subdivision levels for the integration. As stated above, for the regular element we pick the 9th subdivision level as a reference. This means, we do not integrate over around $\lambda^{2n} = 0.5^{18} < 5 \cdot 10^{-6}\%$ of the area of the unit square. This value describes an area error. It corresponds to the area of the portion of Ω_ν close to the extraordinary vertex over that we do not integrate. Based on the area error for the regular element with valence $\nu = 4$, we determine the number of subdivision levels for arbitrary valences. In Table 4.2, we show the results for different area errors and valences $\nu = 3, 4, 5, 6, 7, 8$.

Lvl	Torus 1			Torus 2			Torus 3		
	2^2	3^2	4^2	2^2	3^2	4^2	2^2	3^2	4^2
3	2.231020	2.231744	2.231756	0.641268	0.641265	0.641265	0.170561	0.170561	0.170561
5	2.263691	2.264415	2.264427	0.652192	0.652188	0.652189	0.172805	0.172805	0.172805
7	2.265726	2.266450	2.266462	0.652879	0.652876	0.652877	0.172944	0.172945	0.172945
9	2.265853	2.266577	2.266589	0.652922	0.652919	0.652920	0.172953	0.172953	0.172953
11	2.265861	2.266585	2.266597	0.652925	0.652922	0.652922	0.172953	0.172954	0.172954
Rgl	2.263683	2.265468	2.266603	0.653083	0.652904	0.652924	0.172946	0.172955	0.172954

Table 4.3: Evaluation of the row-sum norm of the mass matrices using the 2^2 -, 3^2 - and 4^2 -point Gaussian quadrature. We consider the regular approach (Rgl) and compare this with the piecewise approach where we apply the quadrature up to a prescribed subdivision level (Lvl).

Lvl	Torus 1			Torus 2			Torus 3		
	2^2	3^2	4^2	2^2	3^2	4^2	2^2	3^2	4^2
3	2.474550	2.475921	2.475905	1.247064	1.246974	1.246976	0.626446	0.626381	0.626382
5	2.510169	2.511538	2.511522	1.265854	1.265763	1.265765	0.635919	0.635854	0.635855
7	2.512383	2.513752	2.513736	1.267032	1.266941	1.266943	0.636514	0.636448	0.636450
9	2.512522	2.513890	2.513875	1.267106	1.267015	1.267017	0.636551	0.636486	0.636487
11	2.512530	2.513899	2.513883	1.267110	1.267020	1.267022	0.636553	0.636488	0.636489
Rgl	2.502769	2.512307	2.514004	1.271519	1.266799	1.267027	0.639064	0.636386	0.636490

Table 4.4: Evaluation of the Frobenius norm of the mass matrices using the 2^2 -, 3^2 - and 4^2 -point Gaussian quadrature. We consider the regular approach (Rgl) and compare this with the piecewise approach where we apply the quadrature up to a prescribed subdivision level (Lvl).

Lvl	Torus 1			Torus 2			Torus 3		
	2^2	3^2	4^2	2^2	3^2	4^2	2^2	3^2	4^2
3	7.315856	7.340588	7.340447	2.313356	2.318608	2.318599	0.630258	0.631582	0.631581
5	7.380651	7.405383	7.405242	2.330065	2.335316	2.335307	0.639797	0.641120	0.641120
7	7.384340	7.409072	7.408932	2.330995	2.336247	2.336238	0.640382	0.641706	0.641705
9	7.384570	7.409301	7.409161	2.331053	2.336305	2.336296	0.640418	0.641742	0.641742
11	7.384584	7.409315	7.409175	2.331057	2.336308	2.336300	0.640421	0.641745	0.641743
Rgl	6.799427	7.420669	7.409264	2.217221	2.337085	2.336314	0.613206	0.641814	0.641748

Table 4.5: Evaluation of the row-sum norm of the stiffness matrices using the 2^2 -, 3^2 - and 4^2 -point Gaussian quadrature. We consider the regular approach (Rgl) and compare this with the piecewise approach where we apply the quadrature up to a prescribed subdivision level (Lvl).

Lvl	Torus 1			Torus 2			Torus 3		
	2^2	3^2	4^2	2^2	3^2	4^2	2^2	3^2	4^2
3	8.960035	8.977788	8.977728	4.398076	4.405576	4.405576	2.228604	2.232251	2.232253
5	9.066537	9.084199	9.084140	4.451415	4.458884	4.458884	2.255917	2.259549	2.259551
7	9.072966	9.090622	9.090562	4.454651	4.462117	4.462117	2.257577	2.261207	2.261210
9	9.073367	9.091022	9.090963	4.454852	4.462318	4.462319	2.257680	2.261310	2.261313
11	9.073392	9.091047	9.090988	4.454865	4.462331	4.462331	2.257687	2.261317	2.261319
Rgl	8.745034	9.090202	9.091336	4.311921	4.462149	4.462367	2.189318	2.261111	2.261333

Table 4.6: Evaluation of the Frobenius norm of the stiffness matrices using the 2^2 -, 3^2 - and 4^2 -point Gaussian quadrature. We consider the regular approach (Rgl) and compare this with the piecewise approach where we apply the quadrature up to a prescribed subdivision level (Lvl).

CHAPTER 5

BOUNDARY CONDITIONS FOR PDEs

So far, we know how to handle closed limit surfaces. The corresponding control grids are closed too, the limit surface is thereby determined for each control grid element. In doing so, we are able to specify a complete one-ring structure (see Section 2.1.2) for each control grid element, this is needed for the evaluation of the limit surface or basis functions over the element. However, we do not want to limit ourselves to closed surfaces. In particular, we are interested in handling of surfaces with boundaries for our applications. Given a control grid with boundary, the one-ring of a boundary element is incomplete, see Definition 2.10. That is, elements are missing in the one-ring of such an element that are needed to assign the associated element based and, equivalently, subdivision basis functions. On the other hand, using the common subdivision method, there is no hierarchical subdivision of elements on the boundary, see Figure 3.2. This means, in order to handle the limit surface on the boundary, concepts to compensate this defect have to be found.

In this chapter, we present concepts to parameterize subdivision surfaces on boundary elements. We describe the required mathematical tools to construct surfaces with periodic boundaries, i.e. that can be reflected along the boundary, such that the extended surface fulfils the general smoothness given by the subdivision scheme, that is, the surface is C^2 -continuous everywhere except at the extraordinary vertices. Additionally, we review the boundary conditions for PDE problems known from the literature. As a result, based on the periodic boundary construction, we introduce boundary conditions within the subdivision finite elements that are suitable for the construction of periodic minimal surfaces. Regarding this, the proposed framework allows to reduce the evaluation of the total surface to an adequate symmetrical component. Additionally, our framework does not impose any combinatorial requirements upon the control mesh. It even allows for extraordinary vertices at the boundary.

5.1 Subdivision boundary issue

A general problem with B-spline based geometries is the handling of control grids with boundaries. The reason for this is that the boundary part of the surface is shrinking more and more in the course of subdivision, i.e. there are missing conditions to describe a hierarchical subdivision of the boundary elements. Considering the parameterization concept, the boundary elements are lacking of a complete one-ring structure too. Owing to missing information, the concept of generating spline cannot be used.

In the literature, different approaches have been proposed to get rid of the individual boundary issues, for instance, new subdivision rules, an extension of the control grid by an additional set of elements at the boundary, and sub-implicit pointwise boundary constraints. In general, all approaches require appropriate conditions to the boundary curve and the outer-pointing normal. By the outer-pointing normal we mean the vector in the tangent space of a point on the surface at the boundary that is perpendicular to the velocity vector of the boundary curve. However, each approach make use of additional elements along the boundary. It is noteworthy that the use of additional elements allows for extra freedom in defining and readjusting of the geometric boundary conditions.

Concerning the issue of new subdivision rules on the boundary, these are given by prescribing new masks for the repositioning of vertices along the boundary. For example, masks that meet the cubic endpoint interpolation rules for B-splines. This approach has been firstly presented in [Halstead et al., 1993; Biermann et al., 2000]. Thus, it allows for connecting additional surface patches without gaps and even for combining them with other surface representations supporting B-spline boundaries. However, this concept leaves too little flexibility. Every small change of constraints requires the complete recalculation of the subdivision rules.

In the second approach, additional elements along the boundary of the control grid have to be attached in order to complete the one-ring of the boundary elements. The newly added components are called artificial or ghost vertices and elements. The ghost components are treated as an extension of the control grid and have to be included in all calculations with respect to the boundary elements. Moreover, the extended geometry, called ghost geometry, is seen as a supplementary geometry of the original geometry.

In the literature, ghost elements have been introduced and used to handle thin shell boundary problems in [Schweitzer, 1996; Cirak et al., 2000]. The construction rules have been determined to be compatible with prior approaches in the engineering and the applied sciences area. Generally, the position of a newly added vertex is specified by means of point symmetry at the boundary. Consequently, the positions and the gradients at the boundary are fixed by the boundary and the ghost elements. In [Barendrecht, 2013], this standard boundary approach has been used to define boundary B-spline functions to avoid the construction of additional elements. A negative aspect of this idea is that we are anchored to only one kind of boundary constraints. Although the attachment of missing vertices and elements on the boundary can be a cumbersome and tedious procedure, we can use the common set of subdivision rules. The boundary elements can be therefore treated as any other element in the grid. Additionally, we gain an increased flexibility, due to the fact that changing the position of the vertices is providing a direct change of the boundary conditions, and vice versa.

Finally, the concept of so-called sub-implicit pointwise constraints has been firstly described in [Green, 2003] and used for solving boundary value problems on thin-shell structures. It is based on a minimization technique that also make use of the other two approaches. A ghost geometry is constructed, but in contrast to the previous concepts, the conditions can be applied to any point on the boundary of the surface. In doing so, conceptual similarities with the ghost geometry approach can be found, i.e. additional vertices will be taken into account to determine

the limit surface positions at the boundary. The conditions describing the positions, tangents and normals of points on the boundary base on the classical theory of subdivision surfaces. That is, the eigenvectors of the subdivision matrix are used to specify the points on the limit surface.

5.1.1 Point reflection

Boundary constraints obtained by adding new points and elements that are using point reflection along the boundary have been presented in [Cirak et al., 2000; Smith et al., 2004; Lacewell and Burley, 2007]. Consider a control grid with boundary, there are two possible configurations of the boundary element in the control grid. By that we mean that either one or rather two adjacent edges of a boundary element are boundary edges. In this manner, we distinguish between the so-called boundary or corner elements, respectively. Both configurations are shown in Figure 5.1. We require that after extending the control grid with ghost elements, the boundary points are regular points. Therefore, the non-boundary vertices are reflected through the boundary and the corner elements need a special treatment. As a result, constructing the ghost geometry by this convention causes the boundary of the limit surface to be a cubic B-spline curve.

Given a boundary element, we consider the incomplete one-ring. We will complete it as shown in Figure 5.1 (a). Therefore, the vertices of the boundary elements that are not contained in the boundary polygon will be reflected through the boundary vertices that share an edge with these vertices. The positions of the ghost vertices c_i , for $i \in \{0, 1, 2, 3\}$ can be generated due to the formula

$$c_i = 2c_{i+4} - c_{i+8}. \quad (5.1)$$

The boundary curve is parametrized by the curve $s(u, 0)$, $u \in [0, 1]$, along the boundary of the surface. Moreover, the boundary curve corresponding to this element is equivalent to the limit curve of the boundary polygon described by the vertices c_{i+4} , for $i \in \{0, 1, 2, 3\}$.

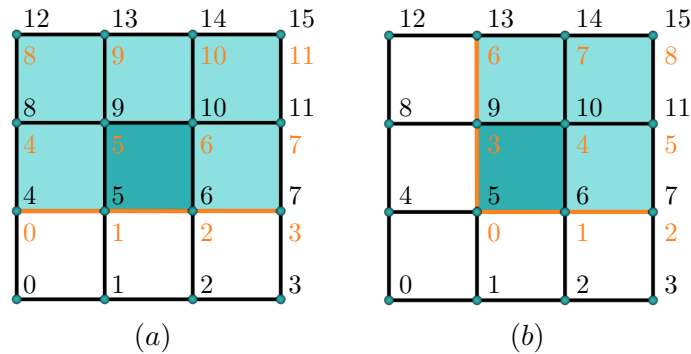


Figure 5.1: Illustration of (a) a boundary element and (a) a corner element in a control grid (blue) with boundary (orange line). The two corresponding elements are coloured in dark blue, whereas the existing geometry is shown by the blue quads. The newly added ghost elements are coloured in white. The order of the vertices in the complete one-ring (black indices) and the order for the calculation of the boundary functions (orange indices) is presented.

Given a corner element, we follow a similar approach. That is, we complete the one-ring of the corner element, in such a way that the two boundary edges are cubic B-splines. In doing so, for the vertex contained in both boundary edges, called corner vertex, it is required to be regular in the ghost geometry. The initial one-ring (coloured in blue) and the completed one-ring (all elements) of a corner element (coloured in dark blue) is shown in Figure 5.1 (b). After the extension, we obtain again a corner element in the ghost geometry. For all new ghost vertices except the ghost corner vertex, we calculate the position of the vertices c_i for $i = 1, 2, 3$ by $c_i = 2c_{i+4} - c_{i+8}$ and for $i = 4, 8, 12$ by $c_i = 2c_{i+1} - c_{i+2}$. The position of the corner vertex is

computed by

$$c_0 = 4c_5 + c_{10} - 2c_6 - 2c_9. \quad (5.2)$$

The boundary curves are two bicubic B-spline curves described by the vertices c_1, c_5, c_9, c_{13} and c_4, c_5, c_6, c_7 . Both curves can be also determined using the surface parameterization, whereby, either the first or the second argument is fixed to be zero, i.e. $s(0, v)$ or $s(u, 0)$ for all $u, v \in [0, 1]$, respectively. The limit position of the corner vertex is given by the surface point $s(0, 0)$.

Due to the linearity of the constraints, we can assign a set of boundary functions. These can be used to parameterize the boundary element without explicitly adding new vertices or elements. The set of boundary functions is determined in correspondence to the vertices in the incomplete one-ring of the boundary element. In the following, we assume that all boundary vertices have valence two or three. In this way, the one-ring of the boundary and the corner element is described by 12 and 9 control vertices, respectively. Consider the blue elements in Figure 5.1, where the dark blue element illustrates one of the described cases. For the boundary element, the control vertex matrix corresponding to the vertices in the incomplete one-ring is given by

$$C^T = (c_0, \dots, c_{11}),$$

where the order is described by the orange coloured numbers in Figure 5.1 (a). For the completed one-ring we have

$$C_g^T = (c_0^g, \dots, c_{15}^g),$$

the order is described by the black coloured numbers in Figure 5.1 (a). Using the linearity of the constraints describing the relation between the newly added ghost vertices and the vertices in the original geometry, see Formula 5.1, we consider the following equation

$$C_g = R_b C \quad (5.3)$$

where the matrix R_b is determined by the weights given in the formula. Hence, the parameterization of the surface patch for the boundary element is described by

$$s(u, v) = C_g^T b(u, v) = C^T R_b^T b(u, v), \quad (u, v) \in [0, 1]^2.$$

In doing so, using this relation the construction of ghost vertices can be avoided. For the computation of the limit surface on boundary elements, new basis functions $b^b(u, v) = R_b^T b(u, v)$ are defined by

$$b_i^b(u, v) = \begin{cases} 2b_i(u, v) + b_{i+4}(u, v) & \text{for } i = 0, \dots, 3 \\ -b_{i-4}(u, v) + b_{i+4}(u, v) & \text{for } i = 4, \dots, 7 \\ b_{i+4}(u, v) & \text{for } i = 8, \dots, 11 \end{cases}.$$

Using the B-spline basis function definition, see Formula 3.1, we can rewrite these equations in

$$b_i^b(u, v) = \begin{cases} n_{i \% 4}(u) (2n_0(v) + n_1(v)) & \text{for } i = 0, \dots, 3 \\ n_{i \% 4}(u) (-n_0(v) + n_2(v)) & \text{for } i = 4, \dots, 7 \\ n_{i \% 4}(u) n_3(v) & \text{for } i = 8, \dots, 11 \end{cases},$$

where the cubic boundary basis functions are given by

$$\begin{aligned} n_0^b(t) &= 2n_0(t) + n_1(t) \\ n_1^b(t) &= -n_0(t) + n_2(t) \\ n_2^b(t) &= n_3(t) \end{aligned} \quad (5.4)$$

We obtain a reduced number of basis functions in the v -component of the bivariate functions $b_i(u, v)$. The functions n_j^b are given by a linear combination of the cubic B-spline functions n_i . We consider the linear dependency $n^b(t) = (R_b^c)^T n(t)$, with the matrix R_b^c given by

$$R_b^c = \begin{pmatrix} 2 & -1 & 0 \\ 1 & 0 & 0 \\ 0 & 1 & 0 \\ 0 & 0 & 1 \end{pmatrix}.$$

The vector n denotes the vector of cubic B-spline basis functions (see Formula 3.2). The vector n^b replace the regular basis in the bivariate functions on boundary elements, where the one-ring of the element is incomplete. For the bivariate boundary basis functions we have

$$b_i^b(u, v) = n_{i\%4}(u) n_{i/4}^b(v), \quad \text{for } i = 0, \dots, 12.$$

Now we consider the same idea to determine the boundary basis of the corner element. Without loss of generality, we follow a similar approach and replace the matrix R_b by matrix R_c that describes the relation between ghost vertices and geometry vertices for the corner element. In this case, the control vertex matrix C is given by the 9 vertices in the one-ring of the corner element. A closer look at the corner element reveals that the corresponding bivariate boundary basis functions can be defined by the basis functions n_j^b , i.e.

$$b_i^c(u, v) = n_{i\%3}^b(u) n_{i/3}^b(v), \quad \text{for } i = 0, \dots, 9,$$

where the order of the vertices is shown by the orange coloured vertices in Figure 5.1. Consequently, the surface patches corresponding to the boundary and the corner elements can be parametrized by using the following representation

$$s(u, v) = C^T b^b(u, v) \quad \text{and} \quad s(u, v) = C^T b^c(u, v),$$

for $(u, v) \in [0, 1]^2$, respectively. The vectors b^b and b^c are describing the generating spline of a boundary and a corner element with respect to the described boundary conditions. The matrices C describe the position of the control vertices in the incomplete one-ring of this element. Therefore, the boundaries are pure B-spline curves defined by the vertices on the boundary. Keep in mind, here we consider specified boundary conditions based on point reflection. Due to the simplicity of the construction, a similar idea independently has appeared in [Barendrecht, 2013].

5.1.2 Pointwise constraints

On the basis of the classical subdivision surface theory, the limit positions, the tangent vectors and the normal vector of the control grid vertices can be uniquely determined using the eigenstructure of the subdivision matrix, see Section 2.3.3. Thus, the dominant and subdominant eigenvalues together with the associated eigenvectors ensure the position of the limit surface in the control grid vertices.

For the construction of pointwise limit surface constraints, a reversed problem has been established. This is, knowing the combinatorial structure of the control grid, we are able to determine the positions of the control grid vertices from its limit positions. This approach has been introduced in [Halstead et al., 1993] for the construction of an interpolating subdivision scheme based on the Catmull-Clark subdivision that, by definition, is an approximating scheme.

The given assumption leads to a linear system

$$Kx = b \quad (5.5)$$

where the vector x corresponds to the unknown positions of the control grid vertices. The left-hand side vector b is given by the predetermined limit features of the control vertices, i.e. the limit positions and normals, if required, of the control vertices that we want to interpolate. The matrix K is determined by the connectivity of the control grid, where the entries are described by vertex weights. For a given control vertex the entries in the related row of K are zero except for the entries corresponding to the vertices in the one-neighbourhood of this vertex. If we want to interpolate the limit positions, then the non-zero entries are given by the relevant entries of the eigenvector corresponding to the dominant eigenvalue $\lambda_0 = 1$ related to the subdivision matrix. Given the one-neighbourhood of a control vertex, a mask can be assigned, using the fact that the eigenvector just depends on the valence ν of the considered vertex. The mask together with the interpolation weights is illustrated in Figure 5.2. The weights for the interpolation of the limit positions of a control vertex with valence ν are given by

$$\alpha = \frac{\nu}{\nu + 5} \quad \beta_i = \frac{4}{\nu(\nu + 5)} \quad \gamma_i = \frac{1}{\nu(\nu + 5)} \quad (5.6)$$

Note, the weights depends only on the valence of the vertex.

The given constraints ensure, that the limit surface associated with the computed control grid interpolates the input limit positions. However, it is not guaranteed that the new surface will be similar to the limit surface used as input. This is because the behaviour of a surface cannot be encoded just on prescribing its positions. Additionally, the tangent plane have an important impact on the preservation of the surface properties. To assign this, we have to constrain additionally the normals of the control grid, if these are known. Again, this can be characterized by using an interpolation mask. To constraint the normals, the weights are characterized by the two eigenvectors associated with the subdominant eigenvalue. The limit masks with respect to the Catmull–Clark scheme are described in detail in [Halstead et al., 1993]. In doing so, the linear system has to be enlarged accordingly. In some cases, the matrix K is singular or non-square. If this is true, a least-squares solution has to be calculated. However, a significantly improved

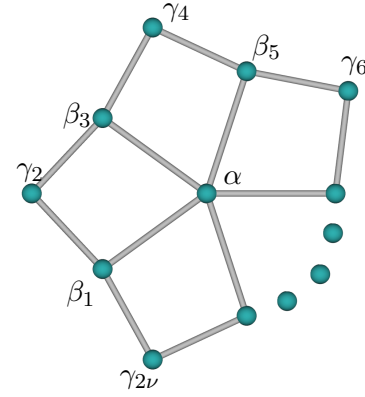


Figure 5.2: *Limit interpolation mask for a vertex of valences ν . The central vertex, its limit position we want to calculate, is weighted by α , β is the weight of the vertices vertices connected by an edge and γ for the remaining vertices in the one-neighbourhood of the central vertex. The weights depend only on the valence of the central vertex, see Equation 5.6.*

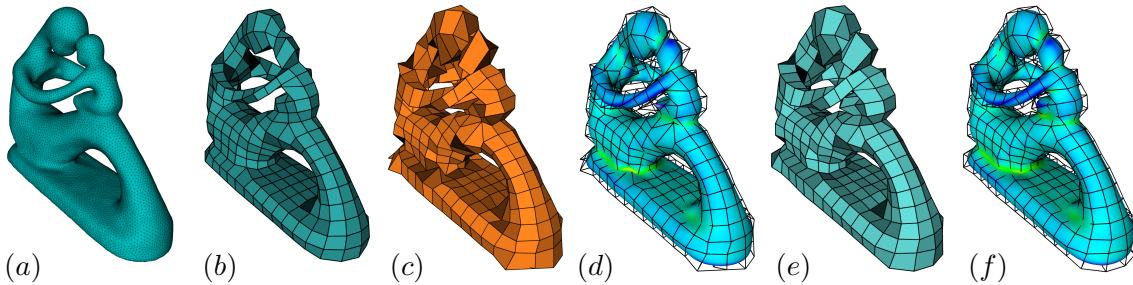


Figure 5.3: *Interpolation of a geometry. We start with an triangular grid (a) and the corresponding Quad-Cover grid (b). This grid is used for the calculation of limit position interpolation (c), and limit position and normal interpolation control grid (e). The corresponding limit surfaces are shown in figure (d) and (f), respectively. The colouring is given by the its mean curvature.*

result can be achieved using the method presented in [Halstead et al., 1993].

We implemented and tested the interpolation of limit positions and normals to have an understanding of the presented constraints, while the construction of our boundary conditions for PDEs. An example of the pointwise constraint is shown in Figure 5.3. The original control grid is obtained by the QuadCover algorithm [Kälberer et al., 2007], where the control grid positions lie on the very fine and detailed resolved input geometry. We use this control grid to obtain a new control grid of the same connectivity that can be used as the Catmull–Clark control grid, i.e. the limit surface of the new control grid interpolates the control grid vertices of the original grid. We compare the resulting control grids achieved by constraining just the limit positions, or the limit positions together with the corresponding normal vectors. In determining the positions and the tangent planes, we obtain a more homogeneous control grid and, consequently, the limit surface better approaches the original surface.

5.2 Symmetry constraints

In this section, we introduce a new construction of boundary constraints for geometries that follow a periodic manner in the space. The construction is adopted into the subdivision surface framework. Due to the problems with the non-existing limit surface on boundary elements, we construct a ghost geometry of the control grid by adding new elements at the boundary in order to obtain complete one-rings for the boundary elements. As mentioned before, an extended control grid allows for extra freedom in modelling of subdivision surfaces along the boundary.

The aim is to construct a ghost geometry which guarantees that the limit surface close to the boundary meets a smooth symmetric behaviour. A model class of surfaces that is built on this behaviour is represented by triply periodic minimal surfaces. Triply periodic means that the surfaces describe a fascinating crystalline structure, in the sense of repeating themselves in three dimensions. The symmetric behaviour of these surfaces is characterized by the Schwarz reflection principle. On the other hand, a direct consequence of the principle is that new valid minimal surfaces can be constructed from pieces of existing minimal surfaces. Therefore, one of the following properties has to be fulfilled: the boundary of the minimal surface is prescribed by a straight line or the surface meets a plane orthogonally on its boundary. In the first case, the minimal surface can be extended to a smooth minimal surface by rotating the surface by 180° about the straight line. The extended minimal surface contains this line as a symmetry line. In the second case, the extension is generated by reflecting the surface through the plane to a smooth minimal surface with this curve contained in its interior.

In the following, we adopt Schwarz’s principle to the construction of periodic boundary constraints. This procedure ensures the imposed symmetric behaviour of the corresponding limit surface close to the boundary.

5.2.1 Rotation by 180°

Considering Schwarz’s reflection principle, if the boundary of a minimal surface is a straight line, then it can be extended to a new valid minimal surface by rotating the surface by 180° about this line. In the following, we want to transform the given surface behaviour onto the control grid. Due to the fact that the limit position of a control vertex depends only on the vertices in its one-neighbourhood, we achieve the specified behaviour of the limit surface by adjusting the control grid appropriately. Namely, the adjustment is done by adding new elements that are equivalent with the rotated copies of the boundary elements along the boundary edge. For the construction, we add new vertices as rotated copies of the element vertices that do not lie in the boundary edge and, as a next step, connect the vertices accordingly.

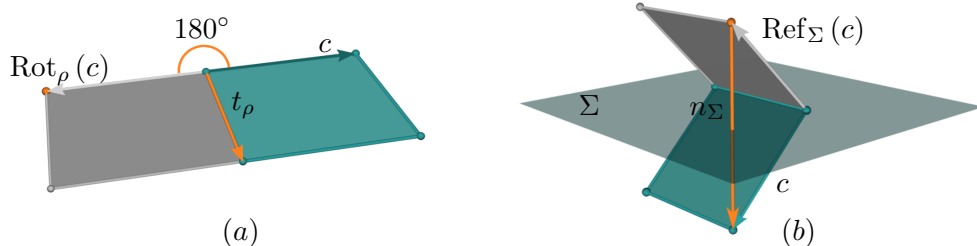


Figure 5.4: Schematic illustration of (a) the 180° rotation of a vector c around line ρ of direction t_ρ and (b) the reflection of vertex c through the plane Σ with the normal vector n_Σ . The blue element shows a geometry element and the grey element the resulting ghost element.

To perform a rotation of a point about a given axis in the Euclidean space \mathbb{R}^3 we make use of a rotation matrix. Given a straight line ρ through the origin, let $t_\rho = (t_x, t_y, t_z)$ be a unit vector that defines its direction and orientation. To perform a rotation by an angle of φ about the axis ρ in the direction of t_ρ , the rotation matrix R is given by

$$R_\varphi = \begin{pmatrix} \cos \varphi + t_x^2 (1 - \cos \varphi) & t_x t_y (1 - \cos \varphi) - t_z \sin \varphi & t_x t_z (1 - \cos \varphi) + t_y \sin \varphi \\ t_x t_y (1 - \cos \varphi) + t_z \sin \varphi & \cos \varphi + t_y^2 (1 - \cos \varphi) & t_y t_z (1 - \cos \varphi) - t_x \sin \varphi \\ t_x t_z (1 - \cos \varphi) - t_y \sin \varphi & t_y t_z (1 - \cos \varphi) + t_x \sin \varphi & \cos \varphi + t_z^2 (1 - \cos \varphi) \end{pmatrix}.$$

For the prescribed rotation angle $\varphi = 180^\circ$, the matrix reduces to

$$R = \begin{pmatrix} 2t_x^2 - 1 & 2t_x t_y & 2t_x t_z \\ 2t_x t_y & 2t_y^2 - 1 & 2t_y t_z \\ 2t_x t_z & 2t_y t_z & 2t_z^2 - 1 \end{pmatrix}. \quad (5.7)$$

The rotation of an arbitrary point c around the straight line ρ can be therefore calculated by

$$\text{Rot}_\rho(c) = Rc, \quad (5.8)$$

where c is a vector through the origin. The rotation Rc will be counter-clockwise related to the right-hand rule, where the right thumb is pointing in the direction of the vector t_ρ . The curled fingers determine the rotation direction.

5.2.2 Householder transformation

In terms of the second Schwarz reflection principle, if the minimal surface meets a plane orthogonally on its boundary, then it can be extended to a new valid minimal surface by reflection about the given plane. Considering the normal vector of the extended surface, we can observe that the normal is contained in the reflection plane. Here, the aim is to achieve the prescribed limit surface behaviour by constructing an appropriate ghost geometry. Thus, a reflection of the boundary elements through the prescribed reflection plane will lead to the required outcome, if the boundary vertices lie in the reflection plane. For the construction, we add new vertices that resemble the reflected copies of the element vertices and, as a next step, connect the vertices accordingly.

A reflection is an isometry from a Euclidean space to itself. Therefore, a hyperplane, called reflection plane, is given as a set of fixed points with a specified origin. To describe a reflection through a plane that contains the origin, we use the Householder transformation, see Householder [1958]. Let Σ be the reflection plane through the origin determined by the vector n_Σ that is orthogonal to the plane, see Figure 5.4. The reflection is defined by a linear transformation.

This is described by the matrix:

$$H = I - \frac{2}{\langle n_\Sigma, n_\Sigma \rangle} n_\Sigma \otimes n_\Sigma, \quad (5.9)$$

where I is the identity matrix. The matrix H is called the Householder-matrix. The denominator $\langle n_\Sigma, n_\Sigma \rangle$ is the scalar product and $n_\Sigma \otimes n_\Sigma$ is the dyadic product of n_Σ with itself. The matrix $\frac{1}{\langle n_\Sigma, n_\Sigma \rangle} n_\Sigma \otimes n_\Sigma$ describes the orthogonal projection in the direction of n_Σ . Is the vector n_Σ of unit length, i.e. $\langle n_\Sigma, n_\Sigma \rangle = 1$, the formula can be simplified to

$$H = I - 2n_\Sigma \otimes n_\Sigma.$$

The reflection of a vector c in the plane Σ is then given by

$$\text{Ref}_\Sigma(c) = Hc = c - 2\langle n_\Sigma, c \rangle n_\Sigma.$$

The term $\langle n_\Sigma, c \rangle$ corresponds to the Euclidean distance of the vertex c to the plane Σ . For a graphic illustration of the reflection see Figure 5.4.

5.2.3 Construction issue

Given an arbitrary control grid with a boundary that fulfils the mentioned symmetry conditions. For the construction of the ghost geometry, we again distinguish between boundary and corner elements. To obtain a valid ghost geometry, the one-rings of the boundary elements have to be completed by adding missing elements that meets the prescribed boundary conditions. A particular attention is required for corner elements its to boundary edges are constrained by two different boundary requirements.

In general, the rotation axis ρ and the reflection plane Σ do not need to go through the origin. If this is the case, we choose a vertex c_O of ρ or, respectively, in Σ that mimic the origin locally. For the rotation or reflection of an arbitrary vertex c , the position of the new vertex related to c is calculated by using the rotation or reflection of the vector $(c - c_O)$. Hence, postponing the origin to c_O means that afterwards we have to add c_O to determine the position of the new ghost vertex in the ambient space. The position of the new vertex $\text{Rot}_\rho(c)$ is obtained from the rotation of the vertex c . This can be computed by using the formula:

$$\text{Rot}_\rho(c) = R(c - c_O) + c_O = (I - R)c_O + Rc, \quad (5.10)$$

where $(c - c_O)$ is a vector that starts in the local origin c_O . The same can be used for the

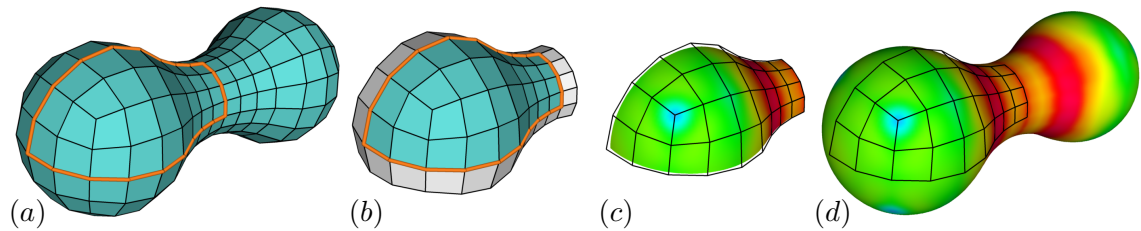


Figure 5.5: Symmetric surfaces. If the initial geometry (a) is symmetric, then a fundamental cell (b) can be obtained for the calculation. The ghost geometry is constructed based on the reflection of the corresponding boundary element vertices. The limit surface of the fundamental cell (c) is again used to construct by reflection the whole limit surface (d).

reflection of a vector c through the plane Σ . The formula is given by

$$\text{Ref}_{\Sigma}(c) = H(c - c_O) + c_O = (I - H)c_O + Hc. \quad (5.11)$$

Given a boundary element, the missing part of the one-ring is obtained by the rotation or reflection of the non-boundary vertices of the boundary elements. Depending on the boundary of the control grid, the completed one-ring of the element has at least one symmetry axis. The parameterization of the limit surface of a boundary element, can now be computed by using one of the presented parameterizations.

As aforementioned, because of the varying boundary constraints for the boundary edges, the corner elements need a special treatment. When thinking of minimal surfaces, it seems not so unlikely to have to handle two boundaries with two different boundary conditions that coincide in a point. If this is the case, the ghost elements result from the sequential execution of different constraints that can be reflections or rotations, or reflection and rotation simultaneously. For this purpose, the task to complete the ghost geometry is highly nontrivial. As an example, let the corner vertex be described by an extraordinary vertex. This can happen when more than two symmetry planes meet at the corner vertex. The corner vertex determines the combinatorics of the one-ring of the corner element. For the construction, only a complete one-ring can be used to parametrize the surface of an element, i.e. the boundary constraints have to be chosen, such that the one-neighbourhood of a corner vertex does not lead to any overlap. In Figure 5.5, an example of a symmetric geometry construction is shown. Given the initial control grid, the ghost geometry is constructed in accordance with the three symmetry planes perpendicular to each coordinate direction.

As a result, the boundary curve of a limit surface can only be determined by using the surface parameterization on the corresponding boundary element. This is due to the nontrivial construction of the ghost geometry.

5.3 Conditions for PDEs

In this section, we are interested in determining boundary conditions for PDEs on subdivision surfaces. A PDE has in general infinitely many solutions. By prescribing constraints, we specify the problem more precisely, whereby for a well-posed problem, a unique solution exists that fulfils the corresponding conditions. Nevertheless, the considered problems can be so complex that only numerical methods can be used to find an approximation of its analytic solution. In this thesis, we use the finite element method. However, constraints are generally a problem in finite element applications. In order to address this problem, the choice of finite elements with sufficient freedom is of crucial importance.

The Catmull–Clark subdivision finite element is known to be H^2 -regular. Nevertheless, there is a price to pay for it. Unlike traditional finite elements, the influence of the element spreads over the its neighbourhood, beyond the vertices of the element. In other words, considering a surface patch, the degrees of freedom describing the limit surface of the patch are distributed to the vertices in the one-ring of the related element. This means, the boundary of the finite element and the boundary of the parameter domain do not coincide. Moreover, the finite element basis functions depend on the element combinatorics. The one-ring of an element provides information about the associated basis functions. Concerning this matters, the concept of boundary constraints within the subdivision finite element needs to be treated carefully. Reasonable boundary conditions are required.

In this section, we discuss how to enforce constraints for subdivision finite elements. A review of different boundary conditions described in the literature is given. Most of these have

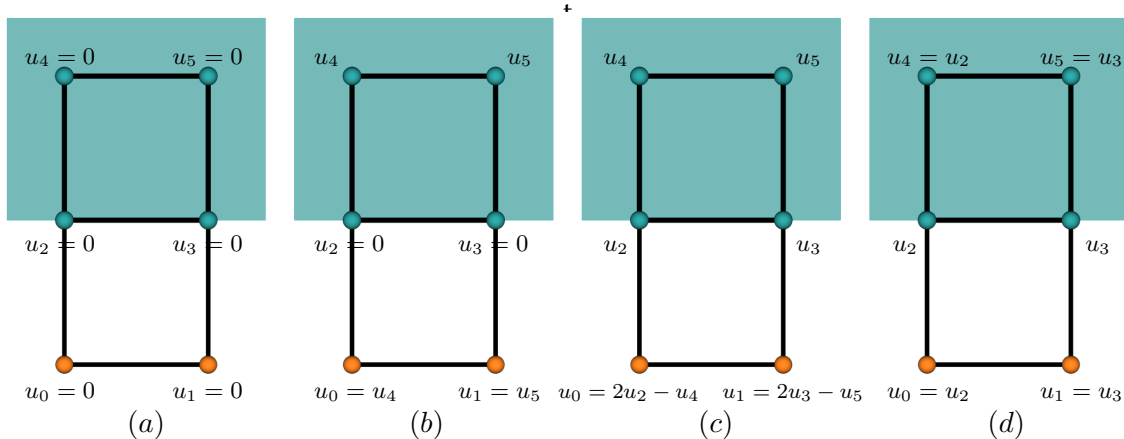


Figure 5.6: *Compatibility conditions: (a) fixed translation and rotation, (b) fixed translation and free rotation, (c) free translation and rotation, and (d) free translation and fixed rotation. The blue coloured parts represent the actual geometry with exemplary elements, the white quads represent the ghost elements. The orange vertices correspond to ghost vertices.*

been used for thin shell problems, but, due to their general validity, the conditions can be applied to other PDEs. Furthermore, we give a precise description how to apply our symmetric constraints for solving periodic boundary value problems. As an application we will consider in the next chapter the construction of periodic minimal surfaces by means of the mean curvature flow. Moreover, our boundary conditions do not impose any requirements on the combinatorial structure of the control grid.

5.3.1 Compatibility conditions

The most common conditions in mechanics restrict either the displacement or rotation, or both, along the boundary of the domain. In other words, the solution or its derivative have to meet specified values at the boundary. The subject of the so-called compatibility constraints are translations and rotations in the neighbourhood of the boundary. The naming of the constraints follows from the compatibility with the boundary constraint known from the literature, i.e. Dirichlet or Neumann boundary constraints.

In the framework of subdivision surfaces, compatibility conditions have been presented in [Cirak et al., 2000] and [Schweitzer, 1996] for thin shell problems on triangular meshes. An extension to quadrangular control grids have been described in [Wawrzinek, 2011]. Thus, the constraints can be obtained using a ghost geometry. Based on the point reflection principle described in Section 5.1.1, a set of displacement configurations of the control vertices can be specified that cover all possible motion laws at the boundary.

In Figure 5.6, the compatibility constraints for the Catmull–Clark finite elements are shown. The conditions are specified for a boundary element based on Formula 5.1. Similar relations hold for a corner element in accordance with Formula 5.2. Consequently, the boundary curve is equal to the limit curve of the boundary edge polygon. On the other hand, we do not need to generate the ghost geometry explicitly. If the boundary is prescribed to meet the compatibility conditions, then we can use boundary basis functions for the computation, see Section 5.1.1.

Summarizing, the compatibility constraints are simple to implement. Additionally, they can be applied to geometries with curved boundaries. Unfortunately, the rate of convergence of the subdivision finite element method for thin shells is quite low, see [Cirak et al., 2000]. The reason for this is that the conditions involve locking of surface features, as for example, deformation involving derivatives of higher order, or in-plane deformation modes. This leads to vanishing of in-plane forces. Consequently, natural deformations are violated. In Figure 6.1, an example of a

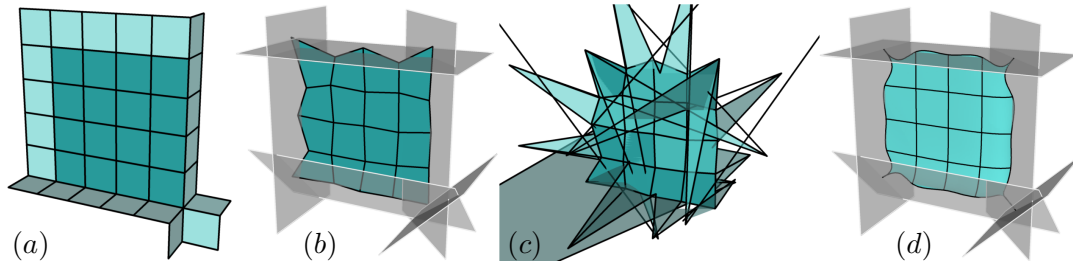


Figure 5.7: *Pointwise constraints. An initial grid with the corresponding ghost geometry (a), the control grid after the first time step of the flow with the corresponding reflection planes (b) and with the resulting ghost geometry (c) are shown. Additionally, the limit surface with the reflection planes is illustrated (d).*

solution of the mean curvature flow with compatibility boundary constraints is shown. Consider the poor quality of the approximation in the neighbourhood of the boundary.

5.3.2 Pointwise constraints

As described in Section 5.1.2, the limit position and the associated tangent space of a control vertex can be easily obtained using limit masks. The masks refer to the vertices in the one-neighbourhood of a control vertex. The underlying concept can also be used for the construction of boundary conditions for PDEs. The so-called pointwise conditions have been introduced in [Green, 2003] to enforce boundary constraints for thin shell problems in the framework of Loop subdivision finite elements on triangular control grids. In the following, we review the conditions determined to enforce different types of boundary constraints on the limit surface. For details, please refer to [Green, 2003].

Let $w^T = (w_0, w_1, w_2, \dots, w_{2\nu}) = (\alpha, \beta_1, \gamma_2, \dots, \gamma_{2\nu})$ be the vector with the interpolation weights, see Section 5.1.2. The displacement of a limit surface point can be described in the form

$$u_\infty = w \cdot u = \sum_{i=0}^{2\nu} w_i u_i, \quad (5.12)$$

where $u = (u_0, u_1, \dots, u_{2\nu})$ is the vector corresponding to the unknown displacements of the vertices in the one-neighbourhood. To enforce the vertices from moving in a given direction d , we require that

$$u_\infty \cdot d = \sum_{i=0}^{2\nu} w_i (u_i \cdot d) = 0.$$

To clamp the position of a vertex, we have to fix its translation and rotation. To assign a given translation, Formula 5.12 is used, where u_∞ determine the provided translation. The rotation can be fixed by constraining the normal vector through some fixed direction r . The required condition is of the form

$$r \cdot n = r \cdot (t_1 \times t_2) \cong \sum_{i=0}^{2\nu} w_i \cdot (w_1^i (t_1 \times r) + w_2^i (r \times t_2)) = 0,$$

where n , t_1 and t_2 are tangent space elements of the deformed surface, and w_1^i and w_2^i are the limit weights of the tangent vector interpolation.

The constraints are very flexible and do not require any symmetry of the neighbourhood. They can be applied directly to the limit surface, not necessarily at the control grid vertices. That is, using Stam's evaluation technique, the pointwise constraints can be applied to any point on the surface. A second order approximation for the pointwise constrain is achieved, for details, see

[Green, 2003]. However, based on the experience in the application, the proposed construction leads easily to an over-determined problem. As pointed out by the author, to find an appropriate set of constraints can be a quite crucial issue.

Moreover, in [Green, 2003], the constraints are applied to the H^2 -regular thin shell problem. However, pointwise constraints applied to H^1 -regular problems may not be strong enough. Considering the trace operator, a single restriction of the problem function cannot be used to meaningfully prescribe a general solution, how it has to behave along the total boundary curve [Braess, 2007]. An example of an application to the H^1 -regular mean curvature flow is considered in Figure 5.7.

5.3.3 Symmetry conditions

In this thesis, we are interested in the construction of symmetric boundary conditions for the following reason: periodic minimal surfaces, their construction is considered in the next chapter, are characterized by symmetry properties. These surfaces are characterized by a symmetry group, i.e. the group of all translations under which the surface is invariant. In doing so, a unit cell can be specified, that determines the total surface by means of the symmetry operations. Using this idea, the computation of periodic minimal surfaces can be reduced to a symmetric patch. On the other hand, the critical points of the mean curvature flow provide minimal surfaces. In other words, an aim of the next section is to solve a mean curvature flow with symmetric boundary conditions.

In the framework of subdivision surfaces, a symmetry at the boundary can be obtained by the extension of the surface using the symmetry constraints described in Section 5.2. According to the boundary representation, i.e. the boundary can be given by a straight line, or an arbitrary curve that is contained in a plane, the ghost vertices are constrained to comply with a rotation or a reflection obligation of the boundary elements. Again, we distinguish between boundary and corner elements.

Given a control grid and the corresponding ghost geometry constructed by means of symmetry conditions. An adequate set of constraints needs to be applied to the ghost vertices. Additionally, to avoid locking of surface features, we allow boundary vertices to move along the specified rotation axis or reflection plane. Let ρ be a straight line, called rotation axis, determined by a part of the boundary polygon of a control grid. The displacement u_g of the ghost vertices is restricted to fulfil the rotation properties by

$$u_g = \text{Rot}_\rho(u_i)$$

where u_i describes the displacement of the associated control vertex. Let $t_\rho = (t_x, t_y, t_z)$ be the vector describing the direction and orientation of the line ρ . The displacement u_b of the boundary vertices contained in ρ can be described by

$$u_b = \alpha t_\rho,$$

where α gives the scaling of the vector t_ρ .

Let Σ be a reflection plane containing a part of the boundary of the control grid. The displacement u_g of the ghost vertices that are constrained using reflection properties is described by the formula

$$u_g = \text{Ref}_\Sigma(u_i),$$

where u_i gives the displacement of the corresponding control vertex. Again, to avoid locking of surface features, we allow boundary vertices to move along the curve or the reflection plane. Let $t_\rho = (t_x, t_y, t_z)$ be the vector describing the direction and orientation of the line ρ . For the reflection plane Σ , the normal n_Σ of Σ be pointing in the outer direction of the control grid. The

displacement u_b of the boundary vertices in Σ is restricted to fulfil

$$n_\Sigma \cdot u_b = 0,$$

or alternatively

$$u_b = \alpha t_1 + \beta t_2,$$

if t_1 and t_2 are the tangential vectors of plane Σ .

Given a corner vertex, we have to take care of the coincidence of two different boundary conditions. Moreover, the ghost geometry has to be constructed such that the consecutive conditions can be achieved. Hence, the corner vertex can be fixed to a point, or allowed to move freely along a straight. That is, a corner vertex is not allowed to move, if one of the boundary edges is constrained by a rotation and the other by a reflection condition, or both edges have to meet rotation conditions. The displacement of the corner vertex is therefore equal to zero, i.e. $u_c = 0$. If the two boundary edges of the corner element are contained in different reflection planes Σ_1 and Σ_2 , the corner vertex is located on the intersection line of Σ_1 and Σ_2 . The vertex is allowed to move along this line. The displacement of the corner vertex can be characterized by

$$u_c = \alpha t_{12},$$

where the vector t_{12} describes the direction and orientation of the intersection line. Additionally, considering the corner element, some of the ghost vertices emerge from the rotation or reflection

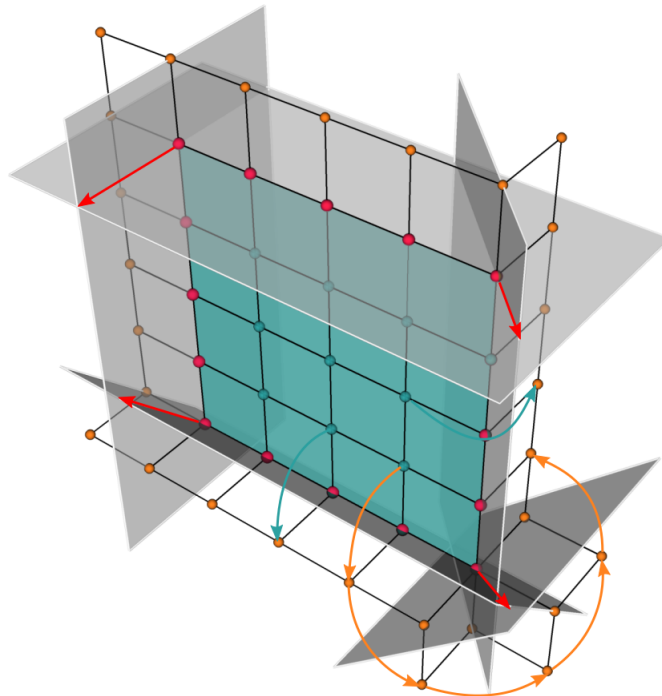


Figure 5.8: An illustration of a geometry (blue) together with the ghost elements (transparent) and the corresponding reflection planes (grey). The geometry vertices (blue) are unconstrained. The boundary vertices (red) are constrained as follows: the red arrows show the allowed movement direction of the corner vertices, i.e. the direction is prescribed by the intersection line of at least two reflection planes. The remaining boundary vertices are allowed to move along the reflection plane in which these are contained. The ghost vertices (orange) are constrained as follows: the ghost vertices are rotations or reflections of the geometry vertices. For example, the blue arrows show the connection of the geometry and the ghost vertices based on the reflection constraint. The orange arrows show a reflection constraint that is consecutively executed around a corner. That is, all the corresponding ghost vertices are constrained by consecutive reflections of a single geometry vertex.

of the boundary vertices of the corner element. In accordance with the nonrigid boundary polygons, these vertices are allowed to move along a rotated copy of the curve ρ or a reflected copy of the reflection plane Σ . The displacement of the associated ghost vertices can be described by

$$u_g = \text{Rot}_\rho(u_b) = \alpha \text{Rot}_\rho(t_\rho)$$

or

$$u_g = \text{Ref}_\Sigma(u_b) = \alpha \text{Ref}_\Sigma(t_1) + \beta \text{Ref}_\Sigma(t_2),$$

respectively, in connection with the suitable rotation axis or reflection plane. The conditions preserve the minimal surface periodicity. Thus, the corresponding limit surface can be extended to a smooth minimal surface containing the boundary curve. In Figure 5.8, an example of a geometry together with the associated ghost geometry and the imposed constraints is shown.

An object in the three-dimensional space has six degrees-of-freedom. Three of them are translations along axes, and the other three are the rotations around these axes. Thus, the presented constraints allow for an explicit calculation of the needed constraints or, equivalently, degrees of freedom.

5.4 Constrained optimization

In this section, we want to integrate the set of specific boundary constraints given by the posed problem into the finite element construction describing a system of linear equation. Due to the fact that B-spline basis functions do not interpolate the associated degrees of freedom, the presented boundary constraints can be resolved using constrained optimization. Moreover, the constraints are linear and finite dimensional. In the following, we consider a set of geometric constraints imposed on the vertices of the control grid. The constraints are intended to ensure to be compatible with the overall finite element system.

Consider a geometric constrained optimization problem. A general representation may be written as follows:

$$\begin{aligned} \min \quad & f(u) \\ \text{subject to} \quad & g_i(u) = c_i \end{aligned}$$

where $f(u)$ is the objective function which is to be minimized and $g_i(u) = c_i$ for $i = 1, \dots, n$ are the set of equality constraints. It is required for the so-called hard constraints to be satisfied with in full. To solve the problem numerically, the problem functions can be restricted to the following standard form

$$\begin{aligned} f(u) &= \frac{1}{2}u^T A u + b^T u + c \\ g_i(u) &= C u - d \end{aligned} \tag{5.13}$$

where A is a symmetric matrix. The matrices C given by the required conditions do not need to be quadratic. This construction implies that the problem to solve is ensured to be a quadratic objective function with linear constraints.

There are two methods that can be applied: reduction of unnecessary degrees of freedom or addition of extra degrees by means of Lagrange multipliers. This is handled as follows: let $Ax = b$ be the final system to be solved, this is given by the gradient of the quadratic Equation 5.13. The compatibility constraints can be resolved by the first method. Therefore, the entries of the problem matrix A needs to be modified in such a way that the required conditions are fulfilled. For example, considering fixed translations and rotations, the rows of the matrix of the corresponding vertices will be set to zero except the one in the column related to the considered vertex. To that

effect, the entry of the left hand side vector b will also be set to zero.

By contrast, using the second method, we have to extend the problem matrix A in accordance with the prescribed conditions. This construction preserves the dynamic of the system by adding additional constrained functions. In doing so, this allows us to enforce the constraints described in Section 5.1.2 and 5.3.3.

5.4.1 The method of Lagrange multipliers

Let $f(u)$ be the function to be extremized, and at the same time be subject to the conditions $g_i(u)$. To put the extremum conditions together with the constraints, we add a new variable λ to the problem. We write down the so called Lagrangian function

$$\mathcal{L}(u, \lambda) = f(u) + \lambda^T g(u),$$

that is a function of the variables u and newly added variable λ . Now, we look for the critical points $\nabla \mathcal{L}(u, \lambda) = 0$ of the Lagrangian function. Extremizing \mathcal{L} with respect to u and λ yields the multiplier form

$$\begin{aligned} \frac{\partial \mathcal{L}}{\partial u} &= Au + b + \lambda^T C = 0, \\ \frac{\partial \mathcal{L}}{\partial \lambda} &= Cu - d = 0 \end{aligned}$$

where the partial derivatives are set to zero. This can be rewritten into the block matrix form

$$\begin{pmatrix} A & C^T \\ C & 0 \end{pmatrix} \begin{pmatrix} u \\ \lambda \end{pmatrix} = \begin{pmatrix} -b \\ d \end{pmatrix}, \quad (5.14)$$

where A is the stiffness matrix of the system and C is the matrix of constrained derivatives with respect to the displacement u . The stiffness matrix A , called the bordered stiffness matrix, is said to be bordered with C and C^T . Solving the system provides a solution for the unknown u and λ , where u describes the displacements of the vertices. The variable λ can be interpreted as a force of constraint in the following sense: a removed constraint can be replaced by a system of forces characterized by λ multiplied by the constraint coefficients. More precisely, the constraint forces are equal to $-C^T \lambda$.

The method of Lagrange multipliers poses a rigorous justification of the problem within the framework of variational calculus. It appears to be the most elegant method for a general-purpose finite element tool that is supposed to work as a "black box" by minimizing guesses and choices from its users. The method enforces the constraints exactly, at the cost of adding one additional variable for each constraint to be enforced. The method provides directly the constraint forces, which are of interest in many applications. On the other hand, the assembling of the extended problem matrix is not simple and highly expensive. Special care should be exercised in detecting singularities and losing the positive definiteness of the bordered stiffness on equation solvers. Due to the B-spline properties, the singularities may occur due to the continuity of the constraints. An initial reduction of the constraint matrix A to a set of independent rows must be performed, because of the fact that the method is sensitive to the degree of linear independence of the constraints. To perform a least-squares fit to the constraint, we consider the normal matrix $A^T A$ and take its independent rows as our constraints. All in all, the method of Lagrange multipliers has the advantage of being exact.

CHAPTER 6

CATMULL-CLARK LIMIT SURFACES OF MINIMAL AREA

Minimal surfaces describe an important class of surfaces in theory and practice, in the area of natural sciences, architecture and art. The interest on minimal surfaces comes from the fact that these surfaces describe an ideal solution to various real world problems. An example of common objects modelled using minimal surfaces are shapes taken by soap films. These objects minimize surface area with respect to their boundaries. According to this, minimal surfaces are those surfaces that have local least surface area of all surfaces enclosed by the same boundary. Minimal area means minimal use of material, minimal amount of material means, in turn, minimal cost of the building material. On the other hand, the minimization is related to mean curvature and therefore provide an effective smoothing method. Moreover, the surface tension is in equilibrium at each point of the minimal surface. All these properties taken together make minimal surfaces very attractive for light weight and yet extremely stable constructions.

Of crucial importance for the construction of minimal surfaces is the following law: given an arbitrary boundary curve, there is a surface of minimal area that fills up the boundary. In practice, to find a surface that fulfils the conditions, numerical methods have to be applied. A minimization problem can be defined that bases on the mean curvature flow. In this framework, at first, an initial geometry has to be constructed. In doing so, we obtain an arbitrary mesh that fits into the given boundary construction.

Considering the state of the art modelling tools, such as used in CAD systems, the design of real world objects is made using smooth surface representations. By reason of easy handling, the most common representations are NURBS, B-spline surfaces or subdivision surfaces. These flexible, but also sophisticated approaches provide a unified framework for the representation and processing of smooth surfaces, and for analytical investigations of the PDE problems. This

is a new approach that is supported by the so-called isogeometric analysis systems. However, the mean curvature flow for the construction of periodic minimal surface problem has not yet been studied.

In this chapter, we give an insight into the construction and design of subdivision limit surfaces that approximate minimal surfaces. We start with a short view on what minimal surfaces are and how these can be constructed. Next, we discuss the mean curvature flow, and derive the corresponding minimization problem and a discretized representation of it. By linking the variational representation of the problem with discrete surface representations, a mathematical framework is established for the computation of discrete minimal surfaces enclosed by prescribed boundaries. Using the framework of subdivision surfaces, minimal Catmull–Clark surfaces will be introduced to the reader. The chapter is rounded off with a set of experiments. A particular focus is laid on the construction of periodic Catmull–Clark surfaces of minimal area.

6.1 Perspectives on minimal spline surfaces

The study and computation of surfaces of minimal area have a long history, where in the course of time various models have been determined for its realisation. Minimal surfaces have been and still are one of the main topics in differential geometry, calculus of variations, complex analysis and other fields of mathematics. They are used to model physical phenomena, as for example soap films, black holes, protein foldings, etc. Many of these fundamental key issues have been solved, whereby new perspectives in different scientific and even industrial areas have opened up. At present, minimal surfaces are a powerful tool that connects various scientific and industrial areas.

This section describes the foundations of the minimal surface theory linking to the construction of spline based approximations of minimal surfaces. We review some representations of the simple but challenging surfaces that have evolved over the course of history. We review some key results of discrete minimal surfaces with a closer look on spline based constructions. Thus, for the classical theory we refer to [Lawson, 1980; Dierkes et al., 1992; Osserman, 2002].

6.1.1 What is a minimal surface?

One can define a minimal surface from different points of view, perfectly showing the richness of this concept. From the classical theory, as the name suggests:

A surface $M \subset \mathbb{R}^3$ is minimal, if each point on the surface has a neighbourhood which is the surface of least area with respect to its boundary.

The least-area property is local, surfaces may still exist that better minimize area within the same boundary.

The history of minimal surfaces goes back to J.L. Lagrange who is one of the founders of calculus of variations. In his famous work [Lagrange, 1761], Lagrange developed an algorithm for the calculation of minimal surfaces, also in higher dimensions. In this work the author introduces the today known as the Euler-Lagrange equation that is a second-order partial differential equation for solving optimization problems related to minimal surfaces. The name of the equation comes from the fact that in 1741, before Lagrange, Euler found the first minimal surface: the catenoid. The catenoid is a surface which minimizes area among surfaces of revolution after prescribing boundary values from the generating curves (in Figure 6.1, an approximation of the catenoid is shown).

In 1776, Meusnier discovered the following geometric interpretation

A surface $M \subset \mathbb{R}^3$ is minimal if and only if its mean curvature vanishes identically.

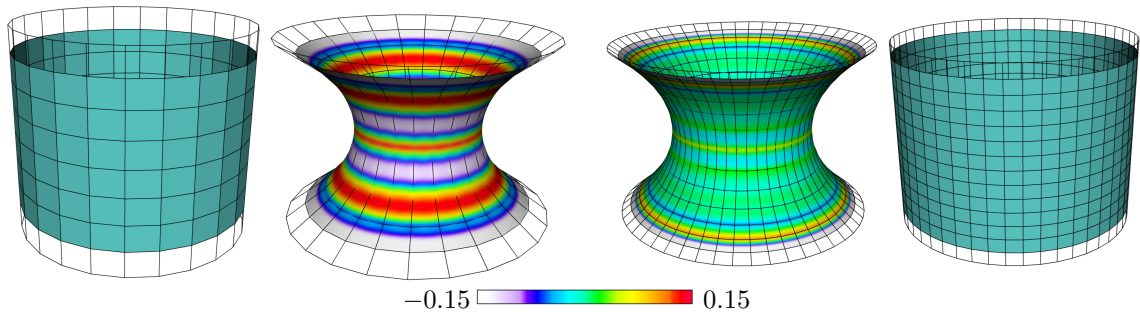


Figure 6.1: *Catmull–Clark catenoid.* Two cylindrical control grids and the corresponding grids and limit surfaces of the critical points of the mean curvature flow are shown. The used boundary conditions are given by compatibility conditions for fixed translation and free rotation of the boundary control vertices (see Section 5.3.1). The colouring of the limit surfaces is given by its mean curvature. The colour bar shows the distribution of the curvature.

By means of this discovery, Meusnier verified that the catenoid has zero mean curvature. Additionally, he found that a right helicoid is a minimal surface. Not counting the plane, the catenoid and the helicoid are the first minimal surfaces that have been discovered. The catenoid and the helicoid have a one-parameter group of symmetries. It means, one can make a continuous and isometric deformation of a catenoid to a helicoid such that every member of the deformation family is minimal. A direct implication of this definition is that every point on the surface is a saddle point with equal and opposite principal curvatures.

It took almost ninety years until a further minimal surface has been explored. In 1835, Scherk [Scherk, 1835] unsuccessfully tried to determine all ruled minimal surfaces that contain a straight line through each point of the surfaces. Nevertheless, his great success are the two Scherk surfaces named after himself. The so-called singly and doubly periodic Scherk's surfaces describe two of the few known complete embedded minimal surfaces. Additionally, these are the first two known periodic surfaces. In 1867 B. Riemann found a one-parameter family of complete embedded singly-periodic minimal surfaces with an infinite number of foliated by circles and lines in parallel planes.

The connection between minimal surfaces and harmonic functions is the following

If the surface is given by a conformal immersion $x = (x_1, x_2, x_3) : M \rightarrow \mathbb{R}^3$ of a Riemannian surface into space, then the surface is minimal, if the components $x_i, i = 1, 2, 3$, of x are harmonic functions on M . This is, $\Delta_M x_i = 0$, where Δ_M is the Laplace–Beltrami on M .

As a consequence of this definition and the maximum principle for harmonic functions, there are no compact complete minimal surfaces in \mathbb{R}^3 .

From a physical point of view, the difference between the pressure at the two sides of a membrane is equal, up to a non-zero multiplicative constant, to the mean curvature of a homogeneous surface separating two materials. Consequently, the membrane has zero mean curvature, if the pressure difference is zero. In 1870, the Belgian physicist J. Plateau observed that minimal surfaces can be physically realized as soap films. From Plateau's experimental observations is known that the surface area of soap films is a relative minimum among nearby surfaces with the same boundary. The soap film corresponds to a physically stable local minimum of the total energy. This means, surfaces that are local minimums to energy are also local minimums to the area and vice versa. As a result, we obtain the following boundary value problem known as the Plateau problem: find the surface of least area which is spanned in a given boundary.

In 1865, H.A. Schwarz derived a representation of minimal surfaces in isothermal coordinates. Isothermal coordinates are local coordinates on a Riemannian manifold their metric is conformal to the Euclidean metric. The minimal surface is the solution to the corresponding

Plateau's problem, where the conditions are fixing the boundary to a polygon consisting of four edges of a tetrahedron. Schwarz's surface is a building block to create a complete minimal surface that is periodic and has a symmetry group containing a three-dimensional lattice of translations. Therefore, the Schwarz primitive triply periodic surface describes a crystallographic cell or space tiling. A fundamental cell exists that fill the whole cube caused by reflection. Conversely, using Schwarz's reflection principle, a triply periodic minimal surface can be divided into identical patches with geodesic boundaries that fulfil prescribed symmetry conditions. This property makes minimal surfaces even more attractive in the area of material science, crystallography, biology, etc. For more information about periodic minimal surfaces, see [Meeks and Rosenberg, 1989, 1993].

A minimal surface is the two-dimensional generalization of a straight line in the plane: any piece of a straight line is the unique curve of minimal length connecting its boundary points. On the other hand, while the straight lines in the plane are essentially the same, the set of all minimal surfaces takes a wide range of surfaces - including those that have not yet been found. The minimal surface can be described as a surface within a given boundary curve that either minimizes or even is a critical point for the mean curvature flow.

A conformal immersion $x : M \rightarrow \mathbb{R}^3$ is minimal, if it is a critical point for the mean curvature flow.

$$\partial_t x(u, t) = -2H(u) n_t(u)$$

We consider an evolutionary motion of surfaces by their mean curvature. This motion allows for a scheme to find minimal surfaces using numerical calculation methods. The first numerical approximation of Plateau's problem have been done by Douglas [Douglas, 1927], Wilson [Wilson, 1961] and Tsuchiya [Tsuchiya, 1986, 1987]. An extended construction problem of this problem is described in [Stahl, 1994]. The author introduces the problem of the mean curvature flow for immersions with Neumann free boundary conditions. In the following, we will use the presented definitions for the construction and investigation of Catmull-Clark surfaces of minimal area.

6.1.2 Overview on minimal spline surfaces

In the framework of surfaces minimizing area, the area of a surface is directly minimized by letting the surface flow in the direction of the surface normal with the magnitude of the mean curvature of the surface. Consequently, the mean curvature flow is the most natural approach to compute minimal surfaces upon a boundary enclosing a domain. Considering numerical methods for solving the given problem, various discrete minimal surfaces bounded by a number of boundary curves can be derived as approximations of its smooth complements. In the following, we give a list of related works on the topic of mean curvature flow and discrete minimal surfaces.

The mean curvature flow has been studied by many authors through different approaches. Investigations on the classical form of the flow have been done in Huisken et al. [1990] and Ecker [2004] where using geometric analysis and PDE techniques regularity properties of the flow are studied. Additionally, unique evolution problems has been solved and families of surfaces constructed under geometric restrictions on the initial surface. Based on geometric measure theory, a general result of the existence and a deep regularity theorem are proven in Brakke [1978]. Therefore, in the setting of varifolds, which describe the generalization of differentiable manifolds in measure theory, a generalized approximate solution is constructed for all specified times. Additionally, geometric properties of the evolution of surfaces has been summarized. In [Dziuk, 1991], the mean curvature flow is used for the computation of stable minimal surfaces using finite elements on surfaces. To reduce numerical difficulties in the construction of the

Laplace operator, Dziuk uses the current surface discretization as the conformal parameter space, that is, the triangles of the mesh define the local surface metric.

Since the 90's, a great deal of interest is being focused on the problem of the mean curvature flow with free boundary conditions. It has started with the work of Stahl [Stahl, 1994], where the author presents his results of the investigations on the geometric flow of immersions. A short time existence result has been shown by writing the evolving hypersurfaces as graphs over the initial hypersurface. The mean curvature flow with free boundary conditions on smooth surfaces is discussed in Buckland [2005]. In particular, the interest of this work is focused on singularities of the mean curvature flow. Thus, singularities are defined as points, where the derivatives do not exist. An introduction to regularity theory for the free-boundary problem is given in [Koeller, 2007].

The concept of discrete minimal surfaces have been established in recent years. In [Bobenko et al., 2006], a non-linear view on discrete mean curvature is provided that allow for finding discrete minimal surfaces arbitrarily close to its smooth analogue. A method to approximate a harmonic map using the finite element method based on linear elements is considered in [Pinkall and Polthier, 1993; Polthier et al., 2002]. Using this approach, various piecewise linear minimal surfaces have been constructed. The construction of discrete minimal surface on PQ meshes is described in [Wallner and Pottmann, 2008]. The integral of the square length of the mean curvature gradient with respect to the to the surface measure has been minimized in [Xu and Zhang, 2007].

The problem of finding a minimal surface have been a big research issue in the area of computer aided design. The first ideas that use CAD tools for the construction of minimal surfaces has been considered in [Cosin and Monterde, 2002] for Bézier surfaces. Corresponding to the approaches of Cosin and Monterde, Bézier control grids have to satisfy certain conditions to be suitable for the construction. As a result, using bicubic Bézier surfaces, the authors have shown that all minimal surfaces are pieces of the Enneper surface, except for their affine transformations. In the context of Bézier surfaces, an equivalent problem to Plateau's problem is the so-called Plateau–Bézier problem that has been studied in [Monterde, 2004]. For the calculation of Bézier surfaces of minimal area, the author consider the Dirichlet functional as an equivalent for the area functional. Therefore, the extremes of the functional can be determined by solving a linear problem. In [Arnal et al., 2003], methods based on the Plateau–Bézier problem are examined for the approximation of triangular Bézier minimal surface with prescribed boundary. Parametrized minimal surfaces bounded by NURBS curves are investigated in [Lian and Lutai, 2005]. The construction of minimal Catmull–Clark subdivision surfaces with prescribed fixed boundaries is discussed in [Pan and Xu, 2010]. An overview on recent results on minimal surfaces and the mean curvature flow is given in [Colding et al., 2011].

6.2 Mean curvature flow

Mean curvature plays a special role among characteristics of surfaces and their dynamics. An example is the mean curvature motion of a manifold, which describes the most natural geometric evolution problem in physics and mathematics. The research into the mean curvature flow is of particular interest in the area of analysis, differential geometry and geometric measure theory. First investigations on this topic has been presented in the pioneering work of Brakke [Brakke, 1978]. Analogously, in this thesis, we study the motion of parametric surfaces in \mathbb{R}^3 with the aim to achieve surfaces of minimal area.

Let M_0 be a regular surface in \mathbb{R}^3 . To perform an evolution of M_0 by its mean curvature, we consider the two principal curvatures κ_1 and κ_2 at each point $p \in M_0$. These curvatures measure how the surface bends in different directions at the point, i.e. it measures the maximal

and minimal bending at $p \in M_0$. The mean curvature H of M_0 is the function $H : M_0 \rightarrow \mathbb{R}$ defined by the average of the two principal curvatures given by the formula

$$H(p) = \frac{\kappa_1(p) + \kappa_2(p)}{2},$$

see Section 4.2.3. For a fixed orientation of the normal vector n_0 , the mean curvature vector H_0 of M_0 is defined by $H_0 = 2Hn_0$. The evolution of the surface M_0 by the mean curvature can be therefore described by

$$-H_0 = \partial_t x_0 \tag{6.1}$$

where $x_0 : \mathbb{R}^2 \rightarrow \mathbb{R}^3$ is the immersion representing M_0 . We consider an evolution of M_0 by the mean curvature flow.

In the sense of the parametric approach, the solution of the geometric flow defines a one-parameter family $\mathcal{M} := \{M_t, t \geq 0\}$ of immersed manifolds M_t in \mathbb{R}^3 . This family evolves in time according to the mean curvature vector that describes the velocity of the flow at each point of the surface. Here, the metric and the immersion is changing during the evolution. Moreover, the flow can be seen as the gradient flow of the area functional on the surface. The stationary points of this extrinsic flow correspond to critical points of the functional. Considering appropriate boundary conditions, in the limit, as time goes to infinity, the evolving immersion emerges as a minimal surface. Furthermore, the surface is characterized by having zero mean curvature everywhere.

In this section, we consider the construction of the mean curvature flow as a geometric partial differential equation on curved surfaces. By assigning appropriate constraints to the flow, various phenomena of evolving surfaces can be obtained. As mentioned before, it can be used to determine minimal surfaces, this is, surfaces having least area among all surfaces spanned by a prescribed boundary. Nevertheless, an initial value problem will lead to a family of shrinking surfaces that degenerate after a finite time.

6.2.1 Motion by mean curvature

For a starting time $t = t_0$, we consider a connected non-empty subset M_0 of the space \mathbb{R}^3 . We assume that M_0 is a compact two-dimensional embedded surface. The surface can be locally represented by a C^2 -continuous isometric immersion $x_0 : \Omega \rightarrow \mathbb{R}^3$, where $\Omega \subset \mathbb{R}^2$ and $x_0(\Omega) \subset M_0$. The function $H : M_0 \rightarrow \mathbb{R}$ be the mean curvature function of the immersion x_0 . The mean curvature $H(p)$ in a point $p := x_0(u)$, $u \in \Omega$, of the surface M_0 is an extrinsic measure for how curved is M_0 in the neighbourhood p . Let $n_0 : M_0 \rightarrow \mathbb{S}^2 \subset \mathbb{R}^3$ be the Gauss map of x_0 such that $n_0(p)$ is a unit vector orthogonal to x_0 at point p , i.e. n_0 is the normal vector to x_0 at p . Following the conventional notation, we can abbreviate the function $H \circ x_0$ and $n_0 \circ x_0$ to H and n_0 . Thus, $H(u)$ and $n_0(u)$, $u \in \Omega$, will denote the value of the mean curvature and the normal vector at $x_0(u)$, respectively. Suppose that each point $p \in M_0$ of the surface moves in the normal direction n_0 , this is perpendicular to the surface, with a speed proportional to the magnitude of the mean curvature H_0 at that point. This action is called motion under the influence of curvature.

For a time $t \in \mathbb{R}$, we can define a map $x_t : \Omega \rightarrow \mathbb{R}^3$ by mapping each $p \in M_t$ to the point obtained by following for time t the mean curvature vector H_t . The mean curvature vector H_t is defined by $H_t = 2Hn_t$, where n_t is the normal vector and H is the mean curvature of the surface M_t at $p \in M_t$. This means, the point p is moving in the direction of the normal vector n_t . Furthermore, the tangential velocity does not play a role. Let $\mathcal{M} := \{M_t : x(\Omega, t) \subset M_t, t \geq 0\}$ be the one-parameter family of smooth orientable immersions $x(\cdot, t)$ in \mathbb{R}^3 , obtained by the motion of M_0 under its mean curvature. Thus, the surface M_t is described by the map $x(\cdot, t) :$

$\Omega \rightarrow \mathbb{R}^3$, such that $x(u, t) \in M_t$ is a point of the surface M_t for the spatial variable $u \in \Omega$ and the time variable $t \in \mathbb{R}$. For $t = 0$ we apply $x_0(\cdot) = x(\cdot, 0)$. The mean curvature flow is therefore defined by

Definition 6.1 (Mean Curvature Flow). Let $x_0 : \Omega \rightarrow \mathbb{R}^3$ be a smooth immersion of a two-dimensional manifold without boundary in the Euclidean space \mathbb{R}^3 . The *mean curvature flow* of x_0 is a family of smooth immersions $x(\cdot, t) : \Omega \rightarrow \mathbb{R}^3$ for $t \geq 0$ such that setting $x(\cdot, t) = x_t(\cdot)$ the map $x : \Omega \times \mathbb{R} \rightarrow \mathbb{R}^3$ is a smooth solution of

$$\partial_t x(u, t) = -2H(u) n_t(u)$$

where $H(u)$ and $n_t(u)$ are the mean curvature and the unit normal of the surface M_t at the point $p = x(u, t) \in M_t$, $u \in \Omega$, respectively. The term $\partial_t = \frac{\partial}{\partial t}$ denotes the time derivative.

We call $M_0 = x_0(\Omega)$ the initial surface. Consequently, the mean curvature flow is a flow in the space of embeddings starting from the fixed surface M_0 . Since the curvature can be either positive or negative, some parts of the surface move outwards while others move inwards, based on the orientation of the surface. The points at which the mean curvature is zero will do not move under such a flow. On the other hand, the mean curvature flow is the gradient flow of the area functional on manifolds. The area reduction stops when $H = 0$. We assume that the family \mathcal{M} has a limit M_∞ as $t \rightarrow \infty$. The surface M_∞ is a minimal surface. This is characterized by having zero mean curvature everywhere.

From differential geometry point of view, the mean curvature vector $H_t = 2Hn_t$ corresponds to the invariant Laplacian of the position vector x_t , i.e.

$$2H(u) n_t(u) = -\Delta_{M_t} x(u, t) \tag{6.2}$$

where Δ_{M_t} describes the Laplace–Beltrami operator on M_t induced by the immersion x_t . The Laplace–Beltrami operator is the geometric counterpart of the Laplacian Δ on smooth surfaces in the Euclidean space. In coordinates, the Laplace–Beltrami is given, like in the Laplacian, by the divergence of the gradient of a function defined on a manifold, see Section 4.2.3. Note, Δ_{M_t} is associated with the metric. Consequently, it is a linear operator, which maps functions into functions. For more detailed examination of the mean curvature in the scope of differential geometry see [do Carmo, 1993; Kühnel, 2008].

Providing the restriction of the Euclidean metric in \mathbb{R}^3 to surface M_t , we can write the mean curvature flow as a geometric diffusion. That means, the flow equilibrates spatial variation of the surface. This is given by the formula

$$\frac{\partial x}{\partial t}(u, t) = \Delta_{M_t} x(u, t) \tag{6.3}$$

with the Laplace–Beltrami operator Δ_{M_t} on surface M_t . As a result, successively smoother surfaces M_t will be obtained. Here, the mean curvature flow can also be seen as a heat flow for manifolds. Moreover, it shares many characteristics with other geometric flows such as the harmonic map flow and the Ricci flow. For example, self-shrinking and formation of singularities are common features of these geometric flows. Additionally, the Formula 6.3 is a second order weakly parabolic partial differential equation for the local embedding map of the evolving surface. In the case of a minimal surface the equation turns out to be elliptic, i. e. $\Delta_{M_t} x = 0$. It can be shown that this parabolic problem has a unique solution for a small time interval. On the other hand, due to the fact that the Laplace–Beltrami operator is developing together with the surface at time t , the mean curvature flow is not identical to the heat equation, where the operator remains inalterable. Moreover, the Laplace–Beltrami operator degenerates as soon as

	Analysis	\leftrightarrow	Geometry
Elliptic	Harmonic equation $\Delta f = 0$		Minimal surface $\Delta_{\mathcal{M}}x = 0$
\updownarrow			
Parabolic	Heat flow $\Delta f = \partial_t f$		Mean Curvature flow $\Delta_{\mathcal{M}}x = \partial_t x$

Table 6.1: Schematic illustration of the accompanying connection of the mean curvature flow as a parabolic problem in geometry with the heat flow in analysis. The transition to an elliptic representation leads to minimal surfaces and the harmonic equation, respectively.

zero eigenvalues are achieved. In Table 6.1, a schematic representation of the mean curvature flow and the heat flow is given.

Finally, as a concluding result, we are able to directly derive an initial value problem. In doing so, the following model problem of moving closed surfaces have to be solved

Remark 6.2. Let M_0 be a compact orientable two-dimensional surface without boundary smoothly embedded in \mathbb{R}^3 . Let mapping $x_0 : \Omega \rightarrow \mathbb{R}^3$ describes M_0 locally. The family of surfaces $\mathcal{M} = \{M_t | x(\Omega, t) \subset M_t, x : (\cdot, t) \Omega \rightarrow \mathbb{R}^3, t > 0\}$ is said to be evolving by the mean curvature flow, if

$$\begin{aligned} \frac{\partial x}{\partial t}(u, t) &= \Delta_{M_t} x(u, t) & (u, t) &\in \Omega \times (0, T) \\ x(u, 0) &= x_0(u), & u &\in \Omega \end{aligned} \tag{6.4}$$

for some $T > 0$, where Δ_{M_t} describes the Laplace–Beltrami operator on M_t .

Here, we consider the identity $x(\cdot, t) := id_{M_t}$. The problem describes a nonlinear parabolic system, which is not defined at points (u, t) where the first fundamental form is $G(u) \equiv 0$. The family \mathcal{M} is therefore described by a set of successively smoother and shrinking surfaces. In the following, in order to obtain more interesting surfaces, we extend this problem to surfaces with boundary.

6.2.2 Initial-boundary value problem

Considering the mean curvature flow, the initial condition is described by the initial surface M_0 . In the following, let the initial surface M_0 be a surface with boundary. To obtain the mean curvature flow on M_0 , a set of additional constraints has to be assigned to handle the boundary of M_0 . We require, for the family \mathcal{M} of evolving surfaces to satisfy problem specific boundary constraints. Consequently, the problem to be solved is an initial-boundary value problem. In the following, suitable conditions are described to guarantee the realization of the corresponding physical model.

A soap film is characterized to be a surface of minimal area for constraints caused by the surrounding environment in a prescribed boundary. The soap film describes a stable equilibrium state. Neglecting the environmental constraints, the boundary of soap films satisfy one of the two naturally present boundary models. These are given as follows: the soap film is fixed in a fine wireframe, or it is allowed to slip along a glass surface. For each model a set of compatible boundary conditions can be determined.

Firstly, we consider the model of a soap film enclosed in a fixed wireframe. The geometrical model is given by a surface with a boundary curve conform to the wireframe. Hence, a fixed boundary curve is the basic principle for the Dirichlet boundary conditions. A reverse problem formulation is given by: starting with an arbitrary, flexible surface included in a prescribed boundary, adjust the surface so that the final surface is of minimal area. The surface remains

bounded by the same boundary curve during the movement. We consider the following formulations of the initial-boundary value problem:

Definition 6.3 (Mean curvature flow with Dirichlet boundary conditions). Let M_0 be an initial surface, where $x_0 : \Omega \rightarrow \mathbb{R}^3$ is the smooth embedding describing M_0 that satisfies

$$\partial M_0 = x_0(\partial\Omega).$$

Let the mappings

$$x(\cdot, t) : \Omega \rightarrow \mathbb{R}^3$$

be a one-parameter family of smooth embeddings for all $t \in [0, T)$. The family of resulting surfaces $\mathcal{M} = \{M_t\}$, where $M_t = x(\Omega, t)$, is said to be evolving by *mean curvature flow with Dirichlet boundary conditions*, if

$$\begin{aligned} \partial_t x(u, t) &= \Delta_{M_t} x(u, t) & (u, t) &\in \Omega \times (0, T) \\ x(u, 0) &= x_0(u) & u &\in \Omega \\ x(u, t) &= x_0(u) & (u, t) &\in \partial\Omega \times (0, T) \end{aligned} \tag{6.5}$$

where Δ_{M_t} is the Laplace–Beltrami operator of the embedding of M_t .

The mean curvature flow problem together with the Dirichlet boundary conditions is known as Plateau’s problem. The problem has been initially raised by Joseph-Louis Lagrange [Lagrange, 1761]. However, it is named after Joseph Plateau who experimented on this problem with soap films to show the existence of minimal surfaces. The stationary solutions of the Plateau problem are minimal surfaces within the given boundary. Over the time, solutions of various examples have been discovered. The general existence proof has been presented in [Douglas, 1927]. As a consequence of the boundary conditions, the surface cannot vanish. Moreover, the mean curvature H has to satisfy

$$H(u, T) = 0, \quad \text{for all } u \in \Omega,$$

for a $T \in \mathbb{R}$.

In the second model, the soap film is allowed to move along a smooth surface, called contact surface. Besides the fact that the boundary of the soap film is lying on the contact surface, it is also perpendicular to the contact surface. This boundary principle can be modelled using the Neumann free-boundary conditions. For the geometrical model, we consider the contact surface Σ to be a smooth surface fixed in the Euclidean space. Again, we start with an arbitrary, flexible surface attached to the prescribed contact surface. The boundary conditions can be defined in a purely geometric manner by requiring a vertical contact angle between the unit normal field n_t of the immersions $x(\cdot, t)$ and the given contact surface Σ . The mean curvature flow is therefore defined by

Definition 6.4 (Mean curvature flow with Neumann free-boundary conditions). Let M_0 be an initial surface, where $x_0 : \Omega \rightarrow \mathbb{R}^3$ is a smooth embedding satisfying

$$\begin{aligned} \partial M_0 &= x_0(\partial\Omega) = M_0 \cap \Sigma, \\ \langle n_0, n_\Sigma \circ x_0 \rangle(u, t) &= 0 \quad \forall u \in \partial\Omega, \end{aligned}$$

for unit normal fields n_0 and n_Σ to M_0 and Σ , respectively. Σ is the contact surface given by an arbitrary smooth surface fixed in the space. Let

$$x(\cdot, t) : \Omega \rightarrow \mathbb{R}^3$$

be a one-parameter family of smooth embeddings for all $t \in [0, T)$. The family of surfaces $\mathcal{M} = \{M_t\}$, where $M_t = x(\Omega, t)$, is said to be evolving by *mean curvature flow with homogenous Neumann free-boundary conditions*, if

$$\begin{aligned} \partial_t x(u, t) &= \Delta_{M_t} x(u, t) & (u, t) &\in \Omega \times (0, T) \\ x(u, 0) &= x_0(u) & u &\in \Omega \\ x(u, t) &\in \Sigma & (u, t) &\in \partial\Omega \times (0, T) \\ \langle n_t, n_\Sigma \circ x \rangle(u, t) &= 0 & (u, t) &\in \partial\Omega \times (0, T) \end{aligned} \quad (6.6)$$

where Δ_{M_t} is the Laplace–Beltrami operator of the embedding of M_t . The vector field n_t is the unit normal vector field of the immersion $x(\cdot, t)$.

Here, we assume that Σ has no boundary or the surface M_t keeps away from $\partial\Sigma$. However, even if the initial surface has a parametrized representation, the existence of a solution is guaranteed only for a short time, as the surface may develop knots and other singularities. The problem has been introduced by Stahl in [Stahl, 1994, 1996]. The author present a short time existence of a unique solution to any initial-boundary value problem. In [Buckland, 2005], the problem of singularity formulation on the free-boundary is studied in detail. Additionally, the author presents a classification of the limiting behaviour of boundary singularities for mean convex evolving hypersurfaces.

Finally, we consider a soap film its boundary is partly fixed to a wireframe and partly allowed to move along a contact surface. This corresponds to a mixed boundary value problem. The mean curvature flow on surfaces with appropriate boundary conditions is described by:

Definition 6.5 (Mean curvature flow with mixed boundary conditions). Let M_0 be an initial surface, where $x_0 : \Omega \rightarrow \mathbb{R}^3$ is the smooth embedding describing locally M_0 that satisfies the following boundary characterization

$$\begin{aligned} \partial M_0 &= x_0(\partial\Omega) & u &\in \partial\Omega_D, \\ \partial M_0 &= x_0(\partial\Omega) = M_0 \cap \Sigma & u &\in \partial\Omega_N, \\ \langle n_0, n_\Sigma \circ x_0 \rangle(u, t) &= 0 & u &\in \partial\Omega_N, \end{aligned}$$

for unit normal fields n_0 and n_Σ to M_0 and Σ , respectively. Σ is the contact plane given by an arbitrary smooth surface fixed in the space. Let

$$x(\cdot, t) : \Omega \rightarrow \mathbb{R}^3$$

be a one-parameter family of smooth embeddings for all $t \in [0, T)$. The family of surfaces $\mathcal{M} = \{M_t\}$, where $M_t = x(\Omega, t)$, is said to be evolving by *mean curvature flow with mixed boundary conditions*, if

Flow equation	$\partial_t x(u, t) = \Delta_{M_t} x(u, t)$	$(u, t) \in \Omega \times (0, T)$
Initial condition	$x(u, 0) = x_0(u)$	$u \in \Omega$
Dirichlet condition	$x(u, t) \in \Sigma$	$(u, t) \in \partial\Omega_D \times (0, T)$
Contact condition	$x(u, t) \in \Sigma$	$(u, t) \in \partial\Omega_N \times (0, T)$
Neumann condition	$\langle \nu, \nu_\Sigma \circ x \rangle(u, t) = 0$	$(u, t) \in \partial\Omega_N \times (0, T)$

where Δ_{M_t} is the Laplace–Beltrami operator of the embedding M_t . The vector field n_t is the unit normal vector field of the immersion M_t . Here $\partial\Omega_D$ denotes the Dirichlet boundary part and $\partial\Omega_N$ denotes the Neumann-free boundary part.

For a given embedding $x(\cdot, t)$ we assume that the exterior unit normal to Σ coincide with the unit inner normal of the boundary ∂M_t at all intersection points. The choice of normal will

by always obtained from an exterior normal field to Σ . Note, the Dirichlet and the Neumann-free boundary problem are direct implications of the mixed problem. It can be achieved by neglecting the opposite boundary part in the definition.

In the following, we continue with the mixed boundary problem. For the initialization of a given problem, the boundary of the initial surface has to fulfil the boundary condition of the corresponding problem. At this point, we are left with the objection that the topology of the solution surface of the problem is restricted to the topology of the initial surface.

6.2.3 Weak formulation

Due to the complexity of the mean curvature flow problem, we can only rely on numerical methods to solve the problem. For this purpose, the problem has to be appropriately reformulated. As a first step, we have to find a weak formulation of the problems. This simplified representation of the problem imply that the solution is contained in a suitable subspace of the initial solution space.

The classical discretization method for time-space problems is built on a time stepping method coupled with a spatial discretization technique. As already initiated in Chapter 4, for the spatial discretization, we will make use of the finite element method. There are two methods to solve a given time-space problem: the vertical method of lines and the horizontal method of lines, also called Rothe's method. The basic idea of the vertical method of lines is to discretize first in space and then in time, see [Thomé, 1984]. Here, we replace the spatial derivatives with algebraic approximations, such that only the initial value problem remains to be solved. This gives an ordinary initial value problem for the time discretization where the dimension for the degrees of freedom is very large. The obtained problem is a stiff initial value problem. For a correct solution, an implicit or linear-implicit method should be used. The advantage of this method is that standard methods for the time discretization can be used. The disadvantage is that the spatial discretization is fixed, this means that local time-dependent refinements are not allowed.

Considering Rothe's method the time variable is discretized at first by one of the common time-differencing schemes that deal with stiff initial value problems. This gives at each time step an elliptic boundary value problem that can be solved by a spatial discretization method, as for example the finite element method. The advantage of this method is that we can adaptively refine the grid during the calculation, but the implementation is much more expensive than using the previous approach. In the classical Rothe's method the time-discretization scheme is kept fixed and only the size of the time step may vary. According to that, Rothe's method appear to be the appropriate discretization technique for our purposes.

To get rid of the coupled time-space problem, firstly, we replace the time derivative with an approximation. Here, we use the implicit Euler method. In doing so, there is no restriction in the choice of time steps. Let $\tau > 0$ denote a discrete time step. The k th point in time is then given by $t_k := t_0 + \tau k$, $k \in \mathbb{N} \cup \{0\}$, and $\tau = t^k - t^{k-1}$. Let x^k denote the approximation of the original solution $x(\cdot, t^k) : \Omega \rightarrow \mathbb{R}^3$ at time $t = t_k$. For every $k \in \mathbb{N}$, $M_k = x^k(\Omega)$ be parametrized over Ω . The time derivative $\partial_t x$ is replaced by $\frac{x^{k+1} - x^k}{\tau}$. Therefore, a semi-discrete problem using the mapping x^k can be obtained.

Problem 6.6. Based on Rothe's approximation, the problem is given by

$$x^{k+1}(u) - \tau \Delta_{M_k} x^{k+1}(u) = x^k(u) \quad u \in \Omega \quad (6.7)$$

with the set of initial and boundary constraints

$$\begin{aligned} x^0(u) &= x_0(u) & u &\in \Omega \\ x^k(u) &= x_0(u) & u &\in \partial\Omega_D \\ x^k(u) &\in \Sigma & u &\in \partial\Omega_N \\ \langle \nu, \nu_\Sigma \circ x^k \rangle(u) &= 0 & u &\in \partial\Omega_N. \end{aligned}$$

for the unknown mapping x^{k+1} , $k > 0$.

The difficulty of this task lies in the fact that the Laplace–Beltrami operator Δ_{M_k} is applied to the unknown map x^{k+1} that is defined over $\Omega \subset \mathbb{R}^3$. Fortunately, the operator Δ_{M_k} is still defined by the known surface M_k . We can avoid the difficulty, if we do not use the local parameterization over the domain Ω , but instead consider a global parameterization of M_{k+1} over the previous manifold M_k . Thus, $M_{k+1} = \{x^{k+1} : x^k \rightarrow \mathbb{R}^3\}$ and $M_0 = x_0(\Omega)$. The non-linear differential equations convert therefore into a sequence of linear equations. Nevertheless, for small time steps these elliptic problems are perturbed problems, where under suitable assumptions the solution x^k at the previous time step provides a good initial approximation for x^{k+1} . Note, the existence of a solution for this problem is hard to show.

A weak solution allows one to avoid some of the high smoothness requirements. If we allow for a less smooth solution, we can rewrite the problem into the corresponding weak formulation. In the process, we multiply Equation 6.7 with a test function $w \in C^\infty(M_k)$ and integrate by parts over the domain M_k . Thus, the second order problem can be reduced to solving the following equation:

$$\int_{M_k} x^{k+1} w \, ds + \tau \int_{M_k} \left(\nabla_{M_k} x^{k+1} \right)^T \nabla_{M_k} w \, ds = \int_{M_k} x^k w \, ds \quad \forall w \in C^\infty(M_k),$$

where ∇_{M_k} is the surface gradient on M_k , see Formula 4.11. Here, the surface gradient takes effect along the surface. It is tangential to the surface. This means, the component normal to the surface is neglected. The gradient can be seen as the orthographic projection of the conventional gradient onto the surface. Further, the corresponding solution space of the model equation is $H^1(M_k)$. Due to the fact that $C^\infty(M_k)$ is dense in $H^1(M_k)$, we take as test functions $w \in H^1(M_k)$. Using this assumption, we consider the following problem formulation

Problem 6.7. For $k \geq 0$, find a mapping $x^{k+1} \in H^1(M_k)$ that is a solution of

$$\int_{M_k} x^{k+1} w \, ds + \tau \int_{M_k} \left(\nabla_{M_k} x^{k+1} \right)^T \nabla_{M_k} w \, ds = \int_{M_k} x^k w \, ds \quad \forall w \in H^1(M_k) \quad (6.8)$$

and fulfils the following set of initial-boundary constraints

$$\begin{aligned} x^0(u) &= x_0 & u &\in \Omega \\ x^k(u) &= x_0 & u &\in \partial\Omega_D \\ x^k(u) &\in \Sigma & u &\in \partial\Omega_N \\ \langle \nu^k(u), \nu_\Sigma^k \circ x^k(u) \rangle &= 0 & u &\in \partial\Omega_N \end{aligned}$$

where ∇_{M_k} denote the tangential gradient on surface M_k . The mappings ν^k and ν_Σ^k are the normal vectors of the solution and the contact plane Σ , respectively.

Consequently, this formulation of the problem is well suited for a finite element approximation. By neglecting all boundary constraints, we obtain the problem formulation for closed surfaces. The same applies to the individual boundary conditions, i.e. by omitting the relevant conditions, the mean curvature flow with Dirichlet or Neumann-free boundary conditions can

be achieved. Nevertheless, the difficulty is now to appropriately adapt the boundary constraints to the problem equation.

6.3 Discretization using subdivision finite element

The main goal of this chapter is to derive a finite element formulation of the approximation for the mean curvature flow using Catmull–Clark finite elements. One has again allow for weaker requirements on the solution. For the approximation of Problem 6.7, we replace the solution space $H^1(M_k)$ by the finite dimensional subspace V_h that consists of appropriate subdivision basis functions. Based on the weak formulation, an associated matrix representation can be described. Therefore, we will use the comprehensive previous preparations.

As mentioned before, the Catmull–Clark subdivision splines are H^2 -regular. Using the subdivision finite elements, we consider a conforming discretization of the mean curvature flow, i.e. the space of Catmull–Clark splines is a subspace of the space $H^1(M_k)$ provided by the problem. Considering the finite-dimensional solution space, in contrast to the classical finite element theory, the Catmull–Clark solution space is already prescribed by the connectivity of the initial Catmull–Clark geometry used for the representation of the problem domain. As a rule, the limit surface should represent the smooth domain sufficiently accurate. The Catmull–Clark geometry is given by the limit surface \mathcal{Q} and the appropriate control grid $\mathcal{C}_{\mathcal{Q}}$. For surfaces with boundary, an appropriate ghost geometry have to be constructed. Hence, the finite element decomposition is prescribed by the physical mesh with the surface patches $Q \subset \mathcal{Q}$ related to the control grid elements $Q_c \in \mathcal{C}_{\mathcal{Q}}$. Note that the choice of the discretization or, equivalently, of the basis functions for the calculation affects not only the quality of the results, but also the computational effort.

As next, we consider the associated subdivision finite element space $V_h(\mathcal{Q}) \subset H^1(\mathcal{Q})$ described as follows:

$$V_h(\mathcal{Q}) = \bigcup_Q V_Q = \left\{ x = \bigcup_Q x_Q \mid x_Q \in \text{span} \{ \beta_i \}_{i \in I_Q} \in V_Q, \forall Q \subset \mathcal{Q}, I_Q \subset \mathbb{Z} \right\},$$

where I_Q is the one-ring index set of element Q . The space $V_h(\mathcal{Q})$ is given by the set of subspaces V_Q corresponding to the surface patches Q . Each of the element-based spaces V_Q is determined by the appropriate set of subdivision shape functions $\{ \beta_i \}_{i \in I_Q}$ is given by the relevant set of the shape functions. The choice of shape functions $\beta_i \in \{ b_i^R, b_i^N, b_i^C \}$, $i \in I_Q$, depends on the underlying one-ring of element Q and the type of finite element approach, where we can choose between the natural and the characteristic approach, see Section 4.2.1.

Given a mean curvature flow problem together with an initial Catmull–Clark limit surface \mathcal{Q}_0 and the corresponding control grid $\mathcal{C}_{\mathcal{Q}}$. Let \mathcal{Q}_0 be a suitable Catmull–Clark surface representing the discrete analogon of the smooth surface M_0 . Considering Problem 6.7, we want to find a family $\{ \mathcal{Q}_k \}$ of Catmull–Clark subdivision surfaces \mathcal{Q}_k described on the basis of the initial surface \mathcal{Q}_0 . For $k \geq 0$, let $x_{k+1} \in V_h(\mathcal{Q}_k)$ be the unique solution of the discrete problem. That is, the mapping x_{k+1} defined over the surface \mathcal{Q}_k determine the parameterization of surface \mathcal{Q}_{k+1} . Using the basis expansion

$$x_k = \sum_{Q \in \mathcal{Q}} \sum_{i \in I_Q} x_i^k \beta_i$$

for $k \geq 0$, with coefficients $x_i^k \in \mathbb{R}$, $i \in I_Q$, we are able to rewrite Equation 6.8 into the linear

system

$$(M + \tau D) X^{k+1} = M X^k,$$

where $X_j^k = x_j^k$, $j \in I_Q$, is the j th entry of the coefficient vector in $\mathbb{R}^{|I_Q|}$. The set I_Q denotes the set of global indices, i.e. the indices of the vertices in the geometry or ghost geometry according to the problem treated here. The matrices $M \in \mathbb{R}^{|I_Q| \times |I_Q|}$ and $D \in \mathbb{R}^{|I_Q| \times |I_Q|}$ are the mass matrix and the stiffness matrix on Q^k , respectively, described in Section 4.3. The discrete mean curvature flow is given by the following problem.

Problem 6.8. For $k \geq 0$, find the family of mappings $\{x_{k+1} \in V_h(Q_k)\}$ solving the equation

$$(M + \tau D) X^{k+1} = M X^k, \quad \forall \beta_i \in V_Q \subset V_h(Q_k), \forall Q \subset Q_k, \quad (6.9)$$

where $X_i^{k+1} = x_i^{k+1}$, $i \in I_Q$, and fulfilling the set of initial and boundary constraints

$$\begin{aligned} x_0(u) &\equiv Q_0 & u &\in \Omega \\ x_k(u) &= x_0 & u &\in \partial\Omega_D \\ x_k(u) &\in \Sigma & u &\in \partial\Omega_N \\ \langle \nu^k(u), \nu_\Sigma^k \circ x_k(u) \rangle &= 0 & u &\in \partial\Omega_N \end{aligned}$$

where ∇_{Q_k} denote the surface gradient on surface Q_k . Thus, the solution x_{k+1} is given by the expansion

$$x_{k+1} = \sum_{Q \in \mathcal{Q}} \sum_{i \in I_Q} x_i^{k+1} \beta_i \in V_h(Q_k)$$

defined over the surface Q_k , $k \geq 0$. The mappings v^k and v_Σ^k are the normal vectors of the solution and the contact plane Σ , respectively.

Note, in each step of the flow, the calculation is done over the surface that has been evolved in the previous step. This means we parameterize Q_{k+1} over Q_k .

Summarizing, the above described problem will be studied in the following section. Existence and uniqueness of the discrete solution x_{k+1} is ensured, if the right-hand side matrix $M + \tau D$ is positive definite. The boundary constraints have to be adjusted immediately after each step as they do constitute a major input to the solution. At this point, if needed, we use the Lagrange multipliers to apply the constraints to the problem equation.

6.4 Implementation and experimental results

We have made all preparations that are necessary to set up an algorithm to solve a mean curvature flow on curved surfaces using Catmull–Clark subdivision surfaces. Given a mean curvature flow problem, we distinguish between the initial value problem for closed surfaces and the initial-boundary value problem for surfaces with boundary. We consider a suitable reference Catmull–Clark limit surface $Q_0 \subset \mathbb{R}^3$ that approximate the smooth initial surface. Our aim is to construct Catmull–Clark geometries Q_1, Q_2, Q_3, \dots , such that Q_i is an approximation of the smooth solution at this time. The algorithm is described by

Algorithm 6.9. Input: Let Q_0 be the initial discrete surface

If needed, generate an appropriate ghost geometry, such that Q_0 fulfils the boundary conditions
For all $k=0,1,2,\dots$ define

$$V_h(Q_k) = \left\{ x^k = \bigcup x_Q^k \mid x_Q^k \in \text{span} \left\{ \beta_i^k \right\}_{i \in I_Q} \in V_Q, I_Q \subset \mathbb{Z}, \forall Q \subset Q_k \right\},$$

where $\beta_i^k \in \{b_i^{\mathcal{R}}, b_i^{\mathcal{N}}, b_i^{\mathcal{C}}\}$ corresponds to the used finite element approach on $Q \subset \mathcal{Q}_k$ (see Section 4.2.1) and proceed with:

1. Assemble the mass matrix M and the stiffness matrix D
2. Construct the system:

if initial value problem for closed surfaces

$$(M + \tau D) X^{k+1} = M X^k \quad (6.10)$$

if initial-boundary value problem with specified constraints

$$\begin{pmatrix} M + \tau D & C^T \\ C & 0 \end{pmatrix} \begin{pmatrix} X^{k+1} \\ \lambda \end{pmatrix} = \begin{pmatrix} M X^k \\ Y \end{pmatrix} \quad (6.11)$$

where $C X^{k+1} = Y$ are the corresponding boundary constraints

3. Solve the system
4. Generate the new surface

$$\mathcal{Q}_{k+1} = \{x^{k+1}(p) \mid p \in \mathcal{Q}_k\} \in V_h(\mathcal{Q}_k)$$

Note, the system deal with three degrees of freedom for each coefficient x_i^k corresponding to the position of the control vertices. Consequently, the problem matrix is obtained as one system for the triple amount of degrees of freedom. Considering an initial value problem, the matrix can be decoupled into three equations, and that the problem matrix is the same for these three equations. In the case of a boundary constrained problem, the system is coupled and cannot be disassembled their individual components. To solve the system, we use a solver based on Jacobi preconditioned conjugate gradient method for symmetric linear systems.

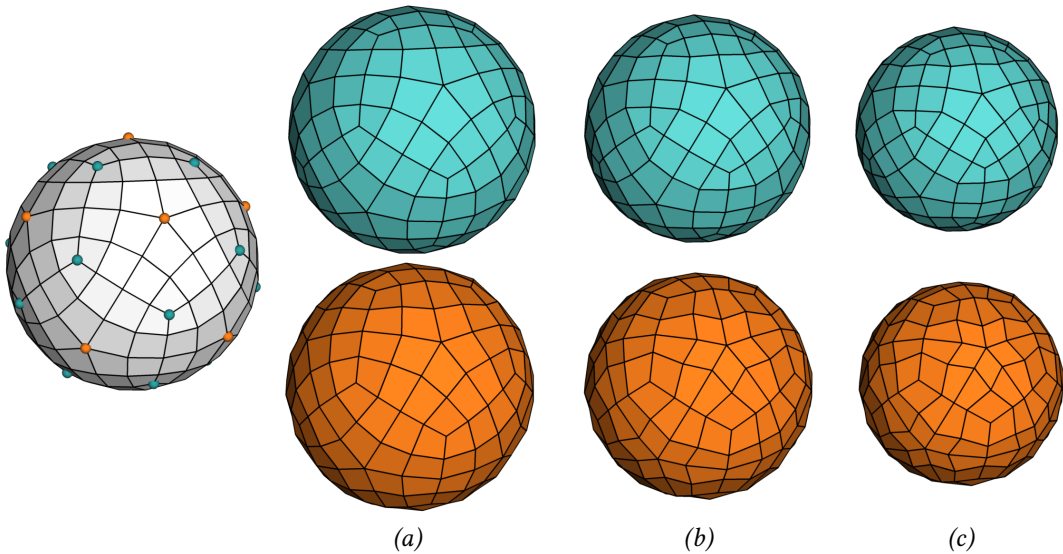


Figure 6.2: The mean curvature flow of a spherical grid (white) with extraordinary vertices of valence 3 and 5. The flow geometries at time (a) t_1 , (b) t_5 and (c) t_{10} for the time step size $\tau = 0.1$ are shown for the characteristic shape functions (blue) and the natural shape function (orange).

6.4.1 Evolution of closed surfaces

In the first experiment, we consider a control grid, which points lie on a sphere. The control grid is derived from a twice subdivided icosahedron, where the control points of the grid have been projected to the unit sphere (symmetrically to the centre of gravity). Because of the properties of the Catmull–Clark scheme, the limit surface of a spherical grid only approximates a sphere. The used control grid has extraordinary vertices of valence 3 and 5. We compute the mean curvature flow on the limit surface by solving the linear system described in Equation 6.10 for a sequence of equidistant time steps τ . The evaluation is done using two Catmull–Clark finite element approaches, this is, the natural and the characteristic finite elements. In Figure 6.2, we illustrate the resulting behaviour of the control grid under the impact of the mean curvature flow for the two finite element approaches.

	t_1	t_3	t_5	t_{10}
characteristic	1.01050	1.00552	1.00314	1.00099
natural	1.01791	1.01650	1.01228	1.00520

Table 6.2: Comparison of the ratio of the maximal radius to the minimal radius of the limit surface at time t_1, t_3, t_5 and t_{10} of the mean curvature flow using characteristic and natural shape functions. For comparison, the ratio of the limit surface of the initial grid is 1.01568.

Additionally, we examine the limit surface of the control grids emerging during the flow. Considering the flow impact, each point of the surface is moving in the mean curvature direction that decreases the absolute value of its curvature. This is, for a convex control grid, the limit surface becomes step-by-step more spherical. Considering the control grid in a given time step, the Catmull–Clark limit surface is an approximation of a sphere with an unknown radius. To get an impression of the deviation from this sphere, we calculate the ratio of the maximal to the minimal radius. In Table 6.2, we show the ratios of the limit surface for a number of time steps. The evaluation of the limit surface has been done using a grid of ten by ten equidistant evaluation points over each element. In both cases, the limit geometry is more and more approaching a sphere. However, in the first step of the natural approach the ratio increases. In Figure 6.3, the mean curvature of the initial limit surfaces and the limit surfaces for both shape function approaches at time t_{10} is shown. In order to obtain comparable curvature values, we scaled the initial grid to a sufficiently equal size. The colour coding illustrates the distribution of the mean curvature. It can be seen by the curvature distribution that for the characteristic approach the

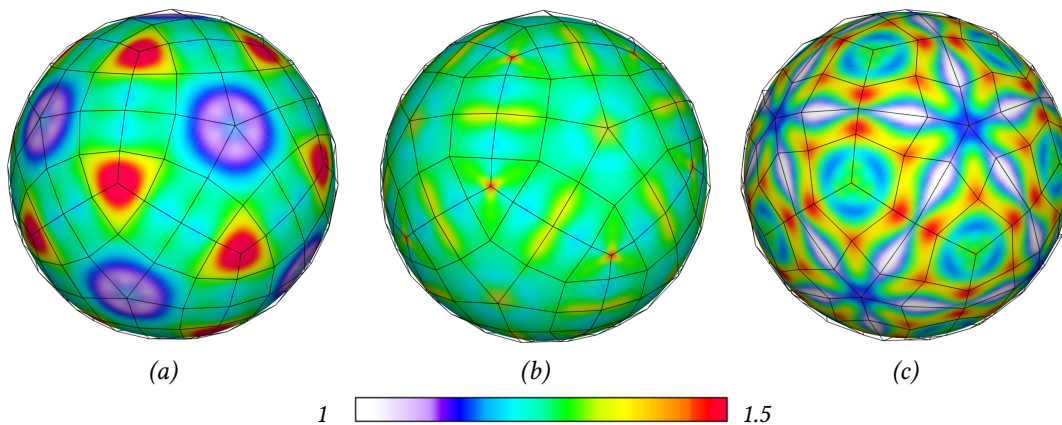


Figure 6.3: Comparison of the mean curvature of the limit surfaces of (a) the initial grid (scaled by 0.8), (b) the grid at time t_{10} using characteristic shape functions and (c) the grid at time t_{10} using natural shape functions. The colours correspond to the values in the range $[1, 1.5]$. The distribution of the colour is shown by the colour bar. The evaluation of the surfaces is done via the natural parameterization.

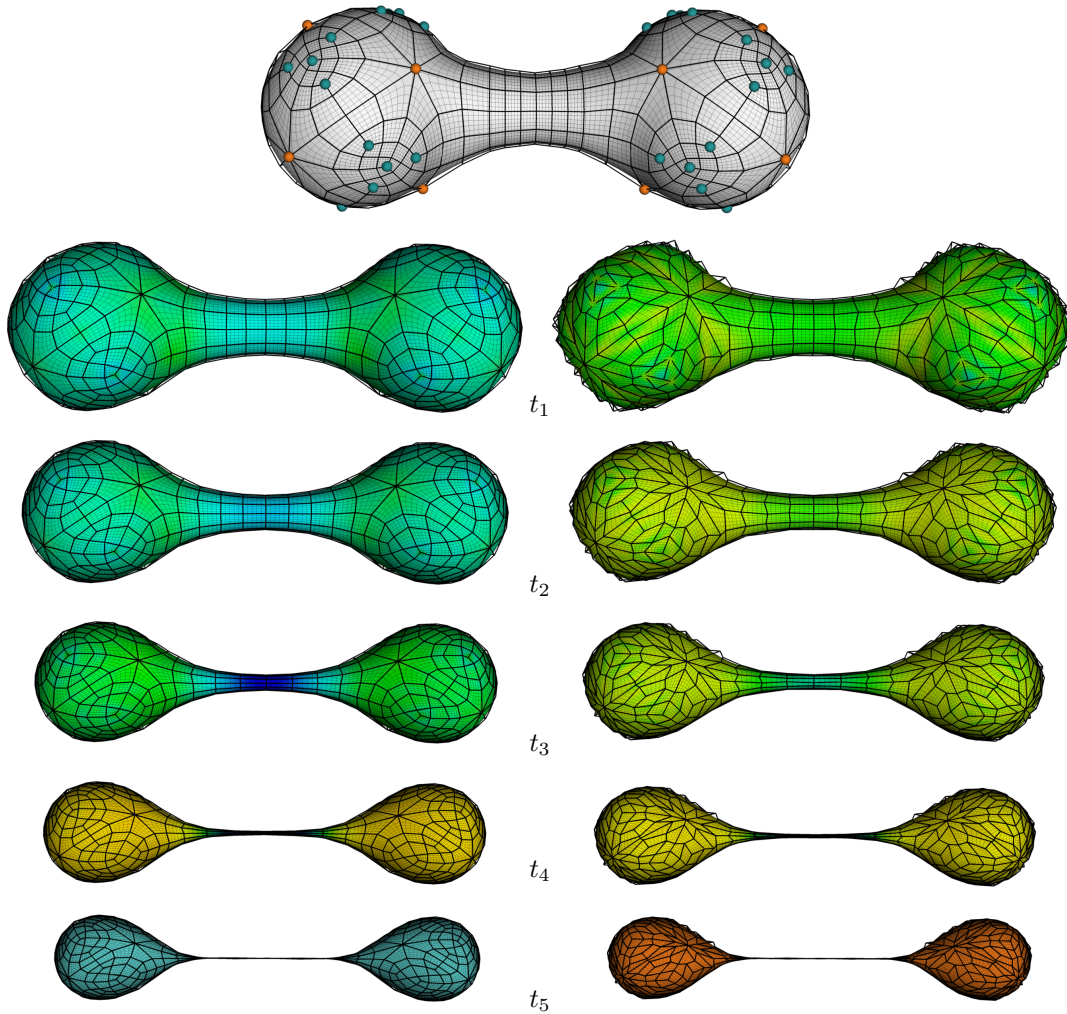


Figure 6.4: The evolution of a singularity on Grayson's dumbbell. We compare the impact of the characteristic and natural subdivision finite elements. In the first row, the initial mesh with its limit surface containing vertices of valence 3 (blue) and 8 (orange) is shown. In the left and right column, the results for the characteristic and the natural approach, respectively, have been shown for a number of time steps t_i , $i = 1, \dots, 5$. The limit surfaces and the control grids are illustrated. The range of the curvature describing to the colouring of the limit surfaces is changing with each step. A singularity appear at time t_5 , for $\tau = 1$.

limit surface is more spherical than with the natural approach.

In the next experiment, we consider a non-convex dumbbell-shaped control grid. The corresponding mean curvature flow problem is called Grayson's dumbbell problem. By definition, any closed surface becomes spoiled in finite time. This means that the flow can only be continued smoothly for some finite. As observed by Grayson, the presented set must develop a singularity when its evolution is not yet reduced to a point. In doing so, before the set become singular, topological changes should be applied, i.e. split of the set in two separate pieces. If the initial surface is embedded, then it remains embedded under the mean curvature flow, we do not consider any geometry splitting. The considered control grid has a large number of extraordinary vertices of valence 3 and 8. In Figure 6.4, the evolution of the surface using the natural and the characteristic approach is shown. After five steps the singularity occurs. Here, a singularity is obtained by a self-intersection of the control grid. We compare the control grids and the limit surfaces of the two approaches. Considering the natural approach, the control grids show a disproportional deviation from the initial grid. On a closer look, this results in significantly undulation of the limit surfaces. A more resistant behaviour is obtained by using the characteristic approach.

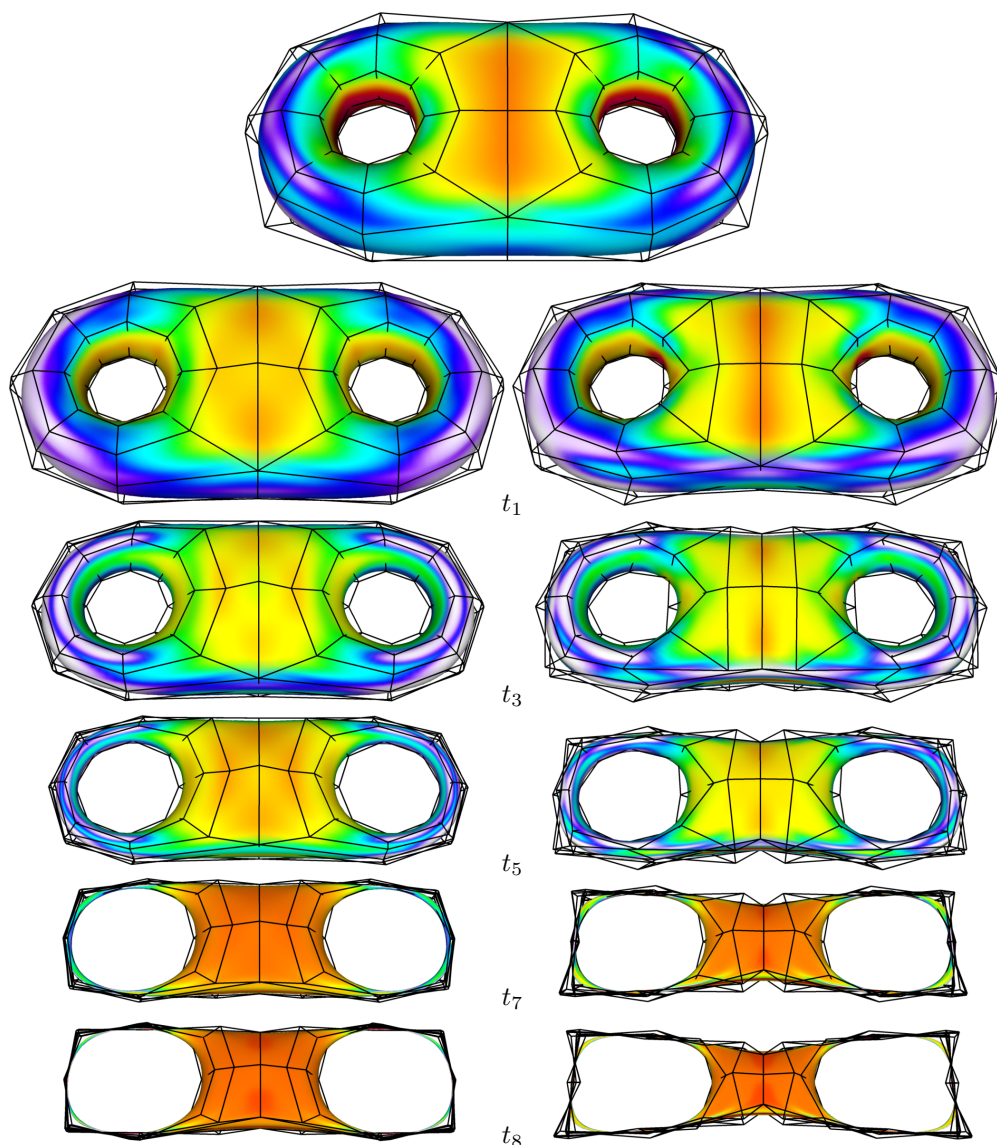


Figure 6.5: Comparison of the impact of the characteristic and natural subdivision finite elements for the mean curvature flow on a non-convex surface with genus two. In the first row, the initial grid and its limit surface are shown. In the left and right column, the characteristic and the natural approaches, respectively, have been shown for a number of time steps t_i , $i = 1, 3, 5, 7, 8$. The range of the curvature corresponding to the colouring is changing with each step. Singularities appear at the handles, at time t_7 for the natural, and at time t_8 for the characteristic approach.

In the last experiment, we examine the behaviour of a non-convex initial surface with genus two under the impact of the mean curvature flow. The control grid has four extraordinary vertices with valence 6. The impact of the flow for a number of steps is shown in Figure 6.5. We compare the control grids and the limit surfaces of the two approaches. The surfaces are coloured by its mean curvature, this allow the investigation of the behaviour of limit surfaces in more detail. In both cases, the surface degenerates at the handles. However, using the natural elements the control grid differs from the initial grid and destroys more and more in the course of time. The distribution of the mean curvature on the handles indicates a perturbed surface behaviour. In contrast to this, the characteristic approach provides a non-destructive grid behaviour and a uniform shrinking of the surface. On the latter point, consider the even shrinking and, equivalently, the uniformly distributed curvature at the handles.

As the experiments show, the characteristic approach leads to better mesh behaviour. The

reason for this can be obtained by comparing both approaches. The difference is due to a factor influencing the calculation. The factor accompanies the pullback onto the domain of the finite element method. It emerges as the scaling factor λ of the partitioned domain (see Figure 3.14) and influence the surface gradient defined in Section 4.3.2. For the natural finite element approach based on the natural generating spline, the factor is the same, regardless of the valence of the extraordinary vertex, i.e. $\lambda = 1/4$ for all valences. Whereas for the characteristic approach λ is changing depending on the extraordinary vertex valence. Keep in mind that λ is here the subdominant eigenvalue of the subdivision matrix and closely connected with the characteristic map.

6.4.2 Periodic minimal surfaces

The main focus of this section is on periodic minimal surfaces given by critical points of the mean curvature flow. We begin with a more elementary example of a symmetric surface. We consider Grayson's dumbbell problem reduced to a symmetric part of the control grid. In Figure 5.5, a schematic construction of the symmetrical problem is illustrated. Due to the problem construction, the surface pieces shrinks in the course of the evolution and remains symmetric to the symmetry planes of the total control grid. As shown previously, it results in a singularity. The minimization of the dumbbell piece is shown in Figure 6.6. We compare the results using the natural and the characteristic approach. As known from the previous section, the surface behaviour using the characteristic finite elements is significantly better than by using the natural approach. We test here the behaviour of our symmetry conditions along the boundary. It can be seen that the results are promising, i.e. the construction do not affects the solution close to the boundary, as it is the case for the compatible constrains (see Figure 6.1).

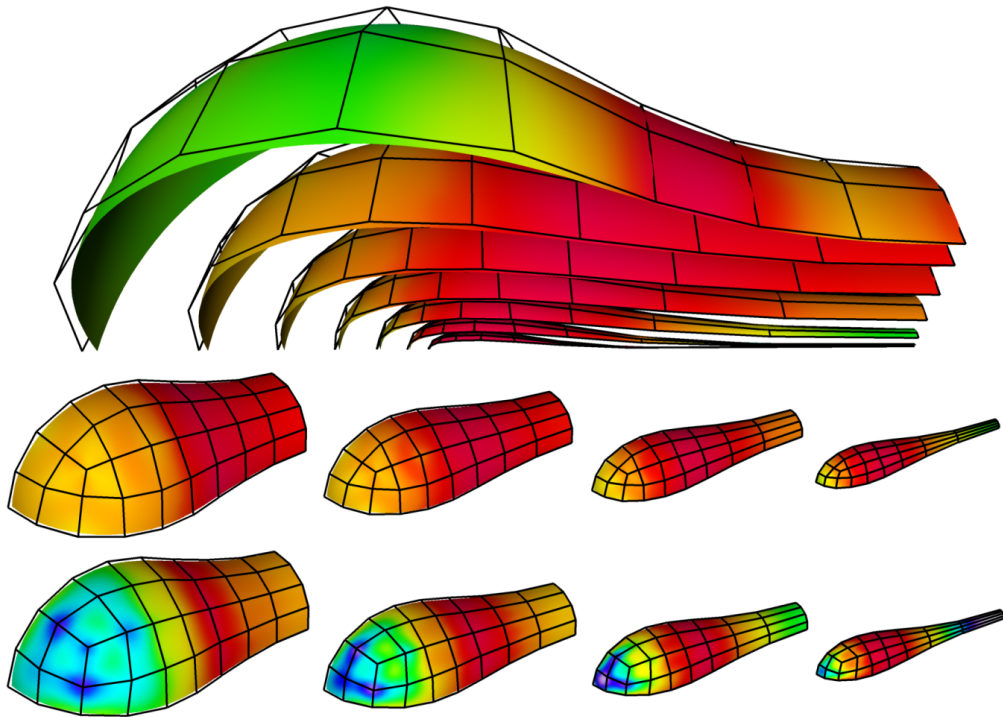


Figure 6.6: The evolution of a singularity on a symmetric piece of Grayson's dumbbell. The construction is shown in Figure 5.5, whereby three symmetry planes perpendicular to the coordinate directions determine the symmetric piece. First four steps using characteristic (middle row) and natural subdivision finite elements (bottom row) are shown. The range of the curvature describing the colouring of the limit surfaces is changing with each step.

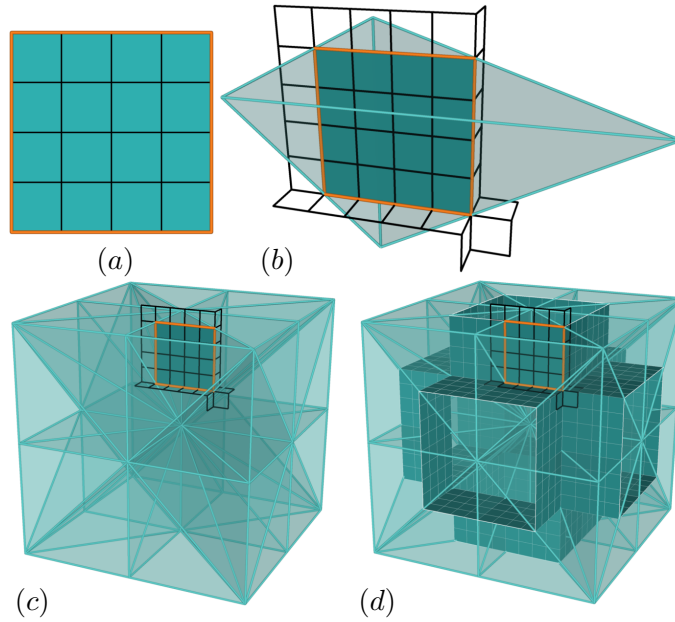


Figure 6.7: Construction of the Schwarz P problem. An (a) initial grid is constructed, and (b) fitted into the fundamental cell that describes the symmetry conditions for the construction of the ghost. Consider (c) the tilling of the unit cell in the reflected pieces of the fundamental cell and (d) the associate surface.

Now, we consider the construction of periodic minimal surfaces based on Catmull–Clark subdivision surfaces. The approximation of the smooth models is initialized on an arbitrary quad grid for that the limit surface fulfils the initial conditions. Based on the principle of the mean curvature flow, a Catmull–Clark minimal surface is defined by

Definition 6.10 (Catmull–Clark minimal surfaces). The limit surface of a control grid that is a critical point of the mean curvature flow, i.e. no single control grid vertex can be moved to decrease the area of the corresponding limit surface, is called a *Catmull–Clark minimal surface*.

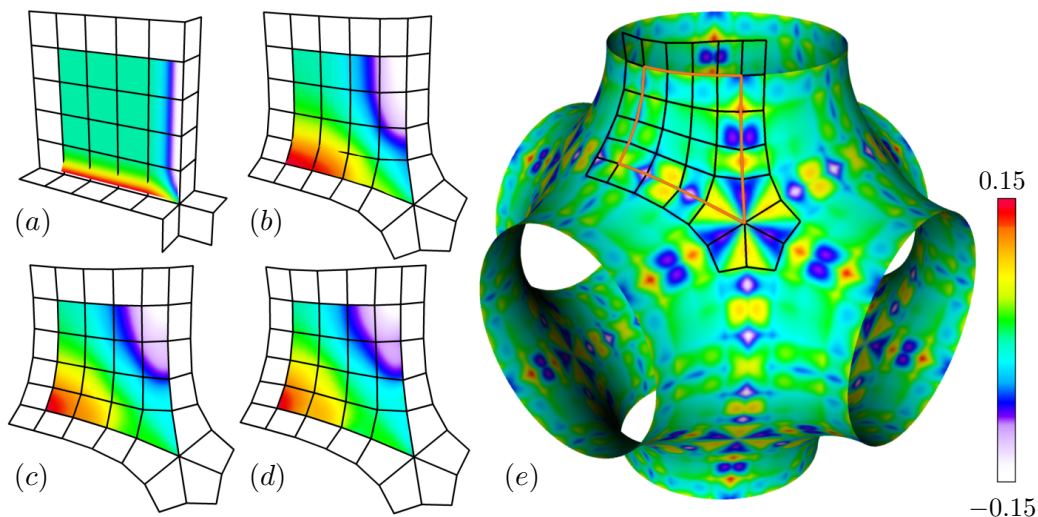


Figure 6.8: Schwarz P surface. The evolution of a surface piece resulting in an approximated Schwarz P surface piece that is used for the construction of the total surface. We use Schwarz reflection to establish a complete smooth surface. The (a) initial Catmull–Clark geometry, and the geometries at time (b) t_5 , (c) t_{10} and (d) t_{15} are shown. The mean curvature flow limit is used for the construction of the total surface (e). The colouring of the limit patches is described by the mean curvature distribution, it changes according to the time. For the flow limit, the distribution of curvature is shown by the colour bar.

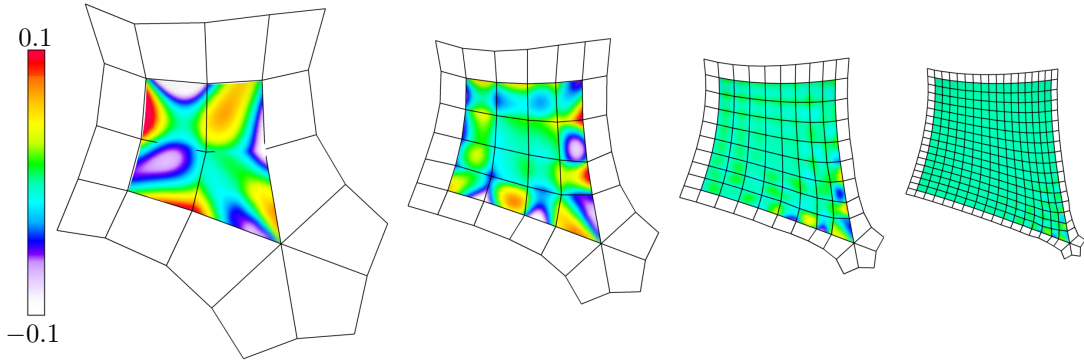


Figure 6.9: The limit of the mean curvature flow for the Schwarz P problem on meshes with increasing resolution using the characteristic approach. The limit surfaces and the corresponding control grids are illustrated. The colouring of the surfaces is given by the distribution of the mean curvature in the range of $(-0.1, 0.1)$.

From the point of view of local geometry, a minimal surface can be also taken as the surface which has the zero average mean curvature at each surface point, e.g. each point is a saddle point. However, the Catmull–Clark surfaces are at most C^2 -continuous. The limit surface is an approximate solution of the real minimal surface in the space of $C^1 \cup H^2$ -continuous surfaces. Additionally, due to the wiggly nature of spline surfaces, the mean curvature of the limit surface can therefore differ from the ideal $H = 0$ state.

To picture the construction process, as an example, we consider the underlying structure of the initial-boundary value problem of the Schwarz P surface shown in Figure 6.7. We consider the symmetry conditions of a fundamental patch for the construction of the total surface. Given an initial Catmull–Clark geometry that fits into an appropriate fundamental cell. Thus, the contact surfaces are equal to the faces of the fundamental cell. Based on the symmetries of the cell, the ghost geometry is constructed using the symmetry conditions along the boundary of the geometry. The initial control grid is the crucial characteristic that specifies the solution space. In Figure 6.8 (a), the initial limit surface of the Schwarz P patch is shown. In general, the limit surface boundary does not interpolate the boundary polygon of the control grid and is not equal to the B-spline curve described by the polygon.

The problem to be solved is described in Equation 6.11. The boundary conditions are established in accordance with the symmetry conditions described in Section 5.3.3. In Figure 6.8, a couple of intermediate steps of the evolving limit surface are shown. Using the resulting configuration, we construct the total limit surface shown in Figure 6.8 (e). The colouring describes

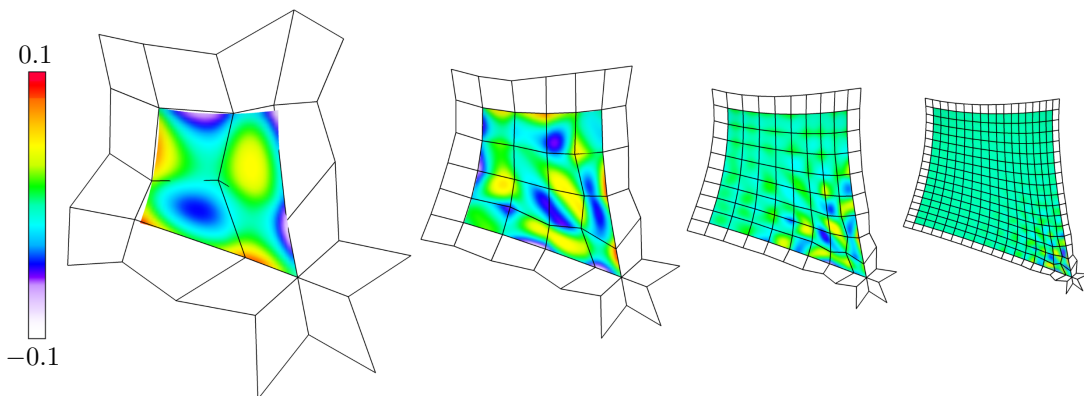


Figure 6.10: The limit of the mean curvature flow for the Schwarz P problem on meshes with increasing resolution using the natural approach. The limit surfaces and the corresponding control grids are illustrated. The colouring of the surfaces is given by the distribution of the mean curvature in the range of $(-0.1, 0.1)$.

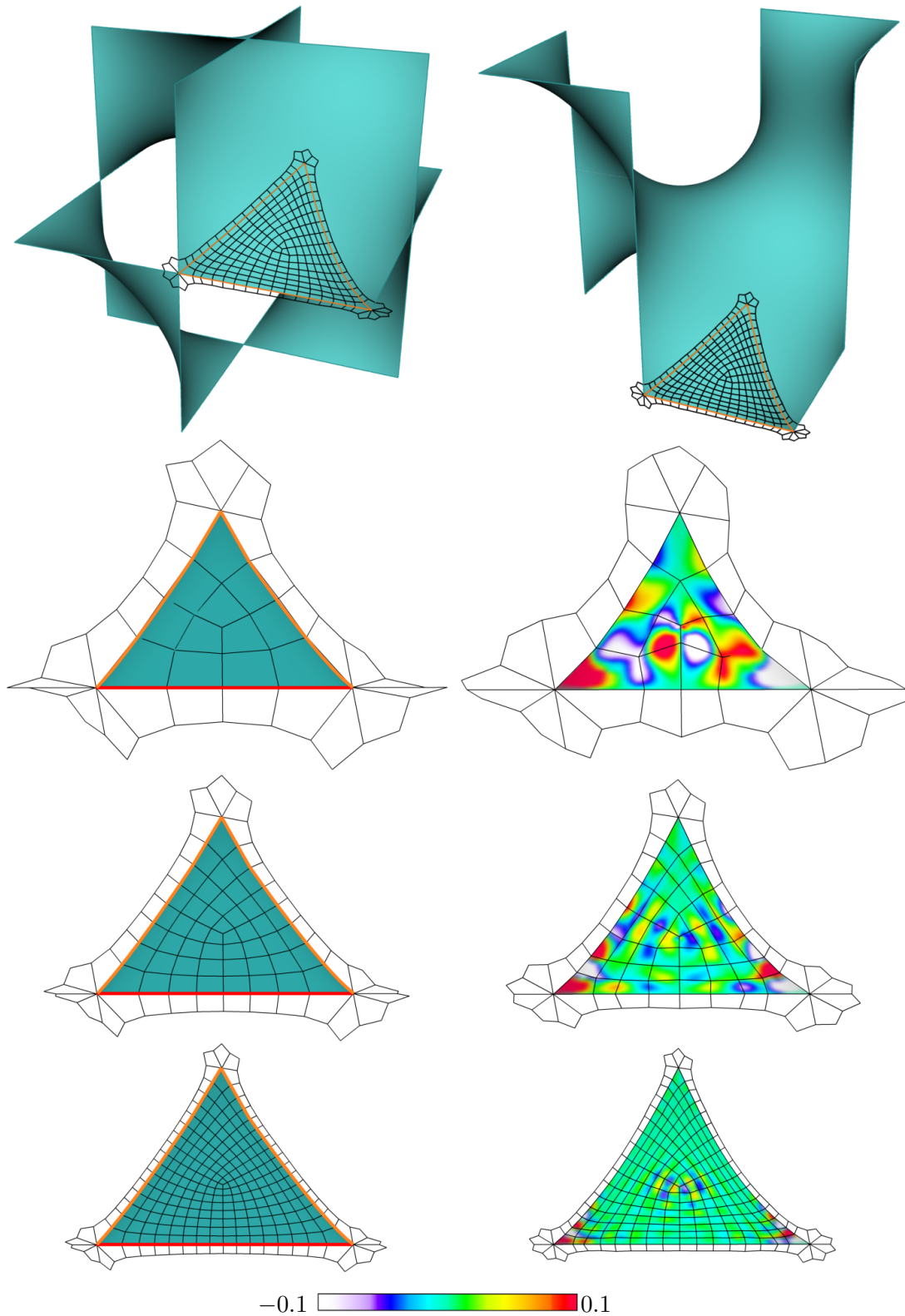


Figure 6.11: Schwarz D surface. Two constructions of the minimal surface (top) are illustrated. The impact of the mean curvature flow on increasingly finer control grids is shown below: the initial meshes (left), and the final limit surfaces (right) coloured by the mean curvature in the range of $(-0.1, 0.1)$. The colour distribution is prescribed by the colour bar. Considering the initial grids, the red line describes the boundary part contained in a rotation axis and the orange line the part allowed to move along the corresponding reflection plane.

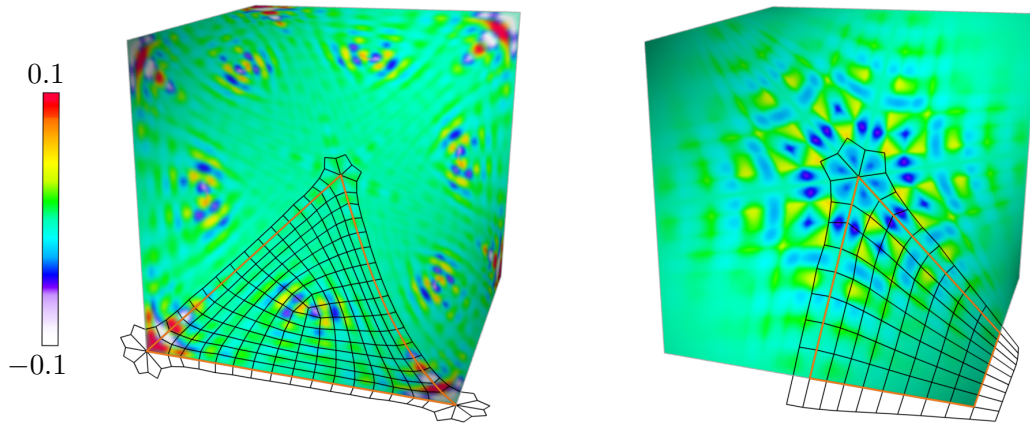


Figure 6.12: Schwarz D surface. Consider two different initial meshes that have been used for the calculation and construction. The resulting minimal surfaces completed by the Schwarz reflection of the minimized fundamental patch are illustrated. The colouring describes the behaviour of the mean curvature of the limit surface. Additionally, the ghost geometry of the control grid (bounded by the orange curves) associated with the fundamental patch is shown.

the mean curvature of the limit surface. The distribution of the mean curvature is shown by the colour bar. For the final geometry, the range of the mean curvature is given by $(-.015; 0.15)$. The distribution of the colours in the range has been illustrated by the colour bar. For the other geometries wider ranges of the mean curvature have been used, then for the final surface. The behaviour of the Catmull–Clark limit surface under the impact of the mean curvature flow on increasingly finer meshes is illustrated in Figure 6.9 for the characteristic approach and in Figure 6.10 for the natural approach. For both approaches, the solutions show a symmetric behaviour, where the finer resolution provides a better approximation of the solution. Note, the ideal solution is here a surface of zero mean curvature. However, as can be seen from the figures, the curvature is very sensitive. Its deviation indicates imprecisions related to the control grid. Thus, the irregular element has a big impact on its neighbourhood. Nevertheless, comparing the two approaches, the characteristic approach provides a homogeneous behaviour of the control grid, whereas for the natural approach the mesh distortion close to the irregular vertex is enormous. Although, up to the two-ring of the irregular element, a relatively small distortion can be noticed in the former case.

In contrast to the Schwarz P problem, where all boundary curves are allowed to move freely along the corresponding reflection surface, the fundamental patch of the Schwarz D surface is constrained to fulfil reflection and rotation constraints along prescribed parts of the boundary, as shown in Figure 6.11. For the computation, we consider control grids of increasing finer resolution, see Figure 6.11, and different combinatorial structure, see Figure 6.12. Meshes of increasing resolution meet the underlying principle of finite element, i.e. finer meshes leads to better approximations. The undesirable effects of the mean curvature improves, the finer meshes are considered. However, the deviations remains attached to the neighbourhood of the irregular elements with extraordinary vertices of valence 3 and 8.

In Figure 6.12, the triangle shaped mesh contains extraordinary vertices of different valences, i.e. of valence 3, 6 and 8, whereby the quadrangular mesh has only one extraordinary vertex of valence 6. At the same time, the vertex of valence 6 behaves differently in every configuration, even while being situated in the same place on the surface. Comparing with the classical Schwarz D surface, the boundary of the triangle shaped control grid coincides with the curved symmetry lines, such that the grid is able to deal with the elastic deformation under the variations of surface pressure along the line. Thus, the boundary of the quad shaped grid coincides with the asymptotic lines, such that the boundary control vertices are allowed to move along these lines.

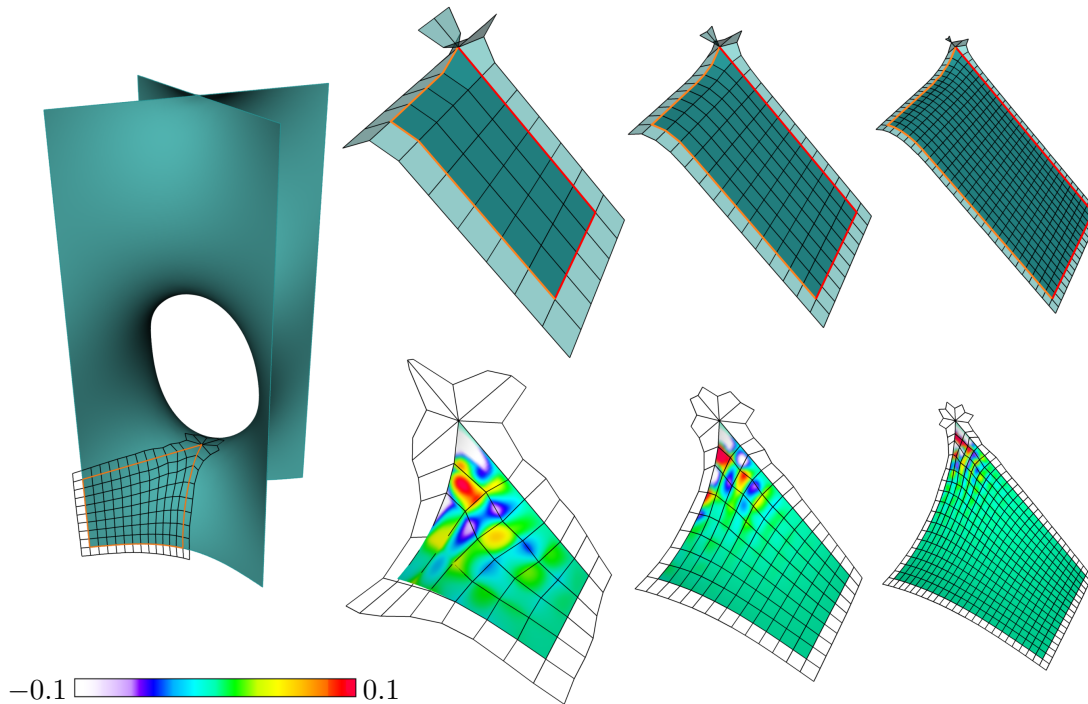


Figure 6.13: Schwarz CLP surface. The impact of the mean curvature flow on increasingly finer control grids is shown: the initial control grids (top), and the deformed control grids together with the final limit surfaces (bottom). The colouring of the final surfaces is described by its mean curvature. Considering the initial grids, the red line describes the boundary part contained in an appropriate rotation axis and the orange line the parts allowed to move along the corresponding reflection plane.

Accordingly, as can be seen by the curvature behaviour, the control grid is too stiff to follow the requirements, the surface behaves rigidly.

In the next example, we deal with the construction of the Schwarz CLP surface. We consider a symmetric fundamental patch that is mostly based on regular elements. The initial control grid used for the calculation contains one extraordinary vertex of valence 8 at the intersection of a reflection plane and a rotation axis, see Figure 6.13. Two of the boundary curves are contained in a rotation axis and two are free to move along a corresponding reflection plane. Therefore, three corners are fixed and one is allowed to move along an intersection line. Additionally, we compare two different control grids shown in Figure 6.14. As the distribution of the mean curvature shows, the undesirable effect of the curvature affect at most the neighbourhood of the extraordinary vertex. However, a closer look at the neighbouring regular elements shows that the defects are the greatest up to the five-ring of the extraordinary vertex. That is to say, considering the two-ring support of the basis function corresponding to the extraordinary vertex, a non-zero mass integral is obtained for functions up to the three-ring. The basis function in the third ring has again a two-ring support. Consequently, disturbances up to the five-ring are the consequence of the approximate integration over the irregular element.

The last example is showing the construction of Sherk's surface, see Figure 6.15. Considering the initial mesh, the elements are rectangles, stretched in one direction. Three of four boundary parts are contained in an appropriate rotation axis and one is allowed to move along a reflection plane. All corner vertices are fixed. The results are similar to the previous one, undesirable effects close to the extraordinary vertex are obtained. The shape of the elements is of second importance since the curvature of the limit surface related to the regular elements are behaving as for the square elements. However, the deviation extends accordingly to the shape of the grid elements.

Considering the minimal surface definitions, a minimal surface is defined to be the surface of

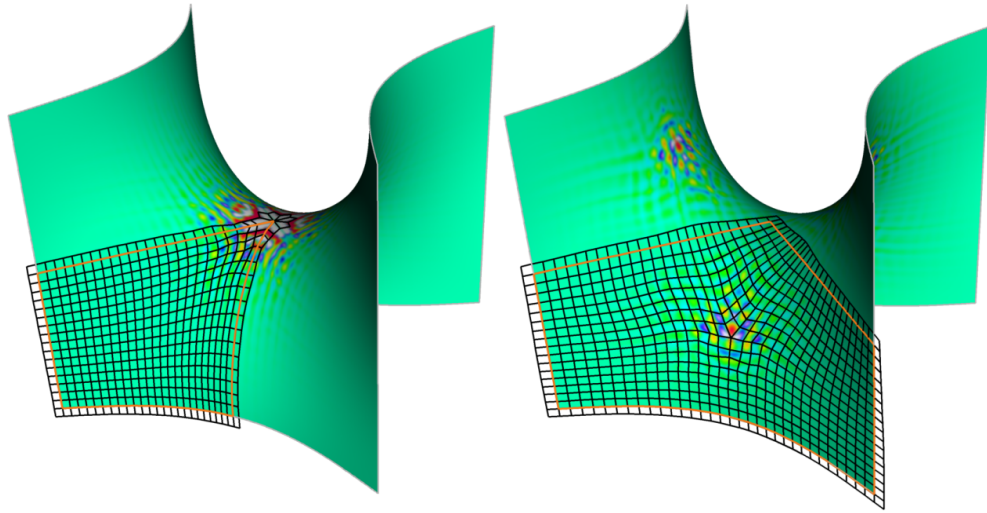


Figure 6.14: Schwarz CLP. Two different minimized grids (bounded by the orange boundary) and its ghost geometries (black grid) obtained for the construction of the Schwarz CLP surface. The first one contains an extraordinary vertex of valence 8 at the boundary. In the second one, an internal extraordinary vertex of valence 5 is obtained.

least area with respect to its boundary. On the other hand, based on the finite element approach, an increasingly finer mesh leads to a better result. In Table 6.3, the relation between the area value and the finer mesh is presented. For the considered examples, the area of the resulting limit surfaces of the presented initial control grid and its two subdivisions is computed. We calculate the area integral over the individual element patches adding all results together. For the extraordinary element, we consider the infinite partition of the patch and perform the calculation up to the 40th, 39th and 38th subdivision level for the initial grid, the 1st and 2nd subdivided mesh, respectively. As can be seen, an area minimization is described, whereby a good approximation is already given for the coarse grid. Considering the different constructions of the initial control grid of one type of surface, the area results are more or less similar. Compare the results on the example of the Schwarz D and the Schwarz CLP surfaces.

Summarizing, the usage of the mean curvature flow for the construction of periodic minimal surfaces has a limitation. That is, only stable minimal surfaces can be constructed. A stable minimal surface is described (where possible) by a soap film when the pressure is equal on each side of the surface. The Schwarz P, Neovius and I-Wp minimal surfaces are unstable, i.e. solving the corresponding mean curvature flow problems for an infinite time leads to degenerations. However, in the first minimal surface example, we constructed a Schwarz P surface using the property that a straight (asymptotic) line connects the extraordinary and the corner vertex located along the diagonal of the control grid.

When looking at the results, the introduced boundary conditions allow to reduce the problem to a symmetric fundamental patch. Although, the construction of the ghost geometry and the corresponding boundary constraints have to be carefully executed. In doing so, the approach is compatible with the given H^1 problem. Nevertheless, we also have studied the problem using pointwise constraints, see Section 5.3.2. However, it was not straight forward to find a set of suitable constraints in order to avoid overdetermining the system. In Figure 5.7, an example of one step of the mean curvature flow is shown. We constrained the limit positions of the boundary vertices of the shown control grid to fulfil the Neumann free-boundary constraints. The outcome shows that the resulting control grid does not fit in the fundamental cell and the ghost geometry is disturbed, but the constrained limit surface vertices do fulfil the constraints. That is, the constrained vertices are attached to the reflection planes, and the surface normals

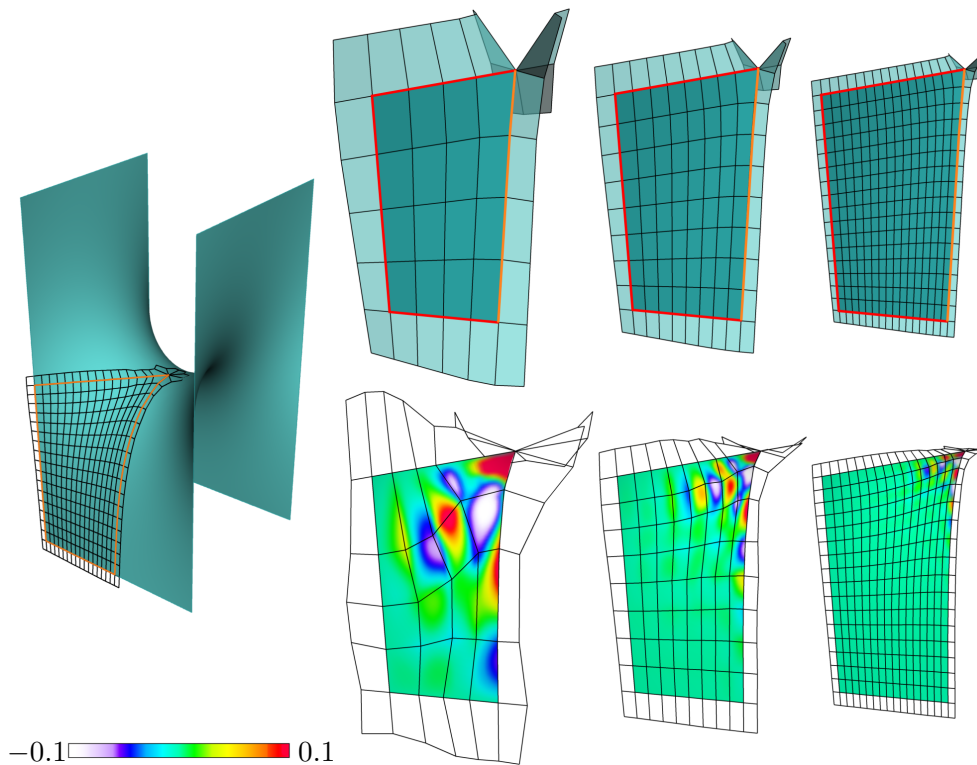


Figure 6.15: *Sherk surface. The impact of the mean curvature flow on increasingly finer control grids is shown: (top) the initial control grids, and (bottom) the deformed control grids together with the final limit surfaces. The colouring of the final surfaces describes the mean curvature of the limit surface. Considering the initial grids, the red lines described the boundary part contained in a rotation axis and the orange line the parts allowed to move along the corresponding reflection plane.*

are contained in the reflection planes. In the presented example, the normals at the corners rotates. We succeeded and rescue the problem by applying our symmetry constraints to the ghost vertices. Consequently, the result is similar to the result shown in Figure 6.9.

In summary, using the Catmull–Clark finite elements to solve the mean curvature flow provide already a good approximation for coarse control grids. However, as shown in the experiments, the highest variation of mean curvature on the subdivision limit surface is detected close to the extraordinary vertices. Consequently, the operations on irregular elements are very sensitive. Please bear in mind that the presented results arise from evolving control grids, and, equivalently, from evolving integral approximation errors. The characteristic approach provides a much better result than the natural approach, but still the integration requires further improvements.

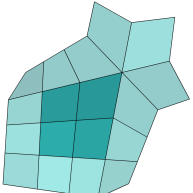
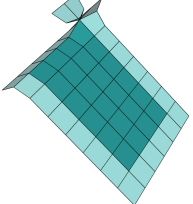
Minimal surface	Initial	1st subdivision	2nd subdivision
Schwarz P 	0.1954255193	0.1954252611	0.1954252497
Schwarz D 	5.1171073274	5.1170527144	5.1170479040
Schwarz D 	1.2792754920	1.2792624760	1.2792616227
Schwarz D 	1.2794327124	1.2792919632	1.2792643118
Schwarz CLP 	0.0515740189	0.0515718827	0.0515713660
Schwarz CLP 	0.1031434178	0.1031427515	0.1031427381
Sherk 	5.4814088101	5.4807817036	5.4806784368

Table 6.3: Area minimization of different Catmull–Clark geometries. The initial control grid with the ghost geometry is shown. We calculated the area of the minimized initial control grid, its first and second subdivisions. Considering the evaluation on the irregular elements, we calculated the area up to the 40th, 39th and 38th subdivision level, respectively. The blue coloured numbers show the position from when the area changes.

CHAPTER 7

CONCLUSIONS

Through this thesis, starting from the classical subdivision theory, we have gained the understanding of the Catmull–Clark subdivision surfaces with the aim to develop a new approach that integrate these into a corresponding finite element method. Although the Catmull–Clark subdivision scheme is not a novelty, its power has still not been completely explored. A first idea on Catmull–Clark subdivision finite elements has been introduced in our previous works [Wawrzinek, 2011; Wawrzinek et al., 2011], however, this work gives a deeper insight into the principles and needs of the underlying basis functions, called here the generalized B-splines of Catmull–Clark type. We present two associated parameterizations, the natural and the characteristic, and look more closely at its properties. In doing so, one can realize the high correlation between the classical subdivision theory and the emergent parametric representation.

Considering the parametric representation of the generalized B-splines, the natural consequence is to aim for finite element methods to solve PDEs on surfaces. Using the expensive characteristic parameterization, we have newly introduced a finite element construction that is compatible with the classical subdivision surfaces. We have shown that the inversion of the characteristic map is done only implicitly, i.e. in the integral representation, the used map reduces to a valence dependent scaling factor. In this connection, the evaluation cost for our approach is comparable to the natural finite element approach known from the literature. This makes our approach equally practicable for PDE applications, as the natural approach is. However, due to the complexity of the problem, an efficient numerical integration method is still an open problem. In doing so, the main crucial issue is the computation of integrals on irregular elements, further developments have to be done in this direction. Using the so far best integration method, i.e. by evaluating the regular subpatches up to a prescribed subdivision level, experimental investigations on the integration requirements on irregular elements has been done. Additionally, we give an valence dependent option for the choice of the number of levels for the integration. That is, we consider a maximal number of levels for a given valence of the extraordinary vertex

corresponding to a prescribed portion of the to be integrated domain.

One of the goals of this thesis is to show our experience regarding the application of subdivision finite elements for PDEs on curved surfaces. In the focus of interest is the mean curvature flow. We describe in detail a conforming discretization of the mean curvature flow using the Catmull–Clark finite element. To understand the behaviour of the method close to singularities, we examine the repeated application of the subdivision finite element method. That is, the computation is done on limit surfaces, changing under the impact of the flow. The problem of evolutionary surfaces in the context of subdivision surfaces has been discussed for the first time in this thesis. In this regard, experimental investigations on closed surfaces and surfaces with boundaries have been performed.

Considering the task of evolving surfaces, an important application of the mean curvature flow is the construction of periodic minimal surfaces. In this context, we present an algorithm to generate periodic Catmull–Clark minimal surfaces as an approximate analogon of the analytical solutions. A set of appropriate symmetric boundary conditions has been constructed that fulfil Schwarz’s reflection principle. On the basis of this, we introduce new boundary conditions for PDEs on subdivision surfaces. However, due to the number of different conceptual aspects that must be taken into account, the assembly of the problem has to be handled very carefully.

In summary, the major benefit of using the subdivision finite element method is that it allows simultaneously for a suitable geometry representation. The results of the experiments show that the introduced characteristic finite elements describe a promising approach for the approximation of PDEs on surfaces. The undesirable effects of the mean curvature close to the irregular vertices are probably due to the fact that the numerical integration on irregular elements leads to a successive increase of the resulting error. Further improvements related to the treatment of irregular elements need be established. Additionally, the main disadvantage of subdivision finite elements is the significantly higher computational cost compared to the classical finite elements. Moreover, using the mean curvature flow for the minimal surface problem has a limitation. That is, only stable minimal surfaces can be constructed. For future works, it will be important to address the investigation of convergence behaviour of the presented finite element method. Additionally, the implementation into traditional numerical codes is essential to get stability.

APPENDIX

We consider the contraction of the subdivision matrices A and \bar{A} described in Section 3.2.3. Here, we use the same notation as derived in Stam [1998]. For the precise derivation of the listed matrices we refer to Stam.

For a valence ν of an extraordinary vertex, the subdivision matrix S associated with the one-neighbourhood of the vertex is described by the form

$$S = \begin{pmatrix} a_\nu & b_\nu & c_\nu & b_\nu & c_\nu & b_\nu & \dots & b_\nu & c_\nu & b_\nu & c_\nu \\ d & d & e & e & 0 & 0 & \dots & 0 & 0 & e & e \\ f & f & f & f & 0 & 0 & \dots & 0 & 0 & 0 & 0 \\ d & e & e & d & e & e & \dots & 0 & 0 & 0 & 0 \\ f & 0 & 0 & f & f & f & \dots & 0 & 0 & 0 & 0 \\ \vdots & \vdots & \vdots & \vdots & \vdots & \vdots & \ddots & \vdots & \vdots & \vdots & \vdots \\ d & e & 0 & 0 & 0 & 0 & \dots & e & e & d & e \\ f & f & 0 & 0 & 0 & 0 & \dots & 0 & 0 & f & f \end{pmatrix},$$

where

$$a_\nu = 1 - \frac{7}{4\nu}, \quad b_\nu = \frac{3}{2\nu^2}, \quad c_\nu = \frac{1}{4\nu^2}, \quad d = \frac{3}{8}, \quad e = \frac{1}{16}, \quad f = \frac{1}{4}.$$

Note, the order of the entries is prescribed by the vertex ordering given in Figure 3.3 (b).

We consider the eigenstructure (Σ, U_0) of S with the diagonal matrix

$$\Sigma = \text{diag}(1, \mu_1, \mu_2, \mu_3, \mu_3, \dots, \mu_{\nu+2}, \mu_{\nu+2}),$$

with

$$\mu_0 = 1, \quad \mu_1, \mu_2 = \frac{1}{8\nu} \left(-7 + 3\nu \mp \sqrt{49 - 30\nu + 5\nu^2} \right)$$

$$\mu_{l+2}, \mu_{l+3} = \frac{1}{16} \left(5 + \cos\left(\frac{2\pi l}{\nu}\right) \mp \cos\left(\frac{\pi l}{\nu}\right) \sqrt{18 + 2 \cos\left(\frac{2\pi l}{\nu}\right)} \right),$$

$l = 1, \dots, \nu - 1$, and the corresponding eigenvectors

$$u_0 = \begin{pmatrix} 1 \\ 1 \\ 1 \\ \vdots \\ 1 \\ 1 \end{pmatrix}, \quad u_1 = \begin{pmatrix} 16\mu_1^2 - 12\mu_1 + 1 \\ 6\mu_1 - 1 \\ 4\mu_1 + 1 \\ \vdots \\ 6\mu_1 - 1 \\ 4\mu_1 + 1 \end{pmatrix}, \quad u_2 = \begin{pmatrix} 16\mu_2^2 - 12\mu_2 + 1 \\ 6\mu_2 - 1 \\ 4\mu_2 + 1 \\ \vdots \\ 6\mu_2 - 1 \\ 4\mu_2 + 1 \end{pmatrix},$$

$$u_{2l+1} = \begin{pmatrix} 0 \\ 4\mu_{l+2} - 1 \\ 1 + C_{\gamma(l)} \\ (4\mu_{l+2} - 1) C_{\gamma(l)} \\ C_{\gamma(l)} + C_{2\gamma(l)} \\ \vdots \\ (4\mu_{l+2} - 1) C_{(\nu-1)\gamma(l)} \\ C_{(\nu-1)\gamma(l)} + 1 \end{pmatrix}, \quad u_{2l+2} = \begin{pmatrix} 0 \\ 0 \\ S_{\gamma(l)} \\ (4\mu_{l+2} - 1) S_{\gamma(l)} \\ S_{\gamma(l)} + S_{2\gamma(l)} \\ \vdots \\ (4\mu_{l+2} - 1) S_{(\nu-1)\gamma(l)} \\ S_{(\nu-1)\gamma(l)} \end{pmatrix},$$

that forms the columns of the eigenvector matrix U_0 , whereby $l = 1, \dots, \nu_2$, $\nu_2 = \nu - 1$ if ν is an odd and $\nu_2 = \nu - 2$ if ν is an even number. The term $\gamma(l)$ is equal to $\gamma(l) = (l + 1) / 2$ if l is an odd and $\gamma(l) = l / 2$ if l is an even number. Additionally, the term C_k is given by the function

$$C_k = \cos\left(\frac{2\pi k}{\nu}\right) \quad \text{und} \quad S_k = \sin\left(\frac{2\pi k}{\nu}\right).$$

Is ν even, then the last two vectors are equal to

$$u_{2\nu-1}^T = (0, 1, 0, -1, 0, 1, 0, \dots, -1, 0) \quad \text{und}$$

$$u_{2\nu}^T = (0, 0, 1, 0, -1, 0, 1, \dots, 0, -1).$$

.

The remaining block matrices of the subdivision matrix A follow directly from the B-spline subdivision, i.e. the given entries correspond to the B-spline subdivision weights. Therefore

$$S_{00} = \begin{pmatrix} c & 0 & 0 & b & a & b & 0 & 0 & 0 \\ e & 0 & 0 & e & d & d & 0 & 0 & 0 \\ b & 0 & 0 & c & b & a & b & c & 0 \\ e & 0 & 0 & 0 & 0 & d & d & e & 0 \\ e & 0 & 0 & d & d & e & 0 & 0 & 0 \\ b & c & b & a & b & c & 0 & 0 & 0 \\ e & e & d & d & 0 & 0 & 0 & 0 & 0 \end{pmatrix}, \quad S_{01} = \begin{pmatrix} c & b & c & 0 & b & c & 0 \\ 0 & e & e & 0 & 0 & 0 & 0 \\ 0 & c & b & c & 0 & 0 & 0 \\ 0 & 0 & e & e & 0 & 0 & 0 \\ 0 & 0 & 0 & 0 & e & e & 0 \\ 0 & 0 & 0 & 0 & c & b & c \\ 0 & 0 & 0 & 0 & 0 & e & e \end{pmatrix},$$

where

$$a = \frac{9}{16}, \quad b = \frac{3}{32}, \quad c = \frac{1}{64}.$$

For $\nu = 3$ the vertex c_7 do not exists, i.e. ($c_7 = c_1$). Due to this, the second column of S_{00} have to be replaced by the vector $(0, 0, c, e, 0, c, e)^T$. Furthermore, we are interested in the eigenstructure of the matrix S_{01} given by the pair (Δ, W_1) . Due to the definition, this can be calculated manually. The diagonal matrix is given by

$$\Delta = \text{diag}\left(\frac{1}{64}, \frac{1}{8}, \frac{1}{16}, \frac{1}{32}, \frac{1}{8}, \frac{1}{16}, \frac{1}{32}\right)$$

with the corresponding eigenvalue matrix

$$W_1 = \begin{pmatrix} 1 & 1 & 2 & 11 & 1 & 2 & 11 \\ 0 & 1 & 1 & 2 & 0 & 0 & 0 \\ 0 & 1 & 0 & -1 & 0 & 0 & 0 \\ 0 & 1 & -1 & 2 & 0 & 0 & 0 \\ 0 & 0 & 0 & 0 & 1 & 1 & 2 \\ 0 & 0 & 0 & 0 & 1 & 0 & -1 \\ 0 & 0 & 0 & 0 & 1 & -1 & 2 \end{pmatrix}.$$

For the enlarged subdivision matrix \bar{A} , the remaining block matrices are given by

$$S_{10} = \begin{pmatrix} 0 & 0 & 0 & 0 & f & 0 & 0 & \mathbf{0} \\ 0 & 0 & 0 & 0 & d & e & 0 & \mathbf{0} \\ 0 & 0 & 0 & 0 & f & f & 0 & \mathbf{0} \\ 0 & 0 & 0 & 0 & e & d & e & \mathbf{0} \\ 0 & 0 & 0 & 0 & 0 & f & f & \mathbf{0} \\ 0 & 0 & 0 & e & d & 0 & 0 & \mathbf{0} \\ 0 & 0 & 0 & f & f & 0 & 0 & \mathbf{0} \\ 0 & 0 & e & d & e & 0 & 0 & \mathbf{0} \\ 0 & 0 & f & f & 0 & 0 & 0 & \mathbf{0} \end{pmatrix}, \quad S_{11} = \begin{pmatrix} f & f & 0 & 0 & f & 0 & 0 \\ e & d & e & 0 & e & 0 & 0 \\ 0 & f & f & 0 & 0 & 0 & 0 \\ 0 & e & d & e & 0 & 0 & 0 \\ 0 & 0 & f & f & 0 & 0 & 0 \\ e & e & 0 & 0 & d & e & 0 \\ 0 & 0 & 0 & 0 & f & f & 0 \\ 0 & 0 & 0 & 0 & e & d & e \\ 0 & 0 & 0 & 0 & 0 & f & f \end{pmatrix}.$$

BIBLIOGRAPHY

- Andersson, L.-E. and Stewart, N. F. (2010). *Introduction to the mathematics of subdivision surfaces*. SIAM.
- Arden, G. (2001). *Approximation properties of subdivision surfaces*. PhD thesis, University of Washington.
- Arnal, A., Lluch, A., and Monterde, J. (2003). Triangular Bézier surfaces of minimal area. In Kumar, V., Gavrilova, M. L., Tan, C. J. K., and LÉcuyer, P., editors, *Computational Science and Its Applications—ICCSA 2003*, volume 2669 of *Lecture Notes in Computer Science*, pages 366–375. Springer Berlin Heidelberg.
- Barendrecht, P. J. (2013). Isogeometric analysis with subdivision surfaces. Master’s thesis, Eindhoven University of Technology: Eindhoven, The Netherland.
- Biermann, H., Levin, A., and Zorin, D. (2000). Piecewise smooth subdivision surfaces with normal control. In *Proceedings of the 27th annual conference on Computer graphics and interactive techniques*, pages 113–120. ACM Press/Addison-Wesley Publishing Co.
- Bobenko, A. I., Hoffmann, T., and Springborn, B. A. (2006). Minimal surfaces from circle patterns: Geometry from combinatorics. *Annals of Mathematics*, pages 231–264.
- Boier-Martin, I. and Zorin, D. (2004). Differentiable parameterization of Catmull–Clark subdivision surfaces. In *Proceedings of the 2004 Eurographics/ACM SIGGRAPH Symposium on Geometry Processing*, pages 155–164. ACM.
- Braess, D. (2007). *Finite Elements: Theory, Fast Solvers, and Applications in Solid Mechanics*. Cambridge University Press.
- Brakke, K. (1978). *The motion of a surface by its mean curvature*, volume 20. Princeton University Press, Princeton, New Jersey.

- Buckland, J. (2005). Mean curvature flow with free boundary on smooth hypersurfaces. *Journal für die reine und angewandte Mathematik*, 586:71–90.
- Cashman, T. J. (2012). Beyond Catmull–Clark? A survey of advances in subdivision surface methods. *Computer Graphics Forum*, 31(1):42–61.
- Catmull, E. and Clark, J. (1978). Recursively generated B-spline surfaces on arbitrary topological meshes. *Computer-Aided Design*, 10(6):350–355.
- Cavaretta, A. S., Dahmen, W., and Micchelli, C. A. (1991). *Stationary subdivision*, volume 453. American Mathematical Soc.
- Ciarlet, P. G. (1978). *The Finite Element Method for Elliptic Problems (Classics in Applied Mathematics)*. North-Holland Publishing Company.
- Cirak, F., Ortiz, M., and Schröder, P. (2000). Subdivision surfaces: A new paradigm for thin-shell finite-element analysis. *International Journal for Numerical Methods in Engineering*, 47:2039–2072.
- Clough, R. W. (September 1960). The finite element method in plane stress analysis. In *Proceedings, 2nd Conference on Electronic Computation, A.S.C.E. Structural Division*, Pittsburgh.
- Colding, T. H., Minicozzi, I., and William, P. (2011). Minimal surfaces and mean curvature flow. *arXiv preprint arXiv:1102.1411*.
- Cosin, C. and Monterde, J. (2002). Bézier surfaces of minimal area. In *Proceedings of the International Conference on Computational Science-Part II, ICCS '02*, pages 72–81. Springer-Verlag.
- Cottrell, J., Bazilevs, Y., and Hughes, T. (2005). Isogeometric analysis: CAD, finite elements, NURBS, exact geometry and mesh refinement. *Computer Methods in Applied Mechanics and Engineering*, 194(39-41):4135–4195.
- Cottrell, J., Hughes, T., and Bazilevs, Y. (2009). *Isogeometric analysis: Toward integration of CAD and FEA*. Wiley, Chichester.
- Dierkes, U., Hildebrandt, S., Küster, A., and Wohlrab, O. (1992). *Minimal surfaces. I, II*, volume 295 of *Grundlehren der Mathematischen Wissenschaften [Fundamental Principles of Mathematical Sciences]*. Springer-Verlag, Berlin.
- do Carmo, M. (1993). *Differentialgeometrie von Kurven und Flächen*, volume 55 of *Vieweg-Studium Aufbaukurs Mathematik*. Vieweg, Braunschweig, 3., durchges. Aufl. edition.
- Doo, D. and Sabin, M. (1978). Behaviour of recursive division surfaces near extraordinary points. *Computer Aided Design*, 10:356–360.
- Douglas, J. (1927). A method of numerical solution of the problem of Plateau. *Annals of Mathematics*, 29(1/4):180–188.
- Dyn, N., Levin, D., and Gregory, J. (1990). A butterfly subdivision scheme for surface interpolation with tension control. *ACM Transactions on Graphics*, 9(2):160–169.
- Dziuk, G. (1991). An algorithm for evolutionary surfaces. *Numerische Mathematik*, 58:603–611.
- Ecker, K. (2004). *Regularity Theory for Mean Curvature Flow*. Birkhauser.
- Fischer, G. (2009). *Lineare Algebra - Eine Einführung für Studienanfänger*. Springer DE, Berlin, 17, akt. Aufl. 2010 edition.

- Green, S. (2003). *Multilevel, subdivision-based, thin shell finite elements: Development and an application to red blood cell modeling*. PhD thesis, Citeseer.
- Halstead, M., Kass, M., and DeRose, T. (1993). Efficient, fair interpolation using Catmull–Clark surfaces. In *Proceedings of the 20th annual conference on Computer graphics and interactive techniques*, SIGGRAPH '93, pages 35–44, New York, NY, USA. ACM.
- Householder, A. S. (1958). Unitary triangularization of a nonsymmetric matrix. *Journal of the ACM (JACM)*, 5(4):339–342.
- Hughes, T. J. (2000). *The finite element method: Linear static and dynamic finite element analysis*. Dover Publications, Mineola, NY, reprint. edition.
- Huisken, G. et al. (1990). Asymptotic behavior for singularities of the mean curvature flow. *Journal of Differential Geometry*, 31(1):285–299.
- Irons, B. and Zienkiewicz, O. (1968). The isoparametric finite element system: A new concept in finite element analysis. In *Proceedings of the Conference on Recent Advances in Stress Analysis*, London. Royal Aeronautical Society.
- Jüttler, B., Mantzaflaris, A., Perl, R., and Rumpf, M. (2016). On numerical integration in isogeometric subdivision methods for PDEs on surfaces. *Computer Methods in Applied Mechanics and Engineering*.
- Kälberer, F., Nieser, M., and Polthier, K. (2007). QuadCover - surface parameterization using branched coverings. *Computer Graphics Forum*, 26(3):375–384.
- Kobbelt, L. (1996). Interpolatory subdivision on open quadrilateral nets with arbitrary topology. *Computer Graphics Forum*, 15(3):409–420.
- Kobbelt, L. (2000). $\sqrt{3}$ -subdivision. In *SIGGRAPH 00: Proceedings of the 27th Annual Conference on Computer Graphics and Interactive Techniques*, pages 103–112. ACM Press/Addison-Wesley Publishing Co.
- Koeller, A. N. (2007). *On the Singularity Sets of Minimal Surfaces and a Mean Curvature Flow*. PhD thesis, Freie Universität Berlin, Fachbereich Mathematik und Informatik, Berlin, Germany.
- Kühnel, W. (2008). *Differentialgeometrie: Kurven - Flächen - Mannigfaltigkeiten*. Friedr. Vieweg & Sohn Verlag | GWV Fachverlage GmbH Wiesbaden, Wiesbaden, 4., überarb. Aufl. edition.
- Lacewell, D. and Burley, B. (2007). Exact evaluation of Catmull-Clark subdivision surfaces near B-spline boundaries. *Journal of Graphics, GPU, and Game Tools*, 12(3):7–15.
- Lagrange, J.-L. (1760-1761). Essai d'une nouvelle méthode pour déterminer les Maxima et les Minima des formules intégrales indéfinies. *Miscellanea Taurinensia II*, 325(1):173–195. A German translation by P. Stäckel can be found in "Ostwalds Klassiker der exakten Wissenschaften" No. 47, Engelmann, Leipzig, 1894.
- Lawson, H. (1980). *Lectures on minimal submanifolds*. Number v. 1 in Mathematics lecture series. Publish or Perish.
- Li, G., Ma, W., and Bao, H. (2004). $\sqrt{2}$ -subdivision for quadrilateral meshes. *Visual Computer*, 20(2):180–198.
- Lian, Q. and Lutai, G. (2005). Minimal surfaces design based on NURBS. *Numerical Mathematics A Journal of Chinese Universities*, pages 175–181.

- Loop, C. (1987). Smooth subdivision surfaces based in triangles. Master's thesis, University of Utah, Departure of Mathematics.
- Loop, C. (2002). Smooth ternary subdivision of triangle meshes. In *Proceedings on Curves and Surfaces Fitting: Saint-Malo 2002*, pages 3–6.
- Ma, W. (2005). Subdivision surfaces for CAD - an overview. *Computer Aided Design*, 37:693–709.
- Meeks, W. H. and Rosenberg, H. (1989). The global theory of doubly periodic minimal surfaces. *Inventiones mathematicae*, 97(2):351–379.
- Meeks, W. H. and Rosenberg, H. (1993). The geometry of periodic minimal surfaces. *Commentarii Mathematici Helvetici*, 68(1):538–578.
- Monterde, J. (2004). Bézier surfaces of minimal area: The Dirichlet approach. *Computer Aided Geometric Design*, 21(2):117–136.
- Morin, G., Warren, J. D., and Weimer, H. (2001). A subdivision scheme for surfaces of revolution. *Computer Aided Geometric Design*, 5(18):483–502.
- Munkres, J. R. (1984). *Elements of Algebraic Topology*. Westview Press.
- Nguyen, T., Karčiauskas, K., and Peters, J. (2014). A comparative study of several classical, discrete differential and isogeometric methods for solving Poisson's equation on the disk. *Axioms*, 3(2):280–299.
- Osserman, R. (2002). *A Survey of Minimal Surfaces*. Phoenix Edition Series. Dover Publications.
- Pan, Q. and Xu, G. (2010). Construction of minimal Catmull-Clark's subdivision surfaces with given boundaries. In *Proceedings of the 6th international conference on Advances in Geometric Modeling and Processing*, GMP'10, pages 206–218, Berlin, Heidelberg. Springer-Verlag.
- Peters, J. and Reif, U. (1997). The simplest subdivision scheme for smoothing polyhedra. *ACM Transactions on Graphics*, 16(4):420–431.
- Peters, J. and Reif, U. (1998). Analysis of algorithms generalizing B-spline subdivision. *SIAM Journal on Numerical Analysis*, 35(2):728–748.
- Peters, J. and Reif, U. (2008). *Subdivision Surfaces*, volume 3 of *Geometry and Computing*. Springer-Verlag, New York.
- Peters, J. and Shiue, L. (2004). Combining 4- and 3-direction subdivision. *ACM Transactions on Graphics*, 23(4):980–1003.
- Pinkall, U. and Polthier, K. (1993). Computing discrete minimal surfaces and their conjugates. *Experimental mathematics*, 2(1):15–36.
- Polthier, K. et al. (2002). *Polyhedral surfaces of constant mean curvature*. PhD thesis, Habilitationsschrift TU Berlin.
- Prautzsch, H. (1997). Freeform splines. *Computer Aided Geometric Design*, 14(3):201–206.
- Prautzsch, H. (1998). Smoothness of subdivision surfaces at extraordinary points. In *Advances in Computational Mathematics*, volume 9, pages 377–390.
- Reif, U. (1995). A unified approach to subdivision algorithms near extraordinary vertices. *Computer Aided Geometric Design*, 12(2):153–174.

- Reif, U. (1998). TURBS: topologically unrestricted rational B-splines. *Constructive Approximation. An International Journal for Approximations and Expansions*, 14(1):57–77.
- Reif, U. and Schröder, P. (2001). Curvature integrability of subdivision surfaces. *Advances in Computational Mathematics*, 14(2):157–174.
- Scherk, H. F. (1835). Bemerkungen über die kleinste Fläche innerhalb gegebener Grenzen. *Journal für die reine und angewandte Mathematik*, 13:185–208.
- Schröder, P. and Zorin, D. (1998). Subdivision for modeling and animation. Website. Available online at <http://www.multires.caltech.edu/teaching/courses/subdivision/>.
- Schweitzer, J. E. (1996). *Analysis and Application of Subdivision Surfaces*. PhD thesis, Department of Computer Science and Engineering, University of Washington.
- Sederberg, T. W., Zheng, J., Bakenov, A., and Nasri, A. (2003). T-splines and T-NURCCs. In *ACM transactions on graphics (TOG)*, volume 22, pages 477–484. ACM.
- Smith, J., Epps, D., and Sequin, C. (2004). Exact evaluation of pieewise smooth Catmull–Clark surfaces using Jordan blocks. *Journal of Graphics, GPU, & Game Tools*.
- Spanier, E. (1981). Algebraic topology. corrected reprint of the 1966 original.
- Stahl, A. (1994). *Über den mittleren Krümmungsfluss mit Neumannrandbedingungen auf glatten Hyperflächen*. PhD thesis, Fachbereich Mathematik, Eberhard Karls Universität, Tübingen, Germany.
- Stahl, A. (1996). Regularity estimates for solutions to the mean curvature flow with a Neumann boundary condition. *Calculus of Variations and Partial Differential Equations*, 4(4):385–407.
- Stam, J. (1998). Exact evaluation of Catmull–Clark subdivision surfaces at arbitrary parameter values. In *Proceedings of the 25th annual conference on Computer graphics and interactive techniques, SIGGRAPH '98*, pages 395–404, New York, NY, USA. ACM.
- Stam, J. and Loop, C. T. (2003). Quad/triangle subdivision. *Computer Graphics Forum*, 22(1):79–86.
- Strang, G. and Fix, G. J. (1973). *An analysis of the finite element method*, volume 212. Prentice-Hall Englewood Cliffs, NJ.
- Thomée, V. (1984). *Galerkin finite element methods for parabolic problems*, volume 1054. Springer.
- Tsuchiya, T. (1986). On two methods for approximating minimal surfaces in parametric form. *Mathematics of Computation*, 46(174):517–529.
- Tsuchiya, T. (1987). Discrete solution of the Plateau problem and its convergence. *Mathematics of Computation*, 49(179):157–165.
- Velho, L. and Zorin, D. (2001). 4-8 subdivision. *Computer Aided Geometric Design*, 18(5):397–427.
- Wallner, J. and Pottmann, H. (2008). Infinitesimally flexible meshes and discrete minimal surfaces. *Monatshefte für Mathematik*, 153(4):347–365.
- Warren, J. (1995). Subdivision methods for geometric design. *Unpublished manuscript, November*.
- Warren, J. and Weimer, H. (2001). *Subdivision methods for geometric design: A constructive approach*. Morgan Kaufmann.

- Wawrzinek, A. (2011). Koiter's Modell für dünne Schalen auf Catmull-Clark Limitflächen. Diploma thesis, Freie Universität Berlin, Department of Mathematics and Computer Science.
- Wawrzinek, A., Hildebrandt, K., and Polthier, K. (2011). Koiter's thin shells on Catmull-Clark limit surfaces. In *Proceedings of the Vision, Modeling & Visualization Workshop 2011, VMV 2011*, pages 113–120, Berlin, Germany. Eurographics Association.
- Wawrzinek, A. and Polthier, K. (2016). Integration of generalized B-spline functions on Catmull-Clark surfaces at singularities. *Computer-Aided Design*, 78:60–70. SPM 2016.
- Wilson, Walter L., J. (1961). On discrete Dirichlet and Plateau problems. *Numerische Mathematik*, 3:359–373.
- Xu, G. and Zhang, Q. (2007). G^2 surface modeling using minimal mean-curvature-variation flow. *Computer-Aided Design*, 39(5):342–351.
- Zorin, D. and Schröder, P. (2000). Subdivision for modeling and animation. *SIGGRAPH '00 Course Notes*.
- Zorin, D. N. (1998). *Stationary Subdivision and Multiresolution Surface Representation*. PhD thesis, California Institute of Technology, Pasadena, CA.

ZUSAMMENFASSUNG

Unterteilungsflächen sind in dem Bereich der geometrischen Modellierung und Computeranimation weit verbreitet. Sie stellen ein rechnerunterstütztes Werkzeug für die Konstruktion von glatten Oberflächen dar, basierend auf der wiederholten Verfeinerung von groben Gittern. Für manche dieser Konstruktionen lässt sich die Grenzfläche, die als Grenzwert einer solchen Verfeinerung definiert wird, mittels einer Parametrisierung beschreiben. Infolge der Parametrisierung wurde in den letzten Jahren eine neue Klasse von Finite-Elemente-Methoden eingeführt. Die hohen Regularitätseigenschaften, die die sogenannten Unterteilungs-Finite-Elemente-Methoden implizieren, sind von besonderem Interesse für die Lösung von partiellen Differentialgleichungen höherer Ordnung. In Bezug darauf genügen die finiten Elemente den Stetigkeitsbedingungen der Lösung. Allerdings ist dieses Konzept, das auf einem grundsätzlich einfachen Unterteilungsverfahren basiert, noch nicht vollständig analysiert worden. Im Vergleich zu den klassischen Finite-Elemente-Methoden stellt sich ein wesentliches Problem im Hinblick auf die recht komplexe zugrunde liegende Struktur der enthaltenen irregulären Elemente.

Mit der Entwicklung einheitlicher Finite-Elemente-Methoden beschäftigt sich ein neues, rasch wachsendes Gebiet der sogenannten Isogeometrischen Analysis. Ein wesentlicher Vorteil dieser Methoden gegenüber den bislang bekannten finiten Elementen liegt in der Interoperabilität zwischen Systemen des computergestützten Designs und Fertigung (CAD und CAM) und der Finite-Elemente-Simulation. Mittels einheitlicher Basisfunktionen kann die Kluft zwischen der Darstellung von geometrischen Formen und Finite-Elemente-Ansatzräumen überbrückt werden. Der kostenaufwendige und fehleranfällige Datenaustausch zwischen Design- und Analysesystemen kann dadurch übergangen werden.

In dieser Arbeit beschäftigen wir uns mit der Untersuchung von Unterteilungs-Finite-Elemente-Methoden für die Lösung von Differenzialgleichungen auf gekrümmten Flächen basierend auf den Catmull–Clark Unterteilungsflächen. Im Mittelpunkt stehen Vierecksnetze und die charakteristische Parametrisierung der Grenzflächen. Diese werden mittels den generalisierten B-Spline-Basisfunktionen vom Catmull–Clark Typ beschrieben. Insbesondere präsentieren wir einen neuen Finite-Elemente-Ansatz, der mit der klassischen Definition der Unterteilungsflächen kompatibel ist. Im Gegensatz zu den bisher verwendeten natürlichen finiten Elementen bleibt die Form der Gitter und somit die Beständigkeit der Grenzfläche bestehen. Dieses kann erreicht werden, da die charakteristischen finiten Elemente die Stetigkeitseigenschaften der durch Gitterverfeinerung erzeugten Unterteilungsflächen vererben.

Für die numerische Analyse der Catmull–Clark-Finite-Elemente-Methode wird als Modellproblem der mittlere Krümmungsfluss betrachtet. Der mittlere Krümmungsfluss wird durch eine geometrische Evolutionsgleichung definiert, die die zeitliche Änderung von Flächen im dreidimensionalen Raum beschreibt, dabei wird die Richtung und die Geschwindigkeit der Änderung von dem Normalenvektor und der mittleren Krümmung der Fläche vorgegeben. Weiterhin ist darauf hinzuweisen, dass unter der Vorgabe einer Randkurve die kritischen Punkte des Krümmungsflusses eine Minimalfläche beschreiben. Minimalflächen zeichnen sich dadurch aus, dass sie den lokal kleinsten Oberflächeninhalt haben, im Vergleich zu allen von der vorgegebenen Randkurve umschlossenen Flächen. Aufgrund dieser Eigenschaft sind diese Flächen außerordentlich interessant für viele Anwendungen im Bereich der Architektur, Kunst, Molekulartechnik, Materialwissenschaft und Werkstofftechnik. Diese Arbeit beschäftigt sich insbesondere mit der Approximation von periodischen Minimalflächen. Wir beschreiben ein Verfahren zur Konstruktion von stabilen periodischen Catmull–Clark Grenzflächen mit minimalem Oberflächeninhalt. Das Verfahren basiert auf dem numerischen Evolutionsmodell einer gegebenen Fläche unter dem mittleren Krümmungsfluss. Unter Verwendung des Schwarzschen Spiegelungsprinzips beschreiben wir eine Konstruktion für die Assemblierung der entsprechenden Randbedingungen, die im Einklang mit den Unterteilungsflächen ist.

SELBSTSTÄNDIGKEITSERKLÄRUNG

Gemäß §7 (4) der Promotionsordnung versichere ich hiermit, dass ich diese Arbeit selbständig verfasst habe und keine anderen als die angegebenen Hilfsmittel und Hilfen genutzt habe. Des Weiteren versichere ich, dass ich die vorliegende Arbeit zu keinem früheren Promotionsverfahren eingereicht habe.

Berlin, den